

DISSERTATION

STATISTICAL MODELS FOR ANIMAL TELEMETRY DATA WITH APPLICATIONS
TO HARBOR SEALS IN THE GULF OF ALASKA

Submitted by

Brian M. Brost

Graduate Degree Program in Ecology

In partial fulfillment of the requirements

For the Degree of Doctor of Philosophy

Colorado State University

Fort Collins, Colorado

Spring 2017

Doctoral Committee:

Advisor: Mevin B. Hooten

Robert J. Small
George Wittemyer
Randall B. Boone

Copyright by Brian M. Brost 2017

All Rights Reserved

ABSTRACT

STATISTICAL MODELS FOR ANIMAL TELEMETRY DATA WITH APPLICATIONS TO HARBOR SEALS IN THE GULF OF ALASKA

Much is known about the general biology and natural history of harbor seals (*Phoca vitulina*), but questions remain about the aquatic and terrestrial space use of these marine mammals. This is in large part because methods for examining the spatial ecology of harbor seals are poorly developed. The objective of this dissertation is to pair existing telemetry data with contemporary spatio-temporal modeling to quantify the space use and resource selection of harbor seals in the coastal waters of southern Alaska.

Recent extensions to models for analyzing animal telemetry data address complications such as autocorrelation and telemetry measurement error; however, additional challenges remain, especially in the context of analyzing Argos satellite telemetry data collected on marine mammals like harbor seals. For example, existing methods assume elliptical (or circular) patterns of measurement error, even though Argos satellite telemetry devices impose more complicated error structures on the data. Constraints, or barriers, to animal movement present another complication. Harbor seals and other marine mammals are constrained to move within the marine environment, and mechanistic models that do not adhere to movement barriers yield unreliable inference. Therefore, a primary goal of this research is to develop statistical tools that account for these nuances and provide rigorous, ecologically relevant inference. Even though the models presented in this dissertation were specifically developed with Argos satellite telemetry data and harbor seals in mind, the methods are general and can be applied to other species and types of telemetry data. This dissertation consists of five chapters.

In Chapter 1, I briefly discuss the general biology of harbor seals, focusing on what is known about their spatial habits in Alaska. I then summarize trends in Alaskan harbor seal abundance, a topic that motivated my research as well as the work of many others. I describe the existing Alaska Department of Fish and Game telemetry data sets that are available for examining harbor seal spatial ecology, commonly-used statistical methods for analyzing animal telemetry data, and conclude with the objectives of my research and an outline for the remainder of the dissertation.

In Chapter 2, I propose an approach for obtaining resource selection inference from animal location data that accounts for complicated error structures, movement constraints, and temporally autocorrelated observations. The model consists of two general components: a model for the true, but unobserved, animal locations that reflects prior knowledge about constraints to animal movement, and a model for the observed telemetry locations that is conditional on the true locations. I apply the model to simulated data, showing that it outperforms common *ad hoc* approaches used when confronted with telemetry measurement error and movement constraints. I then apply the framework to obtain inference concerning aquatic resource selection and space use for harbor seals near Kodiak Island, Alaska.

Chapters 3 and 4 shift the focus from inference concerning aquatic space use and resource selection, to inference concerning the use of coastal resources (i.e., haul-out sites) by harbor seals. In Chapter 3, I present a fully model-based approach for estimating the location of central places (e.g., haul-out sites, dens, nests, etc.) from telemetry data that accounts for multiple sources of uncertainty and uses all of the available locational data. The model consists of an observation model to account for large telemetry measurement error and animal movement, and a highly flexible mixture model (a Dirichlet process) to identify the location of central places. Ancillary behavioral data (e.g., harbor seal dive data obtained

from the satellite-linked depth recorders) are also incorporated into the modeling framework to obtain inference concerning temporal patterns in central place use. Based on the methods developed in Chapter 3, I present a comprehensive analysis of the spatio-temporal patterns of haul-out use for harbor seals near Kodiak Island in Chapter 4. Chapter 4 also extends previously developed methods to examine the affect of covariates on haul-out site selection and to obtain population-level inference concerning haul-out use.

I conclude, in Chapter 5, with some general thoughts about analyzing animal telemetry data, as well as potential future research directions.

ACKNOWLEDGEMENTS

First, I thank my advisor, Mevin Hooten, for his support and encouragement over the past 4 years. Mevin taught me a more flexible and creative (and *fun*) way to approach ecological modeling, for which I am deeply grateful. My other committee members, Bob Small, George Wittemyer, and Randy Boone, provided perspective on issues of wildlife management and conservation, insight into the means and meanings of ecological models, and wisdom concerning the scientific process itself. I thank Bob Small, in particular, for the many discussions about harbor seal biology and the harbor seal telemetry data sets that helped guide my research.

Past and present members of the Hooten Lab have been a terrific source of intellectual companionship. Thanks also to my closest friends and family. I am fortunate to have a life enriched by many remarkable people, and their friendship, love, and unconditional support has not only made my journey possible, but also worthwhile. Thank you.

Financial support for this research came from the Alaska Department of Fish and Game, through award NA11NMF4390200 from the National Oceanic and Atmospheric Administration Fisheries, Alaska Region, and award 1614392 from the National Science Foundation Division of Mathematical Sciences.

TABLE OF CONTENTS

	Page
Abstract	ii
Acknowledgements	v
Table of Contents	vi
List of Tables	ix
List of Figures	x
Chapter 1. Introduction	1
1.1 General biology of harbor seals	1
1.1.1 Description and life history	1
1.1.2 Distribution	2
1.1.3 Aquatic space use and movements	2
1.1.4 Terrestrial haul-out use	4
1.1.5 Prey and predators	6
1.2 Population biology of harbor seals in Alaska	7
1.3 Harbor seal telemetry data	9
1.4 Statistical methods for animal telemetry data	10
1.4.1 Spatial point process models	12
1.4.2 Movement models	15
1.5 Objectives and dissertation structure	19
Chapter 2. Animal movement constraints improve resource selection inference in the presence of telemetry error	22
2.1 Introduction	23
2.2 Telemetry location data	25
2.3 Model formulation	26
2.3.1 Observation model	26
2.3.2 Process model	27
2.3.3 Prior distributions	29
2.4 Model application	29
2.4.1 Model evaluation using simulated data	29
2.4.2 Case study: harbor seals	31
2.5 Discussion	32
2.5.1 Constraints in space and time	34
2.5.2 Guidance	35

Chapter 3. Leveraging constraints and biotelemetry data to pinpoint repetitively used spatial features	40
3.1 Introduction	41
3.2 Telemetry data	42
3.3 Model formulation	43
3.3.1 Observation model	44
3.3.2 Spatial process model	46
3.3.3 Temporal process model	48
3.3.4 Prior distributions	49
3.4 Model application	50
3.4.1 Simulated data example	50
3.4.2 Case study: harbor seals	51
3.5 Discussion	52
3.5.1 Observation model	53
3.5.2 Process models	53
3.5.3 Guidance	55
Chapter 4. Model-based clustering reveals spatio-temporal patterns in central place use of a marine top predator	59
4.1 Introduction	60
4.2 Methods	63
4.2.1 Harbor seal telemetry data	63
4.2.2 Statistical notation	64
4.2.3 Haul-out site location estimation	65
4.2.4 Haul-out site selection	68
4.2.5 Temporal patterns in haul-out use	72
4.3 Results	73
4.3.1 Harbor seal telemetry data	73
4.3.2 Haul-out site location estimation	74
4.3.3 Haul-out site selection	75
4.3.4 Temporal patterns in haul-out use	75
4.4 Discussion	76
4.4.1 Harbor seal haul-out behavior	77
4.4.2 Conclusion	79
Chapter 5. Conclusion	85
5.1 Overarching themes	86
5.2 Future directions	88
Bibliography	91
Appendix A. Supplementary material for Chapter 2	111
A1 Complete mixture model specification	112

A2	Full-conditional distributions and Markov chain Monte Carlo algorithm	113
A3	Performance of mixture model in simulation study	118
A4	Results for harbor seal case study	119
A5	Estimated Argos satellite telemetry error by location class	120
	Appendix B. Supplementary material for Chapter 3	122
B1	Model statement, posterior distribution, and full-conditional distributions	123
B2	Markov chain Monte Carlo algorithm for parameter estimation	132
B3	Posterior quantities for the simulated data example	138
B4	Simulated examples using location data that arises from a movement model .	141
B5	Results for harbor seal case study	143
B6	Alternative model specifications	147
	Appendix C. Supplementary material for Chapter 4	152
C1	Details concerning model for haul-out site locations	153
C2	Details concerning model for haul-out site selection	164
C3	Details concerning model for temporal haul-out use	170
C4	Inference concerning haul-out site locations by individual	175
C5	Inference concerning observation model parameters	187
C6	Inference concerning haul-out site selection	194

LIST OF TABLES

2.1	Performance of five methods for estimating μ_t based on 250 simulations of 1,000 telemetry locations each. The notation $E(\cdot)$ denotes the expectation, or mean value over the simulations. Specifically, $E(n)$ is the expected sample size and $E[d(\hat{\mu}_t, \mu_t)]$ is the expected distance in meters between $\hat{\mu}_t$ (the estimated location) and μ_t as measured through the domain defined by \mathcal{S} . For the mixture t and normal models, $\hat{\mu}_t$ was calculated as $\text{Mode}(\boldsymbol{\mu} \mathbf{s})$. The expected distance $E[d(\hat{\mu}_t, \mu_t)]$ for all locations combined was weighted to account for varying sample sizes in the “Exclude $\mathbf{s}_t \notin \mathcal{S}$ ” and “Speed filter” methods.	36
2.2	Performance of five methods for estimating β based on 250 simulations of 1,000 telemetry locations each.	37

LIST OF FIGURES

1.1	Harbor seals occur in the coastal waters of Alaska from southeastern Alaska (i.e., the Alaskan Panhandle) to Bristol Bay. Areas in which the Alaska Department of Fish and Game telemetered harbor seals are circled in red. From left to right, the circled regions are Bristol Bay, Tugidak and Kodiak Islands, Prince William Sound, and southeast Alaska.	3
1.2	Aerial photograph of harbor seals at a haul-out site in Glacier Bay National Park, Alaska.	5
1.3	Example of Argos satellite telemetry locations (red crosses) collected on a single harbor seal monitored on the southern coast of Kodiak Island, Alaska. (a) The magnitude of error in Argos satellite telemetry data is evident given that telemetry locations in the interior of Alaska are implausible for a marine mammal (e.g., the northern telemetry location that is circled in red). Similarly, even though harbor seals are capable of extensive movements at sea, telemetry locations like the one circled in the Pacific Ocean are most likely errors because harbor seals favor shallow water near shore. (b) Telemetry locations in the vicinity of Kodiak Island. Because of telemetry measurement error, many of the locations occur on land in areas inaccessible by harbor seals.	11
2.1	Simulation of 300 true animal locations (μ_t , black circles) according to the process model (Eq. 2.3) using two resource selection covariates, namely distance to a point of attraction (e.g., a haul-out site; blue triangle) and bathymetry. The blue polygon represents \mathcal{S} , the spatial support of the movement process within which all μ_t occur. (a) Observed telemetry locations (s_t ; crosses) were simulated according to the observation model (Eq. 2.1) with three levels of telemetry measurement error corresponding to high (yellow), medium (orange), and low (red) accuracy Argos locations (i.e., Argos location classes 3, 0, and B, respectively). The lines connect a subset of observed locations with their corresponding true location. (b) The posterior distribution of μ_t (blue to purple color gradient in \mathcal{S} ; darker colors represent higher posterior probability). Lines connect a subset of true animal locations (black circles) with their corresponding observed locations (yellow crosses) and posterior modes (red crosses).	38
2.2	Argos satellite telemetry locations (red crosses) of an adult female harbor seal monitored from 09 OCT 1995 to 04 JUN 1996 along the southern coast of Kodiak Island, Alaska, USA. The blue polygon represents \mathcal{S} , the spatial support of the movement process; for seals, this is the marine environment and adjacent coastlines. Our analysis focused on resource selection inference pertaining to distance to haul-out site (blue triangle) and bathymetry (gray contour lines). The posterior distribution of μ_t is represented by the blue to purple color gradient in \mathcal{S} ; darker colors indicate higher posterior probability.	39

3.1 Simulation of 1,000 telemetry locations ($\mathbf{s}(t)$) arising from three central places ($\boldsymbol{\mu}_j$). The point symbology associates telemetry locations (black and gray numerals; most are smaller gray numerals to reduce clutter) to their corresponding central places (white, numbered circles). For example, a telemetry location labeled “1” is associated with the central place labeled “1.” The spatial support of central places ($\tilde{\mathcal{S}}$) exists at the intersection of the blue and gray polygons (black line). The posterior distribution of $\boldsymbol{\mu}(t)$ (red gradient) in the vicinity of the central places is shown in the bottom panels; brighter red corresponds to higher posterior probability. Inference concerning the location of central place “3,” which was associated with 608 telemetry locations, is most certain. Inference concerning central places “1” and “2,” which were associated with fewer telemetry locations (approximately 200 locations each), is more diffuse. All inference was based on 20,000 MCMC samples after convergence. Note that 326 simulated telemetry locations are beyond the extent of this map, occurring up to 880 km away.

3.2 Telemetry locations (top panel) of a subadult female harbor seal monitored from 09 OCT 1995 to 04 JUN 1996 in Ugak Bay (57.42982°N, -152.5715°W) on the southern coast of Kodiak Island, Alaska, USA. Point symbology reflects whether the individual was hauled-out (black points) or at-sea (black crosses) at the time a telemetry location was recorded. Telemetry locations were collected on average every 5.7 h (range: 0.0 – 54.8 h) using an Argos satellite telemetry device. The animal’s position was measured on 1,004 occasions, with $\approx 72\%$ of locations coming from the three least accurate Argos location classes. Approximately 40% of locations were collected while the individual was at a haul-out site ($y(t) = 1$). The spatial support of haul-out sites ($\tilde{\mathcal{S}}$) exists along the coastline (black line) at the intersection of the blue (water) and gray (land) polygons. The insets show three regions where the posterior probability of $\boldsymbol{\mu}(t)$ (red gradient) is most concentrated (bottom panels). Brighter red corresponds to higher posterior probability. All inference was based on 50,000 MCMC samples after convergence. Note that 190 telemetry locations are beyond the extent of this map, occurring up to 1,100 km away from Ugak Bay.

4.1 Simulation demonstrating the signal of central place behavior in telemetry location data (gray closed circles). (a) When telemetry location error is small, clusters of locations (large black open circles) indicate the location of central places. (b) When telemetry location error is large, the number and location of central places is much less certain. The locations shown in (b) are the same as those shown in (a) but with additional error.

4.2	Posterior distribution of $\mu_i(t)$ (red gradient) for 12 harbor seals telemetered near Kodiak Island, Alaska (a); brighter red corresponds to higher posterior probability. Gray segments of shoreline either have very low or no posterior probability of haul-out use. The inset in the top right shows the location of Kodiak Island and inset (a) (red box) within the state of Alaska, USA (light gray). Boxes in (a) reflect the location of insets (b)–(e) where high posterior probability of $\mu_i(t)$ occurs. The posterior distribution for each individual harbor seal is presented in Appendix C4.	82
4.3	Individual- and population-level inference concerning parameters examined in the haul-out site selection model. The top row (blue box) represents inference concerning the population-level parameter (μ_β) that represents an average affect across the 12 harbor seals analyzed. The remaining rows show individual-level parameters (β_i), and individual seals are labeled according their sex and age class. The points indicate the posterior mean, the thick lines represent the 50% credible interval, and the thin lines represent the 95% credible interval.	83
4.4	Individual- and population-level inference concerning parameters examined in the temporal haul-out use model. The top row (blue box) represents inference concerning the population-level parameter (μ_γ) that represents an average affect across the 12 harbor seals analyzed. The remaining rows show individual-level parameters (γ_i), and individual seals are labeled according their sex and age class. The points indicate the posterior mean, the thick lines represent the 50% credible interval, and the thin lines represent the 95% credible interval.	84

*The great advantage of the model-based over the ad hoc approach,
it seems to me, is that at any given time we know what we are doing.*

—George Box (1979)

CHAPTER ONE

Introduction

Much is known about the general biology and natural history of harbor seals (*Phoca vitulina*), but questions remain about the aquatic and terrestrial space use of these marine mammals. This is in large part because methods for examining the spatial ecology of harbor seals are poorly developed. The objective of this dissertation is to pair existing telemetry data with contemporary spatio-temporal modeling to quantify the space use and resource selection of harbor seals in the coastal waters of southern Alaska. In particular, this research is mostly focused on methods and modeling contributions that will help us learn more about where harbor seals go, and why they go where they go.

In what follows, I briefly discuss the general biology of harbor seals, focusing on what is known about their spatial habits in Alaska. I then summarize trends in Alaskan harbor seal abundance, a topic that motivated my research as well as the work of many others. I describe the existing Alaska Department of Fish and Game telemetry data sets that are available for examining harbor seal spatial ecology, as well as commonly-used statistical methods for analyzing animal telemetry data. Finally, I conclude Chapter 1 with the objectives of my research and an outline for the remainder of the dissertation.

1.1 GENERAL BIOLOGY OF HARBOR SEALS

1.1.1 Description and life history

Harbor seals belong to the “true seal” family, Phocidae. True seals lack external ear flaps and have short forelimbs that limit their ability to move on land. Adult male harbor seals

are slightly larger than females, weighing approximately 85–170 kg and measuring 160–185 cm in length (Pitcher and Calkins 1979, Perrin et al. 2009). Harbor seals generally live < 30 years in the wild, with males reaching sexual maturity at 5–6 years of age and females at 3–7 years of age. Females usually bear a single pup (although twins have been documented) in May to July (in Alaska), and weaning occurs 3–5 weeks after birth (Scheffer and Slipp 1944, Perrin et al. 2009).

1.1.2 Distribution

Harbor seals are widely distributed in the coastal waters of the temperate and subarctic latitudes of the Northern Hemisphere (Scheffer and Slipp 1944, Perrin et al. 2009). In the Atlantic Ocean, harbor seals are found along the eastern coast of North America from Florida to Greenland, and in Europe from France to Norway. In the Pacific Ocean, harbor seals are found from Baja California north to the Bering Sea and Kamchatka Peninsula, and south to Hokkaido Island, Japan (Scheffer and Slipp 1944, Perrin et al. 2009). In Alaska specifically, harbor seals occur from the panhandle of southeastern Alaska northward to Prince William Sound, westward to the Aleutian Islands, and as far north as Bristol Bay and the Pribilof Islands (Fig. 1.1; Muto 2015).

1.1.3 Aquatic space use and movements

Harbor seals are semi-aquatic in that they depend on the marine environment for their food source but haul out of the water onto beaches, intertidal areas, and floating ice (in glacial fjords) to rest, molt, escape aquatic predators, give birth, and rear their pups (Fig 1.2; Ling 1984, da Silva and Terhune 1988, Thompson 1989, Watts 1992). Harbor seals typically forage near their haul-out sites, favoring shallower waters relatively close to shore



FIGURE 1.1. Harbor seals occur in the coastal waters of Alaska from southeastern Alaska (i.e., the Alaskan Panhandle) to Bristol Bay. Areas in which the Alaska Department of Fish and Game telemetered harbor seals are circled in red. From left to right, the circled regions are Bristol Bay, Tugidak and Kodiak Islands, Prince William Sound, and southeast Alaska.

(Frost et al. 2001, Lowry et al. 2001). For example, previous telemetry studies indicate that nearly all at-sea harbor seal locations occur within 25 km of their haul-out sites in water < 200 m deep (Frost et al. 2001, Lowry et al. 2001, Cunningham et al. 2009). Hastings et al. (2004) found that harbor seals in the Gulf of Alaska typically dove to depths < 20 m, whereas Frost et al. (2001) found 20–100 m water depths to be favored by seals in the same region. Exogenous factors like physical environment (e.g., bathymetry and substrate) and time of year can better predict movement and foraging behavior than intrinsic factors like sex and age (Small et al. 2005, Sharples et al. 2012). For example, movements of harbor seal pups were more extensive at Tugidak Island, which is on the continental shelf adjacent to the Gulf of Alaska, compared to movements of pups in the more bathymetrically complex Prince William Sound (Fig. 1.1; Small et al. 2005). Similarly, seasonal changes in the locations of haul-out sites used by harbor seals is a function of prey availability (Montgomery et al. 2007, Cunningham et al. 2009).

Harbor seals occasionally travel 100 km or more from their haul-out sites (Lowry et al. 2001, Peterson et al. 2012); however, adults exhibit high levels of site fidelity over months to years and typically return to the same haul-out sites between at-sea foraging bouts (Härkönen and Heide-Jørgensen 1990, Thompson et al. 1997, Cunningham et al. 2009). Despite movements that are generally more extensive than adults (Lowry et al. 2001, Hastings et al. 2004), juvenile harbor seals often return to haul-out sites within 20–50 km of their natal sites (Small et al. 2005).

1.1.4 Terrestrial haul-out use

Temporal patterns in haul-out use are influenced by behaviors (e.g., breeding and foraging), physiological functions (e.g., thermoregulation and molting), and environmental con-



FIGURE 1.2. Aerial photograph of harbor seals at a haul-out site in Glacier Bay National Park, Alaska.

ditions (e.g., tidal state) that operate at varying time scales (Boveng et al. 2003, London et al. 2012). At daily time scales, the highest proportion of seals onshore are typically observed at times nearest low tide when favorable haul-out sites are exposed (e.g., sites isolated from terrestrial predators; Schneider and Payne 1983, Pauli and Terhune 1987) and during midday when the air temperature is most conducive to thermoregulation (Stewart 1984, Calambokidis et al. 1987, Pauli and Terhune 1987; see London et al. 2012 for an exception to these patterns in Hood Canal, WA). At annual time scales, temporal patterns in haul-out use are influenced by breeding and molting cycles that can be sex- and age-specific (e.g., adult females nurse pups onshore, pups do not molt, etc.; Everitt and Braham 1980, Brown and Mate 1983, Calambokidis et al. 1987, Huber et al. 2001, Jemison and Kelly 2001, Boveng et al. 2003, Daniel et al. 2003), as well as the distribution and availability of prey.

1.1.5 Prey and predators

Harbor seals are opportunistic consumers and eat a wide variety of fish and invertebrate prey that varies seasonally, and probably annually, depending on availability (Imler and Sarber 1947, Fisher 1952, Wilke 1957, Pitcher and Calkins 1979, Pitcher 1980). Harbor seal diets also vary regionally (Iverson et al. 1997, Jemison 1999). For example, walleye pollock (*Theragra*), arrowtooth flounder (*Atheresthes*), herring (*Clupeidae*), and cephalopods were the most frequent prey items of harbor seals in southeastern Alaska, whereas Irish lord (*Hemilepidotus*) and sandlance (*Ammodytes*) were the predominant prey items among harbor seals in the Kodiak Archipelago (Jemison 1999). The composition of harbor seal diets in the Bering Sea were more diverse and included sandlance, rock sole (*Lepidopsetta*), flounders

(Pleuronectidae), sculpin (Cottidae), yellowfin sole (*Limanda*), rainbow smelts (*Osmerus*), and tomcod (*Microgadus*) (Jemison 1999).

The principal natural predators of harbor seals are killer whales (*Orcinus orca*) and sharks (Selachimorpha), although wolves and bears also depredate harbor seals at haul-out sites that are not protected from terrestrial carnivores (Scheffer and Slipp 1944, Perrin et al. 2009). Aside from natural mortality, other sources of mortality include incidental take related to commercial fisheries, illegal killing, and hunting. As prescribed by the U.S. Marine Mammal Protection Act of 1972, hunting in Alaska is limited to Alaska Natives for subsistence and handicraft purposes. Subsistence harvests usually take fewer than 2,000 individuals per year statewide (Muto 2015).

1.2 POPULATION BIOLOGY OF HARBOR SEALS IN ALASKA

The abundance of harbor seals has declined in many parts of Alaska over the past few decades. For example, there was an 85% decline in harbor seal abundance at Tugidak Island from 1976 to 1988 (Pitcher 1990, Jemison et al. 2006), a 63% decline from 1984 to 1997 in Prince William Sound (Frost et al. 1999), and similar declines along the Aleutian Archipelago (Small et al. 2008), at Kodiak Island (Small et al. 2003), and in Glacier Bay National Park (Mathews and Kelly 1996, Mathews and Pendleton 2006). In contrast, harbor seal abundance was stable or increasing in Bristol Bay and parts of southeastern Alaska over approximately the same periods (Small et al. 2003).

Some populations of harbor seals that were once declining started to rebound in the 1990s. Despite the recent upswing at some locations, like a 67% increase in harbor seal abundance at Kodiak Island from 1993–2003 (Small et al. 2003), harbor seal numbers in the Gulf of Alaska remain substantially reduced (Jemison et al. 2006). Even so, recent

estimates indicate harbor seals are still fairly abundant in Alaska, with approximately 200,000 harbor seals statewide (Muto 2015); however, large declines like those experienced during the 1970s–1990s are alarming nonetheless. Harbor seals are often the most numerous marine mammal in coastal Alaska ecosystems and likely play an important role in structuring marine communities as a consumer and as prey for other upper-trophic level species (Boveng and Ziel 2015). Therefore, sustaining harbor seal populations is important for maintaining the health and stability of marine ecosystems. Indeed, a primary management objective according to the Marine Mammal Protection Act is to maintain “optimum sustainable population levels” and to restore depleted populations of harbor seals.

Declines in harbor seal numbers coincided with the 1976–1977 shift in the Pacific Decadal Oscillation (Pitcher 1990, Hare and Mantua 2000, Jemison and Kelly 2001); however, proximate causes for the declines are undetermined (Wade et al. 2007). Harbor seal population trajectories mirrored those of other marine mammals in the region (e.g., Steller sea lions (*Eumetopias jubatus*), northern fur seals (*Callorhinus ursinus*), and sea otters (*Enhydra lutris*); Braham et al. 1980, Fowler 1982, Merrick et al. 1987, York and Kozloff 1987, Loughlin et al. 1992), leading some to suggest that increased predation by transient, marine-mammal-eating killer whales was the primary mechanism behind the declines (Springer et al. 2003, Springer et al. 2008). In contrast, others asserted that more plausible explanations for the decline of marine mammals in the Gulf of Alaska and Bering sea included factors such as direct mortality (incidental mortality related to fisheries, subsistence hunts, and illegal killing), environmental contaminants, disease, human disturbance, and reduction in the quantity and quality of prey (Mizroch and Rice 2006, DeMaster et al. 2006, Trites et al. 2007, Wade et al. 2007).

Despite the many hypotheses concerning the underlying mechanisms that caused the collapse of harbor seal (and other marine mammal) populations in Alaska, there is little empirical evidence pertaining to the factors that ultimately caused the declines. Consequently, there was a call for expanded research on marine mammals in general, and specifically for harbor seals this led to additional studies pertaining to their physiology (e.g., Atkinson et al. 2015), health and disease (e.g., Hueffer et al. 2011), diet (e.g., Herremans et al. 2009), foraging behavior (e.g., Womble et al. 2014), vital rates (survival and reproductive rate), age structure (e.g., Blundell and Pendleton 2008), and spatial ecology (e.g., Brost et al. 2015).

1.3 HARBOR SEAL TELEMETRY DATA

The Alaska Department of Fish and Game collected a rich telemetry data set on harbor seals during the 1990s and early 2000s. Harbor seals were captured and equipped with satellite telemetry devices in four areas throughout Alaska: Bristol Bay, Kodiak and Tugidak Islands, Prince William Sound, and southeast Alaska (Fig. 1.1). The telemetry devices transmitted to Argos receivers attached to polar orbiting meteorological satellites, a system that uses the Doppler effect (i.e., the shift in frequency observed when the telemetry devices and the satellites are moving relative to each other) for geopositioning.

The Argos least-squares positioning algorithm assigns each telemetry location to one of six quality classes based on the number of transmissions received during a satellite pass. In order of decreasing accuracy, the location quality classes are 3, 2, 1, 0, A, and B. The location quality classes have different error patterns and magnitudes, and some exhibit an x-shaped error distribution that has greatest error variance along the NW-SE and NE-SW axes (Costa et al. 2010, Douglas et al. 2012, Brost et al. 2015, Buderman et al. 2016). The x-shaped error pattern is an artifact of the polar orbiting Argos satellites and error that is

largest in the direction perpendicular to the orbit. The magnitude of Argos location errors are often >10 km and in some cases >100 km (Fig. 1.3; Costa et al. 2010, Douglas et al. 2012, Brost et al. 2015), errors that exceed the typical extent of harbor seal movements (Frost et al. 2001, Lowry et al. 2001, Cunningham et al. 2009).

A subset of the captured harbor seals were equipped with satellite-linked depth recorders that provide information on harbor seal diving behavior (Wildlife Computers, Redmond, WA). The depth recorders measured water depth at 10 second intervals with an accuracy of approximately 2 meters; however, these data were summarized into bins (or histograms) over 6-hours intervals to circumvent data transmission limitations. The number of bins, as well as the thresholds defining the bins, vary by region and year of the telemetry study. The dive data consist of four histogram types: (1) maximum depth for individual dives per 6-hour period tabulated by depth bin; (2) length of dives per 6-hour period tabulated by time bin; (3) proportion of time in each depth bin per 6-hour period; and (4) a binary indicator that records whether the majority of time per 20-minute interval is at-sea or on-land. In addition to these data, an on-board conductivity sensor determined if the device was wet (low resistance) versus dry (high resistance) at the time positional data were recorded. The devices were programmed with a delay (10 consecutive readings at 45 sec. intervals) to prevent spurious wet/dry state transitions associated with splashing on a haul-out or short dry periods experienced by the sensor while a seal was surfaced in the water.

1.4 STATISTICAL METHODS FOR ANIMAL TELEMETRY DATA

Animal telemetry data arise as the outcome of periodic observations of a continuous animal movement process. Telemetry locations are a type of presence-only data because they consist of observations of an animal through space and time, and lack information

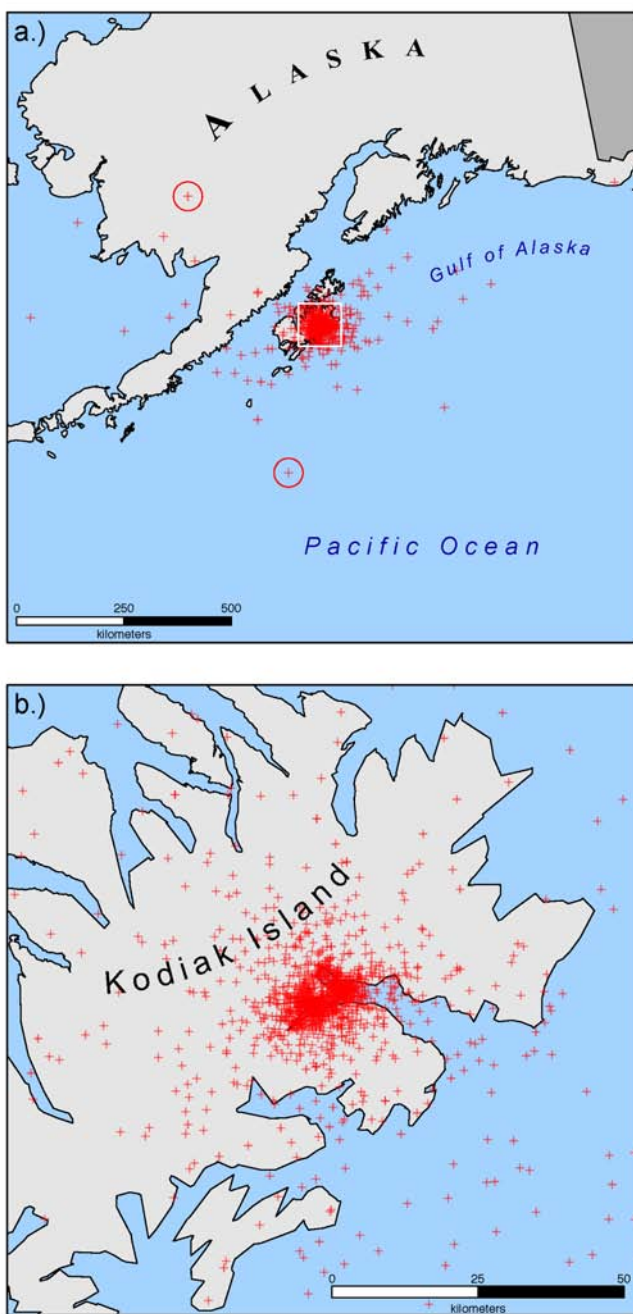


FIGURE 1.3. Example of Argos satellite telemetry locations (red crosses) collected on a single harbor seal monitored on the southern coast of Kodiak Island, Alaska. (a) The magnitude of error in Argos satellite telemetry data is evident given that telemetry locations in the interior of Alaska are implausible for a marine mammal (e.g., the northern telemetry location that is circled in red). Similarly, even though harbor seals are capable of extensive movements at sea, telemetry locations like the one circled in the Pacific Ocean are most likely errors because harbor seals favor shallow water near shore. (b) Telemetry locations in the vicinity of Kodiak Island. Because of telemetry measurement error, many of the locations occur on land in areas inaccessible by harbor seals.

concerning where the animal was not found (Pearce and Boyce 2006). Most statistical models for telemetry data fall into one of two broad classes, namely spatial point process models and models for animal trajectories (“movement models” hereafter). Much overlap exists between these two general approaches to examining animal telemetry data, although spatial point process models often address questions concerning the spatial distribution and habitat use of animals, whereas movement models typically explore behavioral responses and the mechanics of animal movement.

The specific methods for analyzing telemetry data encompassed by the spatial point process and movement modeling approaches are numerous. In fact, entire books cover the topic (e.g., Hooten et al., in press). Therefore, I focus on commonly-used spatial point process and movement models for analyzing animal telemetry data in the exposition below.

1.4.1 Spatial point process models

Spatial point process models describe the relationship among animal locations in geographic space. They focus on the animal’s position and consider movement from a fixed frame of reference (i.e., geographic space). In fact, the “response” variable of interest in a spatial point process model is the animal’s location itself (i.e., the telemetry locations).

Perhaps the most common method used to analyze animal telemetry data is a type of heterogeneous, spatial point process model known as a “resource selection function” (Manly et al. 2002). Denote a telemetry location recorded for a single individual at time t as $\mathbf{s}(t) \equiv (s_x(t), s_y(t))'$. The model takes the form of a weighted distribution (Lele and Keim 2006, Aarts et al. 2012)

$$\mathbf{s}(t) \sim \frac{g(\mathbf{x}(\mathbf{s}(t)), \boldsymbol{\beta}) f(\mathbf{s}(t))}{\int_{\mathcal{S}} g(\mathbf{x}(\mathbf{s}), \boldsymbol{\beta}) f(\mathbf{s}) d\mathbf{s}}, \quad (1.1)$$

where $g(\mathbf{x}(\mathbf{s}), \boldsymbol{\beta})$ represents the “selection function,” $f(\mathbf{s})$ represents the “availability function,” and \mathcal{S} is the spatial support of the point process. The selection function often takes an exponential form (i.e., $g(\mathbf{x}(\mathbf{s}), \boldsymbol{\beta}) \equiv \exp(\mathbf{x}(\mathbf{s})' \boldsymbol{\beta})$) and consists of $\mathbf{x}(\mathbf{s})$, a vector of resource (or habitat) characteristics measured at location \mathbf{s} , and a vector of coefficients, $\boldsymbol{\beta}$, that describes how the individual selects resources from those available to it. The spatial domain \mathcal{S} is often defined as the animal’s estimated home range or as some arbitrary geographic region of interest (Johnson 1980, Manly et al. 2002). The availability function is typically assumed to be uniform over \mathcal{S} (i.e., $f(\mathbf{s}) \equiv \text{Unif}(\mathcal{S})$), implying that all points in \mathcal{S} are equally accessible to the animal at all times (Aarts et al. 2008).

The selection function, $g(\mathbf{x}(\mathbf{s}), \boldsymbol{\beta})$, is said to be proportional to the probability of use, but in practice resource selection functions determine whether resource use is proportional to resource availability (Aarts et al. 2012). Use that is disproportionate to availability is often equated with preference (Manly et al. 2002). A positive relationship between resource use and animal fitness assumes individuals are distributed in proportion to resource availability (i.e., the ideal free distribution); however, animal behavior such as territoriality can undermine this assumption (i.e., the ideal despotic distribution; Fretwell and Lucas 1969, Van Horne 1983, Morris 2011). Nonetheless, resource selection analyses are a valuable starting point for more in-depth studies concerning the resources and conditions that are important drivers of fitness, and by extension species distributions and population dynamics.

In practice, animal resource selection is rarely quantified by evaluating the weighted distribution (Eq. 1.1) directly. Rather, a common approach is to augment the telemetry data with “pseudo-absences,” or randomly selected locations within \mathcal{S} , and subsequently analyze the resulting presence/pseudo-absence data using standard statistical methods such as generalized linear or additive models (McCullagh and Nelder 1989, Ruppert et al. 2003).

Alternatively, a Poisson likelihood can be used to model the counts of telemetry locations within discretized units of \mathcal{S} (i.e., grid cells of a rasterized version of \mathcal{S}). Only recently, however, was it shown that these approaches approximate the spatial point process intensity function (Eq. 1.1; Warton and Shepherd 2010, Aarts et al. 2012).

Most resource selection studies assume the telemetry data are measured without error, and thus the telemetry locations are the same as the true animal locations $\boldsymbol{\mu}(t) \equiv (\mu_x(t), \mu_y(t))'$ (i.e., $\mathbf{s}(t) \equiv \boldsymbol{\mu}(t)$, as assumed in Eq. 1.1). In situations where telemetry measurement error is a concern, the spatial point process model and its approximations (the standard statistical methods described in the preceding paragraph) can be extended to account for an imperfect observation process (Brost et al. 2015, Hefley and Hooten 2016). In particular, hierarchical models are useful for estimating (and separating) uncertainty that results from imperfect observations of the true animal locations, as well as uncertainty related to the biological process that generates the true locations themselves. Consider, for example, the generic hierarchical model

$$\mathbf{s}(t) \sim [\mathbf{s}(t) | \boldsymbol{\mu}(t), \boldsymbol{\theta}_s] \quad (1.2)$$

$$\boldsymbol{\mu}(t) \sim [\boldsymbol{\mu}(t) | \boldsymbol{\theta}_\mu], \quad (1.3)$$

where the bracket notation $[\cdot]$ represents some probability distribution, $\boldsymbol{\theta}_s$ is a vector of parameters that describe telemetry measurement error, and $\boldsymbol{\theta}_\mu$ is a vector of parameters related to the biological process. The “observation” model (Eq. 1.2) describes how telemetry locations ($\mathbf{s}(t)$) arise conditional on the true locations ($\boldsymbol{\mu}(t)$), whereas the “process” model (Eq. 1.3) represents a hypothesis about the mechanics of the ecological process that gives rise to the true but unobserved animal locations. For example, the process model could take

the form of a weighted distribution as in Eq. 1.1, or a Poisson likelihood if one wishes to model the counts of locations within raster cells.

The spatial point process model (Eq. 1.1) can also be adapted to account for dependent telemetry locations. Modern telemetry devices are capable of recording locations at a relatively high temporal frequency, and the time elapsed between locations can be quite short. In these circumstances, the extent of potential movements by an animal within \mathcal{S} is limited, and the common assumption that resource availability is uniform over a predetermined region is dubious (Aarts et al. 2008). Using Eq. 1.1, autocorrelated locations can be accommodated by calculating resource availability as a function of the time elapsed between telemetry locations, thereby reflecting a dynamic animal movement process (e.g., Brost et al. 2015); however, such a space-time point process model is more similar to a movement model than it is to the spatial point process models discussed in this section. Autocorrelated telemetry locations limit application of standard statistical methods in a rigorous, model-based manner.

1.4.2 Movement models

Movement models often focus on the *change* in an animal's position (i.e., the difference between consecutive locations) rather than the locations themselves (e.g., Morales et al. 2004, Johnson et al. 2008, McClintock et al. 2012). They consider the dynamics of animal movement from the perspective of the moving animal, and thus define accessibility of points in space as a function of an individual's starting position, speed, travel duration, and mode of movement. Consequently, movement models naturally account for dependence in telemetry data. Movement models typically yield a spatial surface that represents the likelihood of observing an animal given no habitat preference. Inference concerning the affect of habitat

covariates on animal movement is often left to a secondary analysis (e.g., Hooten et al. 2010, Hanks et al. 2015, Hooten et al. 2016; however, see Morales et al. 2004 for an exception).

Movement models can be divided into discrete-time and continuous-time approaches. Regardless of the manner in which time is treated, movement models typically consist of two hierarchical components: a mechanistic model that describes the animal movement process and a statistical model for the observation process (e.g., Eqs. 1.2 and 1.3). Observation models are interchangeable between the two movement modeling frameworks. Therefore, I specifically focus on common discrete-time and continuous-time process models in the descriptions below. In other words, the quantities discussed are a function of the true animal locations $\mu(t)$, not the observed telemetry data $s(t)$.

Discrete-time movement models.—A widely used discrete-time approach to emulating animal movement is the (discrete-time) correlated random walk, an approach that often deconstructs a movement path into a series of step lengths and turning angles (e.g., Morales et al. 2004, McClintock et al. 2012, McClintock et al. 2013). In this framework, step lengths ($r(t)$) are modeled using some non-negative, right-skewed distribution and turning angles ($\phi(t)$) are given a circular, non-uniform distribution. For example, common specifications are

$$r(t) \sim \text{Weibull}(a(t), b(t)) \quad (1.4)$$

$$\phi(t) \sim \text{wCauchy}(\lambda(t), \rho(t)), \quad (1.5)$$

although other distributions can also be used (Morales et al. 2004, McClintock et al. 2012, McClintock et al. 2013). Correlated movements are captured by turning angles that are concentrated near zero degrees, thus inducing short-term persistence in movement direction (Turchin 1998). Under this modeling framework (Eqs. 1.4 and 1.5), the polar dimensions

of discretized movements are independent; therefore, the model does not account for any relationship between step lengths and turning angles. Alternatively, the “first-difference” discrete-time correlated random walk model of Jonsen et al. (2005) is specified on the velocities, thereby inducing dependence between the speed and direction of movements (e.g., long steps are possible when turning angles are small).

Discrete-time approaches to modeling animal trajectories are highly flexible and have been adapted to accommodate various aspects of animal behavior. For example, mixtures consisting of > 1 discrete-time random walks have been developed to accommodate multiple movement modes associated with latent behavioral states (Morales et al. 2004, Jonsen et al. 2005, McClintock et al. 2012, McClintock et al. 2013). Furthermore, long-term directional persistence has also been incorporated into discrete-time models to allow for movements associated with a specific location in geographic space (e.g., a center of attraction; McClintock et al. 2012). The primary limitation of discrete-time movement models is that they are predicated on observations recorded at regular intervals; however, telemetry data are usually recorded irregularly through time. Thus, discrete-time movement model implementation requires “corrections” to translate the observed data to a regular interval timeline (e.g., interpolation) that matches the desired scale of inference (McClintock et al. 2012).

Continuous-time movement models.—Continuous-time models are appealing because they consider movement more realistically as a process that occurs continuously through time. The inference obtained from a continuous-time model is also not dependent on any particular timescale (as in discrete-time movement models; McClintock et al. 2014). Moreover, modeling animal movement as a continuous stochastic process is a natural way to account

for any relationship (i.e., correlation) between step lengths and turning angles (McClintock et al. 2014).

A common continuous-time movement model is the correlated random walk of Johnson et al. (2008), a continuous time analog of the discrete-time movement model proposed by Jonsen et al. (2005). This model accounts for dependence between locations, as well as a tendency to drift toward a central location, using a stochastic process model known as the Ornstein-Uhlenbeck process. For each separation in time Δ_t , the model is defined by an autoregressive specification for velocity, $\mathbf{v}(t) \equiv (v_x(t), v_y(t))'$, such that

$$v_c(t + \Delta_t) = \gamma_c + \exp(-\beta\Delta_t) \times (v_c(t) - \gamma_c) + \varsigma_c(\Delta_t), \quad (1.6)$$

where $c \in \{x, y\}$, γ_c is the mean velocity, β is an autocorrelation parameter, and $\varsigma_c(\Delta_t)$ is a normal random variable with mean zero and variance $\sigma^2(1 - \exp(-2\beta\Delta_t)) / -2\beta$. The parameter σ^2 controls the overall variability in velocity. Accordingly, the velocity $v_c(t + \Delta_t)$ is a combination of the previous velocity weighted by its difference from the mean velocity, plus a random variable with variance that increases with Δ_t . The animal's position for any time t is subsequently obtained by integrating over the velocities

$$\boldsymbol{\mu}(t) = \boldsymbol{\mu}(0) + \int_0^t \mathbf{v}(u) du, \quad (1.7)$$

where $\boldsymbol{\mu}(0)$ is the initial location. As β approaches ∞ (Eq. 1.6), the location process becomes standard Brownian motion, a continuous-time random walk. Although Brownian motion is another common approach to modeling animal movement (e.g., Hooten and Johnson, in press), its use is motivated by mathematical convenience and ease of implementation rather than its ability to accurately depict animal trajectories.

1.5 OBJECTIVES AND DISSERTATION STRUCTURE

Despite the rapidly increasing number of studies concerning animal resource selection and movement, our ability to analyze telemetry data has not kept pace with our ability to collect individual movement data. Even though recent extensions to models for analyzing animal telemetry data address complications such as autocorrelation and telemetry measurement error, additional challenges remain. This is especially true in the context of analyzing Argos satellite telemetry data collected on marine mammals like harbor seals. For example, existing methods assume elliptical (or circular) patterns of measurement error, even though Argos satellite telemetry devices impose more complicated error structures on the data. Constraints, or barriers, to animal movement present another complication. Harbor seals and other marine mammals are constrained to move within the marine environment, and mechanistic models that do not adhere to movement barriers yield unreliable inference. Therefore, a primary goal of this dissertation is to develop statistical tools that account for these nuances and provide rigorous, ecologically relevant inference. Even though the models presented in this dissertation were specifically developed with Argos satellite telemetry data and harbor seals in mind, the methods are general and can be applied to other species and types of telemetry data. This dissertation consists of three core chapters.

In Chapter 2, I propose an approach for obtaining resource selection inference from animal location data that accounts for complicated error structures, movement constraints, and temporally autocorrelated observations. The model consists of two general components: a model for the true, but unobserved, animal locations that reflects prior knowledge about constraints to animal movement, and a model for the observed telemetry locations that is conditional on the true locations. I apply the model to simulated data, showing that it

outperforms common *ad hoc* approaches used when confronted with telemetry measurement error and movement constraints. I then apply the framework to obtain inference concerning aquatic resource selection and space use for harbor seals near Kodiak Island, Alaska.

Chapters 3 and 4 shift the focus from inference concerning aquatic space use and resource selection, to inference concerning the use of coastal resources (i.e., haul-out sites) by harbor seals. In Chapter 3, I present a fully model-based approach for estimating the location of central places (e.g., haul-out sites, dens, nests, etc.) from telemetry data that accounts for multiple sources of uncertainty and uses all of the available locational data. The model consists of an observation model to account for large telemetry measurement error and animal movement, and a highly flexible mixture model (a Dirichlet process) to identify the location of central places. Ancillary behavioral data (e.g., harbor seal dive data obtained from the satellite-linked depth recorders) are also incorporated into the modeling framework to obtain inference concerning temporal patterns in central place use. Based on the methods developed in Chapter 3, I present a comprehensive analysis of the spatio-temporal patterns of haul-out use for harbor seals near Kodiak Island in Chapter 4. This chapter also extends previously developed methods to examine the affect of covariates on haul-out site selection and to obtain population-level inference concerning haul-out use.

I conclude in Chapter 5 with some general thoughts about analyzing animal telemetry data, as well as potential future research directions. Although each core chapter includes a harbor seal application, this work is primarily methodological. I described the methods in a manner approachable to ecologists with a background in hierarchical modeling, and I included additional resources to help others with model implementation. For example, each chapter includes appendices containing the full model specifications, derivations of the full-conditional distributions, pseudo-code for the Markov chain Monte Carlo algorithms used

for parameter estimation, and annotated R code for model fitting. The statistical rigor, applications, and algorithms presented here may be useful for others to extend my work and tackle a wide variety of problems in animal movement ecology.

CHAPTER TWO

Animal Movement Constraints Improve Resource Selection Inference in the Presence of Telemetry Error¹

Summary. Multiple factors complicate the analysis of animal telemetry location data. Recent advancements address issues such as temporal autocorrelation and telemetry measurement error, but additional challenges remain. Difficulties introduced by complicated error structures or barriers to animal movement can weaken inference. We propose an approach for obtaining resource selection inference from animal location data that accounts for complicated error structures, movement constraints, and temporally autocorrelated observations. We specify a model for telemetry data observed with error conditional on unobserved true locations that reflects prior knowledge about constraints in the animal movement process. The observed telemetry data are modeled using a flexible distribution that accommodates extreme errors and complicated error structures. Although constraints to movement are often viewed as a nuisance, we use constraints to simultaneously estimate and account for telemetry error. We apply the model to simulated data, showing that it outperforms common *ad hoc* approaches used when confronted with measurement error and movement constraints. We then apply our framework to an Argos satellite telemetry data set on harbor seals (*Phoca vitulina*) in the Gulf of Alaska, a species that is constrained to move within the marine environment and adjacent coastlines.

¹The material in Chapter 2 is based on the following publication: Brost, B. M., M. B. Hooten, E. M. Hanks, and R. J. Small. 2015. Animal movement constraints improve resource selection inference in the presence of telemetry error. *Ecology* 96:2590–2597. Thank you to my coauthors, George Wittemyer, and to several anonymous reviewers for comments that improved this manuscript.

2.1 INTRODUCTION

Conservation and management of animal populations requires knowledge of factors affecting their abundance and distribution. The locations of animals, coupled with information about associated environmental characteristics, can be used to quantify species-habitat relationships. This has stimulated the widespread use of telemetry devices to collect animal location data (hereafter telemetry data), which are often analyzed in a resource selection framework (Manly et al. 2002). The goal of such analyses is to quantify the probability of resource (or habitat) use conditional on resource availability (i.e., selection). Use that is disproportionate to availability is often equated with preference (Manly et al. 2002).

Multiple factors complicate the application of resource selection methodology. Modern satellite telemetry devices, for example, can collect multiple locations per day. Although such data increase the prospects for obtaining inference about animal behavior, they often violate the usual independence assumption of basic statistical analyses (Aarts et al. 2008, Fieberg et al. 2010). Telemetry measurement error poses another challenge. Measurement errors, or deviations between recorded telemetry locations and true animal locations, can interact with environmental heterogeneity to bias inferences on species-habitat relationships (Visscher 2006, Johnson and Gillingham 2008, Hefley et al. 2014).

Recent extensions to models for analyzing animal telemetry data address temporal autocorrelation and measurement error. Johnson et al. (2008b), for example, modeled temporally autocorrelated location data using a weighted distribution that combines a resource selection function with a movement model. Morales et al. (2004), Hooten et al. (2010), and Hanks et al. (2011) provide alternatives to the weighted distribution approach that also account for temporally dependent data. So-called “state-space” movement models further account for

telemetry measurement error by coupling a statistical model for the telemetry observation process with a model that describes the true, but unobserved, movement process (Patterson et al. 2008). In principle, state-space movement models can be used to directly quantify species-habitat relationships (McClintock et al. 2012); however, they are typically used only to estimate true animal paths and infer behavioral states.

The contemporary methods highlighted above are important developments for the analysis of telemetry location data; however, additional challenges remain. For example, existing models assume elliptical (or circular) patterns of measurement error, even though some remote sensing devices impose more complicated error structures on the data. Constraints, or barriers, to animal movement present another complication. Constraints modify the spatial support of the animal movement process by limiting where an individual or species exists, and may interact with measurement error to yield telemetry locations that occur in areas not accessible by the telemetered individual (e.g., Fig. 2.1a). Though spatial constraints have been incorporated into animal movement models (e.g., Sumner et al. 2009, McClintock et al. 2012), they have not been used to quantify resource selection.

We propose an approach for obtaining inference concerning resource selection from animal location data that accounts for complicated error structures, constraints to animal movement, and temporally autocorrelated observations. To our knowledge, these objectives have not been addressed previously in a unified framework. We specify a model for observed telemetry data conditional on true but unknown locations that reflects prior knowledge about constraints on the animal movement process. Though constraints to animal movement are typically viewed as a nuisance, our approach uses constraints to simultaneously estimate and account for telemetry error. We first apply the model to a simulated data set and compare it to common *ad hoc* approaches used when confronted with constraints to animal movement.

We also illustrate our framework by analyzing an Argos satellite telemetry data set on harbor seals (*Phoca vitulina*) in the Gulf of Alaska, a species that is constrained to move within the marine environment and adjacent coastlines.

2.2 TELEMETRY LOCATION DATA

The model we propose is general and can be applied to various combinations of telemetry data types (e.g., VHF, GPS, or geolocation telemetry); however, our focus here is on Argos telemetry data. Argos satellite telemetry is a popular platform for collecting animal location data because it is cost effective, and because all location estimates are conveniently delivered to the end user electronically, making tag recovery unnecessary. Argos satellite telemetry has also seen extensive use for more than two decades, resulting in massive historical data sets that are ripe for reanalysis using state-of-the-art methodology (Movebank.org currently contains > 250 Argos telemetry data sets).

Our model application specifically focuses on telemetry locations like those in our harbor seal data set, which were calculated via the Argos least squares positioning algorithm (Service Argos 2015). These location data require special treatment because they exhibit an x-shaped error distribution that has greatest error variance along the NW-SE and NE-SW axes, a consequence of the polar orbiting Argos satellites and error that is largest in the direction perpendicular to the orbit (Costa et al. 2010, Douglas et al. 2012). Analysis of these data is further complicated by the fact that valid Argos telemetry locations are assigned one of six location classes, each exhibiting different error patterns and magnitudes. In order of decreasing accuracy, the location classes are 3, 2, 1, 0, A, and B.

2.3 MODEL FORMULATION

Suppose individuals in a population of animals are constrained to move within \mathcal{S} , the spatial support of the movement process. Let $\mathbf{s}_t \equiv (s_{1,t}, s_{2,t})'$ be the pair of coordinates for an observed telemetry location on a single individual at time t , and $\boldsymbol{\mu}_t \equiv (\mu_{1,t}, \mu_{2,t})'$ be the pair of coordinates for the corresponding latent (i.e., unobserved) true location. Although $\boldsymbol{\mu}_t$ is restricted to be within \mathcal{S} , this is not true for the observed telemetry location which can fall outside of \mathcal{S} due to measurement error (Fig. 2.1a).

2.3.1 Observation model

An appropriate observation model must describe how telemetry locations arise conditional on true locations. We allow for various telemetry error structures using

$$\mathbf{s}_t \sim \begin{cases} t_\nu(\boldsymbol{\mu}_t, \boldsymbol{\Sigma}), & \text{with prob. } p_t \\ t_\nu(\boldsymbol{\mu}_t, \tilde{\boldsymbol{\Sigma}}), & \text{with prob. } 1 - p_t \end{cases}. \quad (2.1)$$

In this expression, the observed telemetry locations \mathbf{s}_t arise from a mixture of multivariate t distributions with mean $\boldsymbol{\mu}_t$ (the true location), scale matrices $\boldsymbol{\Sigma}$ and $\tilde{\boldsymbol{\Sigma}}$, and ‘degrees of freedom’ ν . The parameters $\boldsymbol{\Sigma}$, $\tilde{\boldsymbol{\Sigma}}$, and ν describe error in the telemetry measurement process. The degrees of freedom parameter ν specifically adjusts the heaviness of the tails in the t distribution, thereby accommodating extreme errors commonly seen in telemetry data (Jonsen et al. 2005, Hoenner et al. 2012). Note that the t distribution approximates a Gaussian distribution for $\nu \geq 30$. The scale matrix $\boldsymbol{\Sigma}$ is parametrized in a flexible manner:

$$\boldsymbol{\Sigma} = \sigma^2 \begin{bmatrix} 1 & \rho\sqrt{a} \\ \rho\sqrt{a} & a \end{bmatrix}, \quad (2.2)$$

where σ^2 quantifies scale in the longitude direction, a modifies σ^2 to describe scale in the latitude direction, and ρ describes the correlation between variation in the two directions. The scale matrix $\tilde{\Sigma}$ is identical to Σ except for the off-diagonal elements which are multiplied by -1 ; thus, the off-diagonals of $\tilde{\Sigma}$ are $-\rho\sqrt{a}$.

When $\rho = 0$, Eq. 2.1 collapses to a single multivariate t distribution that is appropriate for circular ($a = 1$) and elliptical error distributions ($a \neq 1$). Alternatively, $\rho \neq 0$ results in two distributions that are reflected across the vertical axis. Consequently, when $\rho \neq 0$, Eq. 2.1 specifies a mixture distribution that decomposes potentially complicated error structures like the x-shaped pattern evident in Argos telemetry data into two simpler forms, with one mixture component for errors along the NE-SW axis (described by Σ) and another for errors along the SE-NW axis (described by $\tilde{\Sigma}$). We define $p_t = 0.5$ because the orbital plane of Argos satellites changes continuously; therefore, observations are equally likely to come from either mixture component.

The parameters relating to measurement error (i.e., σ^2 , ρ , a , and ν) can be estimated independently for different error classes (e.g., Argos location quality classes) or adapted to accommodate a continuous metric of location quality (e.g., GPS dilution of precision). Since 2011, Argos has also provided error ellipses associated with locations processed via a Kalman filtering algorithm. Error ellipses better characterize the magnitude and orientation of errors than location classes, and can be used to inform observation model parameters (e.g., McClintock et al. 2014).

2.3.2 Process model

Animal locations are naturally viewed as a realization of a point process that has a spatially heterogeneous intensity function (Aarts et al. 2012, Johnson et al. 2013). The

intensity function summarizes the ecological processes that give rise to animal locations, and thus provides inference for species-habitat relationships. A weighted distribution is often used to model this intensity function (Lele and Keim 2006, Aarts et al. 2012), which is the approach we adopt as a model for the true locations:

$$\boldsymbol{\mu}_t \sim \frac{\exp \left\{ \mathbf{x}'(\boldsymbol{\mu}_t) \boldsymbol{\beta} - \eta(\boldsymbol{\mu}_t, \boldsymbol{\mu}_{t-\Delta_t}) \right\}}{\int_{\mathcal{S}} \exp \left\{ \mathbf{x}'(\boldsymbol{\mu}) \boldsymbol{\beta} - \eta(\boldsymbol{\mu}, \boldsymbol{\mu}_{t-\Delta_t}) \right\} d\boldsymbol{\mu}}. \quad (2.3)$$

In Eq. 2.3, $\mathbf{x}(\boldsymbol{\mu}_t)$ is a vector of spatially-referenced resource or habitat covariates at location $\boldsymbol{\mu}_t$, $\boldsymbol{\beta}$ is a vector of resource selection coefficients, and $\eta(\boldsymbol{\mu}_t, \boldsymbol{\mu}_{t-\Delta_t})$ is a spatially-explicit movement kernel centered at $\boldsymbol{\mu}_{t-\Delta_t}$, the previous true location (Δ_t denotes the time elapsed between $\boldsymbol{\mu}_t$ and the previous true location). We approximate the integral in the denominator of Eq. 2.3 by numerical quadrature (Dorazio 2012). The kernel $\eta(\boldsymbol{\mu}_t, \boldsymbol{\mu}_{t-\Delta_t})$ governs the distribution of available habitat and accounts for temporal autocorrelation among locations.

The movement kernel is modeled as

$$\eta(\boldsymbol{\mu}_t, \boldsymbol{\mu}_{t-\Delta_t}) = \frac{d(\boldsymbol{\mu}_t, \boldsymbol{\mu}_{t-\Delta_t})}{\Delta_t \phi}, \quad (2.4)$$

where $d(\boldsymbol{\mu}_t, \boldsymbol{\mu}_{t-\Delta_t})$ is the distance between $\boldsymbol{\mu}_t$ and $\boldsymbol{\mu}_{t-\Delta_t}$, and ϕ is a scaling parameter. Importantly, $d(\cdot, \cdot)$ must adhere to animal movement constraints and is thus measured exclusively through the domain defined by \mathcal{S} . In the case of marine mammals like harbor seals, $d(\cdot, \cdot)$ represents the distance through water (i.e., the swim distance). In practice, we calculate $d(\cdot, \cdot)$ using least-cost distance (Dijkstra 1959). Given that Eq. 2.4 takes the form of an exponential kernel, the range of correlation between consecutive locations can be inferred by noting that $\eta(\boldsymbol{\mu}_t, \boldsymbol{\mu}_{t-\Delta_t}) \approx 0$ when $d(\boldsymbol{\mu}_t, \boldsymbol{\mu}_{t-\Delta_t})/\Delta_t > 3\phi$.

2.3.3 Prior distributions

To complete the Bayesian formulation of this model, we specify prior distributions for the unknown parameters. We assume $\sigma \sim \text{Uniform}(0, u)$ with similar uniform priors for ρ , a , ν , and ϕ , and $\beta \sim N(\mathbf{0}, \tau^2 \mathbf{I})$. See Appendix A1 for the full model specification and Appendix A2 for details regarding model implementation.

2.4 MODEL APPLICATION

2.4.1 Model evaluation using simulated data

An example realization from the model described above is shown in Fig. 2.1a. All parameters in the simulation were chosen to be similar to those estimated in an analysis of harbor seal telemetry data (see *Case study* below). To simplify presentation of results, telemetry measurement error corresponded to high, medium, and low accuracy Argos locations (i.e., location classes 3, 0, and B, respectively).

We fit the model using a Markov chain Monte Carlo (MCMC) algorithm written in R (provided in the Supplement; R Core Team 2013) to 250 data sets simulated using the process described above, each containing 1,000 locations randomly allocated to the three error classes. Inference was based on 2,000 MCMC samples after convergence. An example of posterior inference for the true locations μ_t is shown in Fig. 2.1b.

We compare inference for μ_t and β from our model to three *ad hoc* alternatives commonly used when confronted with telemetry measurement error and constraints to animal movement. These alternative approaches approximate μ_t by (1) “snapping” observed telemetry locations to the nearest location in \mathcal{S} ; (2) excluding from analysis all observed locations not in \mathcal{S} ; or (3) using a speed filter (Frietas et al. 2008) to first remove particularly aberrant

observations, then eliminating remaining observations that are not in \mathcal{S} . A spatial point process model is then used for resource selection inference (Aarts et al. 2012). Specifically, we modeled the counts of μ_t per spatial unit (e.g., raster grid cell) using a Poisson generalized linear model. We make one additional comparison with a model wherein Eq. 2.1 is updated to be a normal distribution with $\rho = 0$. This modification mimics the simpler observation models commonly used in other approaches (e.g., Jonsen et al. 2003, Johnson et al. 2008a, Sumner et al. 2009) and provides a benchmark for assessing the performance of a mixture model that accommodates complicated error distributions.

Inference pertaining to the latent state variable μ_t and resource selection coefficients β from the approaches described above are summarized in Table 2.1. Our model retains all telemetry locations to estimate μ_t with greater accuracy than the alternative approaches, and particularly excels for the lower quality error classes that often dominate animal telemetry data sets (Douglas et al. 2012). Censoring observations (approaches 2 and 3) eliminated $> 66\%$ of the observed locations; data loss was particularly severe for the lower quality error classes. Estimates of β were overly confident when μ_t was approximated by filtering, snapping telemetry locations to \mathcal{S} , or excluding observations not in \mathcal{S} (Table 2.1). For example, interval coverage for one of the resource selection coefficients was 0% for all of these approaches. Coverage of intervals for the mixture t model was comparable to coverage attained when Eq. 2.1 was updated to a bivariate normal observation model. Both provided nominal coverage for β , as well as estimates of β that were the least biased among all approaches (Table 2.1). Estimates of other parameters in our model were satisfactory and are described in detail in Appendix A3.

2.4.2 Case study: harbor seals

To demonstrate our approach with real data, we apply our model to telemetry locations of an adult female harbor seal monitored near Kodiak Island, Alaska during 1995 and 1996 (Fig. 2.2). Telemetry locations were collected on average every 4.3 hours (range: 0.02, 131.9 hours) using an Argos satellite telemetry device. The animal's position was measured on 1,457 occasions, with $\approx 80\%$ of locations coming from the three least accurate Argos location classes (i.e., large measurement error). We used a 250-m resolution raster of the marine environment to define \mathcal{S} , the extent of which was limited to 60 km (measured through the water) from the haul-out location. Defining \mathcal{S} in this way should capture all potential μ_t because harbor seals typically stay within 30 km of their haul-outs (Lowry et al. 2001, Small et al. 2005), and nothing suggests this individual exhibited longer distance movements. For illustration purposes, we focused on selection inference pertaining to distance to haul-out site and bathymetry. Both covariates were represented as 250-m resolution rasters and were only marginally correlated ($r = 0.14$).

Point estimates for μ_t (posterior mode) were 4.2 km from the haul-out site, on average, and 95% of the posterior probability for μ_t was within 13.0 km of the haul-out site in water 55-m deep or less (Fig. 2.2). Resource selection coefficients for distance to haul-out and bathymetry were estimated as $\beta_1 = -2.03$ (95% CI: $-2.45, -1.62$) and $\beta_2 = -0.82$ (95% CI: $-1.12, -0.53$), respectively, indicating that habitat far from the haul-out site and deeper water were selected against. These results are consistent with other findings that harbor seals generally use shallower water near their haul-out sites (Lowry et al. 2001, Small et al. 2005). Estimates for ν were less than 30 for all Argos error classes, supporting our use of the t distribution to ensure extreme observations do not exert undue influence on inferences.

Estimates for all parameters are provided in Appendix A4 and we illustrate the flexibility of our observation model in Appendix A5. All inference was based on 100,000 MCMC samples, which required 55 hours of processing time on a computer equipped with a 3.0 GHz Intel Xeon processor.

2.5 DISCUSSION

Our model for resource selection inference addresses several complicating factors in the analysis of animal telemetry data. Our model accounts for telemetry measurement error and temporally autocorrelated observations, and, unlike other approaches, it also accommodates complicated error structures and constraints to animal movement. In fact, we show that constraints to movement are helpful in estimating and accounting for measurement error.

Our model consists of two general components, one “process” model for the true animal locations and another for the observed telemetry locations that is conditional on the true locations (the “observation” model). These components are implemented in a unified framework such that uncertainty naturally propagates through the model, thereby properly accounting for uncertainty in parameter estimates. This unification further allows resource or habitat covariates to improve estimation of μ_t . Methods that are implemented in two stages, where the true locations are first estimated and then used in a secondary analysis to quantify resource selection, do not allow uncertainty in the first stage to propagate through the second stage unless a bootstrapping or multiple imputation procedure is used (e.g., Hanks et al. 2011). The *ad hoc* alternatives presented in our simulation study bear this shortcoming, as do state-space movement models which are often applied in a two-step fashion. Our framework also allows for generalizations such as the joint analysis of multi-

ple individuals using random effects for β and ϕ , which could themselves be functions of auxiliary demographic information such as gender or age.

Methods that account for sampling artifacts improve ecological inference. Ignoring telemetry measurement errors, or hiding them in a pre-processing stage, yields inaccurate estimates of true animal locations and inference for resource selection coefficients that is biased and overly confident (Table 2.1). Censoring poor quality locations leads to substantial data loss, particularly when dealing with wildlife data sets that often largely consist of low-quality observations (Douglas et al. 2012). Given the x-shaped error pattern in Argos telemetry data, true animal locations are more likely to occur on a diagonal from the observed location, rather than, for example, due north of the observed location. Our observation model incorporates this nuance and estimates μ_t with greater accuracy than one that assumes simpler, elliptical error structures (Table 2.1). However, both approaches account for uncertainty in μ_t and thus provided comparable inference for β .

Animal behavior, such as increased milling by harbor seals near haul-out sites, can bias times at which satellite telemetry locations are acquired and may therefore affect resource selection inference (Frair et al. 2010). The telemetry device used in our case study was programmed to suspend transmissions after 6 hours during haul-out bouts, mitigating this concern. Alternatively, predicting μ_t at a fixed time interval may account for bias (e.g., McClintock et al. 2012, 2013), although this general technique appears to be untested. Nonetheless, augmenting our model to obtain predictions for unobserved μ_t at any time or sequence of times is straightforward; however, methods that are conceptually based on locations collected at regular time intervals may not be applicable when data are as intermittent as those in our harbor seal data set (Breed et al. 2011, Silva et al 2014). Methods for

point process data collected under preferential sampling present another promising option for modeling temporally biased telemetry locations (Diggle et al. 2010).

2.5.1 Constraints in space and time

Many animals such as African elephants, European bison, Asiatic wild asses, and Mongolian gazelles encounter fences, railroads, roads, and other barriers that prevent free-ranging movements (Loarie et al. 2009, Kowalczyk et al. 2012, Ito et al. 2013). Our model could easily be extended to accurately estimate the locations of these species in their spatially constrained environments. Features that restrict but do not preclude movement, such as proximity to water, a nest site, or escape terrain, also represent constraints. These “soft” constraints can be modeled in much the same way as we modeled attraction to a haul-out site for harbor seals (i.e., as a component of the resource selection function).

Methods that account for measurement error, like state-space movement models, often require an *a priori* understanding of error patterns, usually obtained from published studies (Jonsen et al. 2003, Jonsen et al. 2005, Johnson et al. 2008a). Unfortunately, observed error patterns can differ in unpredictable ways due to differences in animal behavior, habitat obstructions, environmental conditions, and geographic locations (Cargnelutti et al. 2007, Lewis et al. 2007, Douglas et al. 2012). Consequently, no single description of measurement error may be universally applicable to a tracking technology. Constraints to movement, and the subsequent discrepancy between the spatial support of μ_t and s_t , allow our model to estimate species- and system-specific telemetry measurement error without the expense of collecting additional data (e.g., Costa et al. 2010 and Douglas et al. 2012, who used two telemetry technologies to simultaneously collect locations on free-ranging animals). As such, we view constraints as an aid in the modeling and estimation process.

A second constraint, namely a mechanistic temporal movement constraint (Eq. 2.4), also operates in our model. This movement kernel expands and contracts inversely with Δ_t , thereby accounting for temporal autocorrelation between consecutive locations (Aarts et al. 2008, Johnson et al. 2008b, Forester et al. 2009, Hooten et al. 2014). The kernel also defines the distribution of resources available to the individual, which is data-driven as it is governed by the estimated scale parameter ϕ and the previous location $\mu_{t-\Delta t}$. The process model (Eq. 2.3) balances the effect of $\eta(\mu_t, \mu_{t-\Delta t})$ with that of the resource selection function; both are modified by the spatial constraint when $\mu_{t-\Delta t}$ is near the boundary of \mathcal{S} .

2.5.2 Guidance

Methods that accommodate barriers to movement are important for obtaining reliable inference on animals living in highly constrained environments; however, such methods are computationally expensive compared to alternatives that do not incorporate movement constraints (e.g., Johnson et al. 2008a). Future work comparing approaches, as well as varying degrees of constrained movements, will help provide additional guidance. We encourage researchers to model the mechanisms affecting their measurements. Other ecological models have emphasized the observation process with much success (e.g., models for occupancy and capture-recapture abundance estimation). Analyses of telemetry data merit the same attention.

TABLE 2.1. Performance of five methods for estimating μ_t based on 250 simulations of 1,000 telemetry locations each. The notation $E(\cdot)$ denotes the expectation, or mean value over the simulations. Specifically, $E(n)$ is the expected sample size and $E[d(\hat{\mu}_t, \mu_t)]$ is the expected distance in meters between $\hat{\mu}_t$ (the estimated location) and μ_t as measured through the domain defined by \mathcal{S} . For the mixture t and normal models, $\hat{\mu}_t$ was calculated as $\text{Mode}(\boldsymbol{\mu}|\mathbf{s})$. The expected distance $E[d(\hat{\mu}_t, \mu_t)]$ for all locations combined was weighted to account for varying sample sizes in the “Exclude $\mathbf{s}_t \notin \mathcal{S}$ ” and “Speed filter” methods.

Estimation method	All locations		High accuracy locations		Medium accuracy locations		Low accuracy locations	
	E(n)	$E[d(\hat{\mu}_t, \mu_t)]$	E(n)	$E[d(\hat{\mu}_t, \mu_t)]$	E(n)	$E[d(\hat{\mu}_t, \mu_t)]$	E(n)	$E[d(\hat{\mu}_t, \mu_t)]$
Mixture t model	1000	2178	333	1811	334	2208	333	2513
Snap \mathbf{s}_t to \mathcal{S}	1000	10890	333	3173	334	6108	333	23393
Exclude $\mathbf{s}_t \notin \mathcal{S}$	326	9867	160	2715	125	4416	40	22472
Speed filter	211	4971	117	2460	83	3116	11	9357
Normal model	1000	2615	333	2162	334	2778	333	2905

Notes: High, medium, and low accuracy observed locations were simulated to be consistent with Argos location classes 3, 0, and B, respectively.

TABLE 2.2. Performance of five methods for estimating β based on 250 simulations of 1,000 telemetry locations each.

Estimation method	Distance to haul-out (β_1)				Bathymetry (β_2)	
	Relative		Relative		Coverage	Coverage
	bias	Coverage	bias	Coverage		
Mixture t model	0.01	0.96	0.01	0.90		
Snap \mathbf{s}_t to \mathcal{S}	-0.33	0.00	0.02	0.83		
Exclude $\mathbf{s}_t \notin \mathcal{S}$	-0.05	0.63	-0.94	0.00		
Speed filter	0.28	0.10	-0.92	0.00		
Normal model	0.02	0.92	0.02	0.85		

Notes: Relative bias in estimating β was calculated as $(E(\beta) - \beta)/\beta$ and “Coverage” is the percentage of 95% intervals that contained the true β .

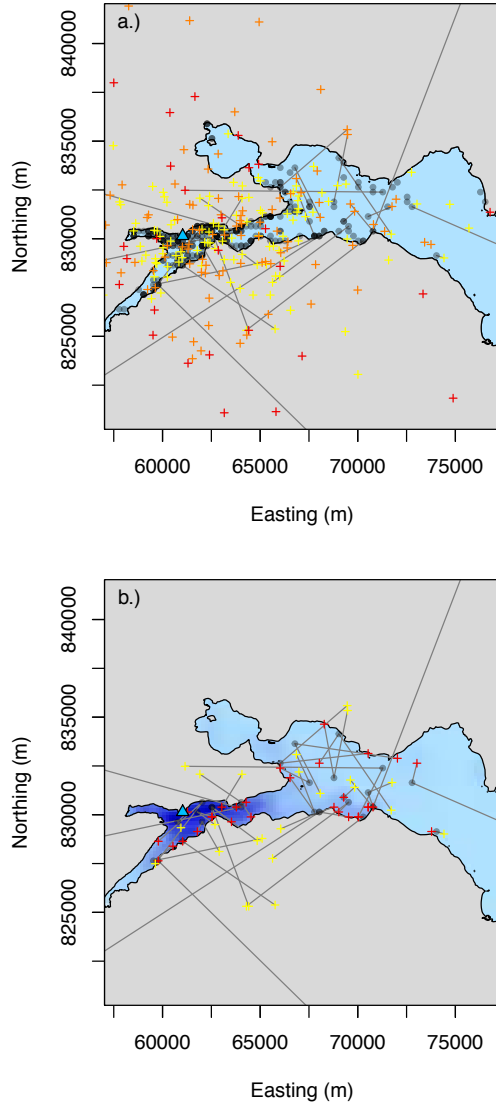


FIGURE 2.1. Simulation of 300 true animal locations (μ_t , black circles) according to the process model (Eq. 2.3) using two resource selection covariates, namely distance to a point of attraction (e.g., a haul-out site; blue triangle) and bathymetry. The blue polygon represents \mathcal{S} , the spatial support of the movement process within which all μ_t occur. (a) Observed telemetry locations (s_t ; crosses) were simulated according to the observation model (Eq. 2.1) with three levels of telemetry measurement error corresponding to high (yellow), medium (orange), and low (red) accuracy Argos locations (i.e., Argos location classes 3, 0, and B, respectively). The lines connect a subset of observed locations with their corresponding true location. (b) The posterior distribution of μ_t (blue to purple color gradient in \mathcal{S} ; darker colors represent higher posterior probability). Lines connect a subset of true animal locations (black circles) with their corresponding observed locations (yellow crosses) and posterior modes (red crosses).

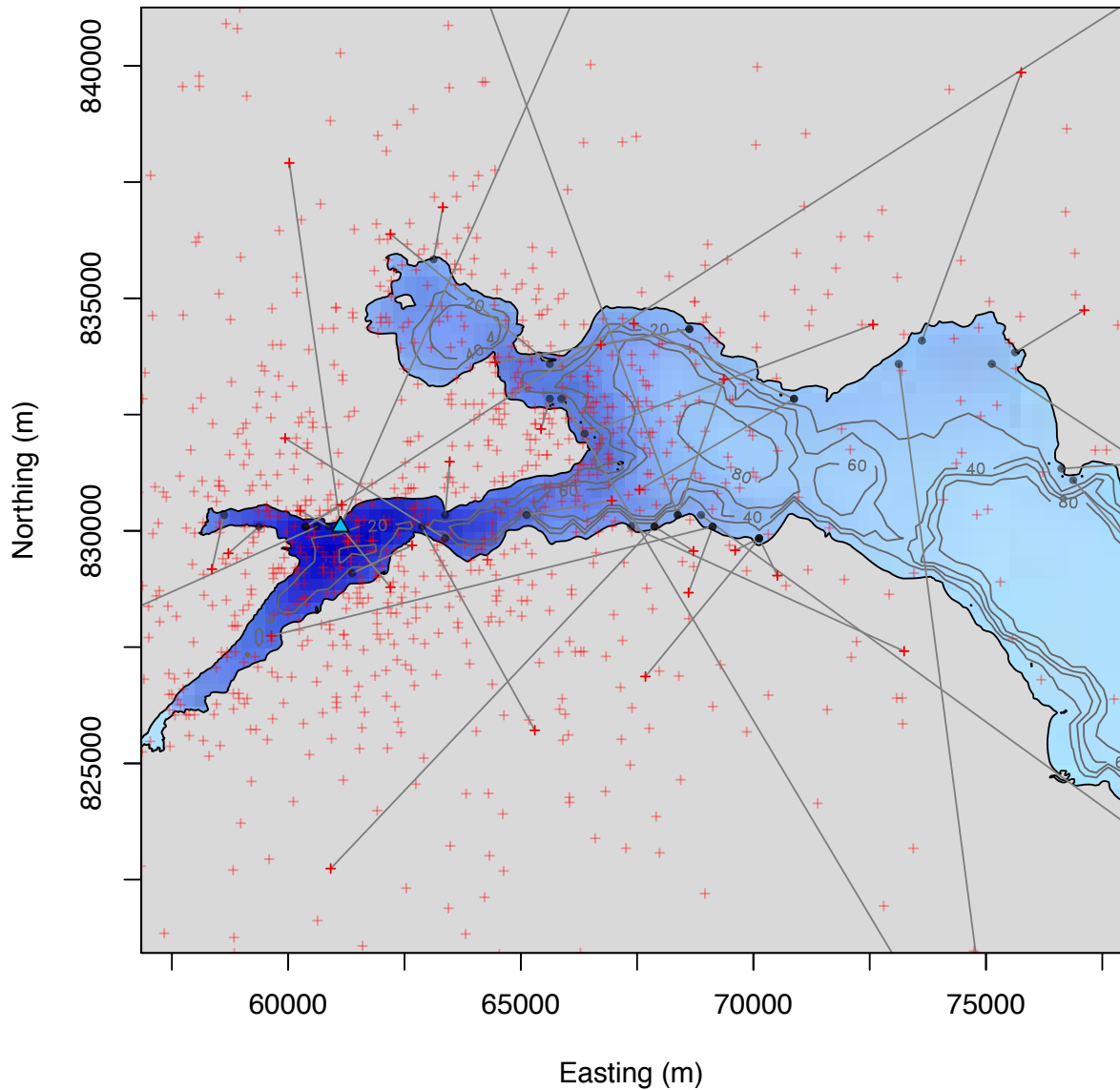


FIGURE 2.2. Argos satellite telemetry locations (red crosses) of an adult female harbor seal monitored from 09 OCT 1995 to 04 JUN 1996 along the southern coast of Kodiak Island, Alaska, USA. The blue polygon represents \mathcal{S} , the spatial support of the movement process; for seals, this is the marine environment and adjacent coastlines. Our analysis focused on resource selection inference pertaining to distance to haul-out site (blue triangle) and bathymetry (gray contour lines). The posterior distribution of μ_t is represented by the blue to purple color gradient in \mathcal{S} ; darker colors indicate higher posterior probability. Lines connect a subset of observed locations with their corresponding posterior modes (black circles). Water depth contours are labeled in meters.

CHAPTER THREE

Leveraging Constraints and Biotelemetry Data to Pinpoint Repetitively Used Spatial Features²

Summary. Satellite telemetry devices collect valuable information concerning the sites visited by animals, including the location of central places like dens, nests, rookeries, or haul-outs. Existing methods for estimating the location of central places from telemetry data require user-specified thresholds and ignore common nuances like measurement error. We present a fully model-based approach for locating central places from telemetry data that accounts for multiple sources of uncertainty and uses all of the available locational data. Our general framework consists of an observation model to account for large telemetry measurement error and animal movement, and a highly flexible mixture model specified using a Dirichlet process to identify the location of central places. We also quantify temporal patterns in central place use by incorporating ancillary behavioral data into the model; however, our framework is also suitable when no such behavioral data exist. We apply the model to a simulated data set as proof of concept. We then illustrate our framework by analyzing an Argos satellite telemetry data set on harbor seals (*Phoca vitulina*) in the Gulf of Alaska, a species that exhibits fidelity to terrestrial haul-out sites.

²The material in Chapter 3 is based on the following publication: Brost, B. M., M. B. Hooten, and R. J. Small. *In press*. Leveraging constraints and biotelemetry data to pinpoint repetitively used spatial features. Ecology. Thank you to my coauthors, as well as to several anonymous reviewers, for comments that improved this manuscript.

3.1 INTRODUCTION

Many animal species return regularly to one or more central places like a den, nest, roost, or foraging site. Central places can be located by sighting individuals during aerial (Montgomery et al. 2007) or ground-based surveys (Blakesley et al. 1992), or by using radio-telemetry equipment to locate individuals in the field (Holloran and Anderson 2005); however, direct observation may only provide a snapshot of the animal's behavior if surveys are infrequent (Ruprecht et al. 2012), and could be altogether impractical when surveys are encumbered by remote locations, rugged terrain, or otherwise difficult conditions. We address these issues using a model-based approach for locating central places from satellite telemetry data.

Satellite telemetry devices collect regular sequences of animal locations (Tomkiewicz et al. 2010), data that contain valuable information concerning the sites visited over a monitoring period. Repeated use of a site often yields multiple telemetry locations collected at that site. Therefore, clusters of locations in mapped telemetry data are important indicators of a central place (Knopff et al. 2009).

When deviations between true animal locations and the observed telemetry locations are small (i.e., small telemetry measurement error), clusters are well-defined. Accordingly, central places can be located by identifying clusters consisting of some pre-specified number of telemetry locations collected within a certain distance and time frame (Anderson and Lindzey 2003, Knopff et al. 2009). However, results are sensitive to the distance and time thresholds used (Zimmermann et al. 2007). Moreover, distance thresholds fail when telemetry measurement error is large. Large errors lead to diffuse clusters, which, in turn, create uncertainty in the location of a central place as well as the composition of the clusters

themselves. For example, observed telemetry locations can plausibly originate from more than one central place (i.e., cluster membership is ambiguous), or locations collected at a central place can be confused with locations collected during movements away from the site. Therefore, a method that accounts for telemetry measurement error is required.

We present a model-based approach for estimating the location of central places from satellite telemetry data. Our approach incorporates an observation model that explicitly accounts for measurement error, and uses a mixture model as a device for exposing latent structure (i.e., clustering) in telemetry location data. The mixture model is specified using a flexible Dirichlet process prior, a well-developed Bayesian nonparametric model that adapts its complexity to the data at hand. We also quantify temporal patterns in central place use (i.e., factors affecting when a central place is used) by incorporating ancillary data related to animal behavior into the model; however, we also extend the model to situations when no such behavioral data exist. We first apply the model to a simulated data set as proof of concept. We then illustrate our framework using an Argos satellite telemetry data set on harbor seals (*Phoca vitulina*) in the Gulf of Alaska. Harbor seals are central place foragers that exhibit fidelity to terrestrial haul-out sites (Lowry et al. 2001).

3.2 TELEMETRY DATA

The model we propose can be applied to various telemetry data types like VHF, GPS, or geolocation telemetry. We focus on Argos satellite telemetry data like those in our harbor seal data set that were calculated via the Argos least-squares positioning algorithm (Service Argos 2015). These data require special treatment because they exhibit an x-shaped error distribution that has greatest error variance along the NW-SE and NE-SW axes, a consequence of the polar orbiting Argos satellites and error that is largest in the direction

perpendicular to the orbit (Costa et al. 2010, Douglas et al. 2012). Furthermore, valid Argos telemetry locations are assigned one of six location classes (3, 2, 1, 0, A, and B), each of which exhibits different error patterns and magnitudes.

In addition to positional data, modern telemetry devices often collect ancillary data related to animal behavior (Tomkiewicz et al. 2010) that can be helpful for partitioning when individuals are actively using a central place versus other resources. The harbor seals in our data set, for example, were equipped with satellite-linked depth recorders that gathered information pertaining to diving behavior. Specifically, we use information from an on-board conductivity sensor that differentiates when a tag is wet (low resistance) versus dry (high resistance) as a surrogate for central place use. Resistance values ranged from 0-255, which we converted into a binary indicator for haul-out status using a threshold value of 127 (i.e., resistance values > 127 were categorized as hauled-out). The devices were programmed with a delay (10 consecutive readings at 45 sec. intervals) to prevent spurious wet/dry state transitions associated with splashing on a haul-out or short dry periods experienced by the sensor while a seal was surfaced but swimming; therefore, these wet/dry data reliably indicate when an individual is hauled-out on shore (dry) or at-sea (wet).

3.3 MODEL FORMULATION

Let $\mathbf{s}(t) \equiv (s_x(t), s_y(t))'$ represent the pair of coordinates for an observed telemetry location at time $t \in \mathcal{T}$, and $\boldsymbol{\mu}(t) \equiv (\mu_x(t), \mu_y(t))'$ represent the coordinates for a corresponding latent central place. We denote the spatial support of central places as $\tilde{\mathcal{S}}$ and the ancillary behavioral data as $y(t)$. In the case of harbor seals, $\tilde{\mathcal{S}}$ represents the coastline where haul-out sites can occur and $y(t) \in \{0, 1\}$, where 0 indicates the individual is at-sea and 1 indicates the individual is on-shore using terrestrial resources.

3.3.1 Observation model

The observed telemetry locations arise from a process that reflects animal movement and measurement error. Movement influences the true animal locations which are then observed imperfectly due to the telemetry measurement process. We accommodate various error patterns using a flexible mixture distribution, which itself is conditioned on the ancillary behavioral data to accommodate movement. First, consider a model for telemetry locations collected while the individual is at a central place (i.e., $y(t) = 1$):

$$\mathbf{s}(t) \sim \begin{cases} \mathcal{N}(\boldsymbol{\mu}(t), \boldsymbol{\Sigma}), & \text{with prob. } p(t) \\ \mathcal{N}(\boldsymbol{\mu}(t), \tilde{\boldsymbol{\Sigma}}), & \text{with prob. } 1 - p(t). \end{cases} \quad (3.1)$$

In Eq. 3.1, an observed telemetry location ($\mathbf{s}(t)$) arises from a mixture of multivariate normal distributions with mean $\boldsymbol{\mu}(t)$ corresponding to the location of a central place, and variance-covariance matrices $\boldsymbol{\Sigma}$ or $\tilde{\boldsymbol{\Sigma}}$ that describe telemetry measurement error. The matrix $\boldsymbol{\Sigma}$ is parameterized in a flexible manner (Brost et al. 2015, Buderman et al. 2016):

$$\boldsymbol{\Sigma} = \sigma^2 \begin{bmatrix} 1 & \rho\sqrt{a} \\ \rho\sqrt{a} & a \end{bmatrix}, \quad (3.2)$$

where σ^2 quantifies measurement error in the longitude direction, a modifies σ^2 to describe error in the latitude direction, and ρ describes the correlation between errors in the two directions. The matrix $\tilde{\boldsymbol{\Sigma}}$ equals $\boldsymbol{\Sigma}$ on the diagonal, but the off-diagonal elements are $-\rho\sqrt{a}$. This model specification accounts for circular ($a = 1$) and elliptical ($a \neq 1$) errors when $\rho = 0$, as well as x-shaped error patterns evident in Argos telemetry data when $\rho \neq 0$.

We model telemetry locations collected while the individual is not at the central place (i.e., $y(t) = 0$) in a fashion similar to Eq. 3.1:

$$\mathbf{s}(t) \sim \begin{cases} \mathcal{N}(\boldsymbol{\mu}(t), \Sigma + \sigma_\mu^2 \mathbf{I}), & \text{with prob. } p(t) \\ \mathcal{N}(\boldsymbol{\mu}(t), \tilde{\Sigma} + \sigma_\mu^2 \mathbf{I}), & \text{with prob. } 1 - p(t), \end{cases} \quad (3.3)$$

except the variance-covariance structure in Eq. 3.3 is augmented by σ_μ^2 , a parameter accounting for dispersion due to animal movement about the central place. In other words, $\boldsymbol{\mu}(t)$ and σ_μ^2 define the center and spread of an individual's "homerange." As in Eq. 3.1, Σ and $\tilde{\Sigma}$ account for error in the telemetry measurement process.

The observation model in Eq. 3.3 represents an integrated likelihood (Berger et al. 1999).

Consider, for example, the hierarchical model

$$\mathbf{s}(t) \sim \mathcal{N}(\tilde{\boldsymbol{\mu}}(t), \sigma^2 \mathbf{I}) \quad (3.4)$$

$$\tilde{\boldsymbol{\mu}}(t) \sim \mathcal{N}(\boldsymbol{\mu}(t), \sigma_\mu^2 \mathbf{I}), \quad (3.5)$$

where $\tilde{\boldsymbol{\mu}}(t)$ is the true but unobserved animal location. The parameters $\boldsymbol{\mu}(t)$, σ^2 , and σ_μ^2 are defined as in Eqs. 3.1–3.3, but note that the telemetry error structure in Eq. 3.4 is simplified for the purposes of illustration. In principle, we could estimate the true location $\tilde{\boldsymbol{\mu}}(t)$; however, our interest here is not the true locations but rather the location of the central place, $\boldsymbol{\mu}(t)$. Therefore, we treat $\tilde{\boldsymbol{\mu}}(t)$ as a "nuisance" parameter and remove it from the likelihood by integration (i.e., Rao-Blackwellization; Berger et al. 1999):

$$\int_{\tilde{\boldsymbol{\mu}}(t)} \mathcal{N}(\mathbf{s}(t) | \tilde{\boldsymbol{\mu}}(t), \sigma^2 \mathbf{I}) \mathcal{N}(\tilde{\boldsymbol{\mu}}(t) | \boldsymbol{\mu}(t), \sigma_\mu^2 \mathbf{I}) d\tilde{\boldsymbol{\mu}}(t) = \mathcal{N}(\mathbf{s}(t) | \boldsymbol{\mu}(t), \sigma^2 \mathbf{I} + \sigma_\mu^2 \mathbf{I}). \quad (3.6)$$

Aside from the simplified error structure, the resulting marginal distribution is the same as Eq. 3.3 and has a reduced parameter space compared to Eqs. 3.4 and 3.5. It also yields a

Markov chain Monte Carlo (MCMC) algorithm that is typically quicker to converge (Finley et al. 2015). Models for animal movement where individuals are attracted to a particular point are also available if inference concerning $\tilde{\mu}(t)$ is desired (Blackwell 2003, McClintock et al. 2012); however, these methods require the number of central places used by an individual to be known.

We define $p(t) = 0.5$ because the orbital plane of Argos satellites changes continuously and observations are equally likely to arise from either mixture component. The parameters related to measurement error (i.e., σ^2 , ρ , and a) are estimated for different Argos location quality classes (Appendix B1). Alternatively, Eq. 3.2 can be adapted to accommodate a continuous metric of location quality (e.g., GPS dilution of precision) or the Argos satellite telemetry location error ellipse (McClintock et al. 2014).

3.3.2 Spatial process model

As specified in the observation model (Eqs. 3.1 and 3.3), a telemetry location arises from an unknown (but estimable) central place, $\mu(t)$. When considering multiple telemetry locations recorded over some period of time, the number of unique central places used by an individual is potentially > 1 , but the exact number is unknown. Modeling central places is further complicated by possible multimodality (central places located in disjoint areas) and skewness (some central places are close together). We resolve these issues (i.e., multimodality, skewness, and an unknown number of central places) by using a Dirichlet process, a widely used probability model for unknown distributions that exhibits an important clustering property (Ferguson 1973, Hjort 2010). Following the constructive, stick-breaking representation of a Dirichlet process (Sethuraman 1994, Ishwaran and James 2001), we model

$\boldsymbol{\mu}(t)$ as a mixture of infinitely many components:

$$\boldsymbol{\mu}(t) \sim \sum_{j=1}^{\infty} \pi_j \delta_{\boldsymbol{\mu}_j}, \quad (3.7)$$

where $\boldsymbol{\mu}_j$ is the location of a potential central place, $\delta_{\boldsymbol{\mu}_j}$ is a point mass (or “atom”) at $\boldsymbol{\mu}_j$, π_j is the corresponding mixing proportion, and $\sum_{j=1}^{\infty} \pi_j = 1$. Because Eq. 3.7 is a discrete distribution, draws from it are generally not distinct, thereby inducing replication in the values for $\boldsymbol{\mu}(t)$. Thus, realizations from the Dirichlet process simultaneously provide a value for $\boldsymbol{\mu}(t)$ and partition telemetry locations with the same value for $\boldsymbol{\mu}(t)$ into clusters. The distinction between $\boldsymbol{\mu}_j$ and $\boldsymbol{\mu}(t)$ is subtle. The $\boldsymbol{\mu}_j$, for $j = 1, \dots, \infty$, are unique and represent the location of potential central places. The $\boldsymbol{\mu}(t)$, on the other hand, have a functional interpretation because they are time-specific and associate a $\boldsymbol{\mu}_j$ to each telemetry location $\mathbf{s}(t)$. Greater replication of $\boldsymbol{\mu}(t)$, for $t \in \mathcal{T}$, confers higher intensity use of the associated central place (i.e., more telemetry locations associated with the same central place). Note that, even though the Dirichlet process assumes infinitely many mixture components (central places), only a finite number are used to generate the observed data.

We formulate π_j using a stick-breaking process (Sethuraman 1994):

$$\pi_j = \eta_j \prod_{l < j} (1 - \eta_l), \quad (3.8)$$

where $\eta_j \sim \text{Beta}(1, \theta)$ and θ is a concentration parameter that controls the prior expected number of mixture components in the Dirichlet process. To describe the stick-breaking process, begin with a stick of unit length that represents the total probability allocated to the infinitely many mixture components in Eq. 3.7. Initially, we break off a piece of length $\eta_1 \sim \text{Beta}(1, \theta)$ from the stick and assign this probability ($\pi_1 = \eta_1$) to the first component, $\boldsymbol{\mu}_1$. Next, we break off another proportion $\eta_2 \sim \text{Beta}(1, \theta)$ from the remaining length of stick ($1 - \eta_1$), and assign this probability ($\pi_2 = \eta_2$) to the second component, $\boldsymbol{\mu}_2$. This process continues until all the probability has been assigned to the components or a stopping criterion is met.

η_1) and assign this probability ($\pi_2 = \eta_2(1 - \eta_1)$) to the second component, μ_2 . As the process is repeated, the stick gets shorter such that the lengths (i.e., mixing proportions) assigned to components with a higher index decrease stochastically. The concentration parameter (θ) controls the rate of decrease.

In practice, we implement the Dirichlet process using a truncation approximation (Ishwaran and James 2001). For a sufficiently high index J , notice that $\sum_{j+1}^{\infty} \pi_j \approx 0$ because the mixing proportions decrease in the index j . Thus, an accurate approximation to the infinite Dirichlet process (Eq. 3.7) can be obtained by letting $\eta_J = 1$, resulting in $\pi_j = 0$ for $j = J + 1, \dots, \infty$. The index J is an upper bound on the number of mixture components in Eq. 3.7, not the number of components necessary to model the observed data.

3.3.3 Temporal process model

We model the ancillary behavioral data using a binary probit regression formulated under a data augmentation approach (Albert and Chib 1993, Johnson et al. 2012, Dorazio and Rodriguez 2012). In particular, we introduce the parameter $v(t)$ as a continuous, latent version of the binary process $y(t)$, which we model as a normal random variable with unit variance:

$$v(t) \sim \mathcal{N}(\mathbf{x}(t)' \boldsymbol{\beta} + \mathbf{w}(t)' \boldsymbol{\alpha}, 1). \quad (3.9)$$

This expression represents a semiparametric regression with mean structure that includes parametric and nonparametric components (Hastie et al. 2009, Ruppert et al. 2003). The parametric component consists of a vector of time-varying covariates that affect the probability of central place use, $\mathbf{x}(t)$, and a corresponding vector of coefficients, $\boldsymbol{\beta}$. The nonparametric component, $\mathbf{w}(t)' \boldsymbol{\alpha}$, is described below. Assuming $y(t) = 1$ if $v(t) > 0$ and $y(t) = 0$

if $v(t) \leq 0$, the specification in Eq. 3.9 implies the probit regression model

$$y(t) \sim \text{Bernoulli}(\Phi(\mathbf{x}(t)' \boldsymbol{\beta} + \mathbf{w}(t)' \boldsymbol{\alpha})), \quad (3.10)$$

where Φ is the standard normal cumulative distribution function. The auxiliary variable specification in Eqs. 3.9 and 3.10 streamlines computation because the associated full-conditional distributions are known and can be sampled in closed form when fitting the model using MCMC.

We use the nonparametric component of Eq. 3.9 to account for temporal autocorrelation, which often occurs in data collected over time from a single individual (e.g., $y(t)$). The nonparametric component consists of a linear combination of basis functions evaluated at time t , $\mathbf{w}(t)$, and the vector of basis coefficients, $\boldsymbol{\alpha}$ (Ruppert et al. 2003). The coefficients weight the basis functions to produce a smooth process through time, thereby inducing dependence among observations. The basis functions are arbitrary and should have features that match those of the underlying process being estimated. Commonly used basis functions include splines, wavelets, and Fourier series. The number of functions should also reflect the temporal resolution of that process (Ruppert et al. 2003).

3.3.4 Prior distributions

To complete the Bayesian formulation of this model, we specify prior distributions for unknown parameters. We assume $\boldsymbol{\beta} \sim N(\boldsymbol{\mu}_\beta, \sigma_\beta^2 \mathbf{I})$, $\theta \sim \text{Gamma}(r_\theta, q_\theta)$, $\log(\sigma_\mu) \sim \mathcal{N}(\mu_\sigma, \sigma_\sigma^2)$, and $\sigma \sim \text{Uniform}(0, u)$, with similar uniform priors for ρ and a . The lognormal distribution for σ_μ allows prior information concerning animal movement and homerange size, if available, to be incorporated into the model. We adopt a penalized approach to avoid overfitting $\boldsymbol{\alpha}$ by assuming $\boldsymbol{\alpha} \sim N(\mathbf{0}, \sigma_\alpha^2 \mathbf{I})$ and $\sigma_\alpha^2 \sim \text{IG}(r_\alpha, q_\alpha)$ (Ruppert et al. 2003). The prior for $\boldsymbol{\mu}_j$,

referred to as the base distribution of the Dirichlet process (Hjort 2010), determines where the atoms δ_{μ_j} tend to be located. We assume $\boldsymbol{\mu}_j \sim f_{\tilde{\mathcal{S}}}(\mathbf{S})$, where \mathbf{S} is a matrix containing all of the observed telemetry locations and $f_{\tilde{\mathcal{S}}}(\mathbf{S})$ represents the density of telemetry locations in $\tilde{\mathcal{S}}$. We approximate $f_{\tilde{\mathcal{S}}}(\mathbf{S})$ using a kernel density estimator evaluated over a rasterized domain $\tilde{\mathcal{S}}$. See Appendix B1 for the full model specification and Appendix B2 for details regarding model implementation.

3.4 MODEL APPLICATION

3.4.1 Simulated data example

We demonstrate our modeling framework when parameters are known in a simulated data example. Figure 3.1 shows 1,000 locations simulated from the model using parameters obtained from an analysis of harbor seal telemetry data (see Case study below). To simplify presentation of results, simulated locations were randomly allocated to Argos location classes 3, 0, and B (high-, medium-, and low-accuracy locations). We set $J = 50$ in the truncation approximation to the Dirichlet process and modeled dependence in central place use with B-spline basis functions ($\mathbf{w}(t)$). B-splines are commonly used in semiparametric regression because they have local support and stable numerical properties (Ruppert et al. 2003). We fit the model using a MCMC algorithm written in R (provided in Data S1; R Development Core Team 2015).

Inference concerning $\boldsymbol{\mu}(t)$, the spatial intensity of central place use, is summarized in Figure 3.1. Posterior probability is concentrated near known central places, and inference is more certain for central places associated with many telemetry locations (i.e., locations that were heavily used). Posterior probability for $\boldsymbol{\mu}_j$, the location of potential central places, is

more diffuse than that of $\mu(t)$, but still generally concentrated near central places (Appendix B3). The model recovers parameters related to telemetry measurement error, animal movement, and the temporal process of central place use (Appendix B3). Additional simulated data examples are presented in Appendix B4.

3.4.2 Case study: harbor seals

To demonstrate our approach with real data, we apply our model to Argos satellite telemetry locations collected from a harbor seal near Kodiak Island, Alaska (Fig. 3.2). Harbor seals repeatedly use terrestrial haul-out sites along the coastline ($\tilde{\mathcal{S}}$), which we represented using a 100-m resolution raster. Haul-out behavior changes over time due to physiological functions (thermoregulation, molting, pupping, etc.) and environmental conditions (e.g., tidal state) that affect the availability of haul-out sites (London et al. 2012). Thus, we evaluated the affect of several temporal covariates on the use of haul-out sites: the number of hours since solar noon (13:00 hours), the number of hours since low tide, and the number of days since August 15 and its quadratic effect. Tide information was obtained from the nearest National Oceanic and Atmospheric Administration station (Kodiak Island, ID: 9457292). We set $J = 50$ in the truncation approximation to the Dirichlet process, which greatly exceeds the expected number of haul-out sites used by a single harbor seal. We modeled the temporal haul-out process using B-splines ($\mathbf{w}(t)$) defined at 6-hour intervals. In addition to allowing for smooth patterns in the probability of haul-out use, a basis expansion defined at this interval allows haul-out behavior to vary throughout day.

Inference concerning the intensity of haul-out site use ($\mu(t)$) is shown in Figure 3.2. Posterior probability is concentrated in three regions, generally occurring near clustered telemetry locations. The highest posterior probability occurs along the northernmost coast-

line of Ugak Bay, indicating this area was most actively used by the individual. Similar to the simulated data example, inference concerning μ_j was more diffuse, but resembles that of $\mu(t)$ (Appendix B5). Parameters in the temporal process model (β) indicate haul-out use was highest at times near solar noon, during summer months, and at high tide (Appendix B5). Inference concerning animal movement (σ_μ) suggests approximately 95% of at-sea locations were within 6.6 km of a haul-out site. Parameters related to telemetry measurement error are provided in Appendix B5. All inference was based on 50,000 MCMC samples, which required 5 hours of processing time on a computer equipped with a 3.4 GHz Intel Core i7 processor.

3.5 DISCUSSION

A fully model-based approach rigorously accommodates multiple sources of uncertainty when estimating the location of central places from satellite telemetry data. Our framework consists of three constituent models: an observation model that accounts for telemetry measurement error and animal movement, a spatial process model for estimating the location of central places, and a temporal process model for quantifying patterns in central place use. Unlike other approaches, our model does not require user-specified distance or time thresholds to identify central places (Anderson and Lindzey 2003), or prior knowledge regarding cluster characteristics (Webb et al. 2008). Model implementation is unified to properly account for uncertainty in parameter estimates.

We demonstrate our model using simulated data examples and an application to harbor seals near Kodiak Island, Alaska. Harbor seals typically exhibit localized movements and regularly return to one or more terrestrial haul-outs between at-sea foraging bouts (Lowry et al. 2001). Our model could also be applied to species that display other behaviors. For

example, our model could be used to examine the location of migratory stopover sites or kill sites (Higuchi et al. 2004, Zimmermann et al. 2007, Chevallier et al. 2010); however, the ability to model ephemeral locations requires telemetry data collected at a relatively high temporal frequency.

3.5.1 Observation model

Our observation model consists of a flexible, finite mixture distribution (Eqs. 3.1 and 3.3) that accounts for potentially complex telemetry measurement errors like those evident in Argos data (Brost et al. 2015, Buderman et al. 2016). The observation model also accounts for movements away from the central place via an integrated likelihood (Eq. 3.3; Berger et al. 1999). Because measurement error and animal movement are incorporated into the observation model, we use all telemetry locations to estimate the location of central places, not just those with small magnitude errors or those collected while the individual is at the central place. Furthermore, we use a constrained spatial support for central places (e.g., haul-out sites that only occur along the coastline), and the subsequent discrepancy between the spatial supports of $\mathbf{s}(t)$ and $\boldsymbol{\mu}(t)$, to simultaneously estimate telemetry measurement error (Brost et al. 2015). In applications where central places do not have a constrained support, telemetry error must be known *a priori* or estimated from a secondary data source (e.g., Jonsen et al. 2005, Costa et al. 2010, Douglas et al. 2012).

3.5.2 Process models

The spatial process model consists of a Dirichlet process, a Bayesian nonparametric model that adapts its complexity (e.g., the number of central places) to the observed data. In conjunction with the observation model, the spatial model comprises a Dirichlet process

mixture model, a highly flexible framework that includes a large class of distributions (Hjort 2010). As such, the model accommodates multimodal and skewed distributions, like the distribution of central places.

The Dirichlet process allows for potentially infinite clusters as T , the number of observations, approaches ∞ ; however, the number of occupied components cannot exceed T and is generally much smaller than T . Consequently, a mixture of a finite number of components could be used in practice, which is the strategy we adopt by using a truncation approximation to produce a computationally efficient algorithm for parameter estimation (Ishwaran and James 2001). Other representations of the Dirichlet process, like the Chinese restaurant process, do not rely on truncations for model fitting (Teh et al. 2006).

Our spatial process model could be adapted to include temporal dynamics in the location of central places. For example, seasonal patterns in the location of harbor seal haul-out sites could be incorporated by modeling the central places in a Markovian fashion such that $\boldsymbol{\mu}(t)$ is a function of previous central places. Adjusting our model to differentiate between behaviors would also be necessary if the goal is to examine multiple types of central places in a single dataset (i.e., long-term use of a den site and short-term use of kill sites). One approach to accommodating different behaviors is to formulate the Dirichlet process as a hidden Markov model, a commonly-used method for identifying multiple behavioral states in telemetry data (Patterson et al. 2009, Langrock et al. 2012).

We use a semiparametric regression to model the temporal process of central place use and account for dependence in the behavioral data (Ruppert et al. 2003). Telemetry data are generally not equally spaced in time; thus, serial correlation would be difficult to model using, for example, an autoregressive process. The basis function approach that we implement is a flexible alternative to modeling autocorrelated data (Hefley et al. in revision).

The basis functions, which are continuous in time, also facilitate prediction of animal behavior. For example, animal behavior can be predicted at times associated with telemetry locations when the positional and behavioral data are temporally misaligned (Appendix B6). Our model can even be adapted to estimate animal behavior when ancillary data are not available (Appendix B6). Indeed, prediction is a key advantage of a probabilistic framework like the one we present.

3.5.3 *Guidance*

The joint analysis of multiple individuals can be achieved by applying our model to several individuals separately, and then combining inference across individuals to obtain population-level parameters with a meta-analysis (e.g., Hartung et al. 2008, Hooten et al. 2016). Alternatively, multiple individuals could be analyzed concurrently using a hierarchical Dirichlet process (Teh et al. 2006, Hjort 2010). A hierarchical approach extends our model by placing individual-specific Dirichlet processes under a common prior (another Dirichlet process), thereby allowing central places to be unique to, or shared amongst, individuals. In either approach, heterogeneity among individuals can be accommodated and explained through the introduction of demographic covariates (e.g., sex and age), and the location of central places could be modeled as a function of environmental covariates to examine site selection.

Bayesian nonparametric models, like the Dirichlet process we use to examine the location of central places, have been adapted to analyze time series data, grouped data, data in a tree, binary data, relational data, and spatial data (Gershman and Blei 2012). This highly flexible framework has been widely used in other fields (Rodriguez and Dunson 2011), although we are aware of few examples from ecology. However, potential ecological applications are

numerous and include abundance estimation (Dorazio et al. 2008, Johnson et al. 2013), population genetics (Huelsenbeck and Andolfatto 2007), and disease spread (Verity et al. 2014), among other applications where the goal is to infer latent structure based on empirical data (Morales et al. 2004, Brost and Beier 2012).

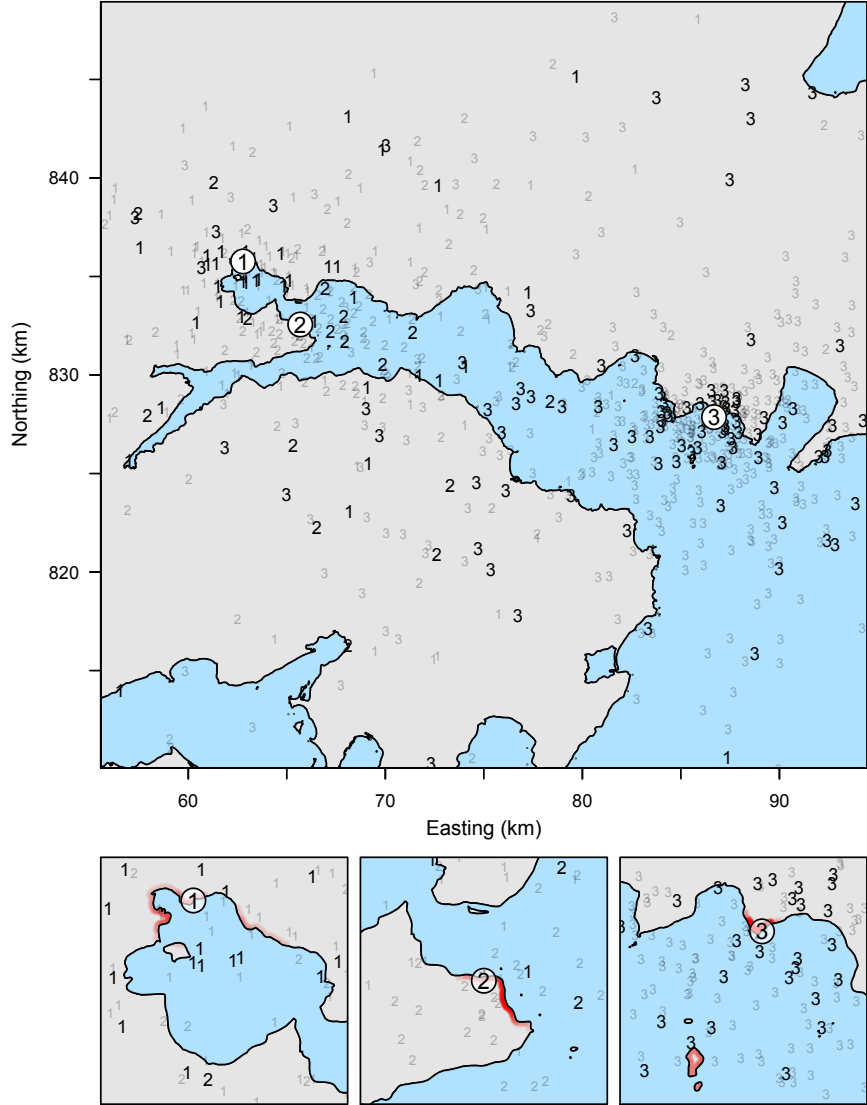


FIGURE 3.1. Simulation of 1,000 telemetry locations ($\mathbf{s}(t)$) arising from three central places ($\boldsymbol{\mu}_j$). The point symbology associates telemetry locations (black and gray numerals; most are smaller gray numerals to reduce clutter) to their corresponding central places (white, numbered circles). For example, a telemetry location labeled “1” is associated with the central place labeled “1.” The spatial support of central places ($\tilde{\mathcal{S}}$) exists at the intersection of the blue and gray polygons (black line). The posterior distribution of $\boldsymbol{\mu}(t)$ (red gradient) in the vicinity of the central places is shown in the bottom panels; brighter red corresponds to higher posterior probability. Inference concerning the location of central place “3,” which was associated with 608 telemetry locations, is most certain. Inference concerning central places “1” and “2,” which were associated with fewer telemetry locations (approximately 200 locations each), is more diffuse. All inference was based on 20,000 MCMC samples after convergence. Note that 326 simulated telemetry locations are beyond the extent of this map, occurring up to 880 km away.

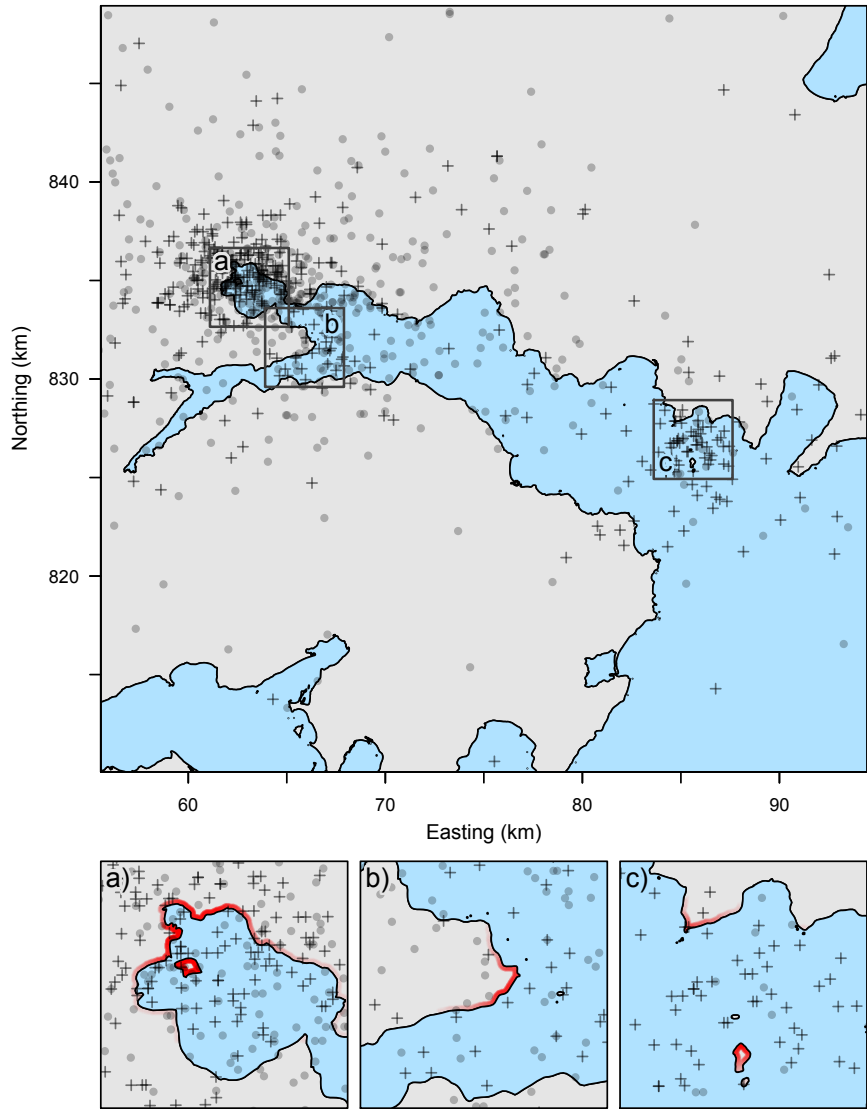


FIGURE 3.2. Telemetry locations (top panel) of a subadult female harbor seal monitored from 09 OCT 1995 to 04 JUN 1996 in Ugak Bay (57.42982°N , $-152.5715^{\circ}\text{W}$) on the southern coast of Kodiak Island, Alaska, USA. Point symbology reflects whether the individual was hauled-out (black points) or at-sea (black crosses) at the time a telemetry location was recorded. Telemetry locations were collected on average every 5.7 h (range: 0.0 – 54.8 h) using an Argos satellite telemetry device. The animal's position was measured on 1,004 occasions, with $\approx 72\%$ of locations coming from the three least accurate Argos location classes. Approximately 40% of locations were collected while the individual was at a haul-out site ($y(t) = 1$). The spatial support of haul-out sites (\hat{S}) exists along the coastline (black line) at the intersection of the blue (water) and gray (land) polygons. The insets show three regions where the posterior probability of $\mu(t)$ (red gradient) is most concentrated (bottom panels). Brighter red corresponds to higher posterior probability. All inference was based on 50,000 MCMC samples after convergence. Note that 190 telemetry locations are beyond the extent of this map, occurring up to 1,100 km away from Ugak Bay.

CHAPTER FOUR

Model-based Clustering Reveals Spatio-temporal Patterns in Central Place Use of a Marine Top Predator³

Summary. Central places like dens, nests, roosts, and rendezvous sites are often associated with important life history events and may exhibit unique characteristics. Consequently, information concerning the location of these sites, as well as the temporal patterns in their use, is essential for the effective management and conservation of many species. Satellite telemetry data contain valuable information concerning the behavior associated with central places; however, using satellite telemetry data to study central places is complicated by common nuances like locational error and animal movement. We coupled a recently developed modeling framework with Argos satellite telemetry data to examine the spatio-temporal behavior associated with harbor seal haul-out sites on Kodiak Island, Alaska, USA. Information concerning harbor seal haul-out behavior has implications for mitigating human-caused disturbances, as well as improving population monitoring programs. The novel modeling framework we used incorporates an observation model that accommodates multiple sources of uncertainty in telemetry data, and a flexible Bayesian nonparametric model called a Dirichlet process to uncover latent clustering in the telemetry locations. We also extend previously developed methods to examine the affect of covariates on haul-out site selection and to obtain population-level inference concerning haul-out use. Our analysis indicates that haul-out sites generally occurred in inlets and bays, areas that are isolated from the

³The material in Chapter 4 is similar to a manuscript of the same title by B. M. Brost, M. B. Hooten, and R. J. Small soon to be submitted to Ecological Applications. Thank you to my coauthors and George Wittemyer for their helpful feedback on this manuscript.

open water of the Gulf of Alaska. Accordingly, most individuals selected haul-out sites that were protected from waves; effects of bathymetry and shoreline complexity on haul-out site selection were variable amongst individual seals. The affects of time of day, time since low tide, and day of year on temporal patterns of haul-out use were also highly variable. The model-based approach we describe is general and offers a practical and rigorous means for using satellite telemetry data to learn about the location of central places, as well as the temporal patterns in their use.

4.1 INTRODUCTION

Central places like dens, nests, roosts, and rendezvous sites are often associated with important life history events (e.g., rearing of young) and may exhibit unique characteristics (e.g., protection from predators or proximity to water). Consequently, information concerning the location of these sites, as well as the temporal patterns in their use, is essential for the effective management and conservation of many species (e.g., Quinlan and Hughes 1990, Blakesley et al. 1992, Brigham et al. 1997, Ciarniello et al. 2005, Holloran and Anderson 2005, Baldwin and Bender 2008). Central places can be studied by sighting individuals during aerial (Montgomery et al. 2007) or ground-based surveys (Blakesley et al. 1992), or by using radio-telemetry equipment to locate tagged individuals in the field; however, direct observation may only provide a snapshot of an animal's behavior if surveys are infrequent, and may be impractical when remote locations, rugged terrain, or otherwise difficult conditions hamper survey efforts. Satellite telemetry data provide regular information over extended periods of time, and thus offer a more complete account of an animal's central place use. Moreover, as repositories of satellite telemetry data on a wide variety of species accumulate,

so do opportunities for using this information to learn about the locations of central places, as well as the temporal patterns in their use.

Satellite telemetry devices record regular sequences of animal locations (Tomkiewicz et al. 2010). Consequently, repeated use of a site yields multiple telemetry locations collected at that site, and central places are often identified by clusters of locations in mapped telemetry data (Knopff et al. 2009). When telemetry location errors are small (i.e., the observed telemetry locations are near the true animal locations), clusters are conspicuous and central places can be easily identified visually or by using a series of user-specified time and distance thresholds (Fig. 4.1a; Anderson and Lindzey 2003, Knopff et al. 2009); however, a more sophisticated methodology is required when errors are large because clusters are poorly defined, and the number and location of central places are highly uncertain (Fig. 4.1b).

Brost et al. (in press) recently proposed a model-based approach to estimate the location of central places that rigorously accommodates multiple sources of uncertainty in telemetry data. Their modeling framework is general and can be applied to different types of telemetry data or used to examine various marine and terrestrial animals and their associated central places. The hierarchical approach incorporates an observation model that allows for telemetry location error and animal movement, and a flexible Bayesian nonparametric model called a Dirichlet process to uncover latent clustering in telemetry location data. They further incorporated ancillary behavioral data (e.g., accelerometer data, wet/dry status) into the model to improve location estimation, as well as to quantify temporal patterns in central place use. In this paper, we extend the framework of Brost et al. (in press) to investigate the spatio-temporal haul-out behavior of a marine top predator, the harbor seal (*Phoca vitulina*).

Harbor seals are widely distributed in the temperate and arctic waters of the Northern Hemisphere (Scheffer and Slipp 1944). Harbor seals regularly leave the water and haul-out

on beaches, intertidal areas, and floating ice (in glacial fjords) to rest, molt, escape aquatic predators, give birth, and rear their pups (Ling 1984, da Silva and Terhune 1988, Thompson 1989, Watts 1992). The locations of haul-out sites may change seasonally to track available food sources (Montgomery et al 2007, Cunningham et al. 2009), although harbor seals exhibit high levels of site fidelity over months to years and typically return to the same haul-out sites between at-sea foraging bouts (Härkönen and Heide-Jørgensen 1990; Thompson et al. 1997; Cunningham et al. 2009).

Knowledge of harbor seal haul-out behavior is necessary to effectively manage and conserve this species. For example, human-caused disturbances can flush harbor seals from their haul-out sites, resulting in increased energy expenditure and potentially decreased fitness (Suryan and Harvey 1999, Jansen et al. 2010, Cordes et al. 2011, Blundell and Pendleton 2015). In particular, the impact of tourism vessels (i.e., cruise ships) on hauled-out harbor seals has received much attention recently (Jansen et al. 2010, Young et al. 2014, Blundell and Pendleton 2015, Mathews et al. 2016), and mitigation efforts require an understanding of harbor seal haul-out behavior. Furthermore, harbor seal population monitoring, which relies on counts of haul-out groups for abundance estimation, can benefit from additional information concerning when and where harbor seals haul out of the water (e.g., to estimate and maximize detection probability during aerial surveys; Boveng et al. 2003, Small et al. 2003, Ver Hoef and Frost 2003).

Although harbor seal haul-out behavior has been studied via direct observation (e.g., Cordes et al. 2011), remote locations and harsh conditions often inhibit extensive field investigations. In Alaska, for example, current knowledge concerning the location of haul-out sites is limited to aerial surveys conducted during August and September (Boveng et al. 2003, Small et al. 2003, Ver Hoef and Frost 2003). Existing satellite telemetry datasets

provide a practical means for learning about harbor seal haul-out behavior throughout the full annual cycle, without the expense of conducting additional fieldwork. We examined an existing Argos satellite telemetry dataset, collected on a population of harbor seals monitored near Kodiak Island, Alaska, USA, to understand the spatial distribution of haul-out sites used by individuals in this population, as well as the temporal patterns in haul-out use. We extend the methods presented by Brost et al. (in press) to examine the affect of covariates on haul-out site selection and to obtain population-level inference concerning haul-out use. Our study simultaneously offers insight into harbor seal haul-out behavior, extends a previously developed modeling framework, and demonstrates how satellite telemetry data are useful for examining spatio-temporal patterns in central place use by marine and terrestrial animals.

4.2 METHODS

4.2.1 Harbor seal telemetry data

Harbor seals were captured near Kodiak Island, Alaska (Fig. 4.2) and equipped with satellite-linked depth recorders (SDRs; Wildlife Computers, Redmond, WA) during 1993–1997. The SDRs transmitted to Argos receivers onboard polar orbiting meteorological satellites, a system that uses the Doppler effect (i.e., the shift in frequency observed when the SDRs and the satellites are moving relative to each other) for geopositioning. The Argos least-squares positioning algorithm assigns each telemetry location to one of six quality classes based on the number of transmissions received during a satellite pass. In order of decreasing accuracy, the location quality classes are 3, 2, 1, 0, A, and B. The location quality classes have different error patterns and magnitudes, and some exhibit an x-shaped error distribution that has greatest error variance along the NW-SE and NE-SW axes (Costa et

al. 2010, Douglas et al. 2012, McClintock et al. 2014, Brost et al. 2015, Buderman et al. 2016). The magnitude of Argos location errors are often >10 km, and in some cases >100 km (Costa et al. 2010, Brost et al. 2015), errors that exceed the typical extent of harbor seal movements (Frost et al. 2001, Lowry et al. 2001, Cunningham et al. 2009).

The SDRs included a conductivity sensor that determined when the device was wet (low resistance) versus dry (high resistance), ancillary behavioral data that we used as a proxy for haul-out use. In other words, instances when the device was dry indicate the individual was out of the water at a haul-out site when the location was recorded, whereas locations collected while the device was wet indicate the individual was at-sea. The devices were programmed with a delay (10 consecutive readings at 45 sec. intervals) to prevent spurious wet/dry state transitions associated with splashing on a haul-out or short dry periods experienced by the sensor while a seal was surfaced in the water. Therefore, the wet/dry data reliably indicate a harbor seal's haul-out status.

4.2.2 Statistical notation

Let $\mathbf{s}_{ic}(t) \equiv (s_{i,c,x}(t), s_{i,c,y}(t))'$ represent the pair of coordinates for an observed telemetry location collected at time $t \in \mathcal{T}$, where i indexes an individual harbor seal ($i = 1, \dots, N$) and c indexes Argos location quality class ($c \in \{3, 2, 1, 0, A, B\}$). Also let $\boldsymbol{\mu}_i(t) \equiv (\mu_{i,x}(t), \mu_{i,y}(t))'$ be the coordinates for the corresponding latent haul-out site. We denote the ancillary behavioral data as $y_i(t)$, where $y_i(t) = 0$ indicates the telemetry device on individual i was wet at time t and thus the harbor seal was at-sea, and $y_i(t) = 1$ indicates the device was dry and the individual was at a haul-out site. We also denote the spatial domain within which haul-out sites can exist as \mathcal{S} (e.g., the shoreline).

4.2.3 Haul-out site location estimation

Haul-out site location estimation was performed using a hierarchical model that consists of two primary components, an observation model and a process model (Brost et al., in press). The observation model accounts for telemetry location error and animal movement, whereas the process model is used to estimate the true but unobserved locations of the haul-out sites.

The observation model consists of two parts, one part for telemetry locations collected while the harbor seal is hauled-out of the water and another part for locations collected while it is at-sea. First, we consider a model for telemetry locations collected while the individual is at a haul-out site (i.e., $y_i(t) = 1$) and the true but unknown harbor seal location is the same as $\mu_i(t)$, the location of the latent haul-out site. In this case, the observation model accounts for the various error patterns evident in Argos telemetry data (Brost et al., in press):

$$\mathbf{s}_{ic}(t) \sim \begin{cases} \mathcal{N}(\boldsymbol{\mu}_i(t), \boldsymbol{\Sigma}_{ic}), & \text{with prob. } p_i(t) \\ \mathcal{N}(\boldsymbol{\mu}_i(t), \tilde{\boldsymbol{\Sigma}}_{ic}), & \text{with prob. } 1 - p_i(t) \end{cases}. \quad (4.1)$$

In Eq. 4.1, an observed telemetry location arises from a mixture of two multivariate normal distributions centered at $\boldsymbol{\mu}_i(t)$ with variance-covariance matrices $\boldsymbol{\Sigma}_{ic}$ or $\tilde{\boldsymbol{\Sigma}}_{ic}$ that describe Argos telemetry measurement error. The parameter $p_i(t)$ defines the probability associated with the mixture components. The matrix $\boldsymbol{\Sigma}_{ic}$ is parameterized as

$$\boldsymbol{\Sigma}_{ic} = \sigma_{ic}^2 \begin{bmatrix} 1 & \rho_{ic}\sqrt{a_{ic}} \\ \rho_{ic}\sqrt{a_{ic}} & a_{ic} \end{bmatrix} \quad (4.2)$$

to allow for various error structures (Brost et al. 2015, Buderman et al. 2016), where σ_{ic}^2 quantifies measurement error in the longitude direction, a_{ic} modifies σ_{ic}^2 to describe error in

the latitude direction, and ρ_{ic} describes the correlation between errors in the two directions. The matrix $\tilde{\Sigma}_{ic}$ is identical to Σ_{ic} except for the off-diagonal elements which are $-\rho_{ic}\sqrt{a_{ic}}$. When $\rho_{ic} = 0$, the model specification in Eq. 4.2 allows for circular ($a_{ic} = 1$) and elliptical ($a_{ic} \neq 1$) error patterns. Alternatively, the error covariance model allows for the x-shaped error pattern evident in Argos telemetry data when $\rho_{ic} \neq 0$, where the mixture component with variance-covariance matrix Σ_{ic} describes error along the SW-NE axis and the mixture component with variance-covariance matrix $\tilde{\Sigma}_{ic}$ describes error along the NW-SE axis. The parameters related to telemetry location error are also indexed by c , allowing the characteristics of locational error to vary for each Argos location quality class.

For telemetry locations collected while the individual is at-sea (i.e., $y_i(t) = 0$), the true harbor seal location is not the same as the location of the haul-out site (as in Eq. 4.1), but, rather, is in the vicinity of $\mu_i(t)$. In this case, the observation model is similar to Eq. 4.1, except that the variance-covariance structure includes an extra component, τ_i^2 , to account for additional uncertainty due to animal movement around the haul-out site (Brost et al., in press), resulting in

$$\mathbf{s}_{ic}(t) \sim \begin{cases} \mathcal{N}(\boldsymbol{\mu}_i(t), \Sigma_{ic} + \tau_i^2 \mathbf{I}), & \text{with prob. } p_i(t) \\ \mathcal{N}(\boldsymbol{\mu}_i(t), \tilde{\Sigma}_{ic} + \tau_i^2 \mathbf{I}), & \text{with prob. } 1 - p_i(t) \end{cases}. \quad (4.3)$$

As in Eq. 4.1, Σ_{ic} and $\tilde{\Sigma}_{ic}$ account for various error patterns in the telemetry measurement process, whereas $\boldsymbol{\mu}_i(t)$ and τ_i^2 define the center and spread of the “home range” for individual i . The mixture probabilities in Eqs. 4.1 and 4.3 are defined as $p_i(t) = 0.5$ because the orbital plane of the Argos satellites changes continuously, and telemetry locations are equally likely to arise from either mixture component (i.e., locations have a 50% chance of arising from either axis of the x-shaped Argos error distribution; Brost et al. 2015).

The process model, which is used to estimate the true but unobserved locations of the haul-out sites ($\boldsymbol{\mu}_i(t)$), consists of a clustering model known as a Dirichlet process that associates telemetry locations with haul-out sites probabilistically. Following Brost et al. (in press), we represent the Dirichlet process as a mixture of infinitely many components

$$\boldsymbol{\mu}_i(t) \sim \sum_{j=1}^{\infty} \pi_{ij} \delta_{\boldsymbol{\mu}_{ij}}, \quad (4.4)$$

where $\boldsymbol{\mu}_{ij}$ are locations within the spatial domain \mathcal{S} , $\delta_{\boldsymbol{\mu}_{ij}}$ is a point mass (or “atom”) at $\boldsymbol{\mu}_{ij}$, π_{ij} is the probability associated with the mixture component, and $\sum_{j=1}^{\infty} \pi_j = 1$. In other words, each mixture component in Eq. 4.4 represents the location of a possible haul-out site and π_{ij} is the probability of the location being used by a harbor seal.

In theory, there are infinitely many possible haul-out sites for a harbor seal to select from (e.g., all locations along the shoreline) and thus infinitely many mixture components in Eq. 4.4; however, only a handful of haul-out sites are likely used by a harbor seal (see next paragraph). The distinction between possible haul-out sites and those actually used by a harbor seal is reflected in the interpretations of $\boldsymbol{\mu}_{ij}$ and $\boldsymbol{\mu}_i(t)$. The $\boldsymbol{\mu}_{ij}$, for $j = 1, \dots, \infty$, are unique locations and represent potential sites where a seal could haul-out. Conversely, the $\boldsymbol{\mu}_i(t)$ have a functional interpretation because they associate a $\boldsymbol{\mu}_{ij}$ to each telemetry location $\mathbf{s}_{ic}(t)$; they are locations that are actually used as a haul-out site. The number of mixture components necessary to generate the observed data can, at most, be the number of telemetry locations collected for an individual (e.g., a harbor seal never uses the same haul-out site twice); however, the number of requisite components is much fewer in practice.

The mixture probabilities are formulated in a manner such that π_{ij} decreases stochastically with increasing index j , favoring fewer clusters (i.e., haul-out sites) with many locations per cluster (Sethuraman 1994, Ishwaran and James 2001). The number of haul-outs used

by an individual seal is unknown; therefore, the rate of decrease in the π_{ij} , and thus the number of clusters, is data-driven, allowing the complexity of the mixture to be tailored to each individual seal. Realizations from Eq. 4.4 are generally not distinct because the Dirichlet process is a discrete distribution (i.e., each mixture component is a discrete entity), and because probability mass is concentrated over the first several components. Therefore, it follows that replication in the values of $\boldsymbol{\mu}_i(t)$, for $t \in \mathcal{T}$, partition telemetry locations into clusters. Replication also provides a measure of intensity of use, such that sites associated with more telemetry locations have higher intensity of use.

We used a custom Markov chain Monte Carlo (MCMC) algorithm written in R (R Core Team 2015) to estimate the observation and process model parameters in a unified framework. Markov chain Monte Carlo is an iterative approach to obtaining random draws, or samples, from the posterior distribution of the unknown parameters (e.g., σ_{ic}^2 , τ_i , $\boldsymbol{\mu}_i(t)$; Gelfand and Smith 1990). The full model statement, including prior distributions for all unknown parameters, is shown in Appendix C1. Inference was based on 100,000 MCMC samples after convergence.

4.2.4 Haul-out site selection

We examined the affect of covariates on haul-out site selection in light of uncertainty in the estimated location of haul-out sites, instead of, say, modeling point estimates for the locations of the haul-out sites themselves. To simplify notation, we let \mathbf{M}_i be a matrix containing estimated haul-out site locations corresponding to the telemetry locations for individual i (i.e., $\mathbf{M}_i \equiv \{\boldsymbol{\mu}_i(t), \forall t\}$). Assuming for now only a single value for \mathbf{M}_i (e.g., obtained from one sample of the posterior distribution of the haul-out site locations, $[\boldsymbol{\mu}_i(t) | \cdot]$), the

posterior distribution is

$$[\boldsymbol{\beta}_i, \boldsymbol{\mu}_\beta | g(\mathbf{M}_i)] \propto \prod_i [g(\mathbf{M}_i) | \boldsymbol{\beta}_i] [\boldsymbol{\beta}_i | \boldsymbol{\mu}_\beta] [\boldsymbol{\mu}_\beta], \quad (4.5)$$

where the notation $[\cdot]$ represents a probability distribution and \mathbf{M}_i may be transformed with some deterministic function $g(\cdot)$. The expression in Eq. 4.5 provides a way to obtain inference for $\boldsymbol{\beta}_i$, a vector of individual-level parameters quantifying the affect of covariates on haul-out site selection, and $\boldsymbol{\mu}_\beta$, a vector of population-level parameters that describe the mean effect across all harbor seals; however, Eq. 4.5 does not incorporate uncertainty in the estimates of $\boldsymbol{\mu}_i(t)$. To account for uncertainty when making inference on the individual- and population-level parameters, we seek the posterior distribution of $\boldsymbol{\beta}_i$ and $\boldsymbol{\mu}_\beta$ given the observed telemetry locations recorded for individual i , which we denote as the matrix \mathbf{S}_i (i.e., $\mathbf{S}_i \equiv \{\mathbf{s}_{ic}(t), \forall t\}$). Accordingly, the desired posterior distribution is obtained by integrating over $[g(\mathbf{M}_i) | \mathbf{S}_i]$:

$$[\boldsymbol{\beta}_i, \boldsymbol{\mu}_\beta | \mathbf{S}_i] = \int [\boldsymbol{\beta}_i, \boldsymbol{\mu}_\beta | g(\mathbf{M}_i), \mathbf{S}_i] [g(\mathbf{M}_i) | \mathbf{S}_i] dg(\mathbf{M}_i). \quad (4.6)$$

Assuming the posterior distribution of \mathbf{M}_i provides complete knowledge of \mathbf{S}_i , we have

$$[\boldsymbol{\beta}_i, \boldsymbol{\mu}_\beta | \mathbf{S}_i] \approx \int [\boldsymbol{\beta}_i, \boldsymbol{\mu}_\beta | g(\mathbf{M}_i)] [g(\mathbf{M}_i) | \mathbf{S}_i] dg(\mathbf{M}_i) \quad (4.7)$$

$$\propto \int \prod_i [g(\mathbf{M}_i) | \boldsymbol{\beta}_i] [\boldsymbol{\beta}_i | \boldsymbol{\mu}_\beta] [\boldsymbol{\mu}_\beta] [g(\mathbf{M}_i) | \mathbf{S}_i] dg(\mathbf{M}_i). \quad (4.8)$$

We perform the integration in Eq. 4.8 using a multiple imputation procedure described by Hooten et al. (2010) and Hanks et al. (2015), where $[g(\mathbf{M}_i) | \mathbf{S}_i]$ is the imputation distribution (see below for procedural details).

In practice, we constructed a model for $\mathbf{w}_i = g(\mathbf{M}_i)$, where the function g aggregates \mathbf{M}_i to obtain the count of telemetry locations for individual i allocated to raster cells in \mathcal{S} , the

spatial support of haul-out sites. In particular, we used a hierarchical mixture model that accommodates zero inflation while also allowing variability among individual harbor seals:

$$w_{ij} \sim \begin{cases} \text{Pois}(\lambda_{ij}), & z_{ij} = 1 \\ 0, & z_{ij} = 0 \end{cases}, \quad (4.9)$$

where w_{ij} is the number of telemetry locations for individual i allocated to raster cell j , λ_{ij} is the intensity of the Poisson distribution, and z_{ij} is a latent indicator variable that specifies the mixture component from which w_{ij} arises. The mixture component consisting of a point mass at 0 (i.e., when $z_{ij} = 0$) accommodates the large number of instances where $w_{ij} = 0$ (i.e., more 0 values than expected under the Poisson distribution alone; Welsh et al. 1996, Martin et al. 2005). We model the mean as a function of environmental characteristics using

$$\log(\lambda_{ij}) = \mathbf{x}'_{ij}\boldsymbol{\beta}_i, \quad (4.10)$$

where \mathbf{x}_{ij} is a vector of covariates associated with raster cell j . The hierarchical specification is completed with individual- and population-level models:

$$\boldsymbol{\beta}_i \sim \mathcal{N}(\boldsymbol{\mu}_\beta, \Sigma_\beta) \quad (4.11)$$

$$\boldsymbol{\mu}_\beta \sim \mathcal{N}(\mathbf{0}, \sigma_{\mu_\beta}^2 \mathbf{I}), \quad (4.12)$$

where Σ_β and $\sigma_{\mu_\beta}^2 \mathbf{I}$ are the respective covariance matrices. The multiple imputation procedure described in Eqs. 4.6–4.8 is implemented by sampling $g(\mathbf{M}_i^{(k)}) \sim [g(\mathbf{M}_i) | \mathbf{S}_i]$ on the k^{th} iteration of an MCMC algorithm used to estimate the parameters in Eqs. 4.9–4.12, which are subsequently updated conditional on the value for $g(\mathbf{M}_i^{(k)})$ (Hooten et al. 2010 and Hanks et al. 2015). See Appendix C2 for the full model statement, prior specifications, and details regarding model implementation.

We investigated the affect of three covariates on the locations of haul-out sites, namely water depth, biological wave exposure, and shoreline complexity. Bathymetric data in the form of depth soundings from National Oceanic and Atmospheric Administration Electronic Navigation Charts were used to examine the relationship between estimated haul-out site locations and distance to water depth. We converted the depth sounding data (points) to a 100-m resolution raster and calculated the distance from each cell in \mathcal{S} to the closest raster cell with water depth 20 m or greater (Montgomery et al. 2007). All distances were calculated as least-cost distance such that measurements were made exclusively through the water, thereby reflecting distances ‘as the seal swims’ (distance measurements did not cross land; Dijkstra 1959). Biological wave exposure, obtained from ShoreZone aerial surveys, was used to determine whether harbor seals selected certain exposures more than others. Biological wave exposure is assigned based on the presence and abundance of coastal biota that have known wave energy tolerances (Harper and Morris 2014). We combined the 6 biological wave exposure categories into 2 broader classes: protected (very protected, protected, and moderately protected categories) and exposed (very exposed, exposed, and moderately exposed categories). Biological wave exposure is considered a better index of exposure than physical wave exposure, which is based on fetch and coastal geomorphology (Harper and Morris 2014). We calculated shoreline complexity as the number of raster cells in \mathcal{S} within 5 km of a focal cell. Thus, raster cells surrounded by neighborhoods consisting of more circuitous sections of shoreline have higher values for shoreline complexity. All inference was based on 100,000 MCMC iterations after convergence.

4.2.5 Temporal patterns in haul-out use

We obtained individual- and population-level inference concerning temporal patterns in haul-out use with a hierarchical model that accommodates the simultaneous analysis of multiple individuals (Gelman and Hill 2007). Specifically, we modeled the behavioral data using binary regression as

$$y_i(t) \sim \text{Bernoulli}(\psi_i(t)), \quad (4.13)$$

where $y_i(t)$ is the haul-out status of individual i at time t and $\psi_i(t)$ is the corresponding probability of being hauled-out. We used the probit link to relate $\psi_i(t)$ to environmental conditions:

$$\psi_i(t) = \Phi(\mathbf{u}_i(t)' \boldsymbol{\gamma}_i), \quad (4.14)$$

where $\mathbf{u}_i(t)$ are covariates measured at time t , $\boldsymbol{\gamma}_i$ are the corresponding individual-level coefficients, and Φ is the standard normal cumulative distribution function. In contrast to the more common logit link used in logistic regression, the probit link streamlines computation when fitting the model using MCMC (Albert and Chib 1993, Hooten et al. 2003, Johnson et al. 2013, Dorazio and Rodriguez 2012). The individual-level parameters were further modeled using

$$\boldsymbol{\gamma}_i \sim \mathcal{N}(\boldsymbol{\mu}_\gamma, \boldsymbol{\Sigma}_\gamma) \quad (4.15)$$

$$\boldsymbol{\mu}_\gamma \sim \mathcal{N}(\mathbf{0}, \sigma_{\mu_\gamma}^2 \mathbf{I}), \quad (4.16)$$

where $\boldsymbol{\mu}_\gamma$ is a population-level parameter that represents the average affect across all individuals, and $\boldsymbol{\Sigma}_\gamma$ and $\sigma_{\mu_\gamma}^2$ are the respective variance-covariance matrices. The full model statement and details pertaining to model implementation are provided in Appendix C3.

Previous studies indicated that temporal patterns in haul-out use are influenced by behaviors (e.g., breeding and foraging), physiological functions (e.g., thermoregulation and molting), and environmental conditions (e.g., tidal state) that operate at varying time scales (Boveng et al. 2003, London et al. 2012). Consequently, we examined the affect of the following covariates on harbor seal haul-out use: the number of hours since solar noon (i.e., 13:00 hours near Kodiak Island), the number hours since low tide, the number of days since August 15, and the quadratic effect associated with days since August 15. August 15 is approximately the beginning of the annual molting period in Alaska when harbor seals are most likely to be hauled out (Calambokidis et al. 1987, Boveng et al. 2003). Tide information was obtained from the National Oceanic and Atmospheric Administration water level monitoring stations nearest the locations of monitored seals (Kodiak Island, Station ID: 9457292 and SW Terror Bay, Station ID: 9457493). Inference was based on 100,000 MCMC samples from the posterior distributions after convergence.

4.3 RESULTS

4.3.1 *Harbor seal telemetry data*

Twelve harbor seals were telemetered near Kodiak Island between October 1994 and June 1996, including 6 males and 6 females (Appendices C.4 and C.5). The age composition of harbor seals at the time of capture included 7 adults, 3 subadults, and 2 pups. The average duration seals were monitored was 183 days (range: 76, 261 days), the average number of telemetry locations per individual was 760 (range: 301, 1460 locations), and the average time elapsed between telemetry locations was 5.8 hours (range: 0, 499 hours). On average,

37% of locations were recorded while an individual was hauled-out of the water (range: 17, 61%).

Overall, 82% of the telemetry locations belonged to the Argos location quality classes that typically have the largest locational errors (classes 0, A, and B). Poor quality location classes were more likely to be associated with telemetry locations recorded while a harbor seal was at-sea and higher quality location classes were more often associated with telemetry locations recorded while a harbor seal was hauled-out. For example, 65% of at-sea locations belonged to Argos location classes A and B, whereas only 35% of locations recorded while a harbor seal was hauled-out of the water belonged to the same classes. Conversely, 31% of telemetry locations recorded while a harbor seal was hauled-out belonged to the highest quality location classes (3, 2, and 1); only 12% of at-sea telemetry locations belonged to these higher quality classes.

4.3.2 Haul-out site location estimation

Inference concerning the intensity of haul-out site use (i.e., $\mu_i(t)$) for all 12 harbor seals is summarized in Figure 4.2. High posterior probability of haul-out use typically occurred in inlets and bays that were isolated from the open ocean (Figs. 4.2b–4.2d). One exception, however, was a subadult female that had high posterior probability of hauling-out on an islet at the southeast corner of Kodiak Island, a location that is adjacent to the Gulf of Alaska (Fig. 4.2e). Inference concerning haul-out use for each individual harbor seal is presented in Appendix C4, and estimates for parameters in the observation model (i.e., parameters related to Argos telemetry error and animal movement) are presented in Appendix C5.

4.3.3 Haul-out site selection

Individual-level coefficients indicate a highly heterogeneous response to distance to 20-m bathymetric depth and shoreline complexity, and responses were not consistent among individuals within sex or age classes (Fig. 4.3). Inference concerning μ_β , the population-level parameters, reflect this heterogeneity and suggest the individual harbor seals we examined lacked a common behavior relative to these two covariates (i.e., 95% credible intervals overlap 0; Fig. 4.3).

We were unable to evaluate the affect of wave exposure on haul-out site selection for most individuals due to complete separation in the counts w_{ij} and the two exposure categories (Albert and Anderson 1984, Hefley and Hooten 2015). Complete separation occurred when all instances of $w_{ij} > 0$ (or $w_{ij} = 0$) for an individual were allocated to one of the exposure categories (protected or exposed), resulting in Markov chains that exhibited poor mixing and failed convergence. Instances of $w_{ij} > 0$ were allocated exclusively to the “protected” category for 6 individuals, whereas all instances of $w_{ij} > 0$ were allocated to the “exposed” category for 1 individual (shown in Fig. 4.2e). A model of the subset of 5 individuals for which complete separation did not occur indicated that haul-out site selection was negatively affected by “exposed” shorelines for 3 individuals; the remaining 2 individuals exhibited no effect for this covariate (Appendix C6). Furthermore, the average affect of “exposed” shoreline was negative for these 5 harbor seals (95% CI for μ_β : -4.55,-0.20).

4.3.4 Temporal patterns in haul-out use

The affect of environmental conditions (time of day, time since low tide, and day of year) on temporal patterns of haul-out use were highly heterogeneous among the 12 harbor seals

we examined (Fig. 4.4). A consistent pattern among individuals within sex or age classes was also not evident (Fig. 4.4). Inference for parameters related to day of year was highly uncertain and 95% credible intervals for most individuals included 0. Inference concerning the population-level parameters reflect the individual-level heterogeneity and show that a common effect across individuals was generally lacking (i.e., 95% credible intervals for μ_γ overlap 0; Fig. 4.4), although there appears to be a weak negative effect for the covariate hours since solar noon (95% CI: -0.37, 0.04).

4.4 DISCUSSION

We combined a previously collected Argos satellite telemetry dataset with a fully model-based framework to examine the spatio-temporal behavior associated with harbor seal haul-out sites on Kodiak Island, Alaska. We adopted a recently developed approach to estimate the location of haul-out sites that rigorously accommodates large telemetry location error and animal movement (Brost et al., in press). We also extended existing methods for examining temporal patterns in central place use to accommodate the simultaneous analysis of multiple individuals and obtain population-level inference (i.e., μ_γ). Our methods are general and can be applied to various types of telemetry data collected on terrestrial or marine species.

We augmented the modeling framework to quantify the affect of environmental characteristics on the location of central places. Our approach uses a multiple imputation procedure that allows the individual-level coefficients (i.e., β_i) to reflect uncertainty in the estimated location of the central places (Hooten et al. 2010, Hanks et al. 2011, Hanks et al. 2015). Inference concerning individual-level parameters is statistically upscaled to obtain population-level inference (μ_β) describing the average effect across individuals.

Our analysis couples positional data with behavioral (wet/dry) data to help inform a model of haul-out site location estimation. We could have also formulated a simpler model by exclusively using telemetry locations collected while harbor seals were hauled-out of the water (i.e., $y_i(t) = 1$) and uncertainty due to animal movement does not degrade inference; however, nearly two-thirds of the locations in our data set were recorded while individuals were at sea (i.e., $y_i(t) = 0$). These “at-sea” locations contain valuable information concerning the true location of the haul-out sites, making it important to incorporate both behavioral states using a two-part observation model that explicitly accounts for animal movement. Other behavioral information, such as accelerometer data, could also be used to partition when individuals were using coastal versus at-sea resources, or the model can be adapted to situations when no such ancillary data are available (e.g., Brost et al., in press).

4.4.1 *Harbor seal haul-out behavior*

Almost all existing information concerning the location of harbor seal haul-out sites in Alaska has been acquired from aerial surveys of haul-out groups that are typically conducted during the molting season in August and September (Boveng et al. 2003, Small et al. 2003, Ver Hoef and Frost 2003). Satellite telemetry data, collected throughout the full annual cycle, provide an opportunity to learn about the location of haul-out sites used at other times of year. Our results suggest that harbor seals favor haul-out sites in isolated bays and inlets (Fig. 4.2); however, one harbor seal in our study used a haul-out site on an islet adjacent to the open water of the Gulf of Alaska (Fig. 4.2e). Locations determined to have high posterior probability of haul-out use in our study match the locations of haul-out sites observed during aerial surveys conducted between 1993 and 2001 (see haul-out sites 7–10

in Fig. 4 of Small et al. 2003 and Fig. 1 of Boveng et al. 2003), serving as an informal evaluation of the methodology we used.

We are aware of only one previous study that examined the relationship between environmental variables and the selection of haul-out sites by harbor seals. Montgomery et al. (2007) used counts of harbor seals obtained from aerial surveys to model terrestrial habitat use in Cook Inlet, a 20,000 km² tidal estuary that opens into the Gulf of Alaska < 100 km north of Kodiak Island. They found that abundance of harbor seals was negatively related to distance to Cook Inlet communities, bathymetric depths of 20 m, and anadromous fish streams, and that harbor seals tended to use haul-out sites with a rock substrate. Montgomery et al. (2007) also examined wave exposure but did not find evidence supporting an effect for this covariate. Our results do not indicate an effect of proximity to a bathymetric depth of 20 m and show a highly heterogeneous response to shoreline complexity (Fig. 4.3). Half of the harbor seals in our analysis exhibited complete separation such that estimated locations of haul-out sites only occurred on “protected” shoreline. This relationship could be coincidental or reflect selection for “protected” shorelines. An analysis of the subset of harbor seals for which complete separation did not occur revealed that 3 of 5 individuals selected against “exposed” shorelines (Appendix C6). The areas in which seals were monitored for this study are isolated from the human communities on Kodiak Island, do not contain substantial variation in shoreline substrate (the majority of shoreline was sedimentary or of mixed types as determined by ShoreZone aerial surveys), and data concerning seasonal variation in prey availability were lacking. Therefore, we did not examine the affect of communities, shoreline substrate, or proximity to fish streams on haul-out use.

Several studies have used counts of harbor seal haul-out groups to investigate patterns in haul-out use at multiple temporal scales. At daily time scales, the highest proportion of seals

onshore are typically observed at times near low tides when favorable haul-outs are exposed (e.g., sites isolated from terrestrial predators; Schneider and Payne 1983, Pauli and Terhune 1987) and during midday when the air temperature is most conducive to thermoregulation (Stewart 1984, Calambokidis et al. 1987, Pauli and Terhune 1987; see London et al. 2012 for an exception to these patterns). At annual time scales, temporal patterns in haul-out use are influenced by breeding and molting cycles that can be sex- and age-specific (e.g., adult females nurse pups onshore, pups do not molt, etc.; Everitt and Braham 1980, Brown and Mate 1983, Calambokidis et al. 1987, Huber et al. 2001, Jemison and Kelly 2001, Boveng et al. 2003, Daniel et al. 2003), as well as the distribution and availability of prey. Our results do not show a consistent affect of environmental conditions on haul-out behavior and thus do not corroborate the conclusions of these earlier studies (Fig. 4.4); however, haul-out behavior is known to vary regionally because seals likely adapt their behavior to local conditions (Simpkins et al. 2003). Patterns related to sex and age class were also not evident in our study, although our analysis of 12 individuals was limited in terms of revealing demographic effects.

4.4.2 Conclusion

Satellite telemetry data provide an important source of animal distribution information and are commonly used to quantify resource selection (Johnson et al. 2008b, Johnson et al. 2013), examine movements (Jonsen et al. 2003, Johnson et al. 2008a, McClintock et al. 2012), and delineate home ranges (Kie et al. 2010). These data also contain information concerning another key aspect of an animal's habitat use, namely the behavior associated with locations that are used repeatedly through time, such as dens, nests, roosts, and rendezvous sites (Anderson and Lindzey 2003, Knopff et al. 2009, Brost et al., in press). As

demonstrated in this paper, examining the spatio-temporal behavior associated with these central places by coupling satellite telemetry data with a model-based approach that rigorously accommodates multiple sources of uncertainty is possible.

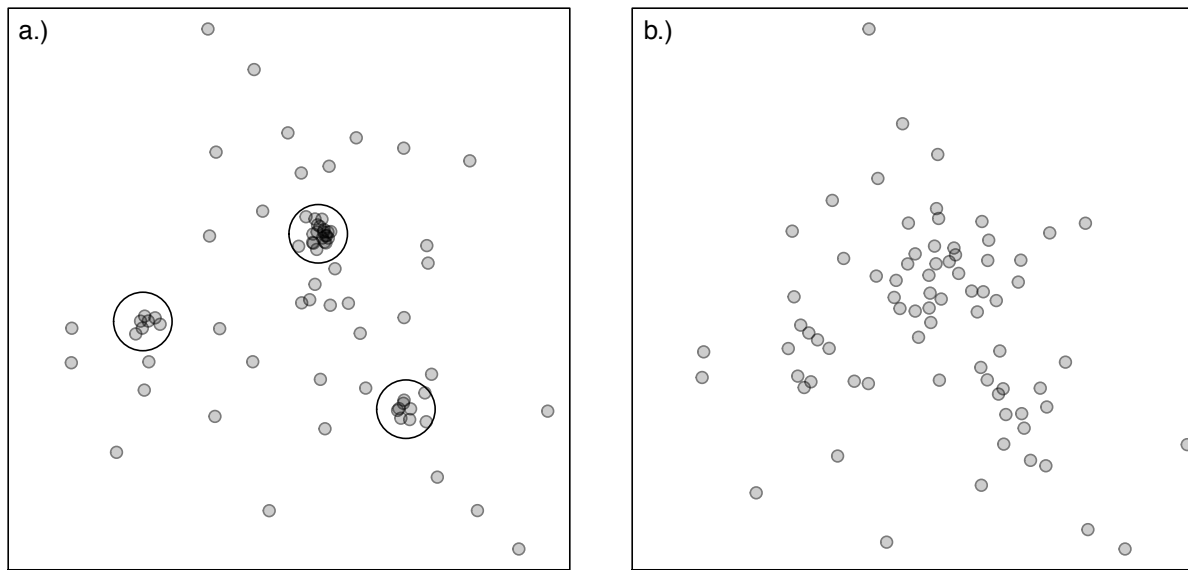


FIGURE 4.1. Simulation demonstrating the signal of central place behavior in telemetry location data (gray closed circles). (a) When telemetry location error is small, clusters of locations (large black open circles) indicate the location of central places. (b) When telemetry location error is large, the number and location of central places is much less certain. The locations shown in (b) are the same as those shown in (a) but with additional error.

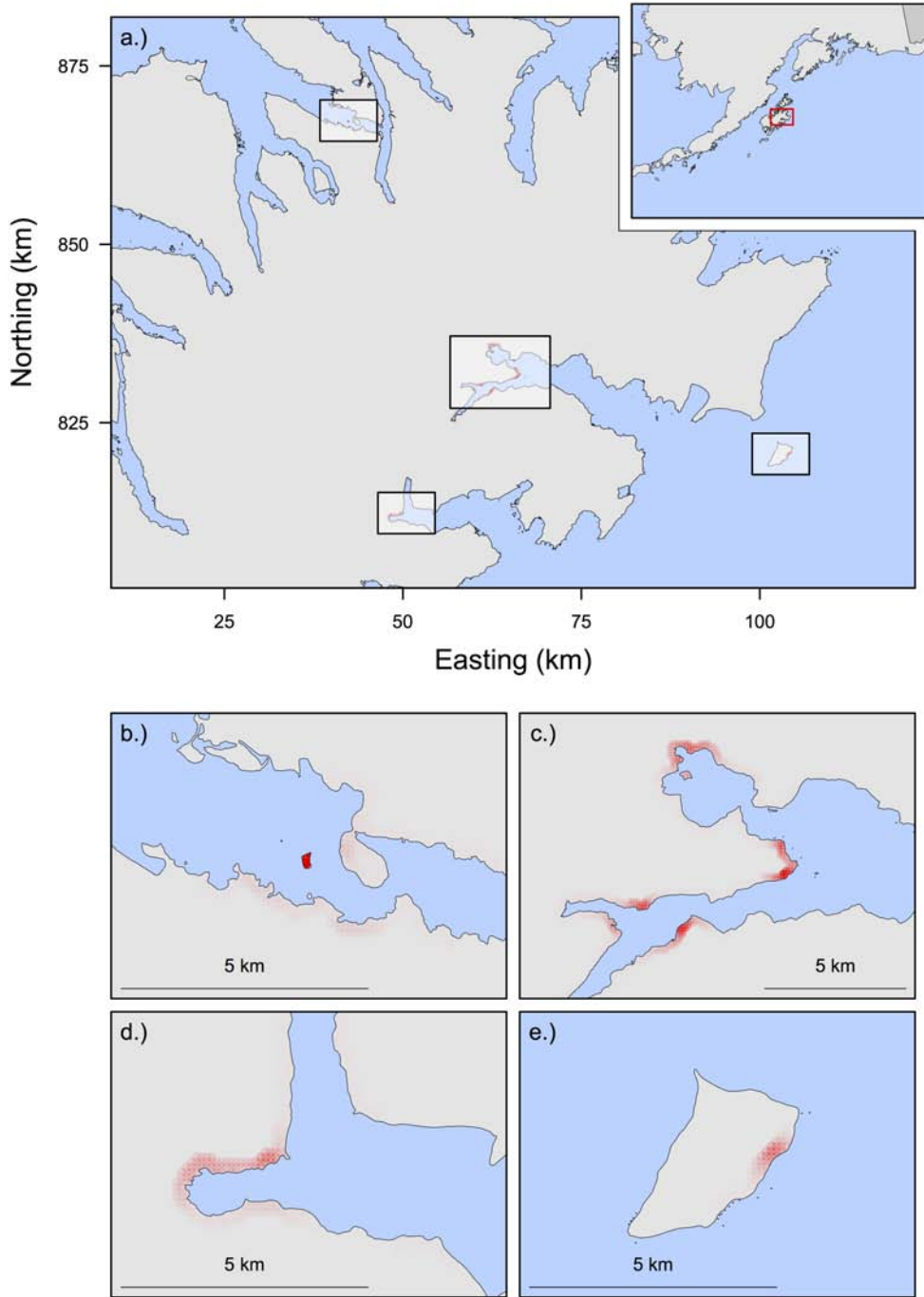


FIGURE 4.2. Posterior distribution of $\mu_i(t)$ (red gradient) for 12 harbor seals telemetered near Kodiak Island, Alaska (a); brighter red corresponds to higher posterior probability. Gray segments of shoreline either have very low or no posterior probability of haul-out use. The inset in the top right shows the location of Kodiak Island and inset (a) (red box) within the state of Alaska, USA (light gray). Boxes in (a) reflect the location of insets (b)–(e) where high posterior probability of $\mu_i(t)$ occurs. The posterior distribution for each individual harbor seal is presented in Appendix C4.

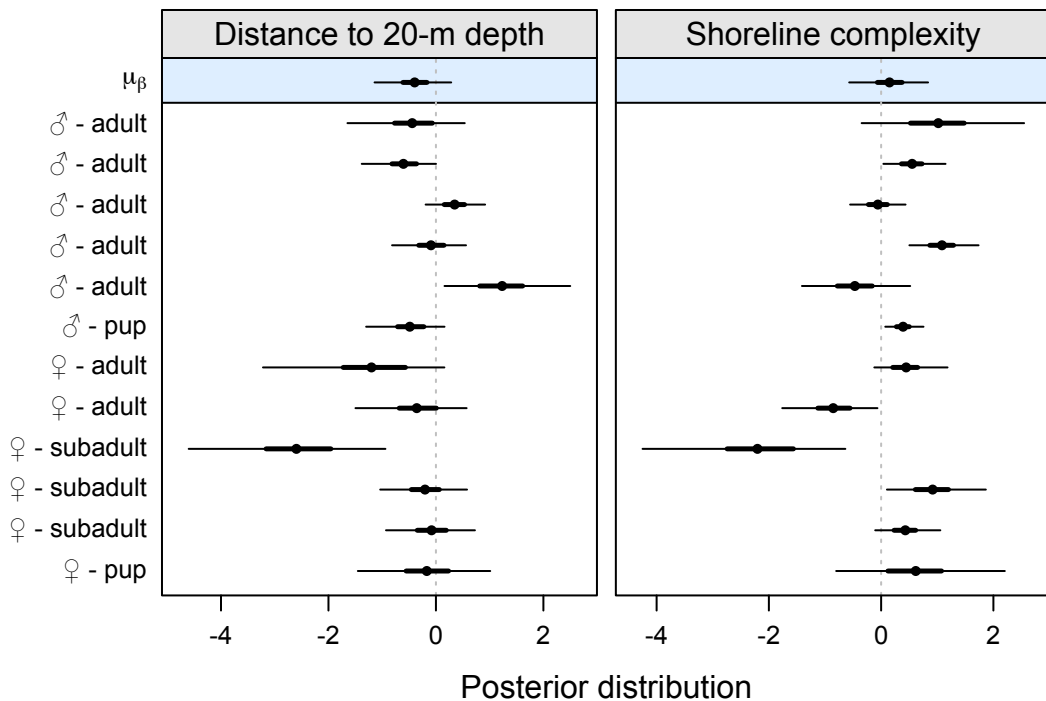


FIGURE 4.3. Individual- and population-level inference concerning parameters examined in the haul-out site selection model. The top row (blue box) represents inference concerning the population-level parameter (μ_β) that represents an average affect across the 12 harbor seals analyzed. The remaining rows show individual-level parameters (β_i), and individual seals are labeled according their sex and age class. The points indicate the posterior mean, the thick lines represent the 50% credible interval, and the thin lines represent the 95% credible interval.

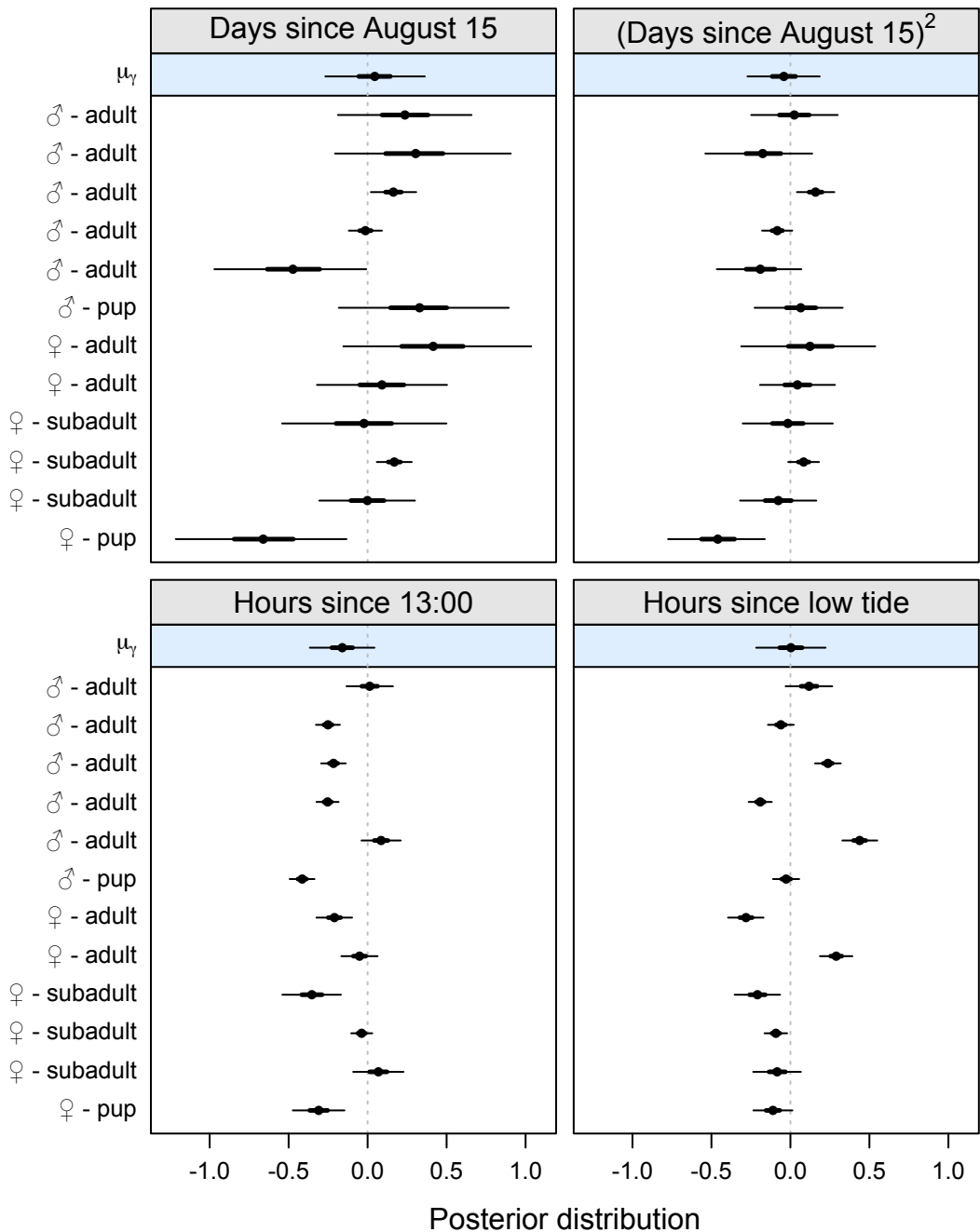


FIGURE 4.4. Individual- and population-level inference concerning parameters examined in the temporal haul-out use model. The top row (blue box) represents inference concerning the population-level parameter (μ_γ) that represents an average affect across the 12 harbor seals analyzed. The remaining rows show individual-level parameters (γ_i), and individual seals are labeled according their sex and age class. The points indicate the posterior mean, the thick lines represent the 50% credible interval, and the thin lines represent the 95% credible interval.

CHAPTER FIVE

Conclusion

The research presented in this dissertation pairs existing Argos satellite telemetry data with contemporary spatio-temporal modeling to quantify harbor seal resource selection and space use in the coastal waters of southern Alaska. Information concerning harbor seal space use and habitat requirements is necessary for assessing the impact of human activities, identifying environmentally sensitive areas, understanding factors that affect population trends (e.g., condition and survival), improving population monitoring programs, and developing effective management strategies for maintaining populations in conjunction with subsistence harvest and commercial fisheries.

Recent methodological advancements address difficulties in the analysis of telemetry data such as temporally autocorrelated observations; however, multiple additional factors complicate the analysis of the harbor seal telemetry data. For example, difficulties introduced by large telemetry location error, complicated error structures, and barriers to animal movement can weaken inference. In addition to developing models that explicitly address these difficulties, obtaining statewide inference concerning harbor seal space use was a central goal of my research. Indeed, the rich harbor seal telemetry data sets collected by the Alaska Department of Fish and Game offer a unique opportunity to examine the spatial ecology of harbor seals from Bristol Bay to the panhandle of southeastern Alaska; however, the difficulties mentioned above make comprehensive analyses of the harbor seal telemetry data particularly challenging, and my work focused on computationally feasible applications to regional groups of harbor seals (e.g., harbors seal monitored near Kodiak Island). Conse-

quently, the primary contributions from this dissertation are novel methods for addressing nuances in telemetry data and obtaining reliable inference concerning harbor seal spatial ecology.

In this concluding chapter, I discuss some of the themes common to the work performed in Chapters 2–4. I then discuss some of the challenges encountered while performing this work, and potential avenues going forward to obtain rigorous, statewide inference concerning harbor seal spatial ecology.

5.1 OVERARCHING THEMES

Each core chapter of this dissertation features a hierarchical model designed to account for various nuances related to animal telemetry data and the behavior of harbor seals. Hierarchical models are commonplace in statistics (Gelman and Hill 2007, Gelman et al. 2014) and are becoming increasingly prevalent in the field of ecology (Royle and Dorazio 2008, Zuur et al. 2009, Hobbs and Hooten 2015, Kery and Royle 2016). For example, hierarchical models are often used to specify overdispersion, accommodate dependence in repeated measurements taken on the same individual or at the same location, and accurately account for uncertainty in prediction and estimation (Gelman and Hill 2007). Some of the most common models in ecology are hierarchical models that formally deal with imperfect observations and provide inference concerning some unobservable state of interest, such as true species occurrence or abundance (e.g., occupancy and N -mixture models; MacKenzie et al. 2002, Tyre et al. 2003, Royle 2004).

The hierarchical models developed in this dissertation also provide inference on a latent state of interest, namely the true location of individual harbor seals, while accounting for imperfect observations. In many cases, observed Argos satellite telemetry locations are more

than 10 km or even 100 km from the corresponding true harbor seal locations (Costa et al. 2010, Douglas et al. 2012, Brost et al. 2015). When ignored, telemetry measurement error can interact with environmental heterogeneity to bias inferences on species-habitat relationships and disguise true patterns in animal space use (Visscher 2006, Johnson and Gillingham 2008, Hefley et al. 2014, Brost et al. 2015). The hierarchical point process model and Dirichlet process mixture models presented in Chapters 2–4 properly account for uncertainty and provide reliable inference concerning the spatial ecology of harbor seals, even though the magnitude of Argos telemetry location error often exceeds the extent of typical harbor seal movements (Lowry et al. 2001).

Although discrete- and continuous-time movement models are often formulated as hierarchical models (e.g., McClintock et al. 2012, McClintock et al. 2013, Buderman et al. 2016), to my knowledge Chapter 2 presents the first point process model applied to animal telemetry data that accounts for non-Gaussian telemetry measurement error. Indeed, a similar hierarchical construction could be used to extend resource selection functions and species distribution models to account for locational error in a model-based framework (Hefley and Hooten 2016).

Another overarching theme is that the models developed here explicitly accommodate constraints to animal movement. In Chapter 2, which focuses on the aquatic space use and resource selection of harbor seals, estimated true harbor seal locations are constrained to be exclusively within the marine environment. The focus shifts to the terrestrial space use and haul-out site selection of harbor seals in Chapters 3 and 4. Accordingly, the estimated locations of haul-out sites are constrained to occur along the coastline in these chapters. Appropriate models for true harbor seal locations require versatile routines for parameter estimation, like the Markov chain Monte Carlo algorithms used throughout this dissertation

for incorporating custom, highly irregular probability distributions that accurately reflect aquatic and terrestrial constraints.

Some discrete-time movement models use a “mask” to constrain estimated true animal locations to occur within some spatial domain (Sumner et al. 2009, McClintock et al. 2012); however, these models assume movements between consecutive locations are Euclidean. Realistically, though, animal movements are constrained to occur within the same domain in which the true locations must exist. The model presented in Chapter 2 is unique in that movements are calculated “as the seal swims.” In other words, distances between estimated true harbor seal locations are non-Euclidean and measured exclusively through the marine environment. The models presented in this dissertation also use constraints to movement, and the subsequent discrepancy between the support of the true harbor seal locations and the observed telemetry locations, to simultaneously estimate and account for telemetry location error. Spatial constraints can similarly be used to account for locational uncertainty in species distribution models (Hefley et al., in review).

5.2 FUTURE DIRECTIONS

Like any other scientific endeavor, there is much research on harbor seal spatial ecology yet to be done. Comprehensive analyses of the existing Argos satellite telemetry data sets to obtain inference concerning the aquatic space use of harbor seals across the entire state of Alaska is a high priority. Rigorous inference concerning aquatic space use requires techniques that deal with the same difficulties addressed throughout this dissertation, namely large telemetry locational error, complicated error structures, temporally autocorrelated observations, and constraints to harbor seal movement. Indeed, given that maps of 2-dimensional

space use are by-products of the resource selection modeling framework presented in Chapter 2, a similar model could be used to accomplish this objective.

A key asset of the current resource selection modeling framework is also its primary downfall. Modeling the animal movement process subject to movement constraints reflects an important aspect of harbor seal biology, but calculating swim distances is computationally expensive. Simplifying the existing model such that telemetry locations are treated as independent observations (i.e., by not modeling the autocorrelated animal movement process) would permit a large-scale, statewide analysis of the harbor seal telemetry data; however, modeling the animal movement process allows high quality telemetry locations (small locational error) to inform estimates corresponding to the poor quality telemetry locations (large locational error). Considering poor quality observed locations comprise > 75% of the harbor seal telemetry data, ignoring the movement process would likely yield spurious inferences. Explicitly modeling the movement process also helps meet critical statistical assumptions. Thus, appropriately modeling movement is vital for characterizing harbor seal space use.

Coupling the current resource selection modeling framework with more advanced computing techniques, such as swim distance calculations that use so-called graphics processing units and cloud computing (e.g., Amazon Web Services), could facilitate a more comprehensive analysis of the harbor seal telemetry data sets; however, model fitting would ideally require no more than a standard personal computer. Perhaps the most promising options going forward, then, will rely on methods for sidestepping the computationally demanding swim distance calculations. For example, one approach might be to interpolate true harbor seal locations at a high temporal frequency in the model fitting and estimation process. Given the temporal resolution of the interpolated locations, assuming straight-line, Euclidean movements in the augmented data set may roughly conform to the spatial support of the

marine environment and approximate the more complex swim distances. Such an approach would trade one computationally demanding procedure (i.e., calculating swim distances) for another (i.e., interpolating many locations), although fast computing languages like C++ may make this a practical option. Another option could be to “warp” the non-Euclidean support of real-life harbor seal movements to create an “artificial” 2- or 3-dimensional space in which Euclidean distances approximate the original swim distances. This approach would require a one-time startup cost of calculating swim distances between all pairs of points in the original non-Euclidean domain, followed by a transformation (e.g., using non-metric multidimensional scaling) to create the new Euclidean space (Borg and Groenen 2005, Manly 2005). Clever indexing could facilitate translation between the two domains, and thus a unified model implementation could be conducted that properly account for uncertainty. These are a few preliminary approaches that require further vetting to assess practicality.

Despite the magnitude of the task, a statewide analysis of harbor seal space use may soon be within reach. Considerable progress has been made toward obtaining reliable inference concerning the spatial ecology of harbor seals while addressing common problems encountered in animal telemetry analyses using rigorous, model-based approaches; however, the research initiated in this dissertation is ongoing and there is potential for improvement. This dissertation serves as a foundation for new innovative ideas that will make comprehensive analyses of the rich telemetry data sets available for harbor seals in Alaska more accessible.

BIBLIOGRAPHY

- Aarts, G., J. Fieberg, and J. Matthiopoulos. 2012. Comparative interpretation of count, presence-absence and point methods for species distribution models. *Methods in Ecology and Evolution* **3**:177–187.
- Aarts, G., M. MacKenzie, B. McConnell, M. Fedak, and J. Matthiopoulos. 2008. Estimating space-use and habitat preference from wildlife telemetry data. *Ecography* **31**:140–160.
- Albert, A., and J. A. Anderson. 1984. On the existence of maximum likelihood estimates in logistic regression models. *Biometrika* **71**:1–10.
- Albert, J. H., and S. Chib. 1993. Bayesian analysis of binary and polychotomous response data. *Journal of the American Statistical Association* **88**:669–679.
- Anderson, C. R., and F. G. Lindzey. 2003. Estimating cougar predation rates from GPS location clusters. *The Journal of Wildlife Management* **67**:307–316.
- Atkinson, S., D. Crocker, D. Houser, and K. Mashburn. 2015. Stress physiology in marine mammals: how well do they fit the terrestrial model? *Journal of Comparative Physiology B* **185**:463–486.
- Baldwin, R. A., and L. C. Bender. 2008. Den-site characteristics of black bears in Rocky Mountain National Park, Colorado. *The Journal of Wildlife Management* **72**:1717–1724.
- Berger, J. O., B. Liseo, and R. L. Wolpert. 1999. Integrated likelihood methods for eliminating nuisance parameters. *Statistical Science* **14**:1–22.
- Blackwell, P. G. 2003. Bayesian inference for Markov processes with diffusion and discrete components. *Biometrika* **90**:613–627.
- Blakesley, J., A. Franklin, and R. Gutiérrez. 1992. Spotted owl roost and nest site selection in northwestern California. *The Journal of Wildlife Management* **56**:388–392.

- Blundell, G. M., and G. W. Pendleton. 2008. Estimating age of harbor seals (*Phoca vitulina*) with incisor teeth and morphometrics. *Marine Mammal Science* **24**:577–590.
- Blundell, G. M., and G. W. Pendleton. 2015. Factors affecting haul-out behavior of harbor seals (*Phoca vitulina*) in tidewater glacier inlets in Alaska: can tourism vessels and seals coexist? *PLoS ONE* **10**:e0125486.
- Borg, I., and P. J. F. Groenen. 2005. Modern multidimensional scaling theory and applications. Springer, New York.
- Boveng, P., J. Bengtson, D. Withrow, J. Cesarone, M. Simpkins, K. Frost, and J. Burns. 2003. The abundance of harbor seals in the Gulf of Alaska. *Marine Mammal Science* **19**:111–127.
- Boveng, P. L., and H. Ziel, 2015. Alaska harbor seal research plan. National Marine Fisheries Service, National Oceanic and Atmospheric Association.
- Braham, H. W., R. D. Everitt, and D. J. Rugh. 1980. Northern sea lion population decline in the eastern Aleutian Islands. *The Journal of Wildlife Management* **44**:25–33.
- Breed, G. A., D. P. Costa, M. E. Goebel, and P. W. Robinson. 2011. Electronic tracking tag programming is critical to data collection for behavioral time-series analysis. *Ecosphere* **2**:art10.
- Brigham, R. M., M. J. Vonhof, R. M. R. Barclay, and J. C. Gwilliam. 1997. Roosting behavior and roost-site preferences of forest-dwelling California bats (*Myotis californicus*). *Journal of Mammalogy* **78**:1231–1239.
- Brost, B. M., and P. Beier. 2012. Use of land facets to design linkages for climate change. *Ecological Applications* **22**:87–103.

- Brost, B. M., M. B. Hooten, E. M. Hanks, and R. J. Small. 2015. Animal movement constraints improve resource selection inference in the presence of telemetry error. *Ecology* **96**:2590–2597.
- Brost, B. M., M. B. Hooten, and R. J. Small. In press. Leveraging constraints and biotelemetry data to pinpoint repetitively used spatial features. *Ecology* .
- Brown, R., and B. Mate. 1983. Abundance, movements, and feeding habits of harbor seals, *Phoca vitulina*, at Netarts and Tillamook Bays, Oregon. *Fishery Bulletin* **81**:291–301.
- Buderman, F., M. Hooten, J. Ivan, and T. Shenk. 2016. A functional model for characterizing long-distance movement behaviour. *Methods in Ecology and Evolution* **7**:264–273.
- Calambokidis, J., B. L. Taylor, S. D. Carter, G. H. Steiger, P. K. Dawson, and L. D. Antrim. 1987. Distribution and haul-out behavior of harbor seals in Glacier Bay, Alaska. *Canadian Journal of Zoology* **65**:1391–1396.
- Cargnelutti, B., A. Coulon, A. J. M. Hewison, M. Goulard, J. Angibault, and N. Morellet. 2007. Testing global positioning system performance for wildlife monitoring using mobile collars and known reference points. *Journal of Wildlife Management* **71**:1380–1387.
- Chevallier, D., Y. Maho, P. Brossault, F. Baillon, and S. Massemin. 2010. The use of stopover sites by Black Storks (*Ciconia nigra*) migrating between West Europe and West Africa as revealed by satellite telemetry. *Journal of Ornithology* **152**:1–13.
- Ciarniello, L. M., M. S. Boyce, D. C. Heard, and D. R. Seip. 2005. Denning behavior and den site selection of grizzly bears along the Parsnip River, British Columbia, Canada. *Ursus* **16**:47–58.

- Cordes, L. S., C. D. Duck, B. L. Mackey, A. J. Hall, and P. M. Thompson. 2011. Long-term patterns in harbour seal site-use and the consequences for managing protected areas. *Animal Conservation* **14**:430–438.
- Costa, D. P., P. W. Robinson, J. P. Y. Arnould, A.-L. Harrison, S. E. Simmons, J. L. Hassrick, A. J. Hoskins, S. P. Kirkman, H. Oosthuizen, S. Villegas-Amtmann, and D. E. Crocker. 2010. Accuracy of Argos locations of Pinnipeds at-sea estimated using Fastloc GPS. *PLoS ONE* **5**:e8677.
- Cunningham, L., J. M. Baxter, I. L. Boyd, C. D. Duck, M. Lonergan, S. E. Moss, and B. McConnell. 2009. Harbour seal movements and haul-out patterns: implications for monitoring and management. *Aquatic Conservation: Marine and Freshwater Ecosystems* **19**:398–407.
- da Silva, J., and J. M. Terhune. 1988. Harbour seal grouping as an anti-predator strategy. *Animal Behaviour* **36**:1309–1316.
- Daniel, R., L. Jemison, G. Pendleton, and S. Crowley. 2003. Molting phenology of harbor seals on Tugidak Island, Alaska. *Marine Mammal Science* **19**:128–140.
- DeMaster, D. P., A. W. Trites, P. Clapham, S. Mizroch, P. Wade, R. J. Small, and J. M. Ver Hoef. 2006. The sequential megafaunal collapse hypothesis: Testing with existing data. *Progress in Oceanography* **68**:329–342.
- Diggle, P. J., R. Menezes, and T. Su. 2010. Geostatistical inference under preferential sampling. *Journal of the Royal Statistical Society: Series C (Applied Statistics)* **59**:191–232.
- Dijkstra, E. 1959. A note on two problems in connexion with graphs. *Numerische Mathematik* **1**:269–271.

- Dorazio, R. M. 2012. Predicting the geographic distribution of a species from presence-only data subject to detection errors. *Biometrics* **68**:1303–1312.
- Dorazio, R. M., B. Mukherjee, L. Zhang, M. Ghosh, H. L. Jelks, and F. Jordan. 2008. Modeling unobserved sources of heterogeneity in animal abundance using a Dirichlet process prior. *Biometrics* **64**:635–644.
- Dorazio, R. M., and D. T. Rodríguez. 2012. A Gibbs sampler for Bayesian analysis of site-occupancy data. *Methods in Ecology and Evolution* **3**:1093–1098.
- Douglas, D. C., R. Weinzierl, S. C. Davidson, R. Kays, M. Wikelski, and G. Bohrer. 2012. Moderating Argos location errors in animal tracking data. *Methods in Ecology and Evolution* **3**:999–1007.
- Everitt, R., and H. W. Braham. 1980. Aerial survey of Pacific harbor seals in the southeastern Bering Sea. *Northwest Science* **54**:281–288.
- Ferguson, T. 1973. A Bayesian analysis of some nonparametric problems. *Statistica Sinica* **1**:209–230.
- Fieberg, J., J. Matthiopoulos, M. Hebblewhite, M. S. Boyce, and J. L. Frair. 2010. Correlation and studies of habitat selection: problem, red herring or opportunity? *Philosophical Transactions of the Royal Society B* **365**:2233–2244.
- Finley, A., S. Banerjee, and A. Gelfand. 2015. spBayes for large univariate and multivariate point-referenced spatio-temporal data models. *Journal of Statistical Software* **63**:1–28.
- Fisher, H. D. 1952. The status of the harbour seal in British Columbia, with particular reference to the Skeena River **93**:
- Forester, J. D., H. K. Im, and P. J. Rathouz. 2009. Accounting for animal movement in estimation of resource selection functions: sampling and data analysis. *Ecology* **90**:3554–3565.

- Fowler, C. W., 1982. Interactions of northern fur seals and commercial fisheries. Transactions of the 47th North American Wildlife and Natural Resources Conference.
- Frair, J. L., J. Fieberg, M. Hebblewhite, F. Cagnacci, N. J. DeCesare, and L. Pedrotti. 2010. Resolving issues of imprecise and habitat-biased locations in ecological analyses using GPS telemetry data. *Philosophical Transactions of the Royal Society B* **365**:2187–2200.
- Freitas, C., C. Lydersen, M. A. Fedak, and K. M. Kovacs. 2008. A simple new algorithm to filter marine mammal Argos locations. *Marine Mammal Science* **24**:315–325.
- Fretwell, S. D., and H. L. Lucas. 1969. On territorial behaviour and other factors influencing habitat distributions in birds. *Acta Biotheoretica* **19**:45–52.
- Frost, K. J., L. F. Lowry, and J. M. Ver Hoef. 1999. Monitoring the trend of harbor seals in Prince William Sound, Alaska, after the Exxon Valdez oil spill. *Marine Mammal Science* **15**:494–506.
- Frost, K. J., M. A. Simpkins, and L. F. Lowry. 2001. Diving behavior of subadult and adult harbor seals in Prince William Sound, Alaska. *Marine Mammal Science* **17**:813–834.
- Gelfand, A. E., and A. F. M. Smith. 1990. Sampling-based approaches to calculating marginal densities. *Journal of the American Statistical Association* **85**:398–409.
- Gelman, A., and J. Hill. 2007. Data analysis using regression and multilevel/hierarchical models. Cambridge University Press.
- Gelman, A., H. S. Stern, D. B. Dunson, A. Vehtari, and D. B. Rubin. 2014. Bayesian data analysis. Chapman & Hall/CRC.
- Gershman, S. J., and D. M. Blei. 2012. A tutorial on Bayesian nonparametric models. *Journal of Mathematical Psychology* **56**:1–12.

- Hanks, E. M., M. B. Hooten, and M. W. Aldredge. 2015. Continuous-time discrete-space models for animal movement. *The Annals of Applied Statistics* **9**:145–165.
- Hanks, E. M., M. B. Hooten, D. S. Johnson, and J. T. Sterling. 2011. Velocity-based movement modeling for individual and population level inference. *PLoS ONE* **6**:e22795.
- Hare, S. R., and N. J. Mantua. 2000. Empirical evidence for North Pacific regime shifts in 1977 and 1989. *Progress in Oceanography* **47**:103–145.
- Harkonen, T., and M. P. Heide-Jorgensen. 1990. Comparative life histories of east Atlantic and other harbor seal populations. *Ophelia* **32**:211–235.
- Harper, J., and M. Morris, 2014. Alaska ShoreZone coastal habitat mapping protocol. Technical report, Bureau of Ocean Energy Management.
- Hartung, J., G. Knapp, and B. Sinha. 2008. Statistical meta-analysis with applications. John Wiley & Sons, Inc.
- Hastie, T., J. H. Friedman, and R. Tibshirani. 2009. The elements of statistical learning data mining, inference, and prediction. Springer, New York.
- Hastings, K. K., K. J. Frost, M. A. Simpkins, G. W. Pendleton, U. G. Swain, and R. J. Small. 2004. Regional differences in diving behavior of harbor seals in the Gulf of Alaska. *Canadian Journal of Zoology* **82**:1755–1773.
- Hefley, T., K. Broms, B. Brost, F. Buderman, S. Kay, H. Scharf, J. Tipton, P. Williams, and M. Hooten. In press. The basis function approach to modeling dependent ecological data. *Ecology* :.
- Hefley, T. J., D. M. Baasch, A. J. Tyre, and E. E. Blankenship. 2014. Correction of location errors for presence-only species distribution models. *Methods in Ecology and Evolution* **5**:207–214.

- Hefley, T. J., B. M. Brost, and M. B. Hooten. In review. Bias correction of bounded locational errors in presence-only data. *Methods in Ecology and Evolution* .
- Hefley, T. J., and M. B. Hooten. 2016. Hierarchical species distribution models. *Current Landscape Ecology Reports* **1**:87–97.
- Herremans, J. K., G. M. Blundell, and M. Ben-David. 2009. Evidence of bottom-up control of diet driven by top-down processes in a declining harbor seal *Phoca vitulina richardsoni* population. *Marine Ecology Progress Series* **374**:287–300.
- Higuchi, H., J. Pierre, V. Krever, V. Andronov, G. Fujita, K. Ozaki, O. Goroshko, M. Ueta, S. Smirensky, and N. Mita. 2004. Using a remote technology in conservation: satellite tracking white-naped cranes in Russia and Asia. *Conservation Biology* **18**:136–147.
- Hjort, N. 2010. Bayesian nonparametrics. Cambridge University Press.
- Hobbs, N. T., and M. B. Hooten. 2015. Bayesian models: A statistical primer for ecologists. Princeton University Press.
- Hoennner, X., S. D. Whiting, M. A. Hindell, and C. R. McMahon. 2012. Enhancing the use of Argos satellite data for home range and long distance migration studies of marine animals. *PLoS ONE* **7**:e40713.
- Holloran, M., and S. Anderson. 2005. Spatial distribution of Greater Sage-Grouse nests in relatively contiguous sagebrush habitats. *The Condor* **107**:742–752.
- Hooten, M. B., F. E. Buderman, B. M. Brost, E. M. Hanks, and J. S. Ivan. 2016. Hierarchical animal movement models for population-level inference. *Environmetrics* **27**:322–333.
- Hooten, M. B., E. M. Hanks, D. S. Johnson, and M. W. Alldredge. 2014. Temporal variation and scale in movement-based resource selection functions. *Statistical Methodology* **17**:82–98.

- Hooten, M. B., and D. S. Johnson. In press. Basis function models for animal movement. *Journal of the American Statistical Association* .
- Hooten, M. B., D. S. Johnson, E. M. Hanks, and J. H. Lowry. 2010. Agent-based inference for animal movement and selection. *Journal of Agricultural, Biological, and Environmental Statistics* **15**:523–538.
- Hooten, M. B., D. S. Johnson, B. T. McClintock, and J. M. Morales. In press. *Animal Movement: Statistical models for telemetry data*. CRC Press/Taylor & Francis Group.
- Hooten, M. B., D. R. Larsen, and C. K. Wikle. 2003. Predicting the spatial distribution of ground flora on large domains using a hierarchical Bayesian model. *Landscape Ecology* **18**:487–502.
- Huber, H. R., S. J. Jeffries, R. F. Brown, R. L. Delong, and G. Vanblaricom. 2001. Correcting aerial survey counts of harbor seals (*Phoca vitulina richardsi*) in Washington and Oregon. *Marine Mammal Science* **17**:276–293.
- Hueffer, K., D. Holcomb, L. R. Ballweber, S. M. Gende, G. Blundell, and T. M. O'Hara. 2011. Serologic surveillance of pathogens in a declining harbor seal (*Phoca vitulina*) population in Glacier Bay National Park, Alaska, USA and a reference site. *Journal of Wildlife Diseases* **47**:984–988.
- Huelsenbeck, J. P., and P. Andolfatto. 2007. Inference of population structure under a Dirichlet process model. *Genetics* **175**:1787–1802.
- Imler, R. H., and H. R. Sarber, 1947. Harbor seals and sea lions in Alaska. Technical Report 28, U.S. Fish and Wildlife Service.
- Ishwaran, H., and L. F. James. 2001. Gibbs sampling methods for stick-breaking priors. *Journal of the American Statistical Association* **96**:161–173.

- Ito, T. Y., B. Lhagvasuren, A. Tsunekawa, M. Shinoda, S. Takatsuki, B. Buuveibaatar, and B. Chimeddorj. 2013. Fragmentation of the habitat of wild ungulates by anthropogenic barriers in Mongolia. *PLoS ONE* **8**:e56995.
- Iverson, S. J., K. J. Frost, and L. F. Lowry. 1997. Fatty acid signatures reveal fine scale structure of foraging distribution of harbor seals and their prey in Prince William Sound, Alaska. *Marine Ecology Progress Series* **151**:255–271.
- Jansen, J., P. Boveng, S. Dahle, and J. Bengston. 2010. Reaction of harbor seals to cruise ships. *The Journal of Wildlife Management* **74**:1186–1194.
- Jemison, L. A., 1999. Summary of harbor seal diet data collected in Alaska from 1990-1999. Technical Report, Alaska Department of Fish and Game.
- Jemison, L. A., and B. P. Kelly. 2001. Pupping phenology and demography of harbor seals (*Phoca vitulina richardsi*) on Tugidak Island, Alaska. *Marine Mammal Science* **17**:585–600.
- Jemison, L. A., G. W. Pendleton, C. A. Wilson, and R. J. Small. 2006. Long-term trends in harbor seal numbers at Tugidak Island and Nanvak Bay, Alaska. *Marine Mammal Science* **22**:339–360.
- Johnson, C. J., and M. P. Gillingham. 2008. Sensitivity of species-distribution models to error, bias, and model design: An application to resource selection functions for woodland caribou. *Ecological Modelling* **213**:143–155.
- Johnson, D. H. 1980. The comparison of usage and availability measurements for evaluating resource preference. *Ecology* **61**:65–71.
- Johnson, D. S., P. B. Conn, M. B. Hooten, J. C. Ray, and B. A. Pond. 2012. Spatial occupancy models for large data sets. *Ecology* **94**:801–808.

- Johnson, D. S., M. B. Hooten, and C. E. Kuhn. 2013a. Estimating animal resource selection from telemetry data using point process models. *Journal of Animal Ecology* **82**:1155–1164.
- Johnson, D. S., J. M. London, M. Lea, and J. W. Durban. 2008a. Continuous-time correlated random walk model for animal telemetry data. *Ecology* **89**:1208–1215.
- Johnson, D. S., R. R. Ream, R. G. Towell, M. T. Williams, and J. D. Leon Guerrero. 2013b. Bayesian clustering of animal abundance trends for inference and dimension reduction. *Journal of Agricultural, Biological, and Environmental Statistics* **18**:299–313.
- Johnson, D. S., D. L. Thomas, J. M. Ver Hoef, and A. Christ. 2008b. A general framework for the analysis of animal resource selection from telemetry data. *Biometrics* **64**:968–976.
- Jonson, I. D., J. M. Flemming, and R. A. Myers. 2005. Robust state-space modeling on animal movement data. *Ecology* **86**:2874–2880.
- Jonson, I. D., R. A. Myers, and J. M. Flemming. 2003. Meta-analysis of animal movement using state-space models. *Ecology* **84**:3055–3063.
- Kery, M., and J. A. Royle. 2016. Applied hierarchical modeling in ecology. Analysis of distribution, abundance and species richness in R and BUGS. Volume 1: Prelude and static models. Elsevier.
- Kie, J. G., J. Matthiopoulos, J. Fieberg, R. A. Powell, F. Cagnacci, M. S. Mitchell, J.-M. Gaillard, and P. R. Moorcroft. 2010. The home-range concept: are traditional estimators still relevant with modern telemetry technology? *Philosophical Transactions of the Royal Society of London B: Biological Sciences* **365**:2221–2231.
- Knopff, K. H., A. A. Knopff, M. B. Warren, and M. S. Boyce. 2009. Evaluating global positioning system telemetry techniques for estimating cougar predation parameters. *Journal of Wildlife Management* **73**:586–597.

- Kowalczyk, R., K. Schmidt, and W. Jedrzejewski. 2012. Do fences or humans inhibit the movements of large mammals in Bialowieza Primeval Forest. Pages 235-244 in M. J. Somers and M. W. Hayward, editors, Fencing for Conservation? Springer.
- Langrock, R., R. King, J. Matthiopoulos, L. Thomas, D. Fortin, and J. M. Morales. 2012. Flexible and practical modeling of animal telemetry data: hidden Markov models and extensions. *Ecology* **93**:2336–2342.
- Lele, S. R., and J. L. Keim. 2006. Weighted distributions and estimation of resource selection probability functions. *Ecology* **87**:3021–3028.
- Lewis, J. S., J. L. Rachlow, E. O. Garton, and L. A. Vierling. 2007. Effects of habitat on GPS collar performance: using data screening to reduce location error. *Journal of Applied Ecology* **44**:663–671.
- Ling, J. K. 1984. Epidermal cycles and moulting in marine mammals. *Acta Zoologica Fennica* **171**:23–26.
- Loarie, S. R., R. J. V. Aarde, and S. L. Pimm. 2009. Fences and artificial water affect African savannah elephant movement patterns. *Biological Conservation* **142**:3086–3098.
- London, J. M., J. M. Ver Hoef, S. J. Jeffries, M. M. Lance, and P. L. Boveng. 2012. Haul-out behavior of harbor seals (*Phoca vitulina*) in Hood Canal, Washington. *PLoS One* **7**:e38180.
- Loughlin, T. R., A. S. Perlov, and V. A. Vladimirov. 1992. Range-wide survey and estimation of total numbers of Steller sea lions in 1989. *Marine Mammal Science* **8**:220–239.
- Lowry, L. F., K. J. Frost, J. M. Ver Hoef, and R. A. Delong. 2001. Movements of satellite-tagged subadult and adult harbor seals in Prince William Sound, Alaska. *Marine Mammal Science* **17**:835–861.

- MacKenzie, D. I., J. D. Nichols, G. B. Lachman, S. Droege, J. Andrew Royle, and C. A. Langtimm. 2002. Estimating site occupancy rates when detection probabilities are less than one. *Ecology* **83**:2248–2255.
- Manly, B. F. J. 2005. Multivariate statistical methods: A primer. 3rd edition. Chapman & Hall/CRC.
- Manly, B. F. J., L. McDonald, D. Thomas, T. L. McDonald, and W. P. Erickson. 2002. Resource selection by animals: Statistical design and analysis for field studies. Kluwer Academic Publishers.
- Martin, T. G., B. A. Wintle, J. R. Rhodes, P. M. Kuhnert, S. A. Field, S. J. Low-Choy, A. J. Tyre, and H. P. Possingham. 2005. Zero tolerance ecology: improving ecological inference by modelling the source of zero observations. *Ecology Letters* **8**:1235–1246.
- Mathews, E. A., L. A. Jemison, G. W. Pendleton, K. M. Blejwas, K. E. Hood, and K. L. Raum-Suryan. 2016. Haul-out patterns and effects of vessel disturbance on harbor seals (*Phoca vitulina*) on glacial ice in Tracy Arm, Alaska. *Fishery Bulletin* **114**:186–202.
- Mathews, E. A., and B. P. Kelly. 1996. Extreme temporal variation in harbor seal (*Phoca vitulina richardsi*) numbers in Glacier Bay, a glacial fjord in southeast Alaska. *Marine Mammal Science* **12**:483–489.
- Mathews, E. A., and G. W. Pendleton. 2006. Declines in harbor seal (*Phoca vitulina*) numbers in Glacier Bay National Park, Alaska, 1992–2002. *Marine Mammal Science* **22**:502.
- McClintock, B. T., D. S. Johnson, M. B. Hooten, J. M. Ver Hoef, and J. M. Morales. 2014a. When to be discrete: the importance of time formulation in understanding animal movement. *Movement Ecology* **2**:21.

- McClintock, B. T., R. King, L. Thomas, J. Matthiopoulos, B. J. McConnell, and J. M. Morales. 2012. A general discrete-time modeling framework for animal movement using multistate random walks. *Ecological Monographs* **82**:335–349.
- McClintock, B. T., J. M. London, M. F. Cameron, and P. L. Boveng. 2014b. Modelling animal movement using the Argos satellite telemetry location error ellipse. *Methods in Ecology and Evolution* **6**:266–277.
- McClintock, B. T., D. J. F. Russell, J. Matthiopoulos, and R. King. 2013. Combining individual animal movement and ancillary biotelemetry data to investigate population-level activity budgets. *Ecology* **94**:838–849.
- McCullagh, P., and J. A. Nelder. 1989. Generalized linear models. Chapman and Hall.
- Merrick, R. L., M. K. Chumbley, and G. V. Byrd. 1997. Diet diversity of Steller sea lions (*Eumetopias jubatus*) and their population decline in Alaska: a potential relationship. *Canadian Journal of Fisheries and Aquatic Sciences* **54**:1342–1348.
- Mizroch, S. A., and D. W. Rice. 2006. Have North Pacific killer whales switched prey species in response to depletion of the great whale populations? *Marine Ecology Progress Series* **310**:235–246.
- Montgomery, R., J. M. Ver Hoef, and P. Boveng. 2007. Spatial modeling of haul-out site use by harbor seals in Cook Inlet, Alaska. *Marine Ecology Progress Series* **341**:257–264.
- Morales, J. M., D. T. Haydon, J. Frair, K. E. Holsiner, and J. M. Fryxell. 2004. Extracting more out of relocation data: Building movement models as mixtures of random walks. *Ecology* **85**:2436–2445.
- Morris, D. W. 2011. Adaptation and habitat selection in the eco-evolutionary process. *Proceedings of the Royal Society B: Biological Sciences* **278**:2401.

- Muto, M. M., 2015. Alaska marine mammal stock assessments: Harbor seal. Technical Report NOAA-TM-AFSC-323, National Marine Fisheries Service, National Oceanic and Atmospheric Association.
- Patterson, T., L. Thomas, C. Wilcox, O. Ovaskainen, and J. Matthiopoulos. 2008. State-space models of individual animal movement. *Trends in Ecology & Evolution* **23**:87–94.
- Patterson, T. A., M. Basson, M. V. Bravington, and J. S. Gunn. 2009. Classifying movement behaviour in relation to environmental conditions using hidden Markov models. *Journal of Animal Ecology* **78**:1113–1123.
- Pauli, B., and J. Terhune. 1987. Tidal and temporal interaction on harbour seal haul-out patterns. *Aquatic Mammals* **13**:93–95.
- Pearce, J. L., and M. S. Boyce. 2006. Modelling distribution and abundance with presence-only data. *Journal of Applied Ecology* **43**:405–412.
- Perrin, W. F., B. G. Würsig, and J. G. M. Thewissen. 2009. Encyclopedia of marine mammals. Academic Press, London.
- Peterson, S. H., M. M. Lance, S. J. Jeffries, and A. Acevedo-Gutierrez. 2012. Long distance movements and disjunct spatial use of harbor seals (*Phoca vitulina*) in the inland waters of the Pacific Northwest. *PLoS ONE* **7**:e39046.
- Pitcher, K. W. 1980. Food of the harbor seal, *Phoca vitulina richardsi*, in the Gulf of Alaska. *Fishery Bulletin* **78**:544–549.
- Pitcher, K. W. 1990. Major decline in number of harbor seals, *Phoca vitulina richardsi*, on Tugidak Island, Gulf of Alaska. *Marine Mammal Science* **6**:121–134.
- Pitcher, K. W., and D. G. Calkins, 1979. Biology of the harbor seal, *Phoca vitulina richardsi*, in the Gulf of Alaska. Technical Report, Alaska Department of Fish and Game.

- Quinlan, S. E., and J. H. Hughes. 1990. Location and description of a Marbled Murrelet tree nest site in Alaska. *The Condor* **92**:1068–1073.
- Rodríguez, A., and D. B. Dunson. 2011. Nonparametric Bayesian models through probit stick-breaking processes. *Bayesian analysis (Online)* **6**:10.1214/11-BA605.
- Royle, J. A. 2004. N-Mixture models for estimating population size from spatially replicated counts. *Biometrics* **60**:108–115.
- Royle, J. A., and R. M. Dorazio. 2008. Hierarchical modeling and inference in ecology the analysis of data from populations, metapopulations and communities. Academic Press, Amsterdam.
- Ruppert, D., M. P. Wand, and R. J. Carroll. 2003. Semiparametric regression. Cambridge University Press.
- Ruprecht, J. S., D. E. Ausband, M. S. Mitchell, E. O. Garton, and P. Zager. 2012. Homesite attendance based on sex, breeding status, and number of helpers in gray wolf packs. *Journal of Mammalogy* **93**:1001–1005.
- Scheffer, V., and J. Slipp. 1944. The harbor seal in Washington State. *The American Midland Naturalist* **32**:373–416.
- Schneider, D. C., and P. M. Payne. 1983. Factors affecting haul-out of harbor seals at a site in southeastern Massachusetts. *Journal of Mammalogy* **64**:518–520.
- Service Argos. 2015. Argos User's Manual. CLS. URL <http://www.argos-system.org> .
- Sethuraman, J. 1994. A constructive definition of Dirichlet priors. *Statistica Sinica* **4**:639–650.
- Sharples, R. J., S. E. Moss, T. A. Patterson, and P. S. Hammond. 2012. Spatial variation in foraging behaviour of a marine top predator (*Phoca vitulina*) determined by a large-scale satellite tagging program. *PLoS One* **7**:e37216.

- Silva, M. A., I. Jonsen, D. J. F. Russell, R. Prieto, D. Thompson, and M. F. Baumgartner. 2014. Assessing performance of Bayesian state-space models fit to Argos satellite telemetry locations processed with Kalman filtering. *PLoS ONE* **9**:e92277.
- Simpkins, M., D. Withrow, J. Cesarone, and P. Boveng. 2003. Stability in the proportion of harbor seals hauled out under locally ideal conditions. *Marine Mammal Science* **19**:791–805.
- Small, R. J., P. L. Boveng, G. V. Byrd, and D. E. Withrow. 2008. Harbor seal population decline in the Aleutian Archipelago. *Marine Mammal Science* **24**:845–863.
- Small, R. J., L. F. Lowry, J. M. ver Hoef, K. J. Frost, R. A. Delong, and M. J. Rehberg. 2005. Differential movements by harbor seal pups in contrastings Alaska environments. *Marine Mammal Science* **21**:671–694.
- Small, R. J., G. W. Pendleton, and K. W. Pitcher. 2003. Trends in abundance of Alaska harbor seals, 1983–2001. *Marine Mammal Science* **19**:344–362.
- Springer, A. M., J. A. Estes, G. B. van Vliet, T. M. Williams, D. F. Doak, E. M. Danner, K. A. Forney, and B. Pfister. 2003. Sequential megafaunal collapse in the North Pacific Ocean: An ongoing legacy of industrial whaling? *Proceedings of the National Academy of Sciences* **100**:12223–12228.
- Springer, A. M., J. A. Estes, G. B. vanvliet, T. M. Williams, D. F. Doak, E. M. Danner, and B. Pfister. 2008. Mammal-eating killer whales, industrial whaling, and the sequential megafaunal collapse in the North Pacific Ocean: a reply to critics of Springer et al. 2003. *Marine Mammal Science* **24**:414.
- Stewart, B. S. 1984. Diurnal hauling patterns of harbor seals at San Miguel Island, California. *The Journal of Wildlife Management* **48**:1459–1461.

- Sumner, M. D., S. J. Wotherspoon, and M. A. Hindell. 2009. Bayesian estimation of animal movement from archival and satellite tags. PLoS ONE **4**:e7324.
- Suryan, R. M., and J. T. Harvey. 1999. Variability in reactions of Pacific harbor seals, *Phoca vitulina richardsi*, to disturbance. Fishery Bulletin **97**:332–339.
- Teh, Y., M. Jordan, M. Beal, and D. Blei. 2006. Hierarchical Dirichlet processes. Journal of the American Statistical Association **101**:1566–1581.
- Thompson, P. M. 1989. Seasonal changes in the distribution and composition of common seal (*Phoca vitulina*) haul-out groups. Journal of Zoology **217**:281–294.
- Thompson, P. M., D. J. Tollit, D. Wood, H. M. Corpe, P. S. Hammond, and A. Mackay. 1997. Estimating harbour seal abundance and status in an estuarine habitat in north-east Scotland. Journal of Applied Ecology **34**:43–52.
- Tomkiewicz, S. M., M. R. Fuller, J. G. Kie, and K. K. Bates. 2010. Global positioning system and associated technologies in animal behaviour and ecological research. Philosophical Transactions of the Royal Society B **365**:2163–2176.
- Trites, A. W., V. B. Deecke, E. J. Gregr, J. K. Ford, and P. F. Olesiuk. 2007. Killer whales, whaling, and sequential megafaunal collapse in the North Pacific: A comparative analysis of the dynamics of marine mammals in Alaska and British Columbia following commercial whaling. Marine Mammal Science **23**:751–765.
- Turchin, P. 1998. Quantitative analysis of movement: Measuring and modeling population redistribution in animals and plants. Sinauer Associates, Sunderland, Massachusetts.
- Tyre, A. J., B. Tenhumberg, S. A. Field, D. Niejalke, K. Parris, and H. P. Possingham. 2003. Improving precision and reducing bias in biological surveys: Estimating false-negative error rates. Ecological Applications **13**:1790–1801.

Van Horne, B. 1983. Density as a misleading indicator of habitat quality. *The Journal of Wildlife Management* **47**:893–901.

Ver Hoef, J., and K. Frost. 2003. A Bayesian hierarchical model for monitoring harbor seal changes in Prince William Sound, Alaska. *Environmental and Ecological Statistics* **10**:201–219.

Verity, R., M. D. Stevenson, D. K. Rossmo, R. A. Nichols, and S. C. Le Comber. 2014. Spatial targeting of infectious disease control: identifying multiple, unknown sources. *Methods in Ecology and Evolution* **5**:647–655.

Visscher, D. 2006. GPS measurement error and resource selection functions in a fragmented landscape. *Ecography* **29**:458–464.

Wade, P. R., V. N. Burkanov, M. E. Dahlheim, N. A. Friday, L. W. Fritz, T. R. Loughlin, S. A. Mizroch, M. M. Muto, D. W. Rice, L. G. Barrett-Lennard, N. A. Black, A. M. Burdin, J. Calambokidis, S. Cerchio, J. K. B. Ford, J. K. Jacobsen, C. O. Matkin, D. R. Matkin, A. V. Mehta, R. J. Small, J. M. Straley, S. M. McCluskey, G. R. VanBlaricom, and P. J. Clapham. 2007. Killer whales and marine mammal trends in the North Pacific—A re-examination of evidence for sequential megafauna collapse and the prey-switching hypothesis. *Marine Mammal Science* **23**:766–802.

Warton, D. I., and L. C. Shepherd. 2010. Poisson point process models solve the "pseudo-absence problem" for presence-only data in ecology. *The Annals of Applied Statistics* **4**:1383–1402.

Watts, P. 1992. Thermal constraints on hauling out by harbour seals (*Phoca vitulina*). *Canadian Journal of Zoology* **70**:553–560.

- Webb, N., M. Hebblewhite, and E. Merrill. 2008. Statistical methods for identifying wolf kill sites using global positioning system locations. *The Journal of Wildlife Management* **72**:798–807.
- Welsh, A. H., R. B. Cunningham, C. F. Donnelly, and D. B. Lindenmayer. 1996. Modelling the abundance of rare species: statistical models for counts with extra zeros. *Ecological Modelling* **88**:297–308.
- Wilke, F. 1957. Food of sea otters and harbor seals at Amchitka Island. *Journal of Wildlife Management* **21**:241–242.
- Womble, J. N., G. M. Blundell, S. M. Gende, M. Horning, M. F. Sigler, and D. J. Csepp. 2014. Linking marine predator diving behavior to local prey fields in contrasting habitats in a subarctic glacial fjord. *Marine Biology* **161**:1361–1374.
- York, A. E., and P. Kozloff. 1987. On the estimation of numbers of northern fur seal, *Callorhinus ursinus*, pups born on St. Paul Island, 1980-86. *Fishery Bulletin* **85**:367–375.
- Young, C., S. M. Gende, and J. T. Harvey. 2014. Effects of vessels on harbor seals in Glacier Bay National Park. *Tourism in Marine Environments* **10**:5–20.
- Zimmermann, B., P. Wabakken, H. Sand, H. C. Pedersen, and Liberg. 2007. Wolf movement patterns: A key to estimation of kill rate? *The Journal of Wildlife Management* **71**:1177–1182.
- Zuur, A. F., E. N. Ieno, N. J. Walker, A. A. Saveliev, and G. M. Smith. 2009. Mixed effects models and extensions in ecology with R. Springer, New York.

APPENDIX A

Supplementary Material for Chapter 2

APPENDIX A1. Complete specification of mixture t model used for the simulation study and harbor seal analysis.

Specification of mixture t model used for the simulation study and harbor seal analysis. Argos location quality class is indexed by c .

$$\begin{aligned}
\mathbf{s}_{tc} &\sim \begin{cases} t(\boldsymbol{\mu}_t, \boldsymbol{\Sigma}_c, \nu_c), & \text{with prob. 0.5} \\ t(\boldsymbol{\mu}_t, \tilde{\boldsymbol{\Sigma}}_c, \nu_c), & \text{with prob. 0.5} \end{cases} \\
\boldsymbol{\Sigma}_c &= \sigma_c^2 \begin{bmatrix} 1 & \rho_c \sqrt{a_c} \\ \rho_c \sqrt{a_c} & a_c \end{bmatrix} \\
\tilde{\boldsymbol{\Sigma}}_c &= \sigma_c^2 \begin{bmatrix} 1 & -\rho_c \sqrt{a_c} \\ -\rho_c \sqrt{a_c} & a_c \end{bmatrix} \\
\boldsymbol{\mu}_t &\sim \frac{\exp \{ \mathbf{x}'(\boldsymbol{\mu}_t) \boldsymbol{\beta} - \eta(\boldsymbol{\mu}_t, \boldsymbol{\mu}_{t-\Delta_t}) \}}{\int_{\mathcal{S}} \exp \{ \mathbf{x}'(\boldsymbol{\mu}) \boldsymbol{\beta} - \eta(\boldsymbol{\mu}, \boldsymbol{\mu}_{t-\Delta_t}) \} d\boldsymbol{\mu}} \\
\eta(\boldsymbol{\mu}_t, \boldsymbol{\mu}_{t-\Delta_t}) &= \frac{d(\boldsymbol{\mu}_t, \boldsymbol{\mu}_{t-\Delta_t})}{\Delta_t \phi} \\
\sigma_c &\sim \text{Unif}(0, 20000) \\
a_c &\sim \text{Unif}(0, 1) \\
\rho_c &\sim \text{Unif}(0, 1) \\
\nu_c &\sim \text{Unif}(0, 30) \\
\phi &\sim \text{Unif}(0, 750) \\
\boldsymbol{\beta} &\sim N(\mathbf{0}, 10^2 \times \mathbf{I})
\end{aligned}$$

APPENDIX A2. Full-conditional distributions and Markov chain Monte Carlo algorithm for parameter estimation.

The model we propose is well-suited to a Bayesian analysis using Markov chain Monte Carlo (MCMC) methods. Such an approach estimates the joint posterior distribution by sampling iteratively from the full-conditional distributions. Below, we use bracket notation to denote a conditional probability distribution. For example, $[x|y]$ indicates the conditional probability distribution of x given the parameter y . The notation “.” represents the data and other parameters in the model. The full-conditional distributions for each of the model parameters are

$$\begin{aligned}
[\sigma_c|\cdot] &\sim \prod_t \left(p_t \times t(\mathbf{s}_{tc}|\boldsymbol{\mu}_t, \boldsymbol{\Sigma}_c, \nu_c) + (1-p_t) \times t(\mathbf{s}_{tc}|\boldsymbol{\mu}_t, \tilde{\boldsymbol{\Sigma}}_c, \nu_c) \right) \times \text{Uniform}(\sigma_c|0, u_\sigma) \\
[a_c|\cdot] &\sim \prod_t \left(p_t \times t(\mathbf{s}_{tc}|\boldsymbol{\mu}_t, \boldsymbol{\Sigma}_c, \nu_c) + (1-p_t) \times t(\mathbf{s}_{tc}|\boldsymbol{\mu}_t, \tilde{\boldsymbol{\Sigma}}_c, \nu_c) \right) \times \text{Uniform}(a_c|0, u_a) \\
[\rho_c|\cdot] &\sim \prod_t \left(p_t \times t(\mathbf{s}_{tc}|\boldsymbol{\mu}_t, \boldsymbol{\Sigma}_c, \nu_c) + (1-p_t) \times t(\mathbf{s}_{tc}|\boldsymbol{\mu}_t, \tilde{\boldsymbol{\Sigma}}_c, \nu_c) \right) \times \text{Uniform}(\rho_c|0, u_\rho) \\
[\nu_c|\cdot] &\sim \prod_t \left(p_t \times t(\mathbf{s}_{tc}|\boldsymbol{\mu}_t, \boldsymbol{\Sigma}_c, \nu_c) + (1-p_t) \times t(\mathbf{s}_{tc}|\boldsymbol{\mu}_t, \tilde{\boldsymbol{\Sigma}}_c, \nu_c) \right) \times \text{Uniform}(\nu_c|0, u_\nu) \\
[\boldsymbol{\mu}_t|\cdot] &\sim \left(\boldsymbol{\mu}_t \left| \frac{\exp \{ \mathbf{x}'(\boldsymbol{\mu}_t) \boldsymbol{\beta} - \eta(\boldsymbol{\mu}_t, \boldsymbol{\mu}_{t-\Delta_t}) \}}{\int_{\mathcal{S}} \exp \{ \mathbf{x}'(\boldsymbol{\mu}) \boldsymbol{\beta} - \eta(\boldsymbol{\mu}, \boldsymbol{\mu}_{t-\Delta_t}) \} d\boldsymbol{\mu}} \right. \right) \times \left(\boldsymbol{\mu}_{t+\Delta_t} \left| \frac{\exp \{ \mathbf{x}'(\boldsymbol{\mu}_{t+\Delta_t}) \boldsymbol{\beta} - \eta(\boldsymbol{\mu}_{t+\Delta_t}, \boldsymbol{\mu}_t) \}}{\int_{\mathcal{S}} \exp \{ \mathbf{x}'(\boldsymbol{\mu}) \boldsymbol{\beta} - \eta(\boldsymbol{\mu}, \boldsymbol{\mu}_t) \} d\boldsymbol{\mu}} \right. \right) \\
&\quad \times \left(p_t \times t(\mathbf{s}_{tc}|\boldsymbol{\mu}_t, \boldsymbol{\Sigma}_c, \nu_c) + (1-p_t) \times t(\mathbf{s}_{tc}|\boldsymbol{\mu}_t, \tilde{\boldsymbol{\Sigma}}_c, \nu_c) \right), \text{ for } t = \Delta_t, \dots, T - \Delta_t \\
[\phi|\cdot] &\sim \prod_t \left(\boldsymbol{\mu}_t \left| \frac{\exp \{ \mathbf{x}'(\boldsymbol{\mu}_t) \boldsymbol{\beta} - \eta(\boldsymbol{\mu}_t, \boldsymbol{\mu}_{t-\Delta_t}) \}}{\int_{\mathcal{S}} \exp \{ \mathbf{x}'(\boldsymbol{\mu}) \boldsymbol{\beta} - \eta(\boldsymbol{\mu}, \boldsymbol{\mu}_{t-\Delta_t}) \} d\boldsymbol{\mu}} \right. \right) \times \text{Uniform}(\phi|0, u_\phi) \\
[\boldsymbol{\beta}|\cdot] &\sim \prod_t \left(\boldsymbol{\mu}_t \left| \frac{\exp \{ \mathbf{x}'(\boldsymbol{\mu}_t) \boldsymbol{\beta} - \eta(\boldsymbol{\mu}_t, \boldsymbol{\mu}_{t-\Delta_t}) \}}{\int_{\mathcal{S}} \exp \{ \mathbf{x}'(\boldsymbol{\mu}) \boldsymbol{\beta} - \eta(\boldsymbol{\mu}, \boldsymbol{\mu}_{t-\Delta_t}) \} d\boldsymbol{\mu}} \right. \right) \times N(\boldsymbol{\beta}|\boldsymbol{\mu}_\beta, \tau^2 \mathbf{I})
\end{aligned}$$

The parameters σ_c , a_c , ρ_c and ν_c are estimated for each error class c ; therefore, the products in their full-conditionals are only over observations \mathbf{s}_{tc} within a single error class. The full-conditionals above are non-conjugate and must be sampled using Metropolis-Hastings updates. Normalizing constants cancel in the Metropolis-Hastings ratio, and thus may be omitted in the pseudocode below (e.g., the uniform prior distributions). One can implement a MCMC algorithm to estimate the parameters of the observation and process models as follows:

1. Define initial values for all model parameters: $\boldsymbol{\mu}_t^{(0)}$ for $t = 0, \dots, T$; $\sigma_c^{(0)}$, $a_c^{(0)}$, $\rho_c^{(0)}$ and $\nu_c^{(0)}$ for $c = 3, 2, 1, 0$, A, and B (i.e., c indexes Argos location quality class); $\phi^{(0)}$; and $\boldsymbol{\beta}^{(0)}$. Set $k = 1$.

2. Let $\tilde{t} \in \{t_1, \dots, t_m\}$, where t_1, \dots, t_m are the times of locations collected for a single error class. Update the observation model parameters (Eqs. 1 and 2) for the corresponding error class by:

(a) Let

$$\boldsymbol{\Sigma}_c^{(k)} = (\sigma_c^{(k-1)})^2 \begin{bmatrix} 1 & \rho_c^{(k-1)} \sqrt{a_c^{(k-1)}} \\ \rho_c^{(k-1)} \sqrt{a_c^{(k-1)}} & a_c^{(k-1)} \end{bmatrix}$$

and

$$\begin{aligned} \tilde{\boldsymbol{\Sigma}}_c^{(k)} &= (\sigma_c^{(k-1)})^2 \begin{bmatrix} 1 & -\rho_c^{(k-1)} \sqrt{a_c^{(k-1)}} \\ -\rho_c^{(k-1)} \sqrt{a_c^{(k-1)}} & a_c^{(k-1)} \end{bmatrix}, \\ &= \mathbf{H} \boldsymbol{\Sigma}_c^{(k)} \mathbf{H}' \end{aligned}$$

where

$$\mathbf{H} = \begin{bmatrix} 1 & 0 \\ 0 & -1 \end{bmatrix}.$$

- (b) Sample $\sigma_c^{(*)}$ from a proposal distribution $[\sigma_c^{(*)} | \sigma_c^{(k-1)}]$ (e.g., $N(\sigma_c^{(*)} | \sigma_c^{(k-1)}, \tau_\sigma^2)$, where τ_σ^2 is a tuning parameter). If $\sigma_c^{(*)} \in [0, u_\sigma]$, calculate the Metropolis-Hastings ratio as

$$r_\sigma = \frac{\prod_{\tilde{t}} \left(p_t \times t(\mathbf{s}_{tc} | \boldsymbol{\mu}_t^{(k-1)}, \boldsymbol{\Sigma}_c^{(*)}, \nu_c^{(k-1)}) + (1-p_t) \times t(\mathbf{s}_{tc} | \boldsymbol{\mu}_t^{(k-1)}, \mathbf{H} \boldsymbol{\Sigma}_c^{(*)} \mathbf{H}', \nu_c^{(k-1)}) \right)}{\prod_{\tilde{t}} \left(p_t \times t(\mathbf{s}_{tc} | \boldsymbol{\mu}_t^{(k-1)}, \boldsymbol{\Sigma}_c^{(k)}, \nu_c^{(k-1)}) + (1-p_t) \times t(\mathbf{s}_{tc} | \boldsymbol{\mu}_t^{(k-1)}, \mathbf{H} \boldsymbol{\Sigma}_c^{(k)} \mathbf{H}', \nu_c^{(k-1)}) \right)},$$

where

$$\boldsymbol{\Sigma}_c^{(*)} = (\sigma_c^{(*)})^2 \begin{bmatrix} 1 & \rho_c^{(k-1)} \sqrt{a_c^{(k-1)}} \\ \rho_c^{(k-1)} \sqrt{a_c^{(k-1)}} & a_c^{(k-1)} \end{bmatrix}.$$

Note that the ratio r_σ assumes the proposal distribution is symmetric with respect to $\sigma_c^{(*)}$ and $\sigma_c^{(k-1)}$. If $r_\sigma > u$, where $u \sim \text{Uniform}(0,1)$, let $\sigma_c^{(k)} = \sigma_c^{(*)}$ and

$$\boldsymbol{\Sigma}_c^{(k)} = (\sigma_c^{(k)})^2 \begin{bmatrix} 1 & \rho_c^{(k-1)} \sqrt{a_c^{(k-1)}} \\ \rho_c^{(k-1)} \sqrt{a_c^{(k-1)}} & a_c^{(k-1)} \end{bmatrix}.$$

Otherwise, let $\sigma_c^{(k)} = \sigma_c^{(k-1)}$ if $r_\sigma < u$, or if $\sigma_c^{(*)} \notin [0, u_\sigma]$.

- (c) Sample $a_c^{(*)}$ from a proposal distribution $[a_c^{(*)}|a_c^{(k-1)}]$ (e.g., $N(a_c^{(*)}|a_c^{(k-1)}, \tau_a^2)$, where τ_a^2 is a tuning parameter). If $a_c^{(*)} \in [0, u_a]$, calculate the Metropolis-Hastings ratio as

$$r_a = \frac{\prod_{\tilde{t}} \left(p_t \times t \left(\mathbf{s}_{tc} | \boldsymbol{\mu}_t^{(k-1)}, \boldsymbol{\Sigma}_c^{(*)}, \nu_c^{(k-1)} \right) + (1-p_t) \times t \left(\mathbf{s}_{tc} | \boldsymbol{\mu}_t^{(k-1)}, \mathbf{H}\boldsymbol{\Sigma}_c^{(*)}\mathbf{H}', \nu_c^{(k-1)} \right) \right)}{\prod_{\tilde{t}} \left(p_t \times t \left(\mathbf{s}_{tc} | \boldsymbol{\mu}_t^{(k-1)}, \boldsymbol{\Sigma}_c^{(k)}, \nu_c^{(k-1)} \right) + (1-p_t) \times t \left(\mathbf{s}_{tc} | \boldsymbol{\mu}_t^{(k-1)}, \mathbf{H}\boldsymbol{\Sigma}_c^{(k)}\mathbf{H}', \nu_c^{(k-1)} \right) \right)},$$

where

$$\boldsymbol{\Sigma}_c^{(*)} = (\sigma_c^{(k)})^2 \begin{bmatrix} 1 & \rho_c^{(k-1)} \sqrt{a_c^{(*)}} \\ \rho_c^{(k-1)} \sqrt{a_c^{(*)}} & a_c^{(*)} \end{bmatrix}.$$

Note that the ratio r_a assumes the proposal distribution is symmetric with respect to $a_c^{(*)}$ and $a_c^{(k-1)}$. If $r_a > u$, where $u \sim \text{Uniform}(0,1)$, let $a_c^{(k)} = a_c^{(*)}$ and

$$\boldsymbol{\Sigma}_c^{(k)} = (\sigma_c^{(k)})^2 \begin{bmatrix} 1 & \rho_c^{(k-1)} \sqrt{a_c^{(k)}} \\ \rho_c^{(k-1)} \sqrt{a_c^{(k)}} & a_c^{(k)} \end{bmatrix}.$$

Otherwise, let $a_c^{(k)} = a_c^{(k-1)}$ if $r_a < u$, or if $a_c^{(*)} \notin [0, u_a]$.

- (d) Sample $\rho_c^{(*)}$ from a proposal distribution $[\rho_c^{(*)}|\rho_c^{(k-1)}]$ (e.g., $N(\rho_c^{(*)}|\rho_c^{(k-1)}, \tau_\rho^2)$, where τ_ρ^2 is a tuning parameter). If $\rho_c^{(*)} \in [0, u_\rho]$, calculate the Metropolis-Hastings ratio as

$$r_\rho = \frac{\prod_{\tilde{t}} \left(p_t \times t \left(\mathbf{s}_{tc} | \boldsymbol{\mu}_t^{(k-1)}, \boldsymbol{\Sigma}_c^{(*)}, \nu_c^{(k-1)} \right) + (1-p_t) \times t \left(\mathbf{s}_{tc} | \boldsymbol{\mu}_t^{(k-1)}, \mathbf{H}\boldsymbol{\Sigma}_c^{(*)}\mathbf{H}', \nu_c^{(k-1)} \right) \right)}{\prod_{\tilde{t}} \left(p_t \times t \left(\mathbf{s}_{tc} | \boldsymbol{\mu}_t^{(k-1)}, \boldsymbol{\Sigma}_c^{(k)}, \nu_c^{(k-1)} \right) + (1-p_t) \times t \left(\mathbf{s}_{tc} | \boldsymbol{\mu}_t^{(k-1)}, \mathbf{H}\boldsymbol{\Sigma}_c^{(k)}\mathbf{H}', \nu_c^{(k-1)} \right) \right)},$$

where

$$\boldsymbol{\Sigma}_c^{(*)} = (\sigma_c^{(k)})^2 \begin{bmatrix} 1 & \rho_c^{(*)} \sqrt{a_c^{(k)}} \\ \rho_c^{(*)} \sqrt{a_c^{(k)}} & a_c^{(k)} \end{bmatrix}.$$

Note that the ratio r_ρ assumes the proposal distribution is symmetric with respect to $\rho_c^{(*)}$ and $\rho_c^{(k-1)}$. If $r_\rho > u$, where $u \sim \text{Uniform}(0,1)$, let $\rho_c^{(k)} = \rho_c^{(*)}$ and

$$\boldsymbol{\Sigma}_c^{(k)} = (\sigma_c^{(k)})^2 \begin{bmatrix} 1 & \rho_c^{(k)} \sqrt{a_c^{(k)}} \\ \rho_c^{(k)} \sqrt{a_c^{(k)}} & a_c^{(k)} \end{bmatrix}.$$

Otherwise, let $\rho_c^{(k)} = \rho_c^{(k-1)}$ if $r_\rho < u$, or if $\rho_c^{(*)} \notin [0, u_\rho]$.

- (e) Sample $\nu_c^{(*)}$ from a proposal distribution $[\nu_c^{(*)}|\nu_c^{(k-1)}]$ (e.g., $N(\nu_c^{(*)}|\nu_c^{(k-1)}, \tau_\nu^2)$, where τ_ν^2 is a tuning parameter). If $\nu_c^{(*)} \in [0, u_\nu]$, calculate the Metropolis-Hastings

ratio as

$$r_\nu = \frac{\prod_{\tilde{t}} \left(p_t \times t \left(\mathbf{s}_{tc} | \boldsymbol{\mu}_t^{(k-1)}, \boldsymbol{\Sigma}_c^{(k)}, \nu_c^{(*)} \right) + (1-p_t) \times t \left(\mathbf{s}_{tc} | \boldsymbol{\mu}_t^{(k-1)}, \mathbf{H}\boldsymbol{\Sigma}_c^{(k)}\mathbf{H}', \nu_c^{(*)} \right) \right)}{\prod_{\tilde{t}} \left(p_t \times t \left(\mathbf{s}_{tc} | \boldsymbol{\mu}_t^{(k-1)}, \boldsymbol{\Sigma}_c^{(k)}, \nu_c^{(k-1)} \right) + (1-p_t) \times t \left(\mathbf{s}_{tc} | \boldsymbol{\mu}_t^{(k-1)}, \mathbf{H}\boldsymbol{\Sigma}_c^{(k)}\mathbf{H}', \nu_c^{(k-1)} \right) \right)}.$$

Note that the ratio r_ν assumes the proposal distribution is symmetric with respect to $\nu_c^{(*)}$ and $\nu_c^{(k-1)}$. If $r_\nu > u$, where $u \sim \text{Uniform}(0,1)$, let $\nu_c^{(k)} = \nu_c^{(*)}$. Otherwise, let $\nu_c^{(k)} = \nu_c^{(k-1)}$ if $r_\nu < u$, or if $\nu_c^{(*)} \notin [0, u_\nu]$.

- (f) Repeat step 2 for each error class c .
- 3. Sample $\phi^{(*)}$ from a proposal distribution $[\phi^{(*)} | \phi^{(k-1)}]$ (e.g., $N(\phi^{(*)} | \phi^{(k-1)}, \tau_\phi^2)$, where τ_ϕ^2 is a tuning parameter). If $\phi^{(*)} \in [0, u_\phi]$, calculate the Metropolis-Hastings ratio as

$$r_\phi = \frac{\prod_{t=0}^T \left(\frac{\exp \left\{ \mathbf{x}'(\boldsymbol{\mu}_t^{(k-1)}) \boldsymbol{\beta}^{(k-1)} - \eta \left(\boldsymbol{\mu}_t^{(k-1)}, \boldsymbol{\mu}_{t-\Delta_t}^{(k-1)}, \phi^{(*)} \right) \right\}}{\int_{\mathcal{S}} \exp \left\{ \mathbf{x}'(\boldsymbol{\mu}) \boldsymbol{\beta}^{(k-1)} - \eta \left(\boldsymbol{\mu}, \boldsymbol{\mu}_{t-\Delta_t}^{(k-1)}, \phi^{(*)} \right) \right\} d\boldsymbol{\mu}} \right)}{\prod_{t=0}^T \left(\frac{\exp \left\{ \mathbf{x}'(\boldsymbol{\mu}_t^{(k-1)}) \boldsymbol{\beta}^{(k-1)} - \eta \left(\boldsymbol{\mu}_t^{(k-1)}, \boldsymbol{\mu}_{t-\Delta_t}^{(k-1)}, \phi^{(k-1)} \right) \right\}}{\int_{\mathcal{S}} \exp \left\{ \mathbf{x}'(\boldsymbol{\mu}) \boldsymbol{\beta}^{(k-1)} - \eta \left(\boldsymbol{\mu}, \boldsymbol{\mu}_{t-\Delta_t}^{(k-1)}, \phi^{(k-1)} \right) \right\} d\boldsymbol{\mu}} \right)},$$

where

$$\eta \left(\boldsymbol{\mu}_t^{(k-1)}, \boldsymbol{\mu}_{t-\Delta_t}^{(k-1)}, \phi^{(*)} \right) = \frac{d \left(\boldsymbol{\mu}_t^{(k-1)}, \boldsymbol{\mu}_{t-\Delta_t}^{(k-1)} \right)}{\Delta_t \phi^{(*)}}$$

and

$$\eta \left(\boldsymbol{\mu}_t^{(k-1)}, \boldsymbol{\mu}_{t-\Delta_t}^{(k-1)}, \phi^{(k-1)} \right) = \frac{d \left(\boldsymbol{\mu}_t^{(k-1)}, \boldsymbol{\mu}_{t-\Delta_t}^{(k-1)} \right)}{\Delta_t \phi^{(k-1)}}.$$

Note that the ratio r_ϕ assumes the proposal distribution is symmetric with respect to $\phi^{(*)}$ and $\phi^{(k-1)}$. If $r_\phi > u$, where $u \sim \text{Uniform}(0,1)$, let $\phi^{(k)} = \phi^{(*)}$. Otherwise, let $\phi^{(k)} = \phi^{(k-1)}$ if $r_\phi < u$, or if $\phi^{(*)} \notin [0, u_\phi]$.

- 4. Sample $\boldsymbol{\beta}^{(*)}$ from a proposal distribution $[\boldsymbol{\beta}^{(*)} | \boldsymbol{\beta}^{(k-1)}]$ (e.g., $N(\boldsymbol{\beta}^{(*)} | \boldsymbol{\beta}^{(k-1)}, \tau_\beta^2 \mathbf{I})$, where τ_β^2 is a tuning parameter). Calculate the Metropolis-Hastings ratio as

$$r_\beta = \frac{\prod_{t=0}^T \left(\frac{\exp \left\{ \mathbf{x}'(\boldsymbol{\mu}_t^{(k-1)}) \boldsymbol{\beta}^{(*)} - \eta \left(\boldsymbol{\mu}_t^{(k-1)}, \boldsymbol{\mu}_{t-\Delta_t}^{(k-1)}, \phi^{(k)} \right) \right\}}{\int_{\mathcal{S}} \exp \left\{ \mathbf{x}'(\boldsymbol{\mu}) \boldsymbol{\beta}^{(*)} - \eta \left(\boldsymbol{\mu}, \boldsymbol{\mu}_{t-\Delta_t}^{(k-1)}, \phi^{(k)} \right) \right\} d\boldsymbol{\mu}} \right) \times N \left(\boldsymbol{\beta}^{(*)} | \boldsymbol{\mu}_\beta, \tau^2 \mathbf{I} \right)}{\prod_{t=0}^T \left(\frac{\exp \left\{ \mathbf{x}'(\boldsymbol{\mu}_t^{(k-1)}) \boldsymbol{\beta}^{(k-1)} - \eta \left(\boldsymbol{\mu}_t^{(k-1)}, \boldsymbol{\mu}_{t-\Delta_t}^{(k-1)}, \phi^{(k)} \right) \right\}}{\int_{\mathcal{S}} \exp \left\{ \mathbf{x}'(\boldsymbol{\mu}) \boldsymbol{\beta}^{(k-1)} - \eta \left(\boldsymbol{\mu}, \boldsymbol{\mu}_{t-\Delta_t}^{(k-1)}, \phi^{(k)} \right) \right\} d\boldsymbol{\mu}} \right) \times N \left(\boldsymbol{\beta}^{(k-1)} | \boldsymbol{\mu}_\beta, \tau^2 \mathbf{I} \right)}.$$

Note that the ratio r_β assumes the proposal distribution is symmetric with respect to $\boldsymbol{\beta}^{(*)}$ and $\boldsymbol{\beta}^{(k-1)}$. If $r_\beta > u$, where $u \sim \text{Uniform}(0,1)$, let $\boldsymbol{\beta}^{(k)} = \boldsymbol{\beta}^{(*)}$. Otherwise, let $\boldsymbol{\beta}^{(k)} = \boldsymbol{\beta}^{(k-1)}$.

- 5. For each $t = \Delta_t, \dots, T - \Delta_t$ in sequence, sample $\boldsymbol{\mu}_t^{(*)}$ from a proposal distribution $[\boldsymbol{\mu}_t^{(*)} | \boldsymbol{\mu}_t^{(k-1)}]$ (e.g., $N(\boldsymbol{\mu}_t^{(*)} | \boldsymbol{\mu}_t^{(k-1)}, \tau_\mu^2 \mathbf{I})$, where τ_μ^2 is a tuning parameter). If $\boldsymbol{\mu}_t^{(*)} \in \mathcal{S}$,

calculate the Metropolis-Hastings ratio as

$$\begin{aligned}
r_\mu &= \frac{\left[\boldsymbol{\mu}_t^{(*)} | \boldsymbol{\mu}_{t-\Delta_t}^{(k)} \right] \times \left[\boldsymbol{\mu}_{t+\Delta_t}^{(k-1)} | \boldsymbol{\mu}_t^{(*)} \right] \times \left[\mathbf{s}_{tc} | \boldsymbol{\mu}_t^{(*)}, \Sigma_c^{(k)}, \nu_c^{(k)} \right]}{\left[\boldsymbol{\mu}_t^{(k-1)} | \boldsymbol{\mu}_{t-\Delta_t}^{(k)} \right] \times \left[\boldsymbol{\mu}_{t+\Delta_t}^{(k-1)} | \boldsymbol{\mu}_t^{(k-1)} \right] \times \left[\mathbf{s}_{tc} | \boldsymbol{\mu}_t^{(k-1)}, \Sigma_c^{(k)}, \nu_c^{(k)} \right]} \\
&= \frac{\left(\frac{\exp\left\{ \mathbf{x}'(\boldsymbol{\mu}_t^{(*)}) \boldsymbol{\beta}^{(k)} - \eta(\boldsymbol{\mu}_t^{(*)}, \boldsymbol{\mu}_{t-\Delta_t}^{(k)}, \phi^{(k)}) \right\}}{\int_{\mathcal{S}} \exp\left\{ \mathbf{x}'(\boldsymbol{\mu}) \boldsymbol{\beta}^{(k)} - \eta(\boldsymbol{\mu}, \boldsymbol{\mu}_{t-\Delta_t}^{(k)}, \phi^{(k)}) \right\} d\boldsymbol{\mu}} \right)}{\left(\frac{\exp\left\{ \mathbf{x}'(\boldsymbol{\mu}_t^{(k-1)}) \boldsymbol{\beta}^{(k)} - \eta(\boldsymbol{\mu}_t^{(k-1)}, \boldsymbol{\mu}_{t-\Delta_t}^{(k)}, \phi^{(k)}) \right\}}{\int_{\mathcal{S}} \exp\left\{ \mathbf{x}'(\boldsymbol{\mu}) \boldsymbol{\beta}^{(k)} - \eta(\boldsymbol{\mu}, \boldsymbol{\mu}_{t-\Delta_t}^{(k)}, \phi^{(k)}) \right\} d\boldsymbol{\mu}} \right)} \times \\
&\quad \frac{\left(\frac{\exp\left\{ \mathbf{x}'(\boldsymbol{\mu}_{t+\Delta_t}^{(k-1)}) \boldsymbol{\beta}^{(k)} - \eta(\boldsymbol{\mu}_{t+\Delta_t}^{(k-1)}, \boldsymbol{\mu}_t^{(*)}, \phi^{(k)}) \right\}}{\int_{\mathcal{S}} \exp\left\{ \mathbf{x}'(\boldsymbol{\mu}) \boldsymbol{\beta}^{(k)} - \eta(\boldsymbol{\mu}, \boldsymbol{\mu}_t^{(*)}, \phi^{(k)}) \right\} d\boldsymbol{\mu}} \right)}{\left(\frac{\exp\left\{ \mathbf{x}'(\boldsymbol{\mu}_{t+\Delta_t}^{(k-1)}) \boldsymbol{\beta}^{(k)} - \eta(\boldsymbol{\mu}_{t+\Delta_t}^{(k-1)}, \boldsymbol{\mu}_t^{(k-1)}, \phi^{(k)}) \right\}}{\int_{\mathcal{S}} \exp\left\{ \mathbf{x}'(\boldsymbol{\mu}) \boldsymbol{\beta}^{(k)} - \eta(\boldsymbol{\mu}, \boldsymbol{\mu}_t^{(k-1)}, \phi^{(k)}) \right\} d\boldsymbol{\mu}} \right)} \times \\
&\quad \frac{\left(p_t \times t\left(\mathbf{s}_{tc} | \boldsymbol{\mu}_t^{(*)}, \Sigma_c^{(k)}, \nu_c^{(k)}\right) + (1-p_t) \times t\left(\mathbf{s}_{tc} | \boldsymbol{\mu}_t^{(*)}, \mathbf{H}\Sigma_c^{(k)}\mathbf{H}', \nu_c^{(k)}\right) \right)}{\left(p_t \times t\left(\mathbf{s}_{tc} | \boldsymbol{\mu}_t^{(k-1)}, \Sigma_c^{(k)}, \nu_c^{(k)}\right) + (1-p_t) \times t\left(\mathbf{s}_{tc} | \boldsymbol{\mu}_t^{(k-1)}, \mathbf{H}\Sigma_c^{(k)}\mathbf{H}', \nu_c^{(k)}\right) \right)}
\end{aligned}$$

Note that the ratio r_μ assumes the proposal distribution is symmetric with respect to $\boldsymbol{\mu}_t^{(*)}$ and $\boldsymbol{\mu}_t^{(k-1)}$. If $r_\mu > u$, where $u \sim \text{Uniform}(0,1)$, let $\boldsymbol{\mu}_t^{(k)} = \boldsymbol{\mu}_t^{(*)}$. Otherwise, let $\boldsymbol{\mu}_t^{(k)} = \boldsymbol{\mu}_t^{(k-1)}$ if $r_\mu < u$, or if $\boldsymbol{\mu}_t^{(*)} \notin \mathcal{S}$.

6. Save $\boldsymbol{\mu}_t^{(k)}$ for $t = 0, \dots, T$; $\sigma_c^{(k)}$, $a_c^{(k)}$, $\rho_c^{(k)}$, and $\nu_c^{(k)}$ for $c = 3, 2, 1, 0, \text{A}, \text{and B}$; $\phi^{(k)}$; and $\boldsymbol{\beta}^{(k)}$.
7. Set $k = k + 1$ and return to step 2. The algorithm is iterated by repeating steps 2 through 7 until a sufficiently large sample has been obtained from which to approximate the posterior distribution.

APPENDIX A3. Performance of mixture t model in simulation study.

Table A3.1. Summary of the performance of our mixture t model in the simulation study. “Mean” and “SD” are the mean and standard deviation across the 250 replicates of the Bayesian point estimate (posterior mean). The parameter β_1 describes selection relative to a point of attraction (e.g., distance to haul-out site), whereas β_2 describes selection for bathymetry. Both covariates were centered and scaled to unit variance prior to model fitting.

Parameter	True value	Mean	SD
σ_H	2291	2279	129
σ_M	2727	2776	203
σ_L	13252	13580	957
a_H	0.70	0.71	0.07
a_M	0.50	0.52	0.08
a_L	0.75	0.75	0.08
ρ_H	0.85	0.84	0.03
ρ_M	0.16	0.25	0.08
ρ_L	0.30	0.28	0.10
ν_H	16.74	18.14	3.36
ν_M	1.60	1.67	0.18
ν_L	1.00	1.03	0.09
ϕ	424	397	31
β_1	-2.12	-2.14	0.21
β_2	-0.82	-0.83	0.14

APPENDIX A4. Summary of results for an analysis of harbor seal data near Kodiak Island, Alaska, USA.

Table A4.1. Parameter estimates from an analysis of an adult female harbor seal near Kodiak Island, AK. Reported values are the posterior mean and 95% equal-tail credible intervals based on 100,000 MCMC samples. Convergence was determined based on potential scale reduction factors < 1.1 (Gelman and Rubin 1992). The parameter β_1 describes selection relative to distance to haul-out site, whereas β_2 describes selection for bathymetry. Both covariates were centered and scaled to unit variance prior to model fitting. Note that ϕ , β_1 , and β_2 are process model parameters that describe harbor seal behavior; therefore, they are global parameters that are not estimated for separate Argos location classes.

Argos							
location class	σ (m)	a	ρ	ν	ϕ (m/hour)	β_1	β_2
3	2259 (1447, 3242)	0.69 (0.42, 0.97)	0.85 (0.51, 0.99)	16.52 (2.80, 29.34)			
2	1089 (614, 1696)	0.42 (0.21, 0.82)	0.73 (0.14, 0.99)	2.29 (1.15, 4.53)			
1	1365 (1051, 1718)	0.64 (0.42, 0.90)	0.40 (0.03, 0.70)	1.72 (1.27, 2.30)	413.00	-2.03	-0.82
0	2720 (2317, 3155)	0.50 (0.37, 0.66)	0.16 (0.01, 0.41)	1.59 (1.29, 1.95)	(350.72, 480.70)	(-2.45, -1.62)	(-1.12, -0.53)
A	2702 (2257, 3186)	0.90 (0.72, 1.00)	0.21 (0.01, 0.48)	1.23 (1.00, 1.50)			
B	13338 (11342, 15542)	0.74 (0.59, 0.92)	0.30 (0.02, 0.53)	1.01 (0.85, 1.18)			

References

Gelman, A. and D. B. Rubin. 1992. Inference from iterative simulation using multiple sequences. Statistical Science 7:457-511.

APPENDIX A5. Estimated Argos satellite telemetry error by location class.

Table A5.1. Estimated percentiles of Argos satellite telemetry error (i.e., $\| \mathbf{s}_t - \boldsymbol{\mu}_t \|$) by location class.

Argos location class	50th percentile error (m)	68th percentile error (m)	95th percentile error (m)
3	2156	3035	6054
2	1158	1727	4975
1	1764	2656	9049
0	3462	5281	19513
A	4203	6760	33920
B	21042	35980	235963

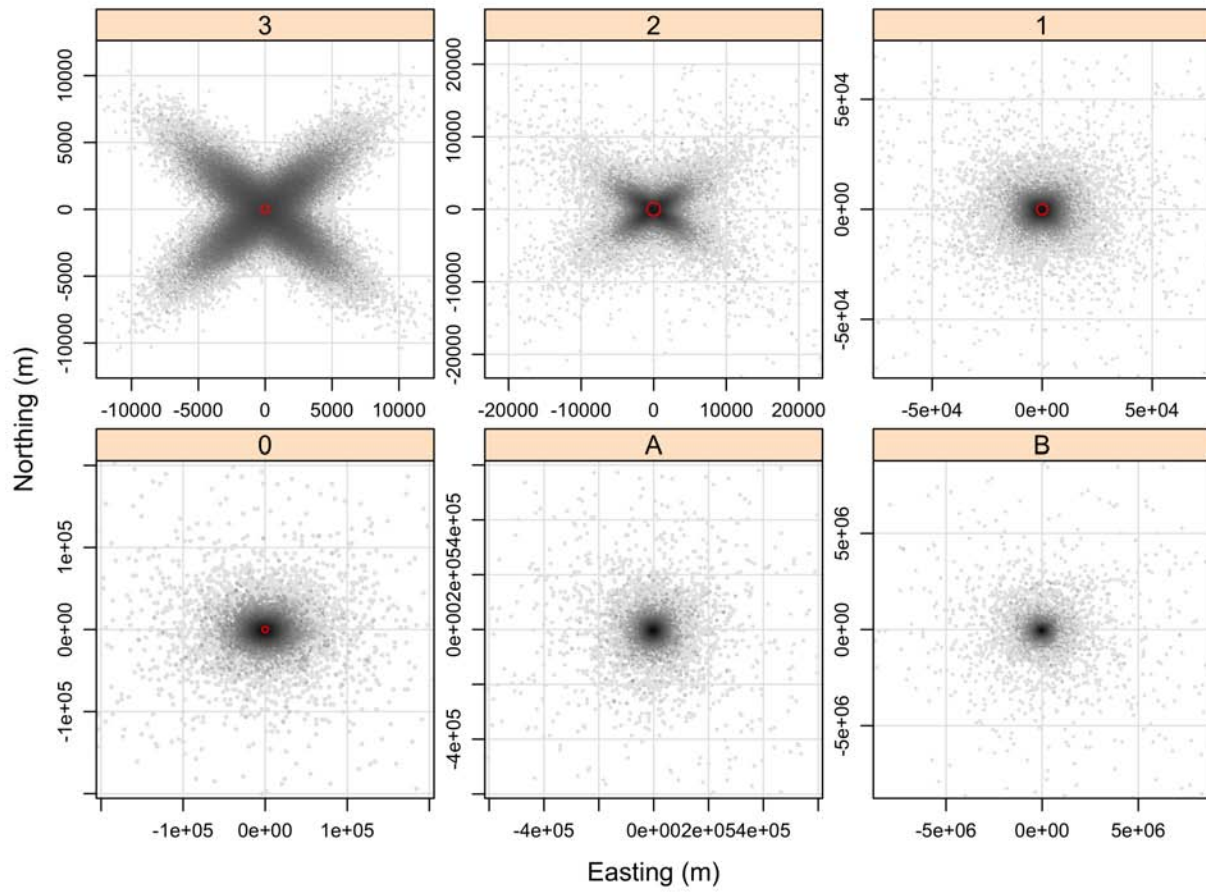


Figure A5.1 Estimated distribution of Argos satellite telemetry errors (i.e., $\mathbf{s}_t - \boldsymbol{\mu}_t$) by location class. Red circles denote error estimates provided by Argos for location classes 3, 2, 1, and 0. Argos does not provide error estimates for location classes A and B. The x-shaped pattern in Argos errors is particularly evident for location classes 3 and 2 ($\rho = 0.85$ and 0.74 , respectively). Errors in class 0 are distinctly elliptical with larger errors in the longitude direction ($a = 0.50$).

APPENDIX B

Supplementary Material for Chapter 3

APPENDIX B1. Model statement, posterior distribution, and full-conditional distributions.

The model we propose is well-suited to a Bayesian analysis using Markov chain Monte Carlo methods. Such an approach estimates the joint posterior distribution by sampling iteratively from the full-conditional distributions. In the posterior and full-conditional distributions below, we use bracket notation to denote a probability distribution. For example, $[x]$ indicates the probability distribution of x . Similarly, $[x|y]$ indicates the probability distribution of x given the parameter y . The notation “.” represents the data and other parameters in the model.

In addition to the notation introduced in the main document, let c index Argos location quality class (i.e., $c \in \{3, 2, 1, 0, \text{A}, \text{and B}\}$).

MODEL STATEMENT

$$\begin{aligned}
\mathbf{s}_c(t) &\sim \begin{cases} \mathcal{N}(\boldsymbol{\mu}(t), \Sigma_c), & \text{with prob. } p(t), y(t) = 1 \\ \mathcal{N}(\boldsymbol{\mu}(t), \tilde{\Sigma}_c), & \text{with prob. } 1 - p(t), y(t) = 1 \\ \mathcal{N}(\boldsymbol{\mu}(t), \sigma_\mu^2 \mathbf{I} + \Sigma_c), & \text{with prob. } p(t), y(t) = 0 \\ \mathcal{N}(\boldsymbol{\mu}(t), \sigma_\mu^2 \mathbf{I} + \tilde{\Sigma}_c), & \text{with prob. } 1 - p(t), y(t) = 0 \end{cases} \\
\Sigma_c &= \sigma_c^2 \begin{bmatrix} 1 & \rho_c \sqrt{a_c} \\ \rho_c \sqrt{a_c} & a_c \end{bmatrix} \\
\tilde{\Sigma}_c &= \sigma_c^2 \begin{bmatrix} 1 & -\rho_c \sqrt{a_c} \\ -\rho_c \sqrt{a_c} & a_c \end{bmatrix} \\
\boldsymbol{\mu}(t) &\sim \sum_{j=1}^J \pi_j \delta_{\boldsymbol{\mu}_j} \\
\pi_j &= \eta_j \prod_{l < j} (1 - \eta_l) \\
\eta_j &\sim \text{Beta}(1, \theta) \\
y(t) &= \begin{cases} 0, & v(t) \leq 0 \\ 1, & v(t) > 0 \end{cases} \\
v(t) &\sim \mathcal{N}(\mathbf{x}(t)' \boldsymbol{\beta} + \mathbf{w}(t)' \boldsymbol{\alpha}, 1) \\
\boldsymbol{\mu}_j &\sim f_{\tilde{\mathcal{S}}}(\mathbf{S}) \\
\theta &\sim \text{Gamma}(r_\theta, q_\theta) \\
\boldsymbol{\beta} &\sim \mathcal{N}(\boldsymbol{\mu}_\beta, \sigma_\beta^2 \mathbf{I}) \\
\boldsymbol{\alpha} &\sim \mathcal{N}(\mathbf{0}, \sigma_\alpha^2 \mathbf{I}) \\
\log(\sigma_\mu) &\sim \mathcal{N}(\mu_\sigma, \sigma_\sigma^2) \\
\sigma_\alpha^2 &\sim \text{IG}(r_\alpha, q_\alpha) \\
\sigma_c &\sim \text{Unif}(l_\sigma, u_\sigma) \\
a_c &\sim \text{Unif}(l_a, u_a) \\
\rho_c &\sim \text{Unif}(l_\rho, u_\rho)
\end{aligned}$$

Note that $f_{\tilde{\mathcal{S}}}(\mathbf{S})$ represents the kernel density estimate of the observed telemetry locations $\mathbf{S} \equiv \{\mathbf{s}_c(t) : t \in \mathcal{T}\}$ at location $\boldsymbol{\mu}_j$, where $f_{\tilde{\mathcal{S}}}(\mathbf{S})$ is truncated and normalized over $\tilde{\mathcal{S}}$.

POSTERIOR DISTRIBUTION

$$\begin{aligned}
[\mathbf{M}_t, \boldsymbol{\eta}, \mathbf{v}, \boldsymbol{\alpha}, \mathbf{M}_j, \theta, \boldsymbol{\beta}, \sigma_\mu, \sigma_\alpha^2, \boldsymbol{\sigma}, \mathbf{a}, \boldsymbol{\rho} | \mathbf{S}, \mathbf{y}] &\propto \prod_{t \in \mathcal{T}} \prod_{j=1}^J \left[\mathbf{s}_c(t) | \boldsymbol{\mu}(t), y(t), \Sigma_c, \tilde{\Sigma}_c, \sigma_\mu \right] \\
&\quad \times [\boldsymbol{\mu}(t) | \boldsymbol{\mu}_j, \eta_j] [\eta_j | \theta] \\
&\quad \times [y(t) | v(t)] [v(t) | \boldsymbol{\alpha}, \boldsymbol{\beta}] [\boldsymbol{\alpha} | \mathbf{0}, \sigma_\alpha^2] \\
&\quad \times [\boldsymbol{\mu}_j] [\theta] [\boldsymbol{\beta}] [\sigma_\mu] [\sigma_\alpha^2] [\boldsymbol{\sigma}] [\mathbf{a}] [\boldsymbol{\rho}],
\end{aligned}$$

where $\mathbf{M}_t \equiv \{\boldsymbol{\mu}(t) : t \in \mathcal{T}\}$ is a matrix of functional central places $\boldsymbol{\mu}(t)$ for all times $t \in \mathcal{T}$; $\boldsymbol{\eta} \equiv (\eta_1, \dots, \eta_J)'$ is a vector of stick-breaking weights η_j for $j = 1, \dots, J$; $\mathbf{v} \equiv \{v(t) : t \in \mathcal{T}\}$ is a vector of latent auxiliary variables $v(t)$ for all times $t \in \mathcal{T}$; $\mathbf{M}_j \equiv \{\boldsymbol{\mu}_j : j = 1, \dots, J\}$ is a matrix of potential central places $\boldsymbol{\mu}_j$ for $j = 1, \dots, J$; $\boldsymbol{\sigma} \equiv (\sigma_3, \sigma_2, \sigma_1, \sigma_0, \sigma_A, \sigma_B)'$, $\mathbf{a} \equiv (a_3, a_2, a_1, a_0, a_A, a_B)'$, and $\boldsymbol{\rho} \equiv (\rho_3, \rho_2, \rho_1, \rho_0, \rho_A, \rho_B)'$ are vectors of parameters describing telemetry measurement error for each Argos location quality class; $\mathbf{S} \equiv \{\mathbf{s}_c(t) : t \in \mathcal{T}\}$ is a matrix of observed telemetry locations $\mathbf{s}_c(t)$ for all times $t \in \mathcal{T}$; and $\mathbf{y} \equiv \{y(t) : t \in \mathcal{T}\}$ is a vector of ancillary behavioral data $y(t)$ for all times $t \in \mathcal{T}$.

FULL-CONDITIONAL DISTRIBUTIONS

Locations of functional central places ($\boldsymbol{\mu}(t)$):

$$\begin{aligned}
[\boldsymbol{\mu}(t) | \cdot] &\propto \left[\mathbf{s}_c(t) | \boldsymbol{\mu}(t), y(t), \Sigma_c, \tilde{\Sigma}_c, \sigma_\mu \right] [\boldsymbol{\mu}(t) | \boldsymbol{\pi}] \\
&\propto \sum_{j=1}^J \pi_j \delta_{\boldsymbol{\mu}_j} \left[\mathbf{s}_c(t) | \boldsymbol{\mu}_j, y(t), \Sigma_c, \tilde{\Sigma}_c, \sigma_\mu \right].
\end{aligned}$$

Here, we introduce a variable for the latent class status, $h(t) \in \{1, \dots, J\}$, that assigns each observed telemetry location $\mathbf{s}_c(t)$ to one of the central places $\boldsymbol{\mu}_j$, for $j = 1, \dots, J$ (i.e., $\boldsymbol{\mu}(t) = \boldsymbol{\mu}_{h(t)}$). The update proceeds just as in multinomial sampling:

$$\begin{aligned}
[h(t) | \cdot] &\sim \text{Cat} \left(\frac{\pi_1 \left[\mathbf{s}_c(t) | \boldsymbol{\mu}_1, \Sigma_c, \tilde{\Sigma}_c \right]^{y(t)} \left[\mathbf{s}_c(t) | \boldsymbol{\mu}_1, \sigma_\mu^2 \mathbf{I} + \Sigma_c, \sigma_\mu^2 \mathbf{I} + \tilde{\Sigma}_c \right]^{1-y(t)}}{\sum_{j=1}^J \pi_j \left[\mathbf{s}_c(t) | \boldsymbol{\mu}_j, \Sigma_c, \tilde{\Sigma}_c \right]^{y(t)} \left[\mathbf{s}_c(t) | \boldsymbol{\mu}_j, \sigma_\mu^2 \mathbf{I} + \Sigma_c, \sigma_\mu^2 \mathbf{I} + \tilde{\Sigma}_c \right]^{1-y(t)}}, \dots, \right. \\
&\quad \left. \frac{\pi_J \left[\mathbf{s}_c(t) | \boldsymbol{\mu}_J, \Sigma_c, \tilde{\Sigma}_c \right]^{y(t)} \left[\mathbf{s}_c(t) | \boldsymbol{\mu}_J, \sigma_\mu^2 \mathbf{I} + \Sigma_c, \sigma_\mu^2 \mathbf{I} + \tilde{\Sigma}_c \right]^{1-y(t)}}{\sum_{j=1}^J \pi_j \left[\mathbf{s}_c(t) | \boldsymbol{\mu}_j, \Sigma_c, \tilde{\Sigma}_c \right]^{y(t)} \left[\mathbf{s}_c(t) | \boldsymbol{\mu}_j, \sigma_\mu^2 \mathbf{I} + \Sigma_c, \sigma_\mu^2 \mathbf{I} + \tilde{\Sigma}_c \right]^{1-y(t)}} \right) \\
&\sim \text{Cat} \left(\frac{a_1}{b}, \dots, \frac{a_J}{b} \right),
\end{aligned}$$

where $a_j = \pi_j \times \left(p(t) \times \mathcal{N}(\mathbf{s}_c(t) | \boldsymbol{\mu}_j, \Sigma_c) + (1 - p(t)) \times \mathcal{N}(\mathbf{s}_c(t) | \boldsymbol{\mu}_j, \tilde{\Sigma}_c) \right)^{y(t)}$
 $\times \left(p(t) \times \mathcal{N}(\mathbf{s}_c(t) | \boldsymbol{\mu}_j, \sigma_\mu^2 \mathbf{I} + \Sigma_c) + (1 - p(t)) \times \mathcal{N}(\mathbf{s}_c(t) | \boldsymbol{\mu}_j, \sigma_\mu^2 \mathbf{I} + \tilde{\Sigma}_c) \right)^{1-y(t)}$
and $b = \sum_{j=1}^J \left\{ \pi_j \times \left(p(t) \times \mathcal{N}(\mathbf{s}_c(t) | \boldsymbol{\mu}_j, \Sigma_c) + (1 - p(t)) \times \mathcal{N}(\mathbf{s}_c(t) | \boldsymbol{\mu}_j, \tilde{\Sigma}_c) \right)^{y(t)} \right.$
 $\left. \times \left(p(t) \times \mathcal{N}(\mathbf{s}_c(t) | \boldsymbol{\mu}_j, \sigma_\mu^2 \mathbf{I} + \Sigma_c) + (1 - p(t)) \times \mathcal{N}(\mathbf{s}_c(t) | \boldsymbol{\mu}_j, \sigma_\mu^2 \mathbf{I} + \tilde{\Sigma}_c) \right)^{1-y(t)} \right\}.$

Stick-breaking weights (η_j):

$$\begin{aligned} [\eta_j | \cdot] &\propto \prod_{t \in \mathcal{T}} [\boldsymbol{\mu}(t) | \pi_j]^{1\{\boldsymbol{\mu}(t)=\boldsymbol{\mu}_j\}} \prod_{i=j+1}^J \prod_{t \in \mathcal{T}} [\boldsymbol{\mu}(t) | \pi_i]^{1\{\boldsymbol{\mu}(t)=\boldsymbol{\mu}_i\}} [\eta_j | 1, \theta] \\ &\propto \prod_{t \in \mathcal{T}} \pi_j^{1\{\boldsymbol{\mu}(t)=\boldsymbol{\mu}_j\}} \prod_{i=j+1}^J \prod_{t \in \mathcal{T}} \pi_i^{1\{\boldsymbol{\mu}(t)=\boldsymbol{\mu}_i\}} \text{Beta}(\eta_j | 1, \theta) \\ &\propto \pi_j^{\sum_{t \in \mathcal{T}} (1\{\boldsymbol{\mu}(t)=\boldsymbol{\mu}_j\})} \prod_{i=j+1}^J \pi_i^{\sum_{t \in \mathcal{T}} (1\{\boldsymbol{\mu}(t)=\boldsymbol{\mu}_i\})} \eta_j^{1-1} (1 - \eta_j)^{\theta-1} \\ &\propto \left(\eta_j \prod_{l < j} (1 - \eta_l) \right)^{m_j} \prod_{i=j+1}^J \left(\eta_i \prod_{l < i} (1 - \eta_l) \right)^{m_i} (1 - \eta_j)^{\theta-1} \\ &\propto \eta_j^{m_j} \prod_{i=j+1}^J \left(\prod_{l < i} (1 - \eta_l) \right)^{m_i} (1 - \eta_j)^{\theta-1} \\ &\propto \eta_j^{m_j} (1 - \eta_j)^{\sum_{i=j+1}^J m_i} (1 - \eta_j)^{\theta-1} \\ &\propto \eta_j^{m_j} (1 - \eta_j)^{\sum_{i=j+1}^J m_i + \theta - 1} \\ &= \text{Beta}\left(m_j + 1, \sum_{i=j+1}^J m_i + \theta\right), \end{aligned}$$

where $m_j = \sum_{t \in \mathcal{T}} (1\{\boldsymbol{\mu}(t)=\boldsymbol{\mu}_j\})$, i.e., the number of observed telemetry locations ($\mathbf{s}_c(t)$) allocated to central place $\boldsymbol{\mu}_j$.

Auxiliary variable for temporal process model ($v(t)$):

$$\begin{aligned} [v(t) | \cdot] &\propto [y(t) | v(t)] [v(t) | \boldsymbol{\alpha}, \boldsymbol{\beta}] \\ &\propto (1_{\{y(t)=0\}} 1_{\{v(t) \leq 0\}} + 1_{\{y(t)=1\}} 1_{\{v(t) > 0\}}) \times \mathcal{N}(v(t) | \mathbf{x}(t)' \boldsymbol{\beta} + \mathbf{w}(t)' \boldsymbol{\alpha}, 1) \\ &= \begin{cases} \mathcal{T}\mathcal{N}(\mathbf{x}(t)' \boldsymbol{\beta} + \mathbf{w}(t)' \boldsymbol{\alpha}, 1) \Big|_{-\infty}^0, & y(t) = 0 \\ \mathcal{T}\mathcal{N}(\mathbf{x}(t)' \boldsymbol{\beta} + \mathbf{w}(t)' \boldsymbol{\alpha}, 1) \Big|_0^\infty, & y(t) = 1 \end{cases}. \end{aligned}$$

Basis coefficients in temporal process model ($\boldsymbol{\alpha}$):

$$\begin{aligned}
[\boldsymbol{\alpha} | \cdot] &\propto [\mathbf{v} | \boldsymbol{\beta}, \boldsymbol{\alpha}] [\boldsymbol{\alpha} | \mathbf{0}, \sigma_\alpha^2] \\
&\propto \mathcal{N}(\mathbf{v} | \mathbf{X}\boldsymbol{\beta} + \mathbf{W}\boldsymbol{\alpha}, \mathbf{1}) \mathcal{N}(\boldsymbol{\alpha} | \mathbf{0}, \sigma_\alpha^2 \mathbf{I}) \\
&\propto \exp \left\{ -\frac{1}{2} (\mathbf{v} - (\mathbf{X}\boldsymbol{\beta} + \mathbf{W}\boldsymbol{\alpha}))' (\mathbf{v} - (\mathbf{X}\boldsymbol{\beta} + \mathbf{W}\boldsymbol{\alpha})) \right\} \\
&\quad \times \exp \left\{ -\frac{1}{2} (\boldsymbol{\alpha} - \mathbf{0})' (\sigma_\alpha^2 \mathbf{I})^{-1} (\boldsymbol{\alpha} - \mathbf{0}) \right\} \\
&\propto \exp \left\{ -\frac{1}{2} ((\mathbf{v} - \mathbf{X}\boldsymbol{\beta}) - \mathbf{W}\boldsymbol{\alpha})' ((\mathbf{v} - \mathbf{X}\boldsymbol{\beta}) - \mathbf{W}\boldsymbol{\alpha}) \right\} \\
&\quad \times \exp \left\{ -\frac{1}{2} \boldsymbol{\alpha}' (\sigma_\alpha^2 \mathbf{I})^{-1} \boldsymbol{\alpha} \right\} \\
&\propto \exp \left\{ -\frac{1}{2} \left(-2 ((\mathbf{v} - \mathbf{X}\boldsymbol{\beta})' \mathbf{W}) \boldsymbol{\alpha} + \boldsymbol{\alpha}' \left(\mathbf{W}' \mathbf{W} + (\sigma_\alpha^2 \mathbf{I})^{-1} \right) \boldsymbol{\alpha} \right) \right\} \\
&= \mathcal{N}(\mathbf{A}^{-1} \mathbf{b}, \mathbf{A}^{-1}),
\end{aligned}$$

where $\mathbf{A} = \mathbf{W}' \mathbf{W} + (\sigma_\alpha^2 \mathbf{I})^{-1}$ and $\mathbf{b}' = (\mathbf{v} - \mathbf{X}\boldsymbol{\beta})' \mathbf{W}$. Note that the matrix $\mathbf{X} \equiv \{\mathbf{x}(t) : t \in \mathcal{T}\}$ contains the vectors $\mathbf{x}(t)$ for all times $t \in \mathcal{T}$. Similarly, $\mathbf{W} \equiv \{\mathbf{w}(t) : t \in \mathcal{T}\}$ is a matrix containing the vectors $\mathbf{w}(t)$ for all times $t \in \mathcal{T}$.

Locations of potential central places ($\boldsymbol{\mu}_j$):

$$\begin{aligned}
[\boldsymbol{\mu}_j | \cdot] &\propto \prod_{t \in \mathcal{T}} \left[\mathbf{s}_c(t) | \boldsymbol{\mu}(t), y(t), \boldsymbol{\Sigma}_c, \tilde{\boldsymbol{\Sigma}}_c, \sigma_\mu \right]^{1_{\{\mu(t)=\mu_j\}}} [\boldsymbol{\mu}_j] \\
&\propto \prod_{\{t: \mu(t)=\mu_j\}} \left\{ \left[\mathbf{s}_c(t) | \boldsymbol{\mu}_j, \boldsymbol{\Sigma}_c, \tilde{\boldsymbol{\Sigma}}_c \right]^{y(t)} \left[\mathbf{s}_c(t) | \boldsymbol{\mu}_j, \sigma_\mu^2 \mathbf{I} + \boldsymbol{\Sigma}_c, \sigma_\mu^2 \mathbf{I} + \tilde{\boldsymbol{\Sigma}}_c \right]^{1-y(t)} \right\} [\boldsymbol{\mu}_j] \\
&\propto \prod_{\{t: \mu(t)=\mu_j\}} \left\{ \left(p(t) \times \mathcal{N}(\mathbf{s}_c(t) | \boldsymbol{\mu}_j, \boldsymbol{\Sigma}_c) + (1-p(t)) \times \mathcal{N}(\mathbf{s}_c(t) | \boldsymbol{\mu}_j, \tilde{\boldsymbol{\Sigma}}_c) \right)^{y(t)} \right. \\
&\quad \times \left. \left(p(t) \times \mathcal{N}(\mathbf{s}_c(t) | \boldsymbol{\mu}_j, \sigma_\mu^2 \mathbf{I} + \boldsymbol{\Sigma}_c) + (1-p(t)) \times \mathcal{N}(\mathbf{s}_c(t) | \boldsymbol{\mu}_j, \sigma_\mu^2 \mathbf{I} + \tilde{\boldsymbol{\Sigma}}_c) \right)^{1-y(t)} \right\} \\
&\quad \times [\boldsymbol{\mu}_j].
\end{aligned}$$

Note that the product is over all $t \in \mathcal{T}$ such that $\mathbf{s}_c(t)$ is allocated to central place $\boldsymbol{\mu}_j$ (i.e., instances where $\boldsymbol{\mu}(t) = \boldsymbol{\mu}_j$).

Dirichlet process concentration parameter (θ):

$$\begin{aligned}
[\theta|\cdot] &\propto \prod_{j=1}^{J-1} [\eta_j \mid 1, \theta] [\theta] \\
&\propto \prod_{j=1}^{J-1} \text{Beta}(\eta_j \mid 1, \theta) \text{Gamma}(\theta \mid r_\theta, q_\theta) \\
&\propto \prod_{j=1}^{J-1} \frac{\Gamma(1+\theta)}{\Gamma(1)\Gamma(\theta)} \eta_j^{1-1} (1-\eta_j)^{\theta-1} \theta^{r_\theta-1} \exp\{-q_\theta\theta\} \\
&\propto \left(\frac{\theta\Gamma(\theta)}{\Gamma(1)\Gamma(\theta)}\right)^{J-1} \theta^{r_\theta-1} \exp\left\{-q_\theta\theta + \log\left(\prod_{j=1}^{J-1} (1-\eta_j)^{\theta-1}\right)\right\} \\
&\propto \left(\frac{\theta\Gamma(\theta)}{\Gamma(1)\Gamma(\theta)}\right)^{J-1} \theta^{r_\theta-1} \exp\left\{-q_\theta\theta + \log\left(\prod_{j=1}^{J-1} (1-\eta_j)^\theta (1-\eta_j)^{-1}\right)\right\} \\
&\propto \left(\frac{\theta\Gamma(\theta)}{\Gamma(1)\Gamma(\theta)}\right)^{J-1} \theta^{r_\theta-1} \exp\left\{-q_\theta\theta + \log\left(\prod_{j=1}^{J-1} (1-\eta_j)^\theta\right)\right\} \\
&\propto \theta^{J-1+r_\theta-1} \exp\left\{-q_\theta\theta + \sum_{j=1}^{J-1} \log(1-\eta_j)^\theta\right\} \\
&\propto \theta^{J-1+r_\theta-1} \exp\left\{-q_\theta\theta + \theta \sum_{j=1}^{J-1} \log(1-\eta_j)\right\} \\
&\propto \theta^{J-1+r_\theta-1} \exp\left\{-\theta \left(q_\theta - \sum_{j=1}^{J-1} \log(1-\eta_j)\right)\right\} \\
&= \text{Gamma}\left(r_\theta + J - 1, q_\theta - \sum_{j=1}^{J-1} \log(1-\eta_j)\right).
\end{aligned}$$

Note that the product is over $j = 1, \dots, J-1$ because $\eta_J = 1$ in the truncation approximation of a Dirichlet process.

Fixed effects in temporal process model (β):

$$\begin{aligned}
[\beta | \cdot] &\propto [\mathbf{v} | \beta, \alpha] [\beta] \\
&\propto \mathcal{N}(\mathbf{v} | \mathbf{X}\beta + \mathbf{W}\alpha, \mathbf{1}) \mathcal{N}(\beta | \mu_\beta, \sigma_\beta^2 \mathbf{I}) \\
&\propto \exp \left\{ -\frac{1}{2} (\mathbf{v} - (\mathbf{X}\beta + \mathbf{W}\alpha))' (\mathbf{v} - (\mathbf{X}\beta + \mathbf{W}\alpha)) \right\} \\
&\quad \times \exp \left\{ -\frac{1}{2} (\beta - \mu_\beta)' (\sigma_\beta^2 \mathbf{I})^{-1} (\beta - \mu_\beta) \right\} \\
&\propto \exp \left\{ -\frac{1}{2} ((\mathbf{v} - \mathbf{W}\alpha) - \mathbf{X}\beta)' ((\mathbf{v} - \mathbf{W}\alpha) - \mathbf{X}\beta) \right\} \\
&\quad \times \exp \left\{ -\frac{1}{2} (\beta - \mu_\beta)' (\sigma_\beta^2 \mathbf{I})^{-1} (\beta - \mu_\beta) \right\} \\
&\propto \exp \left\{ -\frac{1}{2} \left(-2 \left((\mathbf{v} - \mathbf{W}\alpha)' \mathbf{X} + \mu_\beta' (\sigma_\beta^2 \mathbf{I})^{-1} \right) \beta + \beta' \left(\mathbf{X}' \mathbf{X} + (\sigma_\beta^2 \mathbf{I})^{-1} \right) \beta \right) \right\} \\
&= \mathcal{N}(\mathbf{A}^{-1} \mathbf{b}, \mathbf{A}^{-1}),
\end{aligned}$$

where $\mathbf{A} = \mathbf{X}' \mathbf{X} + (\sigma_\beta^2 \mathbf{I})^{-1}$ and $\mathbf{b}' = (\mathbf{v} - \mathbf{W}\alpha)' \mathbf{X} + \mu_\beta' (\sigma_\beta^2 \mathbf{I})^{-1}$. Note that the matrix $\mathbf{X} \equiv \{\mathbf{x}(t) : t \in \mathcal{T}\}$ contains the vectors $\mathbf{x}(t)$ for all times $t \in \mathcal{T}$. Similarly, $\mathbf{W} \equiv \{\mathbf{w}(t) : t \in \mathcal{T}\}$ is a matrix containing the vectors $\mathbf{w}(t)$ for all times $t \in \mathcal{T}$.

Animal movement parameter (σ_μ):

$$\begin{aligned}
[\sigma_\mu | \cdot] &\propto \prod_{t \in \mathcal{T}} \left[\mathbf{s}_c(t) | \mu(t), y(t), \Sigma_c, \tilde{\Sigma}_c, \sigma_\mu \right] [\sigma_\mu] \\
&\propto \prod_{t \in \mathcal{T}} \left[\mathbf{s}_c(t) | \mu(t), \Sigma_c, \tilde{\Sigma}_c, \sigma_\mu^2 \right]^{1-y(t)} [\sigma_\mu] \\
&\propto \prod_{\{t: y(t)=0\}} \left(p(t) \times \mathcal{N}(\mathbf{s}_c(t) | \mu(t), \sigma_\mu^2 \mathbf{I} + \Sigma_c) + (1-p(t)) \times \mathcal{N}(\mathbf{s}_c(t) | \mu(t), \sigma_\mu^2 \mathbf{I} + \tilde{\Sigma}_c) \right) \\
&\quad \times \mathcal{N}(\log(\sigma_\mu) | \log(\mu_\sigma), \sigma_\sigma^2).
\end{aligned}$$

Note that the product is over all $t \in \mathcal{T}$ such that $y(t) = 0$ (i.e., all observed telemetry locations ($\mathbf{s}_c(t)$) collected when the individual is not at the central place).

Variance of basis coefficients (σ_α^2):

$$\begin{aligned}
[\sigma_\alpha^2 | \cdot] &\propto [\boldsymbol{\alpha} | \mathbf{0}, \sigma_\alpha^2] [\sigma_\alpha^2] \\
&\propto \mathcal{N}(\boldsymbol{\alpha} | \mathbf{0}, \sigma_\alpha^2 \mathbf{I}) \text{IG}(\sigma_\alpha^2 | r_\alpha, q_\alpha) \\
&\propto |\sigma_\alpha^2 \mathbf{I}|^{-1/2} \exp \left\{ -\frac{1}{2} \left((\boldsymbol{\alpha} - \mathbf{0})' (\sigma_\alpha^2 \mathbf{I})^{-1} (\boldsymbol{\alpha} - \mathbf{0}) \right) \right\} (\sigma_\alpha^2)^{-(q_\alpha+1)} \exp \left\{ -\frac{1}{r_\alpha \sigma_\alpha^2} \right\} \\
&\propto (\sigma_\alpha^2)^{-M/2} \exp \left\{ -\frac{1}{2\sigma_\alpha^2} \boldsymbol{\alpha}' \boldsymbol{\alpha} \right\} (\sigma_\alpha^2)^{-(q_\alpha+1)} \exp \left\{ -\frac{1}{r_\alpha \sigma_\alpha^2} \right\} \\
&\propto (\sigma_\alpha^2)^{-(M/2+q_\alpha+1)} \exp \left\{ -\frac{1}{\sigma_\alpha^2} \left(\frac{\boldsymbol{\alpha}' \boldsymbol{\alpha}}{2} + \frac{1}{r_\alpha} \right) \right\} \\
&= \text{IG} \left(\left(\frac{\boldsymbol{\alpha}' \boldsymbol{\alpha}}{2} + \frac{1}{r_\alpha} \right)^{-1}, \frac{M}{2} + q_\alpha \right),
\end{aligned}$$

where M is the length of $\boldsymbol{\alpha}$ (or column dimension of \mathbf{W}).

Longitudinal telemetry measurement error (σ_c):

$$\begin{aligned}
[\sigma_c | \cdot] &\propto \prod_{\tilde{t} \in \mathcal{T}} [\mathbf{s}_c(\tilde{t}) | \boldsymbol{\mu}(\tilde{t}), y(\tilde{t}), \boldsymbol{\Sigma}_c, \tilde{\boldsymbol{\Sigma}}_c, \sigma_\mu] [\sigma_c] \\
&\propto \prod_{\tilde{t} \in \mathcal{T}} \left\{ [\mathbf{s}_c(\tilde{t}) | \boldsymbol{\mu}(\tilde{t}), \boldsymbol{\Sigma}_c, \tilde{\boldsymbol{\Sigma}}_c]^{y(\tilde{t})} [\mathbf{s}_c(\tilde{t}) | \boldsymbol{\mu}(\tilde{t}), \sigma_\mu^2 \mathbf{I} + \boldsymbol{\Sigma}_c, \sigma_\mu^2 \mathbf{I} + \tilde{\boldsymbol{\Sigma}}_c]^{1-y(\tilde{t})} \right\} [\sigma_c] \\
&\propto \prod_{\tilde{t} \in \mathcal{T}} \left\{ \left(p(\tilde{t}) \times \mathcal{N}(\mathbf{s}_c(\tilde{t}) | \boldsymbol{\mu}(\tilde{t}), \boldsymbol{\Sigma}_c) + (1-p(\tilde{t})) \times \mathcal{N}(\mathbf{s}_c(\tilde{t}) | \boldsymbol{\mu}(\tilde{t}), \tilde{\boldsymbol{\Sigma}}_c) \right)^{y(\tilde{t})} \right. \\
&\quad \left. \times \left(p(\tilde{t}) \times \mathcal{N}(\mathbf{s}_c(\tilde{t}) | \boldsymbol{\mu}(\tilde{t}), \sigma_\mu^2 \mathbf{I} + \boldsymbol{\Sigma}_c) + (1-p(\tilde{t})) \times \mathcal{N}(\mathbf{s}_c(\tilde{t}) | \boldsymbol{\mu}(\tilde{t}), \sigma_\mu^2 \mathbf{I} + \tilde{\boldsymbol{\Sigma}}_c) \right)^{1-y(\tilde{t})} \right\} \\
&\quad \times \text{Unif}(\sigma_c | l_\sigma, u_\sigma),
\end{aligned}$$

where $\tilde{t} \in \mathcal{T}$ is the subset of times for all observed telemetry locations ($\mathbf{s}_c(t)$) belonging to Argos location quality class c . In other words, the product is over all $t \in \mathcal{T}$ such that $\mathbf{s}_c(t)$ is allocated to location quality class c .

Adjustment for latitudinal telemetry measurement error (a_c):

$$\begin{aligned}
[a_c | \cdot] &\propto \prod_{\tilde{t} \in \mathcal{T}} [\mathbf{s}_c(\tilde{t}) | \boldsymbol{\mu}(\tilde{t}), y(\tilde{t}), \boldsymbol{\Sigma}_c, \tilde{\boldsymbol{\Sigma}}_c, \sigma_\mu] [a_c] \\
&\propto \prod_{\tilde{t} \in \mathcal{T}} \left\{ [\mathbf{s}_c(\tilde{t}) | \boldsymbol{\mu}(\tilde{t}), \boldsymbol{\Sigma}_c, \tilde{\boldsymbol{\Sigma}}_c]^{y(\tilde{t})} [\mathbf{s}_c(\tilde{t}) | \boldsymbol{\mu}(\tilde{t}), \sigma_\mu^2 \mathbf{I} + \boldsymbol{\Sigma}_c, \sigma_\mu^2 \mathbf{I} + \tilde{\boldsymbol{\Sigma}}_c]^{1-y(\tilde{t})} \right\} [a_c] \\
&\propto \prod_{\tilde{t} \in \mathcal{T}} \left\{ \left(p(\tilde{t}) \times \mathcal{N}(\mathbf{s}_c(\tilde{t}) | \boldsymbol{\mu}(\tilde{t}), \boldsymbol{\Sigma}_c) + (1-p(\tilde{t})) \times \mathcal{N}(\mathbf{s}_c(\tilde{t}) | \boldsymbol{\mu}(\tilde{t}), \tilde{\boldsymbol{\Sigma}}_c) \right)^{y(\tilde{t})} \right. \\
&\quad \left. \times \left(p(\tilde{t}) \times \mathcal{N}(\mathbf{s}_c(\tilde{t}) | \boldsymbol{\mu}(\tilde{t}), \sigma_\mu^2 \mathbf{I} + \boldsymbol{\Sigma}_c) + (1-p(\tilde{t})) \times \mathcal{N}(\mathbf{s}_c(\tilde{t}) | \boldsymbol{\mu}(\tilde{t}), \sigma_\mu^2 \mathbf{I} + \tilde{\boldsymbol{\Sigma}}_c) \right)^{1-y(\tilde{t})} \right\} \\
&\quad \times \text{Unif}(a_c | l_a, u_a).
\end{aligned}$$

where $\tilde{\mathcal{T}} \in \mathcal{T}$ is the subset of times for all observed telemetry locations ($\mathbf{s}_c(t)$) belonging to Argos location quality class c . In other words, the product is over all $t \in \mathcal{T}$ such that $\mathbf{s}_c(t)$ is allocated to location quality class c .

Correlation between longitudinal and latitudinal telemetry measurement error (σ_c):

$$\begin{aligned} [\rho_c | \cdot] &\propto \prod_{\tilde{t} \in \tilde{\mathcal{T}}} \left[\mathbf{s}_c(\tilde{t}) | \boldsymbol{\mu}(\tilde{t}), y(\tilde{t}), \boldsymbol{\Sigma}_c, \tilde{\boldsymbol{\Sigma}}_c, \sigma_\mu \right] [\rho_c] \\ &\propto \prod_{\tilde{t} \in \tilde{\mathcal{T}}} \left\{ \left[\mathbf{s}_c(\tilde{t}) | \boldsymbol{\mu}(\tilde{t}), \boldsymbol{\Sigma}_c, \tilde{\boldsymbol{\Sigma}}_c \right]^{y(\tilde{t})} \left[\mathbf{s}_c(\tilde{t}) | \boldsymbol{\mu}(\tilde{t}), \sigma_\mu^2 \mathbf{I} + \boldsymbol{\Sigma}_c, \sigma_\mu^2 \mathbf{I} + \tilde{\boldsymbol{\Sigma}}_c \right]^{1-y(\tilde{t})} \right\} [\rho_c] \\ &\propto \prod_{\tilde{t} \in \tilde{\mathcal{T}}} \left\{ \left(p(\tilde{t}) \times \mathcal{N}(\mathbf{s}_c(\tilde{t}) | \boldsymbol{\mu}(\tilde{t}), \boldsymbol{\Sigma}_c) + (1-p(\tilde{t})) \times \mathcal{N}(\mathbf{s}_c(\tilde{t}) | \boldsymbol{\mu}(\tilde{t}), \tilde{\boldsymbol{\Sigma}}_c) \right)^{y(\tilde{t})} \right. \\ &\quad \left. \times \left(p(\tilde{t}) \times \mathcal{N}(\mathbf{s}_c(\tilde{t}) | \boldsymbol{\mu}(\tilde{t}), \sigma_\mu^2 \mathbf{I} + \boldsymbol{\Sigma}_c) + (1-p(\tilde{t})) \times \mathcal{N}(\mathbf{s}_c(\tilde{t}) | \boldsymbol{\mu}(\tilde{t}), \sigma_\mu^2 \mathbf{I} + \tilde{\boldsymbol{\Sigma}}_c) \right)^{1-y(\tilde{t})} \right\} \\ &\quad \times \text{Unif}(\rho_c | l_\rho, u_\rho). \end{aligned}$$

where $\tilde{\mathcal{T}} \in \mathcal{T}$ is the subset of times for all observed telemetry locations ($\mathbf{s}_c(t)$) belonging to Argos location quality class c . In other words, the product is over all $t \in \mathcal{T}$ such that $\mathbf{s}_c(t)$ is allocated to location quality class c .

APPENDIX B2. Markov chain Monte Carlo algorithm for parameter estimation.

One can implement a Markov chain Monte Carlo algorithm to estimate the parameters of the observation and process models using the sequence of steps outlined below. Proposal distributions for all parameters with non-conjugate full-conditional distributions (i.e., $\boldsymbol{\mu}_j$, σ_μ , σ_c , a_c , and ρ_c) are assumed to be symmetric and updates proceed using Metropolis sampling; therefore, the proposal distribution is not factored into the associated ratios as in Metropolis-Hastings sampling. Also note that normalizing constants cancel in the Metropolis ratios and thus may be omitted for clarity.

1. Define initial values for: $\boldsymbol{\mu}_j^{(0)}$ and $\pi_j^{(0)}$ for $j = 1, \dots, J$; $\theta^{(0)}$; $\sigma_\mu^{(0)}$; $\boldsymbol{\alpha}^{(0)}$; $(\sigma_\alpha^2)^{(0)}$; and $\sigma_c^{(0)}$, $a_c^{(0)}$, and $\rho_c^{(0)}$ for $c = 3, 2, 1, 0, A$, and B .
2. For each Argos location quality class, let

$$\boldsymbol{\Sigma}_c^{(0)} = (\sigma_c^{(0)})^2 \begin{bmatrix} 1 & \rho_c^{(0)} \sqrt{a_c^{(0)}} \\ \rho_c^{(0)} \sqrt{a_c^{(0)}} & a_c^{(0)} \end{bmatrix}$$

and

$$\begin{aligned} \tilde{\boldsymbol{\Sigma}}_c^{(0)} &= (\sigma_c^{(0)})^2 \begin{bmatrix} 1 & -\rho_c^{(0)} \sqrt{a_c^{(0)}} \\ -\rho_c^{(0)} \sqrt{a_c^{(0)}} & a_c^{(0)} \end{bmatrix} \\ &= \mathbf{H} \boldsymbol{\Sigma}_c^{(0)} \mathbf{H}', \end{aligned}$$

where

$$\mathbf{H} = \begin{bmatrix} 1 & 0 \\ 0 & -1 \end{bmatrix}.$$

Also let

$$\mathbf{Q}_c^{(0)} = \boldsymbol{\Sigma}_c^{(0)} + (\sigma_\mu^{(0)})^2 \mathbf{I}$$

and

$$\begin{aligned} \tilde{\mathbf{Q}}_c^{(0)} &= \tilde{\boldsymbol{\Sigma}}_c^{(0)} + (\sigma_\mu^{(0)})^2 \mathbf{I} \\ &= \mathbf{H} \mathbf{Q}_c^{(0)} \mathbf{H}'. \end{aligned}$$

3. Set $k = 1$.
4. Update the spatial process model parameters (i.e., $h(t)$, η_j , θ , and $\boldsymbol{\mu}_j$).
- (a) Sample $h(t)^{(k)}$, for all times $t \in \mathcal{T}$, using a Gibbs step:

$$[h(t)^{(k)} | \cdot] \sim \text{Cat} \left(\frac{a_1^{(k-1)}}{b^{(k-1)}}, \dots, \frac{a_J^{(k-1)}}{b^{(k-1)}} \right),$$

where

$$a_j^{(k-1)} = \pi_j^{(k-1)} \times \left(p(t) \times \mathcal{N}(\mathbf{s}_c(t) | \boldsymbol{\mu}_j^{(k-1)}, \boldsymbol{\Sigma}_c^{(k-1)}) + (1-p(t)) \times \mathcal{N}(\mathbf{s}_c(t) | \boldsymbol{\mu}_j^{(k-1)}, \mathbf{H}\boldsymbol{\Sigma}_c^{(k-1)}\mathbf{H}') \right)^{y(t)} \\ \times \left(p(t) \times \mathcal{N}(\mathbf{s}_c(t) | \boldsymbol{\mu}_j^{(k-1)}, \mathbf{Q}_c^{(k-1)}) + (1-p(t)) \times \mathcal{N}(\mathbf{s}_c(t) | \boldsymbol{\mu}_j^{(k-1)}, \mathbf{H}\mathbf{Q}_c^{(k-1)}\mathbf{H}') \right)^{1-y(t)}$$

and

$$b = \sum_{j=1}^J \left\{ \pi_j^{(k-1)} \times \left(p(t) \times \mathcal{N}(\mathbf{s}_c(t) | \boldsymbol{\mu}_j^{(k-1)}, \boldsymbol{\Sigma}_c^{(k-1)}) + (1-p(t)) \times \mathcal{N}(\mathbf{s}_c(t) | \boldsymbol{\mu}_j^{(k-1)}, \mathbf{H}\boldsymbol{\Sigma}_c^{(k-1)}\mathbf{H}') \right)^{y(t)} \right. \\ \left. \times \left(p(t) \times \mathcal{N}(\mathbf{s}_c(t) | \boldsymbol{\mu}_j^{(k-1)}, \mathbf{Q}_c^{(k-1)}) + (1-p(t)) \times \mathcal{N}(\mathbf{s}_c(t) | \boldsymbol{\mu}_j^{(k-1)}, \mathbf{H}\mathbf{Q}_c^{(k-1)}\mathbf{H}') \right)^{1-y(t)} \right\}.$$

Recall that $h(t)^{(k)} \in \{1, \dots, J\}$ allocates each observed telemetry location ($\mathbf{s}_c(t)$) to a central place $\boldsymbol{\mu}_j$ (i.e., $\boldsymbol{\mu}(t)^{(k)} = \boldsymbol{\mu}_{h(t)^{(k)}}$).

(b) For $j = 1, \dots, J$, tabulate cluster membership:

$$m_j^{(k)} = \sum_{t \in \mathcal{T}} \mathbb{1}_{\{h(t)^{(k)} = j\}}.$$

In other words, $m_j^{(k)}$ denotes the number of observed telemetry locations ($\mathbf{s}_c(t)$) allocated to central place $\boldsymbol{\mu}_j^{(k-1)}$.

(c) Sample $\eta_j^{(k)}$, for $j = 1, \dots, J-1$, using a Gibbs step:

$$[\eta_j^{(k)} | \cdot] \sim \text{Beta} \left(m_j^{(k)} + 1, \sum_{i=j+1}^J m_i^{(k)} + \theta^{(k-1)} \right).$$

Set $\eta_J^{(k)} = 1$.

(d) Update $\pi_j^{(k-1)}$, for $j = 1, \dots, J$, which is calculated as:

$$\pi_j^{(k)} = \eta_j^{(k)} \prod_{l < j} \left(1 - \eta_l^{(k)} \right).$$

Letting $\eta_J^{(k)} = 1$ in Step 4(c) guarantees $\sum_{j=1}^J \pi_j^{(k)} = 1$. Note that a sufficient value for J , the upper bound to the truncation approximation of the Dirichlet process, can be confirmed by ensuring $\pi_J^{(k)} \approx 0$.

(e) Update $\theta^{(k-1)}$ using a Gibbs step:

$$[\theta^{(k)} | \cdot] \propto \text{Gamma} \left(r_\theta + J - 1, q_\theta - \sum_{j=1}^{J-1} \log \left(1 - \eta_j^{(k)} \right) \right).$$

- (f) Update $\boldsymbol{\mu}_j^{(k-1)}$, for each j such that $m_j > 0$, using Metropolis sampling. Sample $\boldsymbol{\mu}_j^{(*)}$ from a proposal distribution $[\boldsymbol{\mu}_j^{(*)} | \boldsymbol{\mu}_j^{(k-1)}]$. Depending on the nature of $\tilde{\mathcal{S}}$ (e.g., linear support like a coastline), proposals generated from $\mathcal{N}(\boldsymbol{\mu}_j^{(*)} | \boldsymbol{\mu}_j^{(k-1)}, \tau_\mu^2 \mathbf{I})$, where τ_μ^2 is a tuning parameter, may rarely occur in $\tilde{\mathcal{S}}$. Therefore, sample locations $\boldsymbol{\mu} \in \tilde{\mathcal{S}}$ with probability proportional to $\mathcal{N}(\boldsymbol{\mu} | \boldsymbol{\mu}_j^{(k-1)}, \tau_\mu^2 \mathbf{I})$, thus guaranteeing $\boldsymbol{\mu}_j^{(*)} \in \tilde{\mathcal{S}}$. Calculate the Metropolis ratio as

$$r_\mu = \left(\frac{\prod_{\{t:h(t)^{(k)}=j\}} \left\{ (p(t) \times \mathcal{N}(\mathbf{s}_c(t) | \boldsymbol{\mu}_j^{(*)}, \boldsymbol{\Sigma}_c^{(k-1)}) + (1-p(t)) \times \mathcal{N}(\mathbf{s}_c(t) | \boldsymbol{\mu}_j^{(*)}, \mathbf{H}\boldsymbol{\Sigma}_c^{(k-1)}\mathbf{H}') \right\}^{y(t)}}{\prod_{\{t:h(t)^{(k)}=j\}} \left\{ (p(t) \times \mathcal{N}(\mathbf{s}_c(t) | \boldsymbol{\mu}_j^{(k-1)}, \boldsymbol{\Sigma}_c^{(k-1)}) + (1-p(t)) \times \mathcal{N}(\mathbf{s}_c(t) | \boldsymbol{\mu}_j^{(k-1)}, \mathbf{H}\boldsymbol{\Sigma}_c^{(k-1)}\mathbf{H}') \right\}^{y(t)}} \right. \\ \times \left. \frac{\left(p(t) \times \mathcal{N}(\mathbf{s}_c(t) | \boldsymbol{\mu}_j^{(*)}, \mathbf{Q}_c^{(k-1)}) + (1-p(t)) \times \mathcal{N}(\mathbf{s}_c(t) | \boldsymbol{\mu}_j^{(*)}, \mathbf{HQ}_c^{(k-1)}\mathbf{H}') \right)^{1-y(t)}}{\left(p(t) \times \mathcal{N}(\mathbf{s}_c(t) | \boldsymbol{\mu}_j^{(k-1)}, \mathbf{Q}_c^{(k-1)}) + (1-p(t)) \times \mathcal{N}(\mathbf{s}_c(t) | \boldsymbol{\mu}_j^{(k-1)}, \mathbf{HQ}_c^{(k-1)}\mathbf{H}') \right)^{1-y(t)}} \right) \\ \times \left(\frac{[\boldsymbol{\mu}_j^{(*)} | f_{\tilde{\mathcal{S}}}(\mathbf{S})]}{[\boldsymbol{\mu}_j^{(k-1)} | f_{\tilde{\mathcal{S}}}(\mathbf{S})]} \right).$$

Note that the product is over all $t \in \mathcal{T}$ such that $\mathbf{s}_c(t)$ is allocated to central place $\boldsymbol{\mu}_j$. If $r_\mu > u$, where $u \sim \text{Uniform}(0,1)$, let $\boldsymbol{\mu}_j^{(k)} = \boldsymbol{\mu}_j^{(*)}$. Otherwise, let $\boldsymbol{\mu}_j^{(k)} = \boldsymbol{\mu}_j^{(k-1)}$ if $r_\mu < u$, or if $\boldsymbol{\mu}_j^{(*)} \notin \tilde{\mathcal{S}}$.

- (g) Update $\boldsymbol{\mu}_j^{(k-1)}$, for each j such that $m_j^{(k)} = 0$ (i.e., central places $\boldsymbol{\mu}_j^{(k-1)}$ with zero membership), by sampling $\boldsymbol{\mu}_j^{(k)}$ from the prior $[\boldsymbol{\mu}_j^{(k)} | f_{\tilde{\mathcal{S}}}(\mathbf{S})]$. As in Step 4(f), sample locations $\boldsymbol{\mu} \in \tilde{\mathcal{S}}$ with probability proportional to $f_{\tilde{\mathcal{S}}}(\mathbf{S})$ to ensure $\boldsymbol{\mu}_j^{(k)} \in \tilde{\mathcal{S}}$.

- (h) Use $h(t)^{(k)}$ to map the potential central places $\boldsymbol{\mu}_j^{(k)}$ to observed telemetry locations $(\mathbf{s}_c(t))$, for all times $t \in \mathcal{T}$:

$$\boldsymbol{\mu}(t)^{(k)} = \boldsymbol{\mu}_{h(t)^{(k)}}^{(k)}.$$

5. Update $\sigma_\mu^{(k-1)}$ using Metropolis sampling. Sample $\sigma_\mu^{(*)}$ from a proposal distribution $[\sigma_\mu^{(*)} | \sigma_\mu^{(k-1)}]$ (e.g., $\mathcal{N}(\sigma_\mu^{(*)} | \sigma_\mu^{(k-1)}, \tau_\sigma^2 \mathbf{I})$, where τ_σ^2 is a tuning parameter). If $\sigma_\mu^{(*)} \geq 0$, let

$$\mathbf{Q}_c^{(*)} = \boldsymbol{\Sigma}_c^{(k-1)} + (\sigma_\mu^{(*)})^2 \mathbf{I}$$

for $c = 3, 2, 1, 0, \text{A}$, and B . Calculate the Metropolis ratio as

$$r_{\sigma_\mu} = \left(\frac{\prod_{\{t:y(t)=0\}} \left\{ p(t) \times \mathcal{N}(\mathbf{s}_c(t) | \boldsymbol{\mu}(t)^{(k)}, \mathbf{Q}_c^{(*)}) + (1-p(t)) \times \mathcal{N}(\mathbf{s}_c(t) | \boldsymbol{\mu}(t)^{(k)}, \mathbf{HQ}_c^{(*)}\mathbf{H}') \right\}}{\prod_{\{t:y(t)=0\}} \left\{ p(t) \times \mathcal{N}(\mathbf{s}_c(t) | \boldsymbol{\mu}(t)^{(k)}, \mathbf{Q}_c^{(k-1)}) + (1-p(t)) \times \mathcal{N}(\mathbf{s}_c(t) | \boldsymbol{\mu}(t)^{(k)}, \mathbf{HQ}_c^{(k-1)}\mathbf{H}') \right\}} \right) \\ \times \left(\frac{\mathcal{N}(\log(\sigma_\mu^{(*)}) | \log(\mu_\sigma), \sigma_\sigma^2)}{\mathcal{N}(\log(\sigma_\mu^{(k-1)}) | \log(\mu_\sigma), \sigma_\sigma^2)} \right).$$

Note that the product is over all $t \in \mathcal{T}$ such that $y(t) = 0$. If $r_{\sigma_\mu} > u$, where $u \sim \text{Uniform}(0,1)$, let $\sigma_\mu^{(k)} = \sigma_\mu^{(*)}$ and $\mathbf{Q}_c^{(k)} = \mathbf{Q}_c^{(*)}$. Otherwise, let $\sigma_\mu^{(k)} = \sigma_\mu^{(k-1)}$ and $\mathbf{Q}_c^{(k)} = \mathbf{Q}_c^{(k-1)}$ if $r_{\sigma_\mu} < u$, or if $\sigma_\mu^{(*)} < 0$.

6. Update the observation model parameters related to telemetry measurement error (i.e., σ_c , a_c , and ρ_c).

- (a) Let $\tilde{t} \in \mathcal{T}$ be the times of all observed telemetry locations ($\mathbf{s}_c(t)$) belonging to a single Argos location quality class c .
- (b) Update $\sigma_c^{(k-1)}$ using Metropolis sampling. Sample $\sigma_c^{(*)}$ from a proposal distribution $\left[\sigma_c^{(*)} | \sigma_c^{(k-1)} \right]$ (e.g., $\mathcal{N}\left(\sigma_c^{(*)} | \sigma_c^{(k-1)}, \tau_\sigma^2\right)$, where τ_σ^2 is a tuning parameter). If $\sigma_c^{(*)} \in [l_\sigma, u_\sigma]$, let

$$\Sigma_c^{(*)} = (\sigma_c^{(*)})^2 \begin{bmatrix} 1 & \rho_c^{(k-1)} \sqrt{a_c^{(k-1)}} \\ \rho_c^{(k-1)} \sqrt{a_c^{(k-1)}} & a_c^{(k-1)} \end{bmatrix}$$

and

$$\mathbf{Q}_c^{(*)} = \Sigma_c^{(*)} + (\sigma_\mu^{(k)})^2 \mathbf{I}.$$

Calculate the Metropolis ratio as

$$r_\sigma = \frac{\left(\frac{\prod_{\tilde{t}} \left\{ (p(\tilde{t}) \times \mathcal{N}(\mathbf{s}_c(\tilde{t}) | \boldsymbol{\mu}(\tilde{t})^{(k)}, \Sigma_c^{(*)}) + (1 - p(\tilde{t})) \times \mathcal{N}(\mathbf{s}_c(\tilde{t}) | \boldsymbol{\mu}(\tilde{t})^{(k)}, \mathbf{H}\Sigma_c^{(*)}\mathbf{H}') \right)^{y(\tilde{t})}}{\prod_{\tilde{t}} \left\{ (p(\tilde{t}) \times \mathcal{N}(\mathbf{s}_c(\tilde{t}) | \boldsymbol{\mu}(\tilde{t})^{(k)}, \Sigma_c^{(k-1)}) + (1 - p(\tilde{t})) \times \mathcal{N}(\mathbf{s}_c(\tilde{t}) | \boldsymbol{\mu}(\tilde{t})^{(k)}, \mathbf{H}\Sigma_c^{(k-1)}\mathbf{H}') \right)^{y(\tilde{t})}} \times \frac{\left(p(\tilde{t}) \times \mathcal{N}(\mathbf{s}_c(\tilde{t}) | \boldsymbol{\mu}(\tilde{t})^{(k)}, \mathbf{Q}_c^{(*)}) + (1 - p(\tilde{t})) \times \mathcal{N}(\mathbf{s}_c(\tilde{t}) | \boldsymbol{\mu}(\tilde{t})^{(k)}, \mathbf{H}\mathbf{Q}_c^{(*)}\mathbf{H}') \right)^{1-y(\tilde{t})}}{\left(p(\tilde{t}) \times \mathcal{N}(\mathbf{s}_c(\tilde{t}) | \boldsymbol{\mu}(\tilde{t})^{(k)}, \mathbf{Q}_c^{(k)}) + (1 - p(\tilde{t})) \times \mathcal{N}(\mathbf{s}_c(\tilde{t}) | \boldsymbol{\mu}(\tilde{t})^{(k)}, \mathbf{H}\mathbf{Q}_c^{(k)}\mathbf{H}') \right)^{1-y(\tilde{t})}} \right\}}.$$

If $r_\sigma > u$, where $u \sim \text{Uniform}(0,1)$, let $\sigma_c^{(k)} = \sigma_c^{(*)}$, $\Sigma_c^{(k)} = \Sigma_c^{(*)}$, and $\mathbf{Q}_c^{(k)} = \mathbf{Q}_c^{(*)}$. Otherwise, let $\sigma_c^{(k)} = \sigma_c^{(k-1)}$, $\Sigma_c^{(k)} = \Sigma_c^{(k-1)}$, and $\mathbf{Q}_c^{(k)} = \mathbf{Q}_c^{(k)} = \Sigma_c^{(k-1)} + (\sigma_\mu^{(k)})^2 \mathbf{I}$ if $r_\sigma < u$, or if $\sigma_c^{(*)} \notin [l_\sigma, u_\sigma]$.

- (c) Update $a_c^{(k-1)}$ using Metropolis sampling. Sample $a_c^{(*)}$ from a proposal distribution $\left[a_c^{(*)} | a_c^{(k-1)} \right]$ (e.g., $\mathcal{N}\left(a_c^{(*)} | a_c^{(k-1)}, \tau_a^2\right)$, where τ_a^2 is a tuning parameter). If $a_c^{(*)} \in [l_a, u_a]$, let

$$\Sigma_c^{(*)} = (\sigma_c^{(*)})^2 \begin{bmatrix} 1 & \rho_c^{(k-1)} \sqrt{a_c^{(*)}} \\ \rho_c^{(k-1)} \sqrt{a_c^{(*)}} & a_c^{(*)} \end{bmatrix}$$

and

$$\mathbf{Q}_c^{(*)} = \Sigma_c^{(*)} + (\sigma_\mu^{(k)})^2 \mathbf{I}.$$

Calculate the Metropolis ratio as

$$r_a = \left(\frac{\prod_{\tilde{t}} \left\{ (p(\tilde{t}) \times \mathcal{N}(\mathbf{s}_c(\tilde{t}) | \boldsymbol{\mu}(\tilde{t})^{(k)}, \boldsymbol{\Sigma}_c^{(*)}) + (1 - p(\tilde{t})) \times \mathcal{N}(\mathbf{s}_c(\tilde{t}) | \boldsymbol{\mu}(\tilde{t})^{(k)}, \mathbf{H}\boldsymbol{\Sigma}_c^{(*)}\mathbf{H}') \right\})^{y(\tilde{t})}}{\prod_{\tilde{t}} \left\{ (p(\tilde{t}) \times \mathcal{N}(\mathbf{s}_c(\tilde{t}) | \boldsymbol{\mu}(\tilde{t})^{(k)}, \boldsymbol{\Sigma}_c^{(k)}) + (1 - p(\tilde{t})) \times \mathcal{N}(\mathbf{s}_c(\tilde{t}) | \boldsymbol{\mu}(\tilde{t})^{(k)}, \mathbf{H}\boldsymbol{\Sigma}_c^{(k)}\mathbf{H}') \right\})^{y(\tilde{t})}} \right. \\ \times \left. \frac{\left(p(\tilde{t}) \times \mathcal{N}(\mathbf{s}_c(\tilde{t}) | \boldsymbol{\mu}(\tilde{t})^{(k)}, \mathbf{Q}_c^{(*)}) + (1 - p(\tilde{t})) \times \mathcal{N}(\mathbf{s}_c(\tilde{t}) | \boldsymbol{\mu}(\tilde{t})^{(k)}, \mathbf{HQ}_c^{(*)}\mathbf{H}') \right)^{1-y(\tilde{t})}}{\left(p(\tilde{t}) \times \mathcal{N}(\mathbf{s}_c(\tilde{t}) | \boldsymbol{\mu}(\tilde{t})^{(k)}, \mathbf{Q}_c^{(k)}) + (1 - p(\tilde{t})) \times \mathcal{N}(\mathbf{s}_c(\tilde{t}) | \boldsymbol{\mu}(\tilde{t})^{(k)}, \mathbf{HQ}_c^{(k)}\mathbf{H}') \right)^{1-y(\tilde{t})}} \right).$$

If $r_a > u$, where $u \sim \text{Uniform}(0,1)$, let $a_c^{(k)} = a_c^{(*)}$, $\boldsymbol{\Sigma}_c^{(k)} = \boldsymbol{\Sigma}_c^{(*)}$, and $\mathbf{Q}_c^{(k)} = \mathbf{Q}_c^{(*)}$. Otherwise, let $a_c^{(k)} = a_c^{(k-1)}$, $\boldsymbol{\Sigma}_c^{(k)} = \boldsymbol{\Sigma}_c^{(k)}$, and $\mathbf{Q}_c^{(k)} = \mathbf{Q}_c^{(k)}$ if $r_a < u$, or if $a_c^{(*)} \notin [l_a, u_a]$.

- (d) Update $\rho_c^{(k-1)}$ using Metropolis sampling. Sample $\rho_c^{(*)}$ from a proposal distribution $\left[\rho_c^{(*)} | \rho_c^{(k-1)} \right]$ (e.g., $\mathcal{N}(\rho_c^{(*)} | \rho_c^{(k-1)}, \tau_\rho^2)$, where τ_ρ^2 is a tuning parameter). If $\rho_c^{(*)} \in [l_\rho, u_\rho]$, let

$$\boldsymbol{\Sigma}_c^{(*)} = (\sigma_c^{(k)})^2 \begin{bmatrix} 1 & \rho_c^{(*)} \sqrt{a_c^{(k)}} \\ \rho_c^{(*)} \sqrt{a_c^{(k)}} & a_c^{(k)} \end{bmatrix}$$

and

$$\mathbf{Q}_c^{(*)} = \boldsymbol{\Sigma}_c^{(*)} + (\sigma_\mu^{(k)})^2 \mathbf{I}.$$

Calculate the Metropolis ratio as

$$r_\rho = \left(\frac{\prod_{\tilde{t}} \left\{ (p(\tilde{t}) \times \mathcal{N}(\mathbf{s}_c(\tilde{t}) | \boldsymbol{\mu}(\tilde{t})^{(k)}, \boldsymbol{\Sigma}_c^{(*)}) + (1 - p(\tilde{t})) \times \mathcal{N}(\mathbf{s}_c(\tilde{t}) | \boldsymbol{\mu}(\tilde{t})^{(k)}, \mathbf{H}\boldsymbol{\Sigma}_c^{(*)}\mathbf{H}') \right\})^{y(\tilde{t})}}{\prod_{\tilde{t}} \left\{ (p(\tilde{t}) \times \mathcal{N}(\mathbf{s}_c(\tilde{t}) | \boldsymbol{\mu}(\tilde{t})^{(k)}, \boldsymbol{\Sigma}_c^{(k)}) + (1 - p(\tilde{t})) \times \mathcal{N}(\mathbf{s}_c(\tilde{t}) | \boldsymbol{\mu}(\tilde{t})^{(k)}, \mathbf{H}\boldsymbol{\Sigma}_c^{(k)}\mathbf{H}') \right\})^{y(\tilde{t})}} \right. \\ \times \left. \frac{\left(p(\tilde{t}) \times \mathcal{N}(\mathbf{s}_c(\tilde{t}) | \boldsymbol{\mu}(\tilde{t})^{(k)}, \mathbf{Q}_c^{(*)}) + (1 - p(\tilde{t})) \times \mathcal{N}(\mathbf{s}_c(\tilde{t}) | \boldsymbol{\mu}(\tilde{t})^{(k)}, \mathbf{HQ}_c^{(*)}\mathbf{H}') \right)^{1-y(\tilde{t})}}{\left(p(\tilde{t}) \times \mathcal{N}(\mathbf{s}_c(\tilde{t}) | \boldsymbol{\mu}(\tilde{t})^{(k)}, \mathbf{Q}_c^{(k)}) + (1 - p(\tilde{t})) \times \mathcal{N}(\mathbf{s}_c(\tilde{t}) | \boldsymbol{\mu}(\tilde{t})^{(k)}, \mathbf{HQ}_c^{(k)}\mathbf{H}') \right)^{1-y(\tilde{t})}} \right).$$

If $r_\rho > u$, where $u \sim \text{Uniform}(0,1)$, let $\rho_c^{(k)} = \rho_c^{(*)}$, $\boldsymbol{\Sigma}_c^{(k)} = \boldsymbol{\Sigma}_c^{(*)}$, and $\mathbf{Q}_c^{(k)} = \mathbf{Q}_c^{(*)}$. Otherwise, let $\rho_c^{(k)} = \rho_c^{(k-1)}$, $\boldsymbol{\Sigma}_c^{(k)} = \boldsymbol{\Sigma}_c^{(k)}$, and $\mathbf{Q}_c^{(k)} = \mathbf{Q}_c^{(k)}$ if $r_\rho < u$, or if $\rho_c^{(*)} \notin [l_\rho, u_\rho]$.

- (e) Repeat Steps 6(a) through 6(d) for each Argos location quality class c .
7. Update the temporal process model parameters (i.e., $\boldsymbol{\beta}$, $\boldsymbol{\alpha}$, $v(t)$, and σ_α^2).

- (a) Sample $\boldsymbol{\beta}^{(k)}$ using a Gibbs step:

$$\left[\boldsymbol{\beta}^{(k)} | \cdot \right] \sim \mathcal{N}(\mathbf{A}^{-1}\mathbf{b}, \mathbf{A}^{-1}),$$

where $\mathbf{A} = \mathbf{X}'\mathbf{X} + (\sigma_\beta^2 \mathbf{I})^{-1}$ and $\mathbf{b}' = (\mathbf{v}^{(k-1)} - \mathbf{W}\boldsymbol{\alpha}^{(k-1)})'\mathbf{X} + \boldsymbol{\mu}'_\beta (\sigma_\beta^2 \mathbf{I})^{-1}$. Note that the matrix $\mathbf{X} \equiv \{\mathbf{x}(t) : t \in \mathcal{T}\}$ contains the vectors $\mathbf{x}(t)$ for all times $t \in \mathcal{T}$. Similarly, $\mathbf{W} \equiv \{\mathbf{w}(t) : t \in \mathcal{T}\}$ is a matrix containing the vectors $\mathbf{w}(t)$ for all times $t \in \mathcal{T}$.

- (b) Update $\boldsymbol{\alpha}^{(k-1)}$ using a Gibbs step:

$$[\boldsymbol{\alpha}^{(k)} | \cdot] \sim \mathcal{N}(\mathbf{A}^{-1}\mathbf{b}, \mathbf{A}^{-1}),$$

where $\mathbf{A} = \mathbf{W}'\mathbf{W} + ((\sigma_\alpha^2)^{(k-1)} \mathbf{I})^{-1}$ and $\mathbf{b}' = (\mathbf{v}^{(k-1)} - \mathbf{X}\boldsymbol{\beta}^{(k)})'\mathbf{W}$. Note that the matrix $\mathbf{X} \equiv \{\mathbf{x}(t) : t \in \mathcal{T}\}$ contains the vectors $\mathbf{x}(t)$ for all times $t \in \mathcal{T}$. Similarly, $\mathbf{W} \equiv \{\mathbf{w}(t) : t \in \mathcal{T}\}$ is a matrix containing the vectors $\mathbf{w}(t)$ for all times $t \in \mathcal{T}$.

- (c) Sample $v(t)^{(k)}$, for $t \in \mathcal{T}$, using a Gibbs step:

$$\left[v(t)^{(k)} | \cdot \right] = \begin{cases} \mathcal{TN} \left(\mathbf{x}(t)' \boldsymbol{\beta}^{(k)} + \mathbf{w}(t)' \boldsymbol{\alpha}^{(k)}, \mathbf{1} \right)_{-\infty}^0, & y(t) = 0 \\ \mathcal{TN} \left(\mathbf{x}(t)' \boldsymbol{\beta}^{(k)} + \mathbf{w}(t)' \boldsymbol{\alpha}^{(k)}, \mathbf{1} \right)_0^\infty, & y(t) = 1 \end{cases}.$$

- (d) Update $(\sigma_\alpha^2)^{(k-1)}$ using a Gibbs step:

$$\left[(\sigma_\alpha^2)^{(k)} | \cdot \right] \sim \text{IG} \left(\left(\frac{\boldsymbol{\alpha}^{(k)'} \boldsymbol{\alpha}^{(k)}}{2} + \frac{1}{r_\alpha} \right)^{-1}, \frac{M}{2} + q_\alpha \right),$$

where M is the length of $\boldsymbol{\alpha}$ (or column dimension of \mathbf{W}).

8. Save $\boldsymbol{\mu}(t)^{(k)}$ (or $h(t)^{(k)}$ and $\boldsymbol{\mu}_j^{(k)}$ for $j = 1, \dots, J$); $\theta^{(k)}$; $\sigma_\mu^{(k)}$; $\boldsymbol{\beta}^{(k)}$; $\boldsymbol{\alpha}^{(k)}$; $\mathbf{v}^{(k)}$; $(\sigma_\alpha^2)^{(k)}$; and $\sigma_c^{(k)}$, $a_c^{(0)}$, and $\rho_c^{(0)}$ for $c = 3, 2, 1, 0$, A, and B.
9. Set $k = k + 1$ and return to Step 4. The algorithm is iterated by repeating Steps 4 through 8 until a sufficiently large sample has been obtained from which to approximate the posterior distribution.

APPENDIX B3. Posterior quantities for the simulated data example.

Table B3.1. Known observation and process model parameters used in simulation, and the corresponding posterior mean and 95% credible intervals. The subscripts on the observation model parameters (i.e., σ_c , a_c , and ρ_c) index the Argos location quality class and correspond to high (3), medium (0), and low (B) accuracy telemetry locations.

Parameter	True value	Posterior mean	Lower 95% credible bound	Upper 95% credible bound
σ_3 (m)	1448	1521	1366	1693
σ_0 (m)	8616	8559	7657	9564
σ_B (m)	29723	30284	27731	33049
a_3	0.34	0.36	0.26	0.48
a_0	0.36	0.40	0.31	0.52
a_B	0.33	0.36	0.28	0.45
ρ_3	0.34	0.18	0.01	0.42
ρ_0	0.36	0.29	0.02	0.54
ρ_B	0.33	0.23	0.01	0.46
σ_μ (m)	3318	3406	3029	3806
β_1	-0.52	-0.57	-0.79	-0.36
β_2	-0.28	-0.30	-0.40	-0.19
β_3	0.37	0.34	0.24	0.44
β_4	0.03	0.07	-0.06	0.20
β_5	0.20	0.24	0.10	0.39

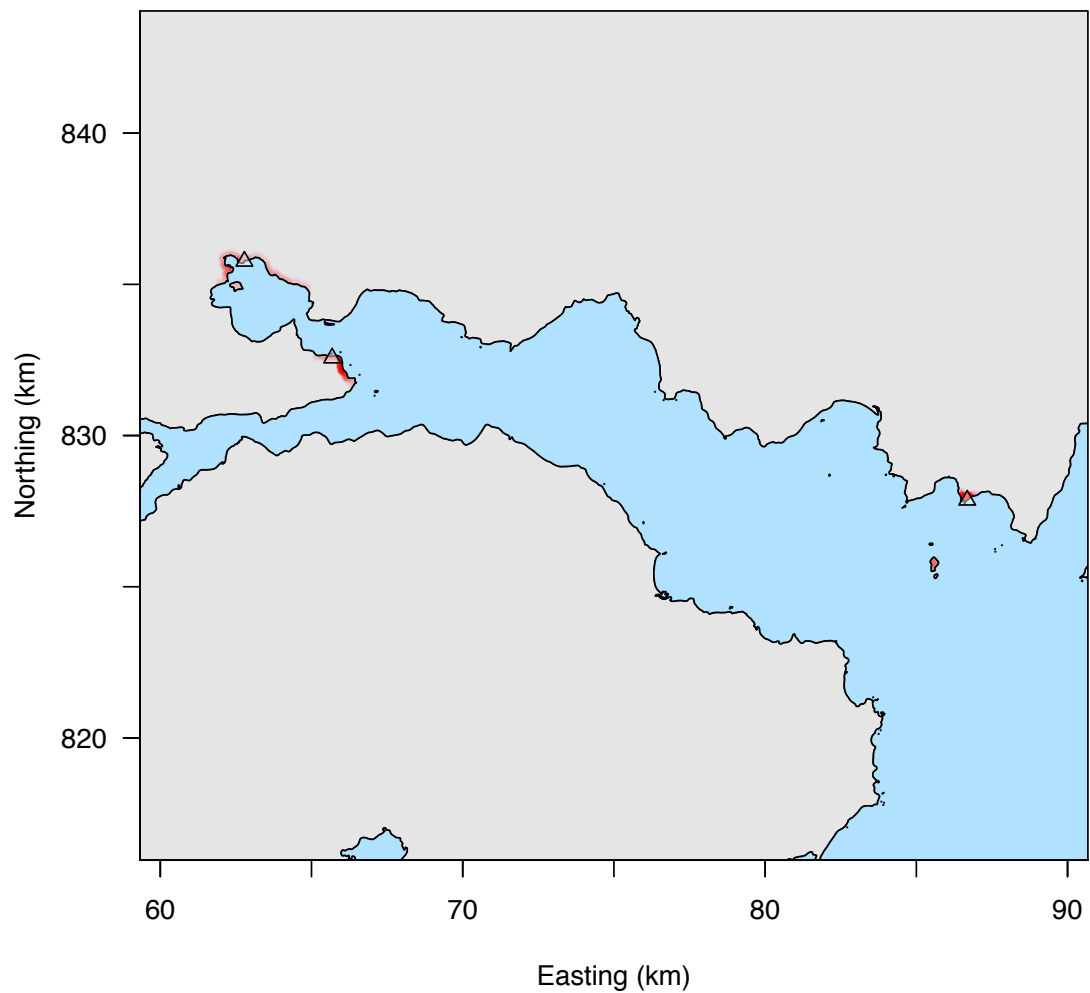


Figure B3.1. The posterior distribution of $\mu(t)$ (red gradient); brighter red indicates higher posterior probability. The spatial support of central places ($\tilde{\mathcal{S}}$) exists at the intersection of the blue and gray polygons (black line). The triangles denote the location of central places used in simulation.

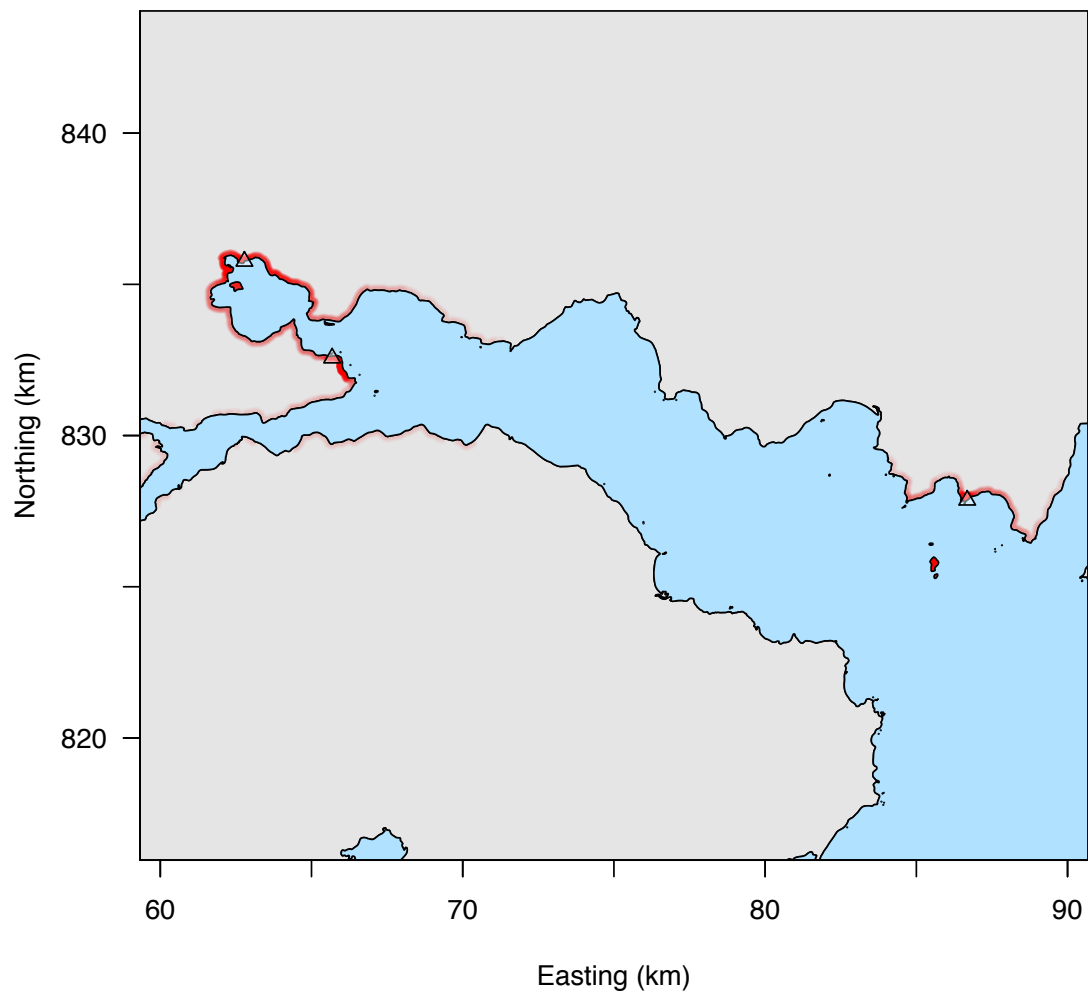


Figure B3.2. The posterior distribution of μ_j (red gradient); brighter red indicates higher posterior probability. The spatial support of central places ($\tilde{\mathcal{S}}$) exists at the intersection of the blue and gray polygons (black line). The triangles denote the location of central places used in simulation.

APPENDIX B4. Simulated examples using location data that arises from a movement model.

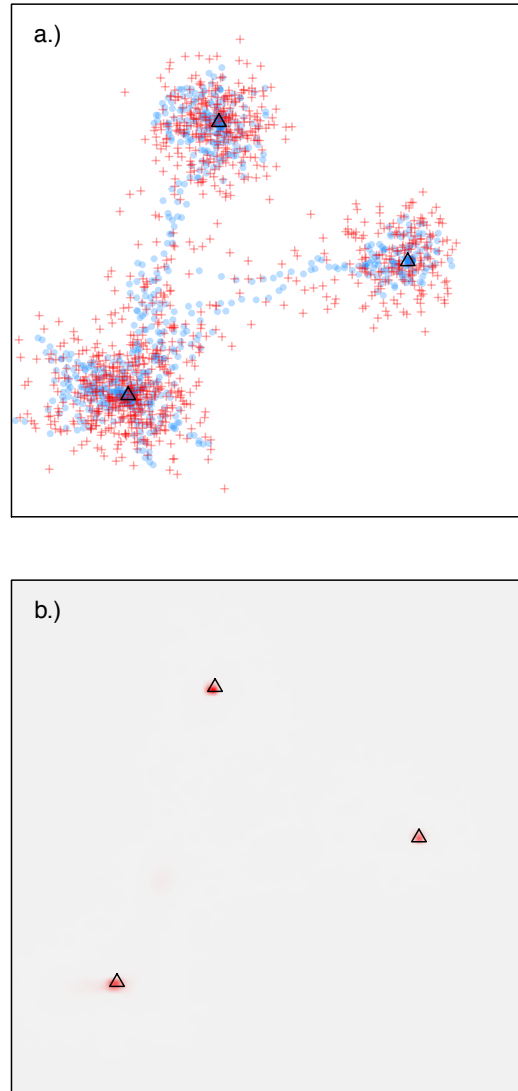


Figure B4.1. Example using simulated movement recorded at a high temporal frequency. (a) True locations ($\tilde{\mu}(t)$; blue circles) and the corresponding observed locations (i.e., with measurement error, $s(t)$; red crosses). Movement was simulated subject to attraction to 3 central places (μ_j ; black triangles). (b) The posterior distribution of $\mu(t)$ (red gradient); brighter red corresponds to higher posterior probability. The spatial support of central places (\bar{S}) covered the entire domain shown in the plots.

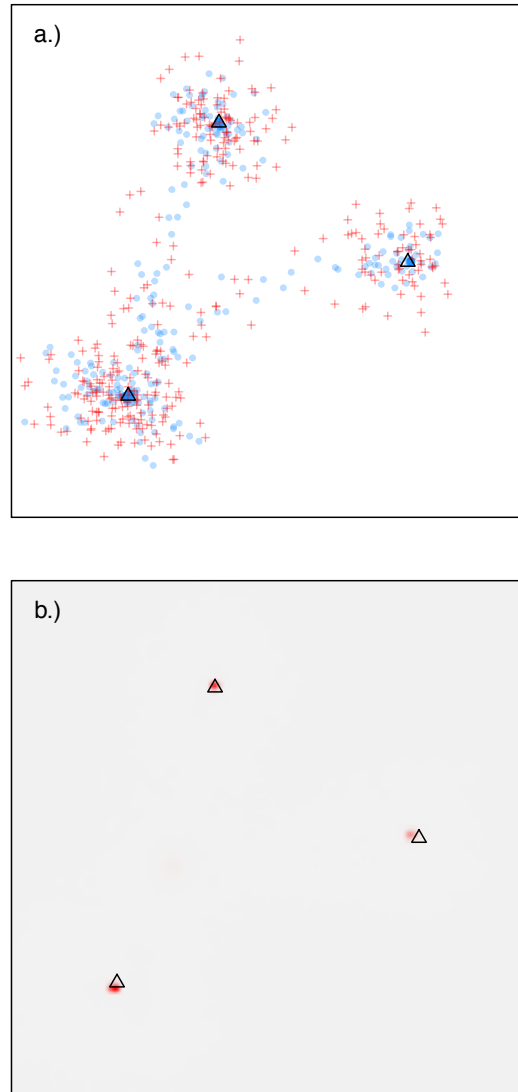


Figure B4.2. Example using simulated movement recorded at a low temporal frequency. (a) Same as Figure D1, except true ($\tilde{\boldsymbol{\mu}}(t)$; blue circles) and observed ($\mathbf{s}(t)$; red crosses) locations were “thinned” to mimic data recorded at a lower temporal frequency. Thinning occurred by keeping every third observation. Movement was simulated subject to attraction to 3 central places ($\boldsymbol{\mu}_j$; black triangles). (b) The posterior distribution of $\boldsymbol{\mu}(t)$ (red gradient); brighter red corresponds to higher posterior probability. The spatial support of central places ($\tilde{\mathcal{S}}$) covered the entire domain shown in the plots.

APPENDIX B5. Summary of results for an analysis of Argos telemetry data collected from a subadult female harbor seal near Kodiak Island, Alaska, USA.

Table B5.1. Posterior mean and 95% credible intervals for observation model parameters related to Argos satellite telemetry error.

Argos				
location class		σ (m)	a	ρ
3		1497 (866, 2477)	0.32 (0.07, 0.82)	0.36 (0.02, 0.86)
2		1689 (1306, 2169)	0.37 (0.19, 0.65)	0.30 (0.02, 0.62)
1		2110 (1818, 2468)	0.30 (0.19, 0.44)	0.41 (0.06, 0.64)
0		8691 (7542, 10018)	0.35 (0.27, 0.44)	0.77 (0.7, 0.83)
A		8144 (7080, 9367)	0.80 (0.62, 0.97)	0.67 (0.56, 0.78)
B		29777 (26898, 32938)	0.33 (0.26, 0.4)	0.67 (0.59, 0.74)

Table B5.2. Posterior mean and 95% credible intervals for parameters related to animal movement (σ_μ), the Dirichlet process concentration parameter (θ), and the temporal process (β). Parameters in the temporal process model correspond to an intercept (β_1), the number of hours since solar noon (13:00 hours, β_2), the number of hours since low tide (β_3), and the number of days since 15 August (β_4) and its quadratic effect (β_5). All covariates in the temporal process model were centered and scaled to unit variance prior to model fitting.

Parameter	Posterior mean	Lower 95% credible bound	Upper 95% credible bound
σ_μ (m)	3314	2663	4057
θ	1.69	0.62	3.24
β_1	-0.76	-1.12	-0.45
β_2	-0.38	-0.55	-0.21
β_3	0.47	0.33	0.63
β_4	0.04	-0.16	0.24
β_5	0.27	0.06	0.49

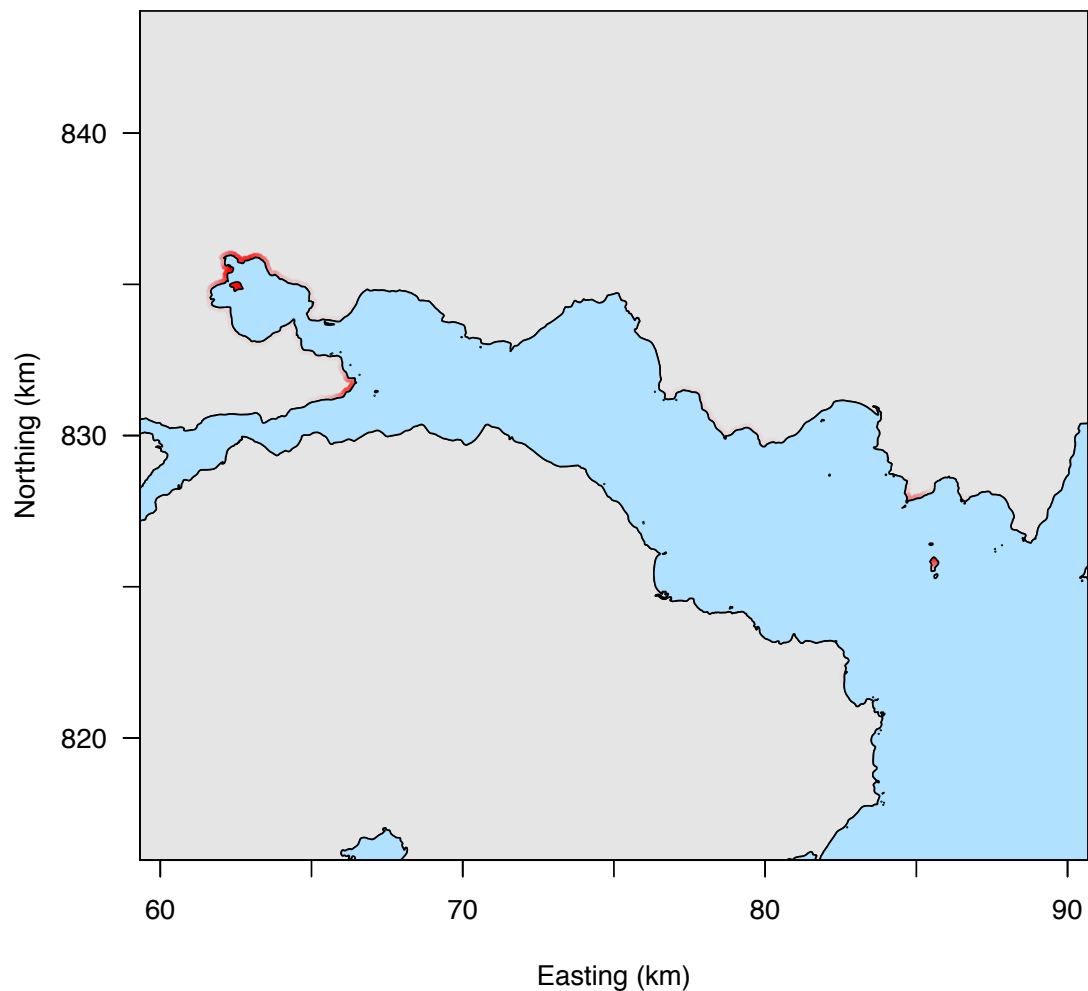


Figure B5.1. The posterior distribution of $\mu(t)$ (red gradient); brighter red indicates higher posterior probability. The spatial support of harbor seal haul-out sites ($\tilde{\mathcal{S}}$) exists along the coastline (black line) at the intersection of the blue (water) and gray (land) polygons.

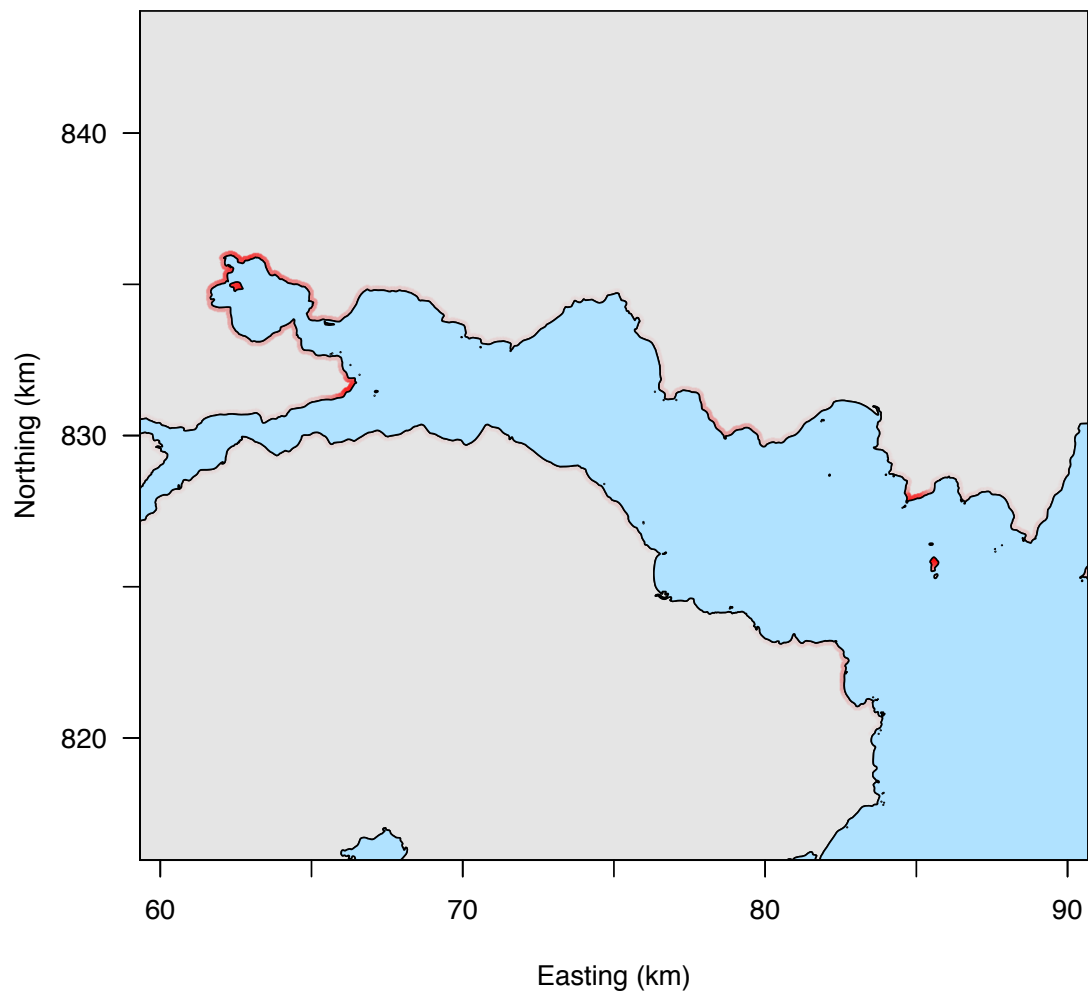


Figure B5.2. The posterior distribution of μ_j (red gradient); brighter red indicates higher posterior probability. The spatial support of harbor seal haul-out sites ($\tilde{\mathcal{S}}$) exists along the coastline (black line) at the intersection of the blue (water) and gray (land) polygons.

APPENDIX B6. Alternative model specifications to accommodate situations when ancillary behavioral data are absent or temporally misaligned with the telemetry locations.

TEMPORAL MISALIGNMENT

Let $y(t_y)$ denote ancillary behavioral data recorded at time $t_y \in \mathcal{T}$ and $z(t_s)$ denote the behavioral state corresponding to the time $t_s \in \mathcal{T}$ that an observed telemetry location is recorded. When times t_y and t_s are not aligned, the behavioral state $z(t_s)$ can be predicted using the following modifications to the model presented in Appendix B1.

MODEL STATEMENT

Update the model statement in Appendix B1 to estimate the latent behavioral state $z(t_s)$ and to reflect the two times t_s and t_y as follows:

$$\begin{aligned} \mathbf{s}_c(t_s) &\sim \begin{cases} \mathcal{N}(\boldsymbol{\mu}(t_s), \Sigma_c), & \text{with prob. } p(t_s), z(t_s) = 1 \\ \mathcal{N}(\boldsymbol{\mu}(t_s), \tilde{\Sigma}_c), & \text{with prob. } 1 - p(t_s), z(t_s) = 1 \\ \mathcal{N}(\boldsymbol{\mu}(t_s), \sigma_\mu^2 \mathbf{I} + \Sigma_c), & \text{with prob. } p(t_s), z(t_s) = 0 \\ \mathcal{N}(\boldsymbol{\mu}(t_s), \sigma_\mu^2 \mathbf{I} + \tilde{\Sigma}_c), & \text{with prob. } 1 - p(t_s), z(t_s) = 0 \end{cases} \\ z(t_s) &\sim \text{Bern}(\phi(t_s)) \\ \phi(t_s) &= \Phi(\mathbf{x}(t_s)' \boldsymbol{\beta} + \mathbf{w}(t_s)' \boldsymbol{\alpha}) \\ y(t_y) &= \begin{cases} 0, & v(t_y) \leq 0 \\ 1, & v(t_y) > 0 \end{cases} \\ v(t_y) &\sim \mathcal{N}(\mathbf{x}(t_y)' \boldsymbol{\beta} + \mathbf{w}(t_y)' \boldsymbol{\alpha}, \mathbf{I}) \\ \boldsymbol{\mu}(t_s) &\sim \sum_{j=1}^J \pi_j \delta_{\mu_j} \end{aligned}$$

FULL-CONDITIONAL DISTRIBUTIONS

Latent class status for update of $\boldsymbol{\mu}(t_s)$ ($h(t_s)$):

$$\begin{aligned} [h(t_s) | \cdot] &\sim \text{Cat} \left(\frac{\pi_1 [\mathbf{s}_c(t_s) | \boldsymbol{\mu}_1, \Sigma_c, \tilde{\Sigma}_c]^{z(t_s)} [\mathbf{s}_c(t_s) | \boldsymbol{\mu}_1, \sigma_\mu^2 \mathbf{I} + \Sigma_c, \sigma_\mu^2 \mathbf{I} + \tilde{\Sigma}_c]^{1-z(t_s)}}{\sum_{j=1}^J \pi_j [\mathbf{s}_c(t_s) | \boldsymbol{\mu}_j, \Sigma_c, \tilde{\Sigma}_c]^{z(t_s)} [\mathbf{s}_c(t_s) | \boldsymbol{\mu}_j, \sigma_\mu^2 \mathbf{I} + \Sigma_c, \sigma_\mu^2 \mathbf{I} + \tilde{\Sigma}_c]^{1-z(t_s)}}, \dots, \right. \\ &\quad \left. \frac{\pi_J [\mathbf{s}_c(t_s) | \boldsymbol{\mu}_J, \Sigma_c, \tilde{\Sigma}_c]^{z(t_s)} [\mathbf{s}_c(t_s) | \boldsymbol{\mu}_J, \sigma_\mu^2 \mathbf{I} + \Sigma_c, \sigma_\mu^2 \mathbf{I} + \tilde{\Sigma}_c]^{1-z(t_s)}}{\sum_{j=1}^J \pi_j [\mathbf{s}_c(t_s) | \boldsymbol{\mu}_j, \Sigma_c, \tilde{\Sigma}_c]^{z(t_s)} [\mathbf{s}_c(t_s) | \boldsymbol{\mu}_j, \sigma_\mu^2 \mathbf{I} + \Sigma_c, \sigma_\mu^2 \mathbf{I} + \tilde{\Sigma}_c]^{1-z(t_s)}} \right) \\ &\sim \text{Cat} \left(\frac{a_1}{b}, \dots, \frac{a_J}{b} \right), \end{aligned}$$

where $a_j = \pi_j \times (p(t_s) \times \mathcal{N}(\mathbf{s}_c(t_s) | \boldsymbol{\mu}_j, \Sigma_c) + (1 - p(t_s)) \times \mathcal{N}(\mathbf{s}_c(t_s) | \boldsymbol{\mu}_j, \tilde{\Sigma}_c))^{z(t_s)}$

$$\times \left(p(t_s) \times \mathcal{N}(\mathbf{s}_c(t_s) | \boldsymbol{\mu}_j, \sigma_\mu^2 \mathbf{I} + \boldsymbol{\Sigma}_c) + (1 - p(t_s)) \times \mathcal{N}(\mathbf{s}_c(t_s) | \boldsymbol{\mu}_j, \sigma_\mu^2 \mathbf{I} + \tilde{\boldsymbol{\Sigma}}_c) \right)^{1-z(t_s)}$$

and $b = \sum_{j=1}^J \left\{ \pi_j \times \left(p(t_s) \times \mathcal{N}(\mathbf{s}_c(t_s) | \boldsymbol{\mu}_j, \boldsymbol{\Sigma}_c) + (1 - p(t_s)) \times \mathcal{N}(\mathbf{s}_c(t_s) | \boldsymbol{\mu}_j, \tilde{\boldsymbol{\Sigma}}_c) \right)^{z(t_s)} \right. \right.$

$$\left. \left. \times \left(p(t_s) \times \mathcal{N}(\mathbf{s}_c(t_s) | \boldsymbol{\mu}_j, \sigma_\mu^2 \mathbf{I} + \boldsymbol{\Sigma}_c) + (1 - p(t_s)) \times \mathcal{N}(\mathbf{s}_c(t_s) | \boldsymbol{\mu}_j, \sigma_\mu^2 \mathbf{I} + \tilde{\boldsymbol{\Sigma}}_c) \right)^{1-z(t_s)} \right\}.$$

Auxiliary variable for the observed behavioral process ($v(t_y)$):

$$\begin{aligned} [v(t_y) | \cdot] &\propto [y(t_y) | v(t_y)] [v(t_y) | \boldsymbol{\alpha}, \boldsymbol{\beta}] \\ &\propto (1_{\{y(t_y)=0\}} 1_{\{v(t_y) \leq 0\}} + 1_{\{y(t_y)=1\}} 1_{\{v(t_y) > 0\}}) \times \mathcal{N}(v(t_y) | \mathbf{x}(t_y)' \boldsymbol{\beta} + \mathbf{w}(t_y)' \boldsymbol{\alpha}, \mathbf{1}) \\ &= \begin{cases} \mathcal{T}\mathcal{N}(\mathbf{x}(t_y)' \boldsymbol{\beta} + \mathbf{w}(t_y)' \boldsymbol{\alpha}, \mathbf{1})_0^0, & y(t_y) = 0 \\ \mathcal{T}\mathcal{N}(\mathbf{x}(t_y)' \boldsymbol{\beta} + \mathbf{w}(t_y)' \boldsymbol{\alpha}, \mathbf{1})_0^\infty, & y(t_y) = 1 \end{cases}. \end{aligned}$$

Prediction of the latent behavioral state ($z(t_s)$):

$$\begin{aligned} [z(t_s) | \cdot] &\propto [\mathbf{s}_c(t_s) | \boldsymbol{\mu}(t_s), z(t_s), \boldsymbol{\Sigma}_c, \tilde{\boldsymbol{\Sigma}}_c, \sigma_\mu] [z(t_s) | \phi(t_s)] \\ &\propto [\mathbf{s}_c(t_s) | \boldsymbol{\mu}(t_s), \boldsymbol{\Sigma}_c, \tilde{\boldsymbol{\Sigma}}_c]^{z(t_s)} [\mathbf{s}_c(t_s) | \boldsymbol{\mu}(t_s), \sigma_\mu^2 \mathbf{I} + \boldsymbol{\Sigma}_c, \sigma_\mu^2 \mathbf{I} + \tilde{\boldsymbol{\Sigma}}_c]^{1-z(t_s)} \text{Bern}(z(t_s) | \phi(t_s)) \\ &\propto (p(t_s) \times \mathcal{N}(\mathbf{s}_c(t_s) | \boldsymbol{\mu}(t_s), \boldsymbol{\Sigma}_c) + (1 - p(t_s)) \times \mathcal{N}(\mathbf{s}_c(t_s) | \boldsymbol{\mu}(t_s), \tilde{\boldsymbol{\Sigma}}_c))^{z(t_s)} \\ &\quad \times (p(t_s) \times \mathcal{N}(\mathbf{s}_c(t_s) | \boldsymbol{\mu}(t_s), \sigma_\mu^2 \mathbf{I} + \boldsymbol{\Sigma}_c) + (1 - p(t_s)) \times \mathcal{N}(\mathbf{s}_c(t_s) | \boldsymbol{\mu}(t_s), \sigma_\mu^2 \mathbf{I} + \tilde{\boldsymbol{\Sigma}}_c))^{1-z(t_s)} \\ &\quad \times \phi(t_s)^{z(t_s)} (1 - \phi(t_s))^{1-z(t_s)} \\ &\propto (\phi(t_s) \times (p(t_s) \times \mathcal{N}(\mathbf{s}_c(t_s) | \boldsymbol{\mu}(t_s), \boldsymbol{\Sigma}_c) + (1 - p(t_s)) \times \mathcal{N}(\mathbf{s}_c(t_s) | \boldsymbol{\mu}(t_s), \tilde{\boldsymbol{\Sigma}}_c)))^{z(t_s)} \\ &\quad \times ((1 - \phi(t_s)) \times (p(t_s) \times \mathcal{N}(\mathbf{s}_c(t_s) | \boldsymbol{\mu}(t_s), \sigma_\mu^2 \mathbf{I} + \boldsymbol{\Sigma}_c) + (1 - p(t_s)) \times \mathcal{N}(\mathbf{s}_c(t_s) | \boldsymbol{\mu}(t_s), \sigma_\mu^2 \mathbf{I} + \tilde{\boldsymbol{\Sigma}}_c)))^{1-z(t_s)} \\ &= \text{Bern}(\tilde{\phi}(t_s)), \end{aligned}$$

where

$$\tilde{\phi}(t_s) = \frac{\phi_1(t_s)}{\phi_1(t_s) + \phi_2(t_s)},$$

$$\begin{aligned} \phi_1(t_s) &= \phi(t_s) \times (p(t_s) \times \mathcal{N}(\mathbf{s}_c(t_s) | \boldsymbol{\mu}(t_s), \boldsymbol{\Sigma}_c) + (1 - p(t_s)) \times \mathcal{N}(\mathbf{s}_c(t_s) | \boldsymbol{\mu}(t_s), \tilde{\boldsymbol{\Sigma}}_c)), \\ \phi_2(t_s) &= (1 - \phi(t_s)) \times (p(t_s) \times \mathcal{N}(\mathbf{s}_c(t_s) | \boldsymbol{\mu}(t_s), \sigma_\mu^2 \mathbf{I} + \boldsymbol{\Sigma}_c) + (1 - p(t_s)) \times \mathcal{N}(\mathbf{s}_c(t_s) | \boldsymbol{\mu}(t_s), \sigma_\mu^2 \mathbf{I} + \tilde{\boldsymbol{\Sigma}}_c)), \\ \text{and } \phi(t_s) &= \Phi(\mathbf{x}(t_s)' \boldsymbol{\beta} + \mathbf{w}(t_s)' \boldsymbol{\alpha}). \end{aligned}$$

MARKOV-CHAIN MONTE CARLO ALGORITHM

Revise steps in the Markov chain Monte Carlo algorithm presented in Appendix B2 as follows:

1. Update Steps 4(a), 4(b), 4(f), 4(h), 5, 6, and 8 to reflect times t_s at which telemetry locations are collected (e.g., $\mathbf{s}(t_s)$, $h(t_s)$, $\boldsymbol{\mu}(t_s)$, $p(t_s)$, etc.).
2. Update Steps 7(a)-7(c) to reflect times t_y at which ancillary behavioral data are collected (e.g., $y(t_y)$, $v(t_y)$, $\mathbf{x}(t_y)$, $\mathbf{w}(t_y)$). Note that updates for $\boldsymbol{\alpha}$ and $\boldsymbol{\beta}$ (Steps 7(a) and 7(b)) are based only on $v(t_y)$ and the covariates measured at times t_y (i.e., $\mathbf{X} \equiv \{\mathbf{x}(t_y) : t_y \in \mathcal{T}\}$ and $\mathbf{W} \equiv \{\mathbf{w}(t_y) : t_y \in \mathcal{T}\}$).

3. Update Steps 4(a), 4(f), 5, and 6 to reflect the latent behavioral state $z(t_s)$ (i.e., change instances of $y(t)$ to $z(t_s)$).

4. Estimate the latent behavioral state $z(t_s)$ by augmenting Step 7 with:

(a) Calculate:

$$\phi(t_s)^{(k)} = \Phi \left(\mathbf{x}(t_s)' \boldsymbol{\beta}^{(k)} + \mathbf{w}(t_s)' \boldsymbol{\alpha}^{(k)} \right),$$

where Φ is the standard normal cumulative distribution function.

(b) Sample $z(t_s)^{(k)}$, for times $t_s \in \mathcal{T}$, using a Gibbs step:

$$[z(t_s)^{(k)} | \cdot] \sim \text{Bern} \left(\frac{\phi_1(t_s)^{(k)}}{\phi_1(t_s)^{(k)} + \phi_2(t_s)^{(k)}} \right),$$

where

$$\phi_1(t_s)^{(k)} = \phi(t_s)^{(k)} \times \left(p(t_s) \times \mathcal{N} \left(\mathbf{s}_c(t_s) | \boldsymbol{\mu}(t_s)^{(k)}, \boldsymbol{\Sigma}_c^{(k)} \right) + (1 - p(t_s)) \times \mathcal{N} \left(\mathbf{s}_c(t_s) | \boldsymbol{\mu}(t_s)^{(k)}, \mathbf{H}\boldsymbol{\Sigma}_c^{(k)}\mathbf{H}' \right) \right)$$

and

$$\phi_2(t_s)^{(k)} = (1 - \phi(t_s)^{(k)}) \times \left(p(t_s) \times \mathcal{N} \left(\mathbf{s}_c(t_s) | \boldsymbol{\mu}(t_s)^{(k)}, \mathbf{Q}_c^{(k)} \right) + (1 - p(t_s)) \times \mathcal{N} \left(\mathbf{s}_c(t_s) | \boldsymbol{\mu}(t_s)^{(k)}, \mathbf{H}\mathbf{Q}_c^{(k)}\mathbf{H}' \right) \right).$$

ANCILLARY BEHAVIORAL DATA IS ABSENT

Consider the case when ancillary behavioral data ($y(t)$) are not available. Let $z(t)$, for $t \in \mathcal{T}$, denote the latent behavioral state corresponding to the time an observed telemetry location is recorded. The behavioral state $z(t)$ can be predicted with the following modifications to the model presented in Appendix B1.

MODEL STATEMENT

Update the model statement in Appendix B1 to estimate the latent behavioral state by replacing all instances of $y(t)$ with $z(t)$ as follows:

$$\begin{aligned} \mathbf{s}_c(t) &\sim \begin{cases} \mathcal{N}(\boldsymbol{\mu}(t), \boldsymbol{\Sigma}_c), & \text{with prob. } p(t), z(t) = 1 \\ \mathcal{N}(\boldsymbol{\mu}(t), \tilde{\boldsymbol{\Sigma}}_c), & \text{with prob. } 1 - p(t), z(t) = 1 \\ \mathcal{N}(\boldsymbol{\mu}(t), \sigma_\mu^2 \mathbf{I} + \boldsymbol{\Sigma}_c), & \text{with prob. } p(t), z(t) = 0 \\ \mathcal{N}(\boldsymbol{\mu}(t), \sigma_\mu^2 \mathbf{I} + \tilde{\boldsymbol{\Sigma}}_c), & \text{with prob. } 1 - p(t), z(t) = 0 \end{cases} \\ z(t) &= \begin{cases} 0, & v(t) \leq 0 \\ 1, & v(t) > 0 \end{cases}. \end{aligned}$$

FULL-CONDITIONAL DISTRIBUTIONS

Auxiliary variable for the latent behavioral process ($v(t)$):

$$\begin{aligned}[v(t) | \cdot] &\propto [z(t) | v(t)] [v(t) | \boldsymbol{\alpha}, \boldsymbol{\beta}] \\ &\propto (1_{\{z(t)=0\}} 1_{\{v(t)\leq 0\}} + 1_{\{z(t)=1\}} 1_{\{v(t)>0\}}) \times \mathcal{N}(v(t) | \mathbf{x}(t)' \boldsymbol{\beta} + \mathbf{w}(t)' \boldsymbol{\alpha}, 1) \\ &= \begin{cases} \mathcal{T}\mathcal{N}(\mathbf{x}(t)' \boldsymbol{\beta} + \mathbf{w}(t)' \boldsymbol{\alpha}, 1)_{-\infty}^0, & z(t) = 0 \\ \mathcal{T}\mathcal{N}(\mathbf{x}(t)' \boldsymbol{\beta} + \mathbf{w}(t)' \boldsymbol{\alpha}, 1)_0^\infty, & z(t) = 1 \end{cases}.\end{aligned}$$

Prediction of the latent behavioral state ($z(t)$):

$$\begin{aligned}[z(t) | \cdot] &\propto [\mathbf{s}_c(t) | \boldsymbol{\mu}(t), z(t), \Sigma_c, \tilde{\Sigma}_c, \sigma_\mu] [z(t) | v(t)] \\ &\propto [\mathbf{s}_c(t) | \boldsymbol{\mu}(t), \Sigma_c, \tilde{\Sigma}_c]^{z(t)} [\mathbf{s}_c(t) | \boldsymbol{\mu}(t), \sigma_\mu^2 \mathbf{I} + \Sigma_c, \sigma_\mu^2 \mathbf{I} + \tilde{\Sigma}_c]^{1-z(t)} \text{Bern}(z(t) | v(t)) \\ &\propto (p(t) \times \mathcal{N}(\mathbf{s}_c(t) | \boldsymbol{\mu}(t), \Sigma_c) + (1-p(t)) \times \mathcal{N}(\mathbf{s}_c(t) | \boldsymbol{\mu}(t), \tilde{\Sigma}_c))^{z(t)} \\ &\quad \times (p(t) \times \mathcal{N}(\mathbf{s}_c(t) | \boldsymbol{\mu}(t), \sigma_\mu^2 \mathbf{I} + \Sigma_c) + (1-p(t)) \times \mathcal{N}(\mathbf{s}_c(t) | \boldsymbol{\mu}(t), \sigma_\mu^2 \mathbf{I} + \tilde{\Sigma}_c))^{1-z(t)} \\ &\quad \times \phi(t)^{z(t)} (1 - \phi(t))^{1-z(t)} \\ &\propto (\phi(t) \times (p(t) \times \mathcal{N}(\mathbf{s}_c(t) | \boldsymbol{\mu}(t), \Sigma_c) + (1-p(t)) \times \mathcal{N}(\mathbf{s}_c(t) | \boldsymbol{\mu}(t), \tilde{\Sigma}_c)))^{z(t)} \\ &\quad \times ((1 - \phi(t)) \times (p(t) \times \mathcal{N}(\mathbf{s}_c(t) | \boldsymbol{\mu}(t), \sigma_\mu^2 \mathbf{I} + \Sigma_c) + (1-p(t)) \times \mathcal{N}(\mathbf{s}_c(t) | \boldsymbol{\mu}(t), \sigma_\mu^2 \mathbf{I} + \tilde{\Sigma}_c)))^{1-z(t)} \\ &= \text{Bern}(\tilde{\phi}(t)),\end{aligned}$$

where

$$\tilde{\phi}(t) = \frac{\phi_1(t)}{\phi_1(t) + \phi_2(t)},$$

$$\begin{aligned}\phi_1(t) &= \phi(t) \times (p(t) \times \mathcal{N}(\mathbf{s}_c(t) | \boldsymbol{\mu}(t), \Sigma_c) + (1-p(t)) \times \mathcal{N}(\mathbf{s}_c(t) | \boldsymbol{\mu}(t), \tilde{\Sigma}_c)), \\ \phi_2(t) &= (1 - \phi(t)) \times (p(t) \times \mathcal{N}(\mathbf{s}_c(t) | \boldsymbol{\mu}(t), \sigma_\mu^2 \mathbf{I} + \Sigma_c) + (1-p(t)) \times \mathcal{N}(\mathbf{s}_c(t) | \boldsymbol{\mu}(t), \sigma_\mu^2 \mathbf{I} + \tilde{\Sigma}_c)), \\ \text{and } \phi(t) &= \Phi(\mathbf{x}(t)' \boldsymbol{\beta} + \mathbf{w}(t)' \boldsymbol{\alpha}).\end{aligned}$$

MARKOV-CHAIN MONTE CARLO ALGORITHM

Revise steps in the Markov chain Monte Carlo algorithm presented in Appendix B2 as follows:

1. Update Steps 4(a), 4(f), 5, 6, and 7(c) to reflect the latent behavioral state $z(t)$ (i.e., change instances of $y(t)$ to $z(t)$).
2. Steps 7(a) and 7(b) remain the same as before.
3. Estimate the latent behavioral state $z(t)$ by augmenting Step 7 with:

(a) Calculate:

$$\phi(t)^{(k)} = \Phi(\mathbf{x}(t)' \boldsymbol{\beta}^{(k)} + \mathbf{w}(t)' \boldsymbol{\alpha}^{(k)}),$$

where Φ is the standard normal cumulative distribution function.

(b) Sample $z(t)^{(k)}$, for $t \in \mathcal{T}$, using a Gibbs step:

$$[z(t)^{(k)} | \cdot] \sim \text{Bern} \left(\frac{\phi_1(t)^{(k)}}{\phi_1(t)^{(k)} + \phi_2(t)^{(k)}} \right),$$

where

$$\phi_1(t)^{(k)} = \phi(t)^{(k)} \times \left(p(t) \times \mathcal{N} \left(\mathbf{s}_c(t) | \boldsymbol{\mu}(t)^{(k)}, \boldsymbol{\Sigma}_c^{(k)} \right) + (1 - p(t)) \times \mathcal{N} \left(\mathbf{s}_c(t) | \boldsymbol{\mu}(t)^{(k)}, \mathbf{H}\boldsymbol{\Sigma}_c^{(k)}\mathbf{H}' \right) \right)$$

and

$$\phi_2(t)^{(k)} = \left(1 - \phi(t)^{(k)} \right) \times \left(p(t) \times \mathcal{N} \left(\mathbf{s}_c(t) | \boldsymbol{\mu}(t)^{(k)}, \mathbf{Q}_c^{(k)} \right) + (1 - p(t)) \times \mathcal{N} \left(\mathbf{s}_c(t) | \boldsymbol{\mu}(t)^{(k)}, \mathbf{H}\mathbf{Q}_c^{(k)}\mathbf{H}' \right) \right).$$

APPENDIX C

Supplementary Material for Chapter 4

APPENDIX C1. Model statement, posterior distribution, full-conditional distributions, and pseudocode detailing a Markov chain Monte Carlo algorithm to implement the model for haul-out site location estimation. We represented \mathcal{S} , the spatial domain of possible haul-out sites, as a 100-m resolution raster consisting of cells along the shoreline of Kodiak Island, and let the locations of potential haul-out sites ($\boldsymbol{\mu}_{ij}$) assume values corresponding to the centroids of cells in \mathcal{S} .

In the posterior and full-conditional distributions below, we use bracket notation to denote a probability distribution. For example, $[x]$ indicates the probability distribution of x . Similarly, $[x|y]$ indicates the probability distribution of x given the parameter y . The notation “.” represents the data and other parameters in the model.

MODEL STATEMENT

$$\begin{aligned}
\mathbf{s}_{ic}(t) &\sim \begin{cases} \mathcal{N}(\boldsymbol{\mu}_i(t), \Sigma_{ic}), & \text{with prob. } 0.5, y_i(t) = 1 \\ \mathcal{N}(\boldsymbol{\mu}_i(t), \tilde{\Sigma}_{ic}), & \text{with prob. } 0.5, y_i(t) = 1 \\ \mathcal{N}(\boldsymbol{\mu}_i(t), \tau_i^2 \mathbf{I} + \Sigma_{ic}), & \text{with prob. } 0.5, y_i(t) = 0 \\ \mathcal{N}(\boldsymbol{\mu}_i(t), \tau_i^2 \mathbf{I} + \tilde{\Sigma}_{ic}), & \text{with prob. } 0.5, y_i(t) = 0 \end{cases} \\
\Sigma_{ic} &= \sigma_{ic}^2 \begin{bmatrix} 1 & \rho_{ic}\sqrt{a_{ic}} \\ \rho_{ic}\sqrt{a_{ic}} & a_{ic} \end{bmatrix} \\
\tilde{\Sigma}_{ic} &= \sigma_{ic}^2 \begin{bmatrix} 1 & -\rho_{ic}\sqrt{a_{ic}} \\ -\rho_{ic}\sqrt{a_{ic}} & a_{ic} \end{bmatrix} \\
\boldsymbol{\mu}_i(t) &\sim \sum_{j=1}^J \pi_{ij} \delta_{\boldsymbol{\mu}_{ij}} \\
\pi_{ij} &= \eta_{ij} \prod_{l < j} (1 - \eta_{il}) \\
\eta_{ij} &\sim \text{Beta}(1, \theta_i) \\
\boldsymbol{\mu}_{ij} &\sim f_{\mathcal{S}}(\mathbf{S}_i) \\
\theta_i &\sim \text{Gamma}(r_\theta, q_\theta) \\
\log(\tau_i) &\sim \mathcal{N}(\mu_\tau, \sigma_\tau^2) \\
\sigma_{ic} &\sim \text{Unif}(l_\sigma, u_\sigma) \\
a_{ic} &\sim \text{Unif}(l_a, u_a) \\
\rho_{ic} &\sim \text{Unif}(l_\rho, u_\rho),
\end{aligned}$$

where J indicates the upper bound to the truncation approximation of the Dirichlet process (Sethuraman 1994, Ishwaran and James 2001), $\mathbf{S}_i = \{\mathbf{s}_{ic}(t), \forall t\}$ is a matrix of the observed telemetry locations for individual i , and $f_{\mathcal{S}}(\mathbf{S}_i)$ is the kernel density estimate of \mathbf{S}_i truncated and normalized over \mathcal{S} .

POSTERIOR DISTRIBUTION

$$[\mathbf{M}_i, \boldsymbol{\eta}_i, \theta_i, \tau_i, \boldsymbol{\sigma}_i, \mathbf{a}_i, \boldsymbol{\rho}_i | \mathbf{S}_i, \mathbf{y}_i] \propto \prod_{t \in \mathcal{T}} \prod_{j=1}^J \left[\mathbf{s}_{ic}(t) | \boldsymbol{\mu}_i(t), y_i(t), \tau_i^2, \boldsymbol{\Sigma}_{ic}, \tilde{\boldsymbol{\Sigma}}_{ic} \right] [\boldsymbol{\mu}_i(t) | \boldsymbol{\mu}_{ij}, \eta_{ij}] \times \\ [\boldsymbol{\mu}_{ij} | f_{\mathcal{S}}(\mathbf{S}_i)] [\eta_{ij} | \theta_i] [\theta_i] [\tau_i] [\boldsymbol{\sigma}_i] [\mathbf{a}_i] [\boldsymbol{\rho}_i],$$

where $\mathbf{M}_i = \{\boldsymbol{\mu}_i(t), \forall t\}$ is a matrix of “functional” haul-out sites associated with the telemetry locations for individual i (\mathbf{M}_i has the same dimensions as \mathbf{S}_i); $\boldsymbol{\eta}_i \equiv (\eta_{i1}, \dots, \eta_{iJ})'$ is a vector of stick-breaking weights; $\mathbf{y}_i = \{y_i(t), \forall t\}$ is a vector of behavioral (wet/dry) data for individual i ; and $\boldsymbol{\sigma}_i \equiv (\sigma_{i3}, \sigma_{i2}, \sigma_{i1}, \sigma_{i0}, \sigma_{iA}, \sigma_{iB})'$, $\mathbf{a}_i \equiv (a_{i3}, a_{i2}, a_{i1}, a_{i0}, a_{iA}, a_{iB})'$, and $\boldsymbol{\rho} \equiv (\rho_{i3}, \rho_{i2}, \rho_{i1}, \rho_{i0}, \rho_{iA}, \rho_{iB})'$ are vectors of parameters that describe Argos telemetry location error.

FULL-CONDITIONAL DISTRIBUTIONS

Location of “potential” haul-out sites ($\boldsymbol{\mu}_{ij}$):

$$[\boldsymbol{\mu}_{ij} | \cdot] \propto \prod_{t \in \mathcal{T}} \left[\mathbf{s}_{ic}(t) | \boldsymbol{\mu}_i(t), y_i(t), \boldsymbol{\Sigma}_{ic}, \tilde{\boldsymbol{\Sigma}}_{ic}, \tau_i^2 \right]^{1\{\boldsymbol{\mu}_i(t)=\boldsymbol{\mu}_{ij}\}} [\boldsymbol{\mu}_{ij} | f_{\mathcal{S}}(\mathbf{S}_i)] \\ \propto \prod_{\{t \in \mathcal{T}: \boldsymbol{\mu}_i(t)=\boldsymbol{\mu}_{ij}\}} \left\{ \left[\mathbf{s}_{ic}(t) | \boldsymbol{\mu}_{ij}, \boldsymbol{\Sigma}_{ic}, \tilde{\boldsymbol{\Sigma}}_{ic} \right]^{y_i(t)} \left[\mathbf{s}_{ic}(t) | \boldsymbol{\mu}_{ij}, \tau_i^2 \mathbf{I} + \boldsymbol{\Sigma}_{ic}, \tau_i^2 \mathbf{I} + \tilde{\boldsymbol{\Sigma}}_{ic} \right]^{1-y_i(t)} \right\} \\ \times [\boldsymbol{\mu}_{ij} | f_{\mathcal{S}}(\mathbf{S}_i)] \\ \propto \prod_{\{t \in \mathcal{T}: \boldsymbol{\mu}_i(t)=\boldsymbol{\mu}_{ij}\}} \left\{ \left(0.5 \times \left(\mathcal{N}(\mathbf{s}_{ic}(t) | \boldsymbol{\mu}_{ij}, \boldsymbol{\Sigma}_{ic}) + \mathcal{N}(\mathbf{s}_{ic}(t) | \boldsymbol{\mu}_{ij}, \tilde{\boldsymbol{\Sigma}}_{ic}) \right) \right)^{y_i(t)} \right. \\ \left. \times \left(0.5 \times \left(\mathcal{N}(\mathbf{s}_{ic}(t) | \boldsymbol{\mu}_{ij}, \tau_i^2 \mathbf{I} + \boldsymbol{\Sigma}_{ic}) + \mathcal{N}(\mathbf{s}_{ic}(t) | \boldsymbol{\mu}_{ij}, \tau_i^2 \mathbf{I} + \tilde{\boldsymbol{\Sigma}}_{ic}) \right) \right)^{1-y_i(t)} \right\} \\ \times [\boldsymbol{\mu}_{ij} | f_{\mathcal{S}}(\mathbf{S}_i)]$$

Note that the product is over all observed telemetry locations ($\mathbf{s}_{ic}(t)$) allocated to haul-out site $\boldsymbol{\mu}_{ij}$.

Stick-breaking weights (η_{ij}):

$$\begin{aligned}
[\eta_{ij} \mid \cdot] &\propto \prod_{t \in \mathcal{T}} [\boldsymbol{\mu}_i(t) \mid \pi_{ij}]^{1\{\boldsymbol{\mu}_i(t)=\boldsymbol{\mu}_{ij}\}} \prod_{l=j+1}^J \prod_{t \in \mathcal{T}} [\boldsymbol{\mu}_i(t) \mid \pi_{il}]^{1\{\boldsymbol{\mu}_i(t)=\boldsymbol{\mu}_{il}\}} [\eta_{ij} \mid 1, \theta_i] \\
&\propto \prod_{t \in \mathcal{T}} \pi_{ij}^{1\{\boldsymbol{\mu}_i(t)=\boldsymbol{\mu}_{ij}\}} \prod_{l=j+1}^J \prod_{t \in \mathcal{T}} \pi_{il}^{1\{\boldsymbol{\mu}_i(t)=\boldsymbol{\mu}_{il}\}} \text{Beta}(\eta_{ij} \mid 1, \theta_i) \\
&\propto \pi_{ij}^{\sum_{t \in \mathcal{T}} (1\{\boldsymbol{\mu}_i(t)=\boldsymbol{\mu}_{ij}\})} \prod_{l=j+1}^J \pi_{il}^{\sum_{t \in \mathcal{T}} (1\{\boldsymbol{\mu}_i(t)=\boldsymbol{\mu}_{il}\})} \eta_{ij}^{1-1} (1 - \eta_{ij})^{\theta_i-1} \\
&\propto \left(\eta_{ij} \prod_{l < j} (1 - \eta_{il}) \right)^{n_{ij}} \prod_{l=j+1}^J \left(\eta_{il} \prod_{m < l} (1 - \eta_{il}) \right)^{n_{il}} (1 - \eta_{ij})^{\theta_i-1} \\
&\propto \eta_{ij}^{n_{ij}} \prod_{l=j+1}^J \left(\prod_{m < l} (1 - \eta_{il}) \right)^{n_{il}} (1 - \eta_{ij})^{\theta_i-1} \\
&\propto \eta_{ij}^{n_{ij}} (1 - \eta_{ij})^{\sum_{l=j+1}^J n_{il}} (1 - \eta_{ij})^{\theta_i-1} \\
&\propto \eta_{ij}^{n_{ij}} (1 - \eta_{ij})^{\sum_{l=j+1}^J n_{il} + \theta_i - 1} \\
&= \text{Beta} \left(n_{ij} + 1, \sum_{l=j+1}^J n_{il} + \theta_i \right),
\end{aligned}$$

where $n_{ij} = \sum_{t \in \mathcal{T}} (1\{\boldsymbol{\mu}_i(t)=\boldsymbol{\mu}_{ij}\})$, i.e., the number of observed telemetry locations ($\mathbf{s}_{ic}(t)$) allocated to haul-out site $\boldsymbol{\mu}_{ij}$.

Dirichlet process concentration parameter (θ_i):

$$\begin{aligned}
[\theta_i \mid \cdot] &\propto \prod_{j=1}^{J-1} [\eta_{ij} \mid 1, \theta_i] [\theta_i \mid r_\theta, q_\theta] \\
&\propto \prod_{j=1}^{J-1} \text{Beta}(\eta_{ij} \mid 1, \theta_i) \text{Gamma}(\theta_i \mid r_\theta, q_\theta) \\
&\propto \prod_{j=1}^{J-1} \frac{\Gamma(1 + \theta_i)}{\Gamma(1)\Gamma(\theta_i)} \eta_{ij}^{1-1} (1 - \eta_{ij})^{\theta_i-1} \theta_i^{r_\theta-1} \exp\{-q_\theta \theta_i\} \\
&\propto \left(\frac{\theta_i \Gamma(\theta_i)}{\Gamma(1)\Gamma(\theta_i)} \right)^{J-1} \theta_i^{r_\theta-1} \exp \left\{ -q_\theta \theta_i + \log \left(\prod_{j=1}^{J-1} (1 - \eta_{ij})^{\theta_i-1} \right) \right\} \\
&\propto \theta_i^{J-1+r_\theta-1} \exp \left\{ -q_\theta \theta_i + \sum_{j=1}^{J-1} \left(\log(1 - \eta_{ij})^{\theta_i} \log(1 - \eta_{ij})^{-1} \right) \right\} \\
&\propto \theta_i^{J-1+r_\theta-1} \exp \left\{ -q_\theta \theta_i + \sum_{j=1}^{J-1} \log(1 - \eta_{ij})^{\theta_i} \right\} \\
&\propto \theta_i^{J-1+r_\theta-1} \exp \left\{ -q_\theta \theta_i + \theta_i \sum_{j=1}^{J-1} \log(1 - \eta_{ij}) \right\} \\
&\propto \theta_i^{J-1+r_\theta-1} \exp \left\{ -\theta_i \left(q_\theta - \sum_{j=1}^{J-1} \log(1 - \eta_{ij}) \right) \right\} \\
&= \text{Gamma} \left(r_\theta + J - 1, q_\theta - \sum_{j=1}^{J-1} \log(1 - \eta_{ij}) \right).
\end{aligned}$$

Note that the product is over $j = 1, \dots, J-1$ because $\eta_{iJ} = 1$ in the truncation approximation of a Dirichlet process (Sethuraman 1994, Ishwaran and James 2001).

Location of “functional” haul-out sites ($\boldsymbol{\mu}_i(t)$):

$$\begin{aligned}
[\boldsymbol{\mu}_i(t) \mid \cdot] &\propto \left[\mathbf{s}_{ic}(t) \mid \boldsymbol{\mu}_i(t), y_i(t), \boldsymbol{\Sigma}_{ic}, \tilde{\boldsymbol{\Sigma}}_{ic}, \tau_i^2 \right] [\boldsymbol{\mu}_i(t) \mid \boldsymbol{\pi}_i, \boldsymbol{\delta}_i] \\
&\propto \sum_{j=1}^J \pi_{ij} \delta_{\boldsymbol{\mu}_{ij}} \left[\mathbf{s}_{ic}(t) \mid \boldsymbol{\mu}_{ij}, y_i(t), \boldsymbol{\Sigma}_{ic}, \tilde{\boldsymbol{\Sigma}}_{ic}, \tau_i^2 \right],
\end{aligned}$$

where $\boldsymbol{\pi}_i = (\pi_{i1}, \dots, \pi_{iJ})$ and $\boldsymbol{\delta}_i = (\delta_{\mu_{i1}}, \dots, \delta_{\mu_{iJ}})$. We introduce an indicator variable for the latent class status, $h_i(t) \in \{1, \dots, J\}$, that assigns each telemetry location $\mathbf{s}_{ic}(t)$ to one of the potential haul-out sites $\boldsymbol{\mu}_{ij}$, for $j = 1, \dots, J$. In other words, $\boldsymbol{\mu}_i(t) = \boldsymbol{\mu}_{i,h_i(t)}$. The

update proceeds just as in multinomial sampling:

$$\begin{aligned}
[h_i(t) | \cdot] &\sim \text{Cat} \left(\frac{\pi_{i1} [\mathbf{s}_{ic}(t) | \boldsymbol{\mu}_{i1}, \Sigma_{ic}, \tilde{\Sigma}_{ic}]^{y_i(t)} [\mathbf{s}_{ic}(t) | \boldsymbol{\mu}_{i1}, \tau_i^2 \mathbf{I} + \Sigma_{ic}, \tau_i^2 \mathbf{I} + \tilde{\Sigma}_{ic}]^{1-y_i(t)}}{\sum_{j=1}^J \pi_{ij} [\mathbf{s}_{ic}(t) | \boldsymbol{\mu}_{ij}, \Sigma_{ic}, \tilde{\Sigma}_{ic}]^{y_i(t)} [\mathbf{s}_{ic}(t) | \boldsymbol{\mu}_{ij}, \tau_i^2 \mathbf{I} + \Sigma_{ic}, \tau_i^2 \mathbf{I} + \tilde{\Sigma}_{ic}]^{1-y_i(t)}}, \dots, \right. \\
&\quad \left. \frac{\pi_{iJ} [\mathbf{s}_{ic}(t) | \boldsymbol{\mu}_{iJ}, \Sigma_{ic}, \tilde{\Sigma}_{ic}]^{y_i(t)} [\mathbf{s}_{ic}(t) | \boldsymbol{\mu}_{iJ}, \tau_i^2 \mathbf{I} + \Sigma_{ic}, \tau_i^2 \mathbf{I} + \tilde{\Sigma}_{ic}]^{1-y_i(t)}}{\sum_{j=1}^J \pi_{ij} [\mathbf{s}_{ic}(t) | \boldsymbol{\mu}_{ij}, \Sigma_{ic}, \tilde{\Sigma}_{ic}]^{y_i(t)} [\mathbf{s}_{ic}(t) | \boldsymbol{\mu}_{ij}, \tau_i^2 \mathbf{I} + \Sigma_{ic}, \tau_i^2 \mathbf{I} + \tilde{\Sigma}_{ic}]^{1-y_i(t)}} \right) \\
&\sim \text{Cat} \left(\frac{a_{i1}}{b_i}, \dots, \frac{a_{iJ}}{b_i} \right),
\end{aligned}$$

where $a_{ij} = \pi_{ij} \times \left(0.5 \times (\mathcal{N}(\mathbf{s}_{ic}(t) | \boldsymbol{\mu}_{ij}, \Sigma_{ic}) + \mathcal{N}(\mathbf{s}_{ic}(t) | \boldsymbol{\mu}_{ij}, \tilde{\Sigma}_{ic})) \right)^{y_i(t)} \times (0.5 \times (\mathcal{N}(\mathbf{s}_{ic}(t) | \boldsymbol{\mu}_{ij}, \tau_i^2 \mathbf{I} + \Sigma_{ic}) + \mathcal{N}(\mathbf{s}_{ic}(t) | \boldsymbol{\mu}_{ij}, \tau_i^2 \mathbf{I} + \tilde{\Sigma}_{ic})) \right)^{1-y_i(t)}$

and $b_i = \sum_{j=1}^J \left\{ \pi_{ij} \left(0.5 \times (\mathcal{N}(\mathbf{s}_{ic}(t) | \boldsymbol{\mu}_{ij}, \Sigma_{ic}) + \mathcal{N}(\mathbf{s}_{ic}(t) | \boldsymbol{\mu}_{ij}, \tilde{\Sigma}_{ic})) \right)^{y_i(t)} \times (0.5 \times (\mathcal{N}(\mathbf{s}_{ic}(t) | \boldsymbol{\mu}_{ij}, \tau_i^2 \mathbf{I} + \Sigma_{ic}) + \mathcal{N}(\mathbf{s}_{ic}(t) | \boldsymbol{\mu}_{ij}, \tau_i^2 \mathbf{I} + \tilde{\Sigma}_{ic})) \right)^{1-y_i(t)} \right\}$.

Animal movement parameter (τ_i):

$$\begin{aligned}
[\tau_i | \cdot] &\propto \prod_{t \in \mathcal{T}} [\mathbf{s}_{ic}(t) | \boldsymbol{\mu}_i(t), y_i(t), \Sigma_{ic}, \tilde{\Sigma}_{ic}, \tau_i^2] [\tau_i | \mu_\tau, \sigma_\tau^2] \\
&\propto \prod_{t \in \mathcal{T}} [\mathbf{s}_{ic}(t) | \boldsymbol{\mu}_i(t), \Sigma_{ic}, \tilde{\Sigma}_{ic}, \tau_i^2]^{1-y_i(t)} [\tau_i | \mu_\tau, \sigma_\tau^2] \\
&\propto \prod_{\{t \in \mathcal{T}: y_i(t)=0\}} 0.5 \times (\mathcal{N}(\mathbf{s}_{ic}(t) | \boldsymbol{\mu}_i(t), \tau_i^2 \mathbf{I} + \Sigma_{ic}) + \mathcal{N}(\mathbf{s}_{ic}(t) | \boldsymbol{\mu}_i(t), \tau_i^2 \mathbf{I} + \tilde{\Sigma}_{ic})) \times \\
&\quad \mathcal{N}(\log(\tau_i) | \log(\mu_\tau), \sigma_\tau^2).
\end{aligned}$$

Note that the product is over all observed telemetry locations ($\mathbf{s}_{ic}(t)$) that are recorded when the individual is at-sea (i.e., $y_i(t) = 0$).

Longitudinal telemetry measurement error (σ_{ic}):

$$\begin{aligned}
[\sigma_{ic} | \cdot] &\propto \prod_{t \in \mathcal{T}} [\mathbf{s}_{ic}(t) | \boldsymbol{\mu}_i(t), y_i(t), \Sigma_{ic}, \tilde{\Sigma}_{ic}, \tau_i^2]^{1 \{ \mathbf{s}_{ic}(t): t \in \mathcal{T}_c \}} [\sigma_{ic} | l_\sigma, u_\sigma] \\
&\propto \prod_{t \in \mathcal{T}_c} \left\{ [\mathbf{s}_{ic}(t) | \boldsymbol{\mu}_i(t), \Sigma_{ic}, \tilde{\Sigma}_{ic}]^{y_i(t)} [\mathbf{s}_{ic}(t) | \boldsymbol{\mu}_i(t), \tau_i^2 \mathbf{I} + \Sigma_{ic}, \tau_i^2 \mathbf{I} + \tilde{\Sigma}_{ic}]^{1-y_i(t)} \right\} [\sigma_{ic} | l_\sigma, u_\sigma] \\
&\propto \prod_{t \in \mathcal{T}_c} \left\{ (0.5 \times (\mathcal{N}(\mathbf{s}_{ic}(t) | \boldsymbol{\mu}_i(t), \Sigma_{ic}) + \mathcal{N}(\mathbf{s}_{ic}(t) | \boldsymbol{\mu}_i(t), \tilde{\Sigma}_{ic})))^{y_i(t)} \times \right. \\
&\quad \left. (0.5 \times (\mathcal{N}(\mathbf{s}_{ic}(t) | \boldsymbol{\mu}_i(t), \tau_i^2 \mathbf{I} + \Sigma_{ic}) + \mathcal{N}(\mathbf{s}_{ic}(t) | \boldsymbol{\mu}_i(t), \tau_i^2 \mathbf{I} + \tilde{\Sigma}_{ic})))^{1-y_i(t)} \right\} \times \\
&\quad \text{Unif}(\sigma_{ic} | l_\sigma, u_\sigma).
\end{aligned}$$

Note that \mathcal{T}_c defines the times at which telemetry locations in Argos location class c were recorded. In other words, the product is over all observed telemetry locations ($\mathbf{s}_{ic}(t)$) in Argos location quality class c .

Adjustment for latitudinal telemetry measurement error (a_{ic}):

$$\begin{aligned} [a_{ic} | \cdot] &\propto \prod_{t \in \mathcal{T}} \left[\mathbf{s}_{ic}(t) | \boldsymbol{\mu}_i(t), y_i(t), \Sigma_{ic}, \tilde{\Sigma}_{ic}, \tau_i^2 \right]^{1_{\{\mathbf{s}_{ic}(t):t \in \mathcal{T}_c\}}} [a_{ic} | l_a, u_a] \\ &\propto \prod_{t \in \mathcal{T}_c} \left\{ \left[\mathbf{s}_{ic}(t) | \boldsymbol{\mu}_i(t), \Sigma_{ic}, \tilde{\Sigma}_{ic} \right]^{y_i(t)} \left[\mathbf{s}_{ic}(t) | \boldsymbol{\mu}_i(t), \tau_i^2 \mathbf{I} + \Sigma_{ic}, \tau_i^2 \mathbf{I} + \tilde{\Sigma}_{ic} \right]^{1-y_i(t)} \right\} [a_{ic} | l_a, u_a] \\ &\propto \prod_{t \in \mathcal{T}_c} \left\{ \left(0.5 \times (\mathcal{N}(\mathbf{s}_{ic}(t) | \boldsymbol{\mu}_i(t), \Sigma_{ic}) + \mathcal{N}(\mathbf{s}_{ic}(t) | \boldsymbol{\mu}_i(t), \tilde{\Sigma}_{ic})) \right)^{y_i(t)} \times \right. \\ &\quad \left. \left(0.5 \times (\mathcal{N}(\mathbf{s}_{ic}(t) | \boldsymbol{\mu}_i(t), \tau_i^2 \mathbf{I} + \Sigma_{ic}) + \mathcal{N}(\mathbf{s}_{ic}(t) | \boldsymbol{\mu}_i(t), \tau_i^2 \mathbf{I} + \tilde{\Sigma}_{ic})) \right)^{1-y_i(t)} \right\} \times \\ &\quad \text{Unif}(a_{ic} | l_a, u_a). \end{aligned}$$

Note that \mathcal{T}_c defines the times at which telemetry locations in Argos location class c were recorded. In other words, the product is over all observed telemetry locations ($\mathbf{s}_{ic}(t)$) in Argos location quality class c .

Correlation between longitudinal and latitudinal telemetry measurement error (ρ_{ic}):

$$\begin{aligned} [\rho_{ic} | \cdot] &\propto \prod_{t \in \mathcal{T}} \left[\mathbf{s}_{ic}(t) | \boldsymbol{\mu}_i(t), y_i(t), \Sigma_{ic}, \tilde{\Sigma}_{ic}, \tau_i^2 \right]^{1_{\{\mathbf{s}_{ic}(t):t \in \mathcal{T}_c\}}} [\rho_{ic} | l_\rho, u_\rho] \\ &\propto \prod_{t \in \mathcal{T}_c} \left\{ \left[\mathbf{s}_{ic}(t) | \boldsymbol{\mu}_i(t), \Sigma_{ic}, \tilde{\Sigma}_{ic} \right]^{y_i(t)} \left[\mathbf{s}_{ic}(t) | \boldsymbol{\mu}_i(t), \tau_i^2 \mathbf{I} + \Sigma_{ic}, \tau_i^2 \mathbf{I} + \tilde{\Sigma}_{ic} \right]^{1-y_i(t)} \right\} [\rho_{ic} | l_\rho, u_\rho] \\ &\propto \prod_{t \in \mathcal{T}_c} \left\{ \left(0.5 \times (\mathcal{N}(\mathbf{s}_{ic}(t) | \boldsymbol{\mu}_i(t), \Sigma_{ic}) + \mathcal{N}(\mathbf{s}_{ic}(t) | \boldsymbol{\mu}_i(t), \tilde{\Sigma}_{ic})) \right)^{y_i(t)} \times \right. \\ &\quad \left. \left(0.5 \times (\mathcal{N}(\mathbf{s}_{ic}(t) | \boldsymbol{\mu}_i(t), \tau_i^2 \mathbf{I} + \Sigma_{ic}) + \mathcal{N}(\mathbf{s}_{ic}(t) | \boldsymbol{\mu}_i(t), \tau_i^2 \mathbf{I} + \tilde{\Sigma}_{ic})) \right)^{1-y_i(t)} \right\} \times \\ &\quad \text{Unif}(\rho_{ic} | l_\rho, u_\rho). \end{aligned}$$

Note that \mathcal{T}_c defines the times at which telemetry locations in Argos location class c were recorded. In other words, the product is over all observed telemetry locations ($\mathbf{s}_{ic}(t)$) in Argos location quality class c .

MCMC ALGORITHM FOR PARAMETER ESTIMATION

One can implement a MCMC algorithm to estimate the parameters of the observation and process models using the sequence of steps outlined below. Proposal distributions for all parameters with non-conjugate full-conditional distributions (i.e., $\boldsymbol{\mu}_{ij}$, τ_i , σ_{ic} , a_{ic} , and ρ_{ic}) are assumed to be symmetric and updates proceed using Metropolis sampling; therefore, the proposal distribution is not factored into the associated ratios as in Metropolis-Hastings sampling. Also note that normalizing constants cancel in the Metropolis ratios and thus may be omitted for clarity.

1. Define initial values for: $\boldsymbol{\mu}_{ij}^{(0)}$ and $\pi_{ij}^{(0)}$ for $j = 1, \dots, J$; $\theta_i^{(0)}$; $\tau_i^{(0)}$; and $\sigma_{ic}^{(0)}$, $a_{ic}^{(0)}$, and $\rho_{ic}^{(0)}$ for $c = 3, 2, 1, 0$, A, and B.

2. For each Argos location quality class, let

$$\boldsymbol{\Sigma}_{ic}^{(0)} = \left(\sigma_{ic}^{(0)}\right)^2 \begin{bmatrix} 1 & \rho_{ic}^{(0)} \sqrt{a_{ic}^{(0)}} \\ \rho_{ic}^{(0)} \sqrt{a_{ic}^{(0)}} & a_{ic}^{(0)} \end{bmatrix}$$

and

$$\begin{aligned} \tilde{\boldsymbol{\Sigma}}_{ic}^{(0)} &= \left(\sigma_{ic}^{(0)}\right)^2 \begin{bmatrix} 1 & -\rho_{ic}^{(0)} \sqrt{a_{ic}^{(0)}} \\ -\rho_{ic}^{(0)} \sqrt{a_{ic}^{(0)}} & a_{ic}^{(0)} \end{bmatrix} \\ &= \mathbf{H} \boldsymbol{\Sigma}_{ic}^{(0)} \mathbf{H}', \end{aligned}$$

where

$$\mathbf{H} = \begin{bmatrix} 1 & 0 \\ 0 & -1 \end{bmatrix}.$$

Also let

$$\mathbf{Q}_{ic}^{(0)} = \boldsymbol{\Sigma}_{ic}^{(0)} + \left(\tau_i^{(0)}\right)^2 \mathbf{I}$$

and

$$\begin{aligned} \tilde{\mathbf{Q}}_{ic}^{(0)} &= \tilde{\boldsymbol{\Sigma}}_{ic}^{(0)} + \left(\tau_i^{(0)}\right)^2 \mathbf{I} \\ &= \mathbf{H} \mathbf{Q}_{ic}^{(0)} \mathbf{H}'. \end{aligned}$$

3. Set $k = 1$.

4. Update the spatial process model parameters (i.e., $h_i(t)$, η_{ij} , θ_i , and $\boldsymbol{\mu}_{ij}$).

(a) Sample $h_i(t)^{(k)}$:

$$[h_i(t)^{(k)} | \cdot] \sim \text{Cat}\left(\frac{a_{ij}}{b_i}, \dots, \frac{a_{iJ}}{b_i}\right),$$

where $a_{ij} = \pi_{ij}^{(k-1)} \times \left(\mathcal{N}(\mathbf{s}_{ic}(t) | \boldsymbol{\mu}_{ij}^{(k-1)}, \boldsymbol{\Sigma}_{ic}^{(k-1)}) + \mathcal{N}(\mathbf{s}_{ic}(t) | \boldsymbol{\mu}_{ij}^{(k-1)}, \tilde{\boldsymbol{\Sigma}}_{ic}^{(k-1)})\right)^{y_{ij}(t)} \times \left(\mathcal{N}(\mathbf{s}_{ic}(t) | \boldsymbol{\mu}_{ij}^{(k-1)}, \mathbf{Q}_{ic}^{(k-1)}) + \mathcal{N}(\mathbf{s}_{ic}(t) | \boldsymbol{\mu}_{ij}^{(k-1)}, \mathbf{H} \mathbf{Q}_{ic}^{(k-1)} \mathbf{H}')\right)^{1-y_{ij}(t)}$
and $b_i = \sum_{j=1}^J \left\{ \pi_{ij}^{(k-1)} \left(\mathcal{N}(\mathbf{s}_{ic}(t) | \boldsymbol{\mu}_{ij}^{(k-1)}, \boldsymbol{\Sigma}_{ic}^{(k-1)}) + \mathcal{N}(\mathbf{s}_{ic}(t) | \boldsymbol{\mu}_{ij}^{(k-1)}, \tilde{\boldsymbol{\Sigma}}_{ic}^{(k-1)}) \right)^{y_{ij}(t)} \times \left(\mathcal{N}(\mathbf{s}_{ic}(t) | \boldsymbol{\mu}_{ij}^{(k-1)}, \mathbf{Q}_{ic}^{(k-1)}) + \mathcal{N}(\mathbf{s}_{ic}(t) | \boldsymbol{\mu}_{ij}^{(k-1)}, \mathbf{H} \mathbf{Q}_{ic}^{(k-1)} \mathbf{H}') \right)^{1-y_{ij}(t)} \right\}$.

(b) Tabulate cluster membership for $j = 1, \dots, J$:

$$n_{ij}^{(k)} = \sum_{t \in \mathcal{T}} 1_{\{h_i(t)^{(k)} = j\}}.$$

In other words, $n_{ij}^{(k)}$ denotes the number of observed telemetry locations ($\mathbf{s}_{ic}(t)$) allocated to haul-out site $\boldsymbol{\mu}_{ij}^{(k-1)}$.

- (c) Update $\eta_{ij}^{(k-1)}$, for $j = 1, \dots, J - 1$, using a Gibbs step:

$$\left[\eta_{ij}^{(k)} \mid \cdot \right] \sim \text{Beta} \left(1 + n_{ij}^{(k)}, \theta_i^{(k-1)} + \sum_{l=j+1}^J n_{il}^{(k)} \right).$$

Set $\eta_{iJ}^{(k)} = 1$.

- (d) Update $\pi_{ij}^{(k-1)}$, for $j = 1, \dots, J$, which is calculated as:

$$\pi_{ij}^{(k)} = \eta_{ij}^{(k)} \prod_{l < j} \left(1 - \eta_{il}^{(k)} \right).$$

Letting $\eta_{iJ}^{(k)} = 1$ ensures $\sum_{j=1}^J \pi_{ij}^{(k)} = 1$.

- (e) Update $\theta_i^{(k-1)}$ using a Gibbs step:

$$\left[\theta_i^{(k)} \mid \cdot \right] \sim \text{Gamma} \left(r_\theta + J - 1, q_\theta - \sum_{j=1}^{J-1} \log \left(1 - \eta_{ij}^{(k)} \right) \right).$$

- (f) Update $\boldsymbol{\mu}_{ij}^{(k-1)}$, for each j such that $n_{ij}^{(k)} > 0$, using Metropolis sampling. Sample $\boldsymbol{\mu}_{ij}^{(*)}$ from a proposal distribution $\left[\boldsymbol{\mu}_{ij}^{(*)} \mid \boldsymbol{\mu}_{ij}^{(k-1)} \right]$. Depending on the nature of \mathcal{S} (e.g., linear support like a coastline), proposals generated from $\mathcal{N} \left(\boldsymbol{\mu}_{ij}^{(*)} \mid \boldsymbol{\mu}_{ij}^{(k-1)}, \tau_\mu^2 \mathbf{I} \right)$, where τ_μ^2 is a tuning parameter, may rarely occur in \mathcal{S} . Therefore, sample all possible locations $\mathbf{M} \in \mathcal{S}$ with probability proportional to $\mathcal{N} \left(\mathbf{M} \mid \boldsymbol{\mu}_{ij}^{(k-1)}, \tau_\mu^2 \mathbf{I} \right)$, thus guaranteeing $\boldsymbol{\mu}_{ij}^{(*)} \in \mathcal{S}$. Calculate the Metropolis ratio as

$$r_\mu = \left(\frac{\prod_{\{t \in \mathcal{T}: h_i(t)^{(k)} = j\}} \left\{ \left(\mathcal{N} \left(\mathbf{s}_{ic}(t) \mid \boldsymbol{\mu}_{ij}^{(*)}, \boldsymbol{\Sigma}_{ic}^{(k-1)} \right) + \mathcal{N} \left(\mathbf{s}_{ic}(t) \mid \boldsymbol{\mu}_{ij}^{(*)}, \mathbf{H} \boldsymbol{\Sigma}_{ic}^{(k-1)} \mathbf{H}' \right) \right)^{y_i(t)} \right\}}{\prod_{\{t \in \mathcal{T}: h_i(t)^{(k)} = j\}} \left\{ \left(\mathcal{N} \left(\mathbf{s}_{ic}(t) \mid \boldsymbol{\mu}_{ij}^{(k-1)}, \boldsymbol{\Sigma}_{ic}^{(k-1)} \right) + \mathcal{N} \left(\mathbf{s}_{ic}(t) \mid \boldsymbol{\mu}_{ij}^{(k-1)}, \mathbf{H} \boldsymbol{\Sigma}_{ic}^{(k-1)} \mathbf{H}' \right) \right)^{y_i(t)} \right\}} \times \frac{\left(\mathcal{N} \left(\mathbf{s}_{ic}(t) \mid \boldsymbol{\mu}_{ij}^{(*)}, \mathbf{Q}_{ic}^{(k-1)} \right) + \mathcal{N} \left(\mathbf{s}_{ic}(t) \mid \boldsymbol{\mu}_{ij}^{(*)}, \mathbf{H} \mathbf{Q}_{ic}^{(k-1)} \mathbf{H}' \right) \right)^{1-y_i(t)}}{\left(\mathcal{N} \left(\mathbf{s}_{ic}(t) \mid \boldsymbol{\mu}_{ij}^{(k-1)}, \mathbf{Q}_{ic}^{(k-1)} \right) + \mathcal{N} \left(\mathbf{s}_{ic}(t) \mid \boldsymbol{\mu}_{ij}^{(k-1)}, \mathbf{H} \mathbf{Q}_{ic}^{(k-1)} \mathbf{H}' \right) \right)^{1-y_i(t)}} \right) \times \left(\frac{\left[\boldsymbol{\mu}_{ij}^{(*)} \mid f_{\mathcal{S}}(\mathbf{s}_i) \right]}{\left[\boldsymbol{\mu}_{ij}^{(k-1)} \mid f_{\mathcal{S}}(\mathbf{s}_i) \right]} \right).$$

Note that the product is over all observed telemetry locations ($\mathbf{s}_{ic}(t)$) that are allocated to haul-out site $\boldsymbol{\mu}_{ij}$ (i.e., $t \in \mathcal{T}$ such that $h_i(t)^{(k)} = j$). If $r_\mu > u$, where $u \sim \text{Uniform}(0,1)$, let $\boldsymbol{\mu}_{ij}^{(k)} = \boldsymbol{\mu}_{ij}^{(*)}$. Otherwise, let $\boldsymbol{\mu}_{ij}^{(k)} = \boldsymbol{\mu}_{ij}^{(k-1)}$ if $r_\mu < u$, or if $\boldsymbol{\mu}_{ij}^{(*)} \notin \mathcal{S}$.

- (g) For each j such that $n_{ij}^{(k)} = 0$ (i.e., potential haul-out sites $\mu_{ij}^{(k-1)}$ with zero membership), sample $\mu_{ij}^{(k)}$ from the prior $[\mu_{ij}^{(k)} | f_S(\mathbf{S}_i)]$. As in Step 4(f), sample all possible locations $\mathbf{M} \in \mathcal{S}$ with probability proportional to $f_S(\mathbf{S}_i)$ to ensure $\mu_{ij}^{(k)} \in \mathcal{S}$.
- (h) Use $h_i(t)^{(k)}$ to map the location of haul-out sites $\mu_{ij}^{(k)}$, for $j = 1, \dots, J$, to telemetry locations $\mathbf{s}_{ic}(t)$, for times $t \in \mathcal{T}$:

$$\boldsymbol{\mu}_i(t)^{(k)} = \boldsymbol{\mu}_{i,h_i(t)^{(k)}}^{(k)}.$$

5. Update $\tau_i^{(k-1)}$ using Metropolis sampling. Sample $\tau_i^{(*)}$ from a proposal distribution $[\tau_i^{(*)} | \tau_i^{(k-1)}]$ (e.g., $\mathcal{N}(\tau_i^{(*)} | \tau_i^{(k-1)}, \tau_\tau^2 \mathbf{I})$, where τ_τ^2 is a tuning parameter). If $\tau_i^{(*)} \geq 0$, let

$$\mathbf{Q}_{ic}^{(*)} = \boldsymbol{\Sigma}_{ic}^{(k-1)} + (\tau_i^{(*)})^2 \mathbf{I}$$

for $c = 3, 2, 1, 0, A$, and B . Calculate the Metropolis ratio as

$$r_\tau = \left(\frac{\prod_{\{t \in \mathcal{T}: y_i(t)=0\}} \left\{ \mathcal{N}(\mathbf{s}_{ic}(t) | \boldsymbol{\mu}_i(t)^{(k)}, \mathbf{Q}_{ic}^{(*)}) + \mathcal{N}(\mathbf{s}_{ic}(t) | \boldsymbol{\mu}_i(t)^{(k)}, \mathbf{H}\mathbf{Q}_{ic}^{(*)}\mathbf{H}') \right\}}{\prod_{\{t \in \mathcal{T}: y_i(t)=0\}} \left\{ \mathcal{N}(\mathbf{s}_{ic}(t) | \boldsymbol{\mu}_i(t)^{(k)}, \mathbf{Q}_{ic}^{(k-1)}) + \mathcal{N}(\mathbf{s}_{ic}(t) | \boldsymbol{\mu}_i(t)^{(k)}, \mathbf{H}\mathbf{Q}_{ic}^{(k-1)}\mathbf{H}') \right\}} \right) \times \left(\frac{\mathcal{N}(\log(\tau_i^{(*)}) | \log(\mu_\tau), \sigma_\tau^2)}{\mathcal{N}(\log(\tau_i^{(k-1)}) | \log(\mu_\tau), \sigma_\tau^2)} \right).$$

Note that the product is over all $t \in \mathcal{T}$ such that $y_i(t) = 0$. If $r_\tau > u$, where $u \sim \text{Uniform}(0,1)$, let $\tau_i^{(k)} = \tau_i^{(*)}$ and $\mathbf{Q}_{ic}^{(k)} = \mathbf{Q}_{ic}^{(*)}$. Otherwise, let $\tau_i^{(k)} = \tau_i^{(k-1)}$ and $\mathbf{Q}_{ic}^{(k)} = \mathbf{Q}_{ic}^{(k-1)}$ if $r_\tau < u$, or if $\tau_i^{(*)} < 0$.

6. For each Argos location quality class $c = 3, 2, 1, 0, A$, and B , update the observation model parameters related to telemetry measurement error (i.e., $\boldsymbol{\sigma}_i$, \mathbf{a}_i , and $\boldsymbol{\rho}_i$).

- (a) Let \mathcal{T}_c define the times at which telemetry locations in Argos location class c were recorded.
- (b) Update $\sigma_{ic}^{(k-1)}$ using Metropolis sampling. Sample $\sigma_{ic}^{(*)}$ from a proposal distribution $[\sigma_{ic}^{(*)} | \sigma_{ic}^{(k-1)}]$ (e.g., $\mathcal{N}(\sigma_{ic}^{(*)} | \sigma_{ic}^{(k-1)}, \tau_\sigma^2)$, where τ_σ^2 is a tuning parameter). If $\sigma_{ic}^{(*)} \in [l_\sigma, u_\sigma]$, let

$$\boldsymbol{\Sigma}_{ic}^{(*)} = (\sigma_{ic}^{(*)})^2 \begin{bmatrix} 1 & \rho_{ic}^{(k-1)} \sqrt{a_{ic}^{(k-1)}} \\ \rho_{ic}^{(k-1)} \sqrt{a_{ic}^{(k-1)}} & a_{ic}^{(k-1)} \end{bmatrix}$$

and

$$\mathbf{Q}_{ic}^{(*)} = \boldsymbol{\Sigma}_{ic}^{(*)} + (\tau_i^{(k)})^2 \mathbf{I}.$$

Calculate the Metropolis ratio as

$$r_\sigma = \left(\frac{\prod_{t \in \mathcal{T}_c} \left\{ (\mathcal{N}(\mathbf{s}_{ic}(t) | \boldsymbol{\mu}_i(t)^{(k)}, \Sigma_{ic}^{(*)}) + \mathcal{N}(\mathbf{s}_{ic}(t) | \boldsymbol{\mu}_i(t)^{(k)}, \mathbf{H}\Sigma_{ic}^{(*)}\mathbf{H}')\right\}^{y_i(t)}}{\prod_{t \in \mathcal{T}_c} \left\{ (\mathcal{N}(\mathbf{s}_{ic}(t) | \boldsymbol{\mu}_i(t)^{(k)}, \Sigma_{ic}^{(k-1)}) + \mathcal{N}(\mathbf{s}_{ic}(t) | \boldsymbol{\mu}_i(t)^{(k)}, \mathbf{H}\Sigma_{ic}^{(k-1)}\mathbf{H}')\right\}^{y_i(t)}} \times \frac{\left(\mathcal{N}(\mathbf{s}_{ic}(t) | \boldsymbol{\mu}_i(t)^{(k)}, \mathbf{Q}_{ic}^{(*)}) + \mathcal{N}(\mathbf{s}_{ic}(t) | \boldsymbol{\mu}_i(t)^{(k)}, \mathbf{HQ}_{ic}^{(*)}\mathbf{H}')\right)^{1-y_i(t)}}{\left(\mathcal{N}(\mathbf{s}_{ic}(t) | \boldsymbol{\mu}_i(t)^{(k)}, \mathbf{Q}_{ic}^{(k)}) + \mathcal{N}(\mathbf{s}_{ic}(t) | \boldsymbol{\mu}_i(t)^{(k)}, \mathbf{HQ}_{ic}^{(k)}\mathbf{H}')\right)^{1-y_i(t)}} \right).$$

If $r_\sigma > u$, where $u \sim \text{Uniform}(0,1)$, let $\sigma_{ic}^{(k)} = \sigma_{ic}^{(*)}$, $\Sigma_{ic}^{(k)} = \Sigma_{ic}^{(*)}$, and $\mathbf{Q}_{ic}^{(k)} = \mathbf{Q}_{ic}^{(*)}$. Otherwise, let $\sigma_{ic}^{(k)} = \sigma_{ic}^{(k-1)}$, $\Sigma_{ic}^{(k)} = \Sigma_{ic}^{(k-1)}$, and $\mathbf{Q}_{ic}^{(k)} = \mathbf{Q}_{ic}^{(k)} = \Sigma_{ic}^{(k-1)} + (\tau_i^{(k)})^2 \mathbf{I}$ if $r_\sigma < u$, or if $\sigma_{ic}^{(*)} \notin [l_\sigma, u_\sigma]$.

- (c) Update $a_{ic}^{(k-1)}$ using Metropolis sampling. Sample $a_{ic}^{(*)}$ from a proposal distribution $[a_{ic}^{(*)} | a_{ic}^{(k-1)}]$ (e.g., $N(a_{ic}^{(*)} | a_{ic}^{(k-1)}, \tau_a^2)$, where τ_a^2 is a tuning parameter). If $a_{ic}^{(*)} \in [l_a, u_a]$, let

$$\Sigma_{ic}^{(*)} = \left(\sigma_{ic}^{(k)} \right)^2 \begin{bmatrix} 1 & \rho_{ic}^{(k-1)} \sqrt{a_{ic}^{(*)}} \\ \rho_{ic}^{(k-1)} \sqrt{a_{ic}^{(*)}} & a_{ic}^{(*)} \end{bmatrix}$$

and

$$\mathbf{Q}_{ic}^{(*)} = \Sigma_{ic}^{(*)} + (\tau_i^{(k)})^2 \mathbf{I}.$$

Calculate the Metropolis ratio as

$$r_a = \left(\frac{\prod_{t \in \mathcal{T}_c} \left\{ (\mathcal{N}(\mathbf{s}_{ic}(t) | \boldsymbol{\mu}_i(t)^{(k)}, \Sigma_{ic}^{(*)}) + \mathcal{N}(\mathbf{s}_{ic}(t) | \boldsymbol{\mu}_i(t)^{(k)}, \mathbf{H}\Sigma_{ic}^{(*)}\mathbf{H}')\right\}^{y_i(t)}}{\prod_{t \in \mathcal{T}_c} \left\{ (\mathcal{N}(\mathbf{s}_{ic}(t) | \boldsymbol{\mu}_i(t)^{(k)}, \Sigma_{ic}^{(k)}) + \mathcal{N}(\mathbf{s}_{ic}(t) | \boldsymbol{\mu}_i(t)^{(k)}, \mathbf{H}\Sigma_{ic}^{(k)}\mathbf{H}')\right\}^{y_i(t)}} \times \frac{\left(\mathcal{N}(\mathbf{s}_{ic}(t) | \boldsymbol{\mu}_i(t)^{(k)}, \mathbf{Q}_{ic}^{(*)}) + \mathcal{N}(\mathbf{s}_{ic}(t) | \boldsymbol{\mu}_i(t)^{(k)}, \mathbf{HQ}_{ic}^{(*)}\mathbf{H}')\right)^{1-y_i(t)}}{\left(\mathcal{N}(\mathbf{s}_{ic}(t) | \boldsymbol{\mu}_i(t)^{(k)}, \mathbf{Q}_{ic}^{(k)}) + \mathcal{N}(\mathbf{s}_{ic}(t) | \boldsymbol{\mu}_i(t)^{(k)}, \mathbf{HQ}_{ic}^{(k)}\mathbf{H}')\right)^{1-y_i(t)}} \right).$$

If $r_a > u$, where $u \sim \text{Uniform}(0,1)$, let $a_{ic}^{(k)} = a_{ic}^{(*)}$, $\Sigma_{ic}^{(k)} = \Sigma_{ic}^{(*)}$, and $\mathbf{Q}_{ic}^{(k)} = \mathbf{Q}_{ic}^{(*)}$. Otherwise, let $a_{ic}^{(k)} = a_{ic}^{(k-1)}$, $\Sigma_{ic}^{(k)} = \Sigma_{ic}^{(k-1)}$, and $\mathbf{Q}_{ic}^{(k)} = \mathbf{Q}_{ic}^{(k)}$ if $r_a < u$, or if $a_{ic}^{(*)} \notin [l_a, u_a]$.

- (d) Update $\rho_{ic}^{(k-1)}$ using Metropolis sampling. Sample $\rho_{ic}^{(*)}$ from a proposal distribution $[\rho_{ic}^{(*)} | \rho_{ic}^{(k-1)}]$ (e.g., $N(\rho_{ic}^{(*)} | \rho_{ic}^{(k-1)}, \tau_\rho^2)$, where τ_ρ^2 is a tuning parameter). If $\rho_{ic}^{(*)} \in [l_\rho, u_\rho]$, let

$$\Sigma_{ic}^{(*)} = \left(\sigma_{ic}^{(k)} \right)^2 \begin{bmatrix} 1 & \rho_{ic}^{(*)} \sqrt{a_{ic}^{(k)}} \\ \rho_{ic}^{(*)} \sqrt{a_{ic}^{(k)}} & a_{ic}^{(k)} \end{bmatrix}$$

and

$$\mathbf{Q}_{ic}^{(*)} = \boldsymbol{\Sigma}_{ic}^{(*)} + \left(\tau_i^{(k)} \right)^2 \mathbf{I}.$$

Calculate the Metropolis ratio as

$$r_\rho = \left(\frac{\prod_{t \in \mathcal{T}_c} \left\{ \left(\mathcal{N}(\mathbf{s}_{ic}(t) | \boldsymbol{\mu}_i(t)^{(k)}, \boldsymbol{\Sigma}_{ic}^{(*)}) + \mathcal{N}(\mathbf{s}_{ic}(t) | \boldsymbol{\mu}_i(t)^{(k)}, \mathbf{H}\boldsymbol{\Sigma}_{ic}^{(*)}\mathbf{H}') \right)^{y_i(t)} \right.}{\prod_{t \in \mathcal{T}_c} \left\{ \left(\mathcal{N}(\mathbf{s}_{ic}(t) | \boldsymbol{\mu}_i(t)^{(k)}, \boldsymbol{\Sigma}_{ic}^{(*)}) + \mathcal{N}(\mathbf{s}_{ic}(t) | \boldsymbol{\mu}_i(t)^{(k)}, \mathbf{H}\boldsymbol{\Sigma}_{ic}^{(*)}\mathbf{H}') \right)^{y_i(t)} \right.} \times \frac{\left. \left(\mathcal{N}(\mathbf{s}_{ic}(t) | \boldsymbol{\mu}_i(t)^{(k)}, \mathbf{Q}_{ic}^{(*)}) + \mathcal{N}(\mathbf{s}_{ic}(t) | \boldsymbol{\mu}_i(t)^{(k)}, \mathbf{H}\mathbf{Q}_{ic}^{(*)}\mathbf{H}') \right)^{1-y_i(t)} \right\}}{\left. \left(\mathcal{N}(\mathbf{s}_{ic}(t) | \boldsymbol{\mu}_i(t)^{(k)}, \mathbf{Q}_{ic}^{(*)}) + \mathcal{N}(\mathbf{s}_{ic}(t) | \boldsymbol{\mu}_i(t)^{(k)}, \mathbf{H}\mathbf{Q}_{ic}^{(*)}\mathbf{H}') \right)^{1-y_i(t)} \right\}} \right).$$

If $r_\rho > u$, where $u \sim \text{Uniform}(0,1)$, let $\rho_{ic}^{(k)} = \rho_{ic}^{(*)}$, $\boldsymbol{\Sigma}_{ic}^{(k)} = \boldsymbol{\Sigma}_{ic}^{(*)}$, and $\mathbf{Q}_{ic}^{(k)} = \mathbf{Q}_{ic}^{(*)}$. Otherwise, let $\rho_{ic}^{(k)} = \rho_{ic}^{(k-1)}$, $\boldsymbol{\Sigma}_{ic}^{(k)} = \boldsymbol{\Sigma}_{ic}^{(k-1)}$, and $\mathbf{Q}_{ic}^{(k)} = \mathbf{Q}_{ic}^{(k-1)}$ if $r_\rho < u$, or if $\rho_{ic}^{(*)} \notin [l_\rho, u_\rho]$.

- (e) Repeat Steps 6(a) through 6(d) for each error class c .
- 7. Save $\boldsymbol{\mu}_i(t)^{(k)}$ for $t \in \mathcal{T}$; $\theta_i^{(k)}$; $\tau_i^{(k)}$; π_{ij} for $j = 1, \dots, J$; and $\sigma_{ic}^{(k)}$, $a_{ic}^{(0)}$, and $\rho_{ic}^{(0)}$ for $c = 3, 2, 1, 0, \text{A}, \text{ and B}$.
- 8. Set $k = k + 1$ and return to Step 4. The algorithm is iterated by repeating Steps 4 through 7 until a sufficiently large sample has been obtained from which to approximate the posterior distribution.

REFERENCES

- Ishwaran, H., and L. F. James. 2001. Gibbs sampling methods for stick-breaking priors. *Journal of the American Statistical Association* **96**:161–173.
 Sethuraman, J. 1994. A constructive definition of Dirichlet priors. *Statistica Sinica* **4**:639–650.

APPENDIX C2. Model statement, posterior distribution, full-conditional distributions, and pseudocode detailing a Markov chain Monte Carlo algorithm for estimating the parameters in the model for examining haul-out site selection.

In the posterior and full-conditional distributions below, we use bracket notation to denote a probability distribution. For example, $[x]$ indicates the probability distribution of x . Similarly, $[x|y]$ indicates the probability distribution of x given the parameter y . The notation “.” represents the data and other parameters in the model.

MODEL STATEMENT

$$\begin{aligned} w_{ij} &\sim \begin{cases} \text{Pois}(\lambda_{ij}), & z_{ij} = 1 \\ 0, & z_{ij} = 0 \end{cases} \\ z_{ij} &\sim \text{Bern}(p_i) \\ \log(\lambda_{ij}) &= \mathbf{x}'_{ij} \boldsymbol{\beta}_i \\ \boldsymbol{\beta}_i &\sim \mathcal{N}(\boldsymbol{\mu}_\beta, \Sigma_\beta) \\ \boldsymbol{\mu}_\beta &\sim \mathcal{N}(\mathbf{0}, \sigma_{\mu_\beta}^2 \mathbf{I}) \\ p_i &\sim \text{Beta}(\alpha_1, \alpha_2) \\ \Sigma_\beta^{-1} &\sim \text{Wish}(\mathbf{S}_0^{-1}, \nu) \end{aligned}$$

POSTERIOR DISTRIBUTION

$$\begin{aligned} [\mathbf{B}, \boldsymbol{\mu}_\beta, \mathbf{p}, \Sigma_\beta | \mathbf{W}, \mathbf{Z}] &\propto \prod_{i=1}^N \prod_{j=1}^{J_i} [w_{ij} | \lambda_{ik}, \boldsymbol{\beta}_i] [\boldsymbol{\beta}_i | \boldsymbol{\mu}_\beta, \Sigma_\beta] \\ &\quad \times [p_i | \alpha_1, \alpha_2] [\boldsymbol{\mu}_\beta | \mathbf{0}, \sigma_{\mu_\beta}^2 \mathbf{I}] [\Sigma_\beta | \mathbf{S}_0, \nu], \end{aligned}$$

where $\mathbf{B} = \{\boldsymbol{\beta}_i, \forall i\}$ is a matrix of regression coefficients for each individual i ; $\mathbf{p} = (p_1, \dots, p_N)$ is vector of probabilities; $\mathbf{W} = \{w_{ij}, \forall i, \forall j\}$ is a matrix containing the counts of telemetry locations for each individual i allocated to each raster cell j in \mathcal{S} ; and $\mathbf{Z} = \{z_{ij}, \forall i, \forall j\}$ is a matrix of indicator variables of the same dimension as \mathbf{W} .

FULL-CONDITIONAL DISTRIBUTIONS

Latent mixture component indicator variable (z_{ij}):

$$\begin{aligned}
[z_{ij} | \cdot] &\propto [w_{ij} | \lambda_{ij}, z_{ij}] [z_{ij} | p_i] \\
&\propto \text{Pois}(w_{ij} | \lambda_{ij})^{z_{ij}} 1_{\{w_{ij}=0\}}^{1-z_{ij}} (p_i)^{z_{ij}} (1-p_i)^{1-z_{ij}} \\
&\propto \left(\frac{(\lambda_{ij})^{w_{ij}} \exp(-\lambda_{ij})}{w_{ij}!} \right)^{z_{ij}} (p_i)^{z_{ij}} (1-p_i)^{1-z_{ij}} \\
&\propto (\exp(-\lambda_{ij}))^{z_{ij}} (p_i)^{z_{ij}} (1-p_i)^{1-z_{ij}} \\
&\propto (p_i \times \exp(-\lambda_{ij}))^{z_{ij}} (1-p_i)^{1-z_{ij}} \\
&= \text{Bern}(\tilde{p}),
\end{aligned}$$

where

$$\tilde{p} = \frac{p_i \times \exp(-\lambda_{ij})}{p_i \times \exp(-\lambda_{ij}) + 1 - p_i}.$$

Note that z_{ij} is only estimated for instances where $w_{ij} = 0$ ($z_{ij} = 1$ when $w_{ij} > 0$).

Individual-level regression coefficients (β_i):

$$\begin{aligned}
[\beta_i | \cdot] &\propto \prod_{j=1}^{J_i} [w_{ij} | \lambda_{ij}, z_{ij}] [\beta_i | \mu_\beta, \Sigma_\beta] \\
&\propto \prod_{j=1}^{J_i} \text{Pois}(w_{ij} | \lambda_{ij})^{z_{ij}} \mathcal{N}(\beta_i | \mu_\beta, \Sigma_\beta).
\end{aligned}$$

The update for β_i proceeds using Metropolis-Hastings.

Population-level regression coefficients ($\boldsymbol{\mu}_\beta$):

$$\begin{aligned}
[\boldsymbol{\mu}_\beta \mid \cdot] &\propto \prod_{i=1}^N [\boldsymbol{\beta}_i \mid \boldsymbol{\mu}_\beta, \Sigma_\beta] [\boldsymbol{\mu}_\beta \mid \mathbf{0}, \sigma_{\mu_\beta}^2 \mathbf{I}] \\
&\propto \prod_{i=1}^N \mathcal{N}(\boldsymbol{\beta}_i \mid \boldsymbol{\mu}_\beta, \Sigma_\beta) \mathcal{N}(\boldsymbol{\mu}_\beta \mid \mathbf{0}, \sigma_{\mu_\beta}^2 \mathbf{I}) \\
&\propto \exp \left\{ \sum_{i=1}^N \left(-\frac{1}{2} (\boldsymbol{\beta}_i - \boldsymbol{\mu}_\beta)' \Sigma_\beta^{-1} (\boldsymbol{\beta}_i - \boldsymbol{\mu}_\beta) \right) \right\} \\
&\quad \times \exp \left\{ -\frac{1}{2} (\boldsymbol{\mu}_\beta - \mathbf{0})' (\sigma_{\mu_\beta}^2 \mathbf{I})^{-1} (\boldsymbol{\mu}_\beta - \mathbf{0}) \right\} \\
&\propto \exp \left\{ -\frac{1}{2} \left(-2 \left(\sum_{i=1}^N \boldsymbol{\beta}_i' \Sigma_\beta^{-1} \right) \boldsymbol{\mu}_\beta + \boldsymbol{\mu}_\beta' (N \Sigma_\beta^{-1}) \boldsymbol{\mu}_\beta \right) \right\} \\
&\quad \times \exp \left\{ -\frac{1}{2} \left(\boldsymbol{\mu}_\beta' (\sigma_{\mu_\beta}^2 \mathbf{I})^{-1} \boldsymbol{\mu}_\beta \right) \right\} \\
&\propto \exp \left\{ -\frac{1}{2} \left(-2 \left(\sum_{i=1}^N \boldsymbol{\beta}_i' \Sigma_\beta^{-1} \right) \boldsymbol{\mu}_\beta + \boldsymbol{\mu}_\beta' \left(N \Sigma_\beta^{-1} + (\sigma_{\mu_\beta}^2 \mathbf{I})^{-1} \right) \boldsymbol{\mu}_\beta \right) \right\} \\
&= \mathcal{N}(\mathbf{A}^{-1} \mathbf{b}, \mathbf{A}^{-1}),
\end{aligned}$$

where $\mathbf{A} = N \Sigma_\beta^{-1} + (\sigma_{\mu_\beta}^2 \mathbf{I})^{-1}$ and $\mathbf{b}' = \boldsymbol{\beta}' \Sigma_\beta^{-1}$, where $\boldsymbol{\beta}$ is the vector sum $\sum_{i=1}^N \boldsymbol{\beta}_i$.

Probability associated with the mixture component indicator variables ($p_i^{(k)}$):

$$\begin{aligned}
[p_i \mid \cdot] &\propto \prod_{j=1}^{J_i} [z_{ij} \mid p_i] [p_i \mid \alpha_1, \alpha_2] \\
&\propto \prod_{j=1}^{J_i} (p_i)^{z_{ij}} (1 - p_i)^{1 - z_{ij}} (p_i)^{\alpha_1 - 1} (1 - p_i)^{\alpha_2 - 1} \\
&\propto (p_i)^{\sum_{j=1}^{J_i} z_{ij}} (1 - p_i)^{J_i - \sum_{j=1}^{J_i} z_{ij}} (p_i)^{\alpha_1 - 1} (1 - p_i)^{\alpha_2 - 1} \\
&= \text{Beta} \left(\sum_{j=1}^{J_i} z_{ij} + \alpha_1, J_i - \sum_{j=1}^{J_i} z_{ij} + \alpha_2 \right)
\end{aligned}$$

Precision matrix of the individual-level regression coefficients (Σ_{β}^{-1}):

$$\begin{aligned}
[\Sigma_{\beta}^{-1} | \cdot] &\propto \prod_{i=1}^N [\beta_i | \mu_{\beta}, \Sigma_{\beta}] [\Sigma_{\beta}^{-1} | S_0^{-1}, \nu] \\
&\propto \prod_{i=1}^N \mathcal{N}(\beta_i | \mu_{\beta}, \Sigma_{\beta}) \text{Wish}(\Sigma_{\beta}^{-1} | S_0^{-1}, \nu) \\
&\propto |\Sigma_{\beta}|^{-\frac{N}{2}} \exp \left\{ -\frac{1}{2} \sum_{i=1}^N (\beta_i - \mu_{\beta})' \Sigma_{\beta}^{-1} (\beta_i - \mu_{\beta}) \right\} \\
&\quad \times |S_0|^{-\frac{\nu}{2}} |\Sigma_{\beta}^{-1}|^{\frac{\nu-p-1}{2}} \exp \left\{ -\frac{1}{2} \text{tr}(S_0 \Sigma_{\beta}^{-1}) \right\} \\
&\propto |\Sigma_{\beta}|^{-\frac{N+\nu-p-1}{2}} \exp \left\{ -\frac{1}{2} \left[\sum_{i=1}^N \text{tr}((\beta_i - \mu_{\beta})' \Sigma_{\beta}^{-1} (\beta_i - \mu_{\beta})) + \text{tr}(S_0 \Sigma_{\beta}^{-1}) \right] \right\} \\
&\propto |\Sigma_{\beta}|^{-\frac{N+\nu-p-1}{2}} \exp \left\{ -\frac{1}{2} \left[\sum_{i=1}^N \text{tr}((\beta_i - \mu_{\beta}) (\beta_i - \mu_{\beta})' \Sigma_{\beta}^{-1}) + \text{tr}(S_0 \Sigma_{\beta}^{-1}) \right] \right\} \\
&\propto |\Sigma_{\beta}|^{-\frac{N+\nu-p-1}{2}} \exp \left\{ -\frac{1}{2} \left[\text{tr} \left(\sum_{i=1}^N ((\beta_i - \mu_{\beta}) (\beta_i - \mu_{\beta})') \Sigma_{\beta}^{-1} + S_0 \Sigma_{\beta}^{-1} \right) \right] \right\} \\
&\propto |\Sigma_{\beta}|^{-\frac{N+\nu-p-1}{2}} \exp \left\{ -\frac{1}{2} \left[\text{tr} \left(\sum_{i=1}^N ((\beta_i - \mu_{\beta}) (\beta_i - \mu_{\beta})') + S_0 \right) \Sigma_{\beta}^{-1} \right] \right\} \\
&= \text{Wish} \left(\left(\sum_{i=1}^N ((\beta_i - \mu_{\beta}) (\beta_i - \mu_{\beta})') + S_0 \right)^{-1}, N + \nu \right).
\end{aligned}$$

MCMC ALGORITHM FOR PARAMETER ESTIMATION

One can implement a MCMC algorithm to estimate the parameters of the observation and process models using the sequence of steps outlined below. Proposal distributions for all parameters with non-conjugate full-conditional distributions (i.e., β_i) are assumed to be symmetric and updates proceed using Metropolis sampling; therefore, the proposal distribution is not factored into the associated ratios as in Metropolis-Hastings sampling. Also note that normalizing constants cancel in the Metropolis ratios and thus may be omitted for clarity.

1. Define initial values for: $\beta_i^{(0)}$ and $p_i^{(0)}$ for $i = 1, \dots, N$; $\mu_{\beta}^{(0)}$; and $\Sigma_{\beta}^{(0)}$.
2. Calculate $\lambda_{ij}^{(0)} = \exp(\mathbf{x}'_{ij} \beta_i^{(0)})$ for $i = 1, \dots, N$ and $j = 1, \dots, J_i$.
3. Set $k = 1$.
4. For each harbor seal, $i = 1, \dots, N$, update the individual-level parameters (i.e., z_{ij} , p_i , and β_i):

- (a) Sample $\mathbf{M}_i^{(k)} \sim [\mathbf{M}_i | \mathbf{S}_i]$, where $[\mathbf{M}_i | \mathbf{S}_i]$ is the posterior distribution of “functional” haul-out sites obtained from the model implemented in Appendix A (i.e., $[\{\boldsymbol{\mu}_i(t), \forall t\} | \{\mathbf{s}_{ic}(t), \forall t\}]$), and $\mathbf{M}_i^{(k)}$ represents the estimated location of “functional” haul-out sites from one iteration of the corresponding MCMC algorithm. Calculate the derived quantity $\mathbf{w}_i = g(\mathbf{M}_i^{(k)})$. Recall the function g aggregates \mathbf{M}_i to obtain the count of telemetry locations for individual i allocated to raster cells in \mathcal{S} ; thus, $\mathbf{w}_i = (w_{i1}, \dots, w_{iJ_i})$ is a vector with each element representing the count of telemetry locations for individual i allocated to raster cell j .

- (b) Update $z_{ij}^{(k-1)}$ using a Gibbs step:

$$[z_{ij}^{(k)} | \cdot] \sim \text{Bern}(\tilde{p}),$$

where

$$\tilde{p} = \frac{p_i^{(k-1)} \times \exp(-\lambda_{ij}^{(k)})}{p_i^{(k-1)} \times \exp(-\lambda_{ij}^{(k)}) + 1 - p_i^{(k-1)}}.$$

- (c) Update $p_i^{(k-1)}$ using a Gibbs step:

$$[p_i^{(k)} | \cdot] \sim \text{Beta}\left(\sum_{j=1}^{J_i} z_{ij}^{(k)} + \alpha_1, J_i - \sum_{j=1}^{J_i} z_{ij}^{(k)} + \alpha_2\right).$$

- (d) Update $\boldsymbol{\beta}_i^{(k-1)}$ using Metropolis sampling. Sample $\boldsymbol{\beta}_i^{(*)}$ from a proposal distribution $[\boldsymbol{\beta}_i^{(*)} | \boldsymbol{\beta}_i^{(k-1)}]$ (e.g., $N(\boldsymbol{\beta}_i^{(*)} | \boldsymbol{\beta}_i^{(k-1)}, \tau_\beta^2 \mathbf{I})$, where τ_β^2 is a tuning parameter) and calculate $\lambda_{ij}^{(*)} = \exp(\mathbf{x}'_{ij} \boldsymbol{\beta}_i^{(*)})$. Calculate the Metropolis ratio as

$$r_\beta = \frac{\prod_{j=1}^{J_i} \text{Pois}\left(w_{ij}^{(k)} | \lambda_{ij}^{(*)}\right)^{z_{ij}^{(k)}} \mathcal{N}\left(\boldsymbol{\beta}_i^{(*)} | \boldsymbol{\mu}_\beta^{(k-1)}, \boldsymbol{\Sigma}_\beta^{(k-1)}\right)}{\prod_{j=1}^{J_i} \text{Pois}\left(w_{ij}^{(k)} | \lambda_{ij}^{(k-1)}\right)^{z_{ij}^{(k)}} \mathcal{N}\left(\boldsymbol{\beta}_i^{(k-1)} | \boldsymbol{\mu}_\beta^{(k-1)}, \boldsymbol{\Sigma}_\beta^{(k-1)}\right)}.$$

If $r_\beta > u$, where $u \sim \text{Uniform}(0,1)$, let $\boldsymbol{\beta}_i^{(k)} = \boldsymbol{\beta}_i^{(*)}$ and $\lambda_{ij}^{(k)} = \lambda_{ij}^{(*)}$. Otherwise, let $\boldsymbol{\beta}_i^{(k)} = \boldsymbol{\beta}_i^{(k-1)}$ and $\lambda_{ij}^{(k)} = \lambda_{ij}^{(k-1)}$.

- (e) Repeat Steps 4(a) through 4(d) for each individual $i = 1, \dots, N$.

5. Update $(\boldsymbol{\Sigma}_\beta^{-1})^{(k-1)}$ using a Gibbs step:

$$[(\boldsymbol{\Sigma}_\beta^{-1})^{(k)} | \cdot] \sim \text{Wish}\left(\left(\sum_{i=1}^N \left(\left(\boldsymbol{\beta}_i^{(k)} - \boldsymbol{\mu}_\beta^{(k-1)}\right) \left(\boldsymbol{\beta}_i^{(k)} - \boldsymbol{\mu}_\beta^{(k-1)}\right)'\right) + \mathbf{S}_0\right)^{-1}, N + \nu\right).$$

6. Update $\boldsymbol{\mu}_\beta^{(k-1)}$ using a Gibbs step:

$$\left[\boldsymbol{\mu}_\beta^{(k)} \mid \cdot \right] \sim \mathcal{N}(\mathbf{A}^{-1}\mathbf{b}, \mathbf{A}^{-1}),$$

where $\mathbf{A} = N(\boldsymbol{\Sigma}_\beta^{-1})^{(k)} + (\sigma_{\mu_\beta}^2 \mathbf{I})^{-1}$, $\mathbf{b}' = (\boldsymbol{\beta}^{(k)})' (\boldsymbol{\Sigma}_\beta^{-1})^{(k)}$, and $\boldsymbol{\beta}^{(k)}$ is the vector sum $\sum_{i=1}^N \boldsymbol{\beta}_i^{(k)}$.

7. Save $z_{ij}^{(k)}$ for $i = 1, \dots, N$ and $j = 1, \dots, J_i$; $\boldsymbol{\beta}_i^{(k)}$ and $p_i^{(k)}$ for $i = 1, \dots, N$; $\boldsymbol{\Sigma}_\beta^{(k)}$; and $\boldsymbol{\mu}_\beta^{(k)}$.
8. Set $k = k + 1$ and return to Step 4. The algorithm is iterated by repeating Steps 4 through 7 until a sufficiently large sample has been obtained from which to approximate the posterior distribution.

APPENDIX C3. Model statement, posterior distribution, full-conditional distributions, and pseudocode detailing a Markov chain Monte Carlo algorithm for estimating the parameters in the model for examining temporal patterns in haul-out use.

In the posterior and full-conditional distributions below, we use bracket notation to denote a probability distribution. For example, $[x]$ indicates the probability distribution of x . Similarly, $[x|y]$ indicates the probability distribution of x given the parameter y . The notation “.” represents the data and other parameters in the model.

MODEL STATEMENT

We formulated the binary probit regression under a data augmentation approach (Albert and Chib 1993, Johnson et al. 2012, Dorazio and Rodriguez 2012). In particular, we introduce the parameter $v_i(t)$ as a continuous, latent version of the binary process $y_i(t)$. Assuming $y_i(t) = 1$ if $v_i(t) > 0$ and $y_i(t) = 0$ if $v_i(t) \leq 0$, the following model specification is equivalent to Eqs. 17 and 18 in the main text.

$$\begin{aligned} y_i(t) &\sim \begin{cases} 0, & v_i(t) \leq 0 \\ 1, & v_i(t) > 1 \end{cases} \\ v_i(t) &\sim \mathcal{N}(\mathbf{u}_i(t)' \boldsymbol{\gamma}_i, 1) \\ \boldsymbol{\gamma}_i(t) &\sim \mathcal{N}(\boldsymbol{\mu}_\gamma, \boldsymbol{\Sigma}_\gamma) \\ \boldsymbol{\mu}_\gamma &\sim \mathcal{N}(\mathbf{0}, \sigma_{\mu_\gamma}^2 \mathbf{I}) \\ \boldsymbol{\Sigma}_\gamma^{-1} &\sim \text{Wish}(\mathbf{S}_0^{-1}, \nu) \end{aligned}$$

POSTERIOR DISTRIBUTION

$$[\mathbf{V}, \boldsymbol{\Gamma}, \boldsymbol{\mu}_\gamma, \boldsymbol{\Sigma}_\gamma | \mathbf{Y}] \propto \prod_{i=1}^N \prod_{t \in \mathcal{T}} [y_i(t) | v_i(t)] [v_i(t) | \boldsymbol{\gamma}_i] [\boldsymbol{\gamma}_i | \boldsymbol{\mu}_\gamma, \boldsymbol{\Sigma}_\gamma] [\boldsymbol{\mu}_\gamma | \mathbf{0}, \sigma_{\mu_\gamma}^2 \mathbf{I}] [\boldsymbol{\Sigma}_\gamma | \mathbf{S}_0, \nu],$$

where $\mathbf{V} = \{v_i(t), \forall i, \forall t\}$ is a matrix of auxiliary variables for $i = 1, \dots, N$ and $t \in \mathcal{T}$; $\boldsymbol{\Gamma} = \{\boldsymbol{\gamma}_i, \forall i\}$ is a matrix of regression coefficients for $i = 1, \dots, N$; and $\mathbf{Y} = \{y_i(t), \forall i, \forall t\}$ is a matrix of behavioral data (wet/dry status) for $i = 1, \dots, N$ and $t \in \mathcal{T}$.

FULL-CONDITIONAL DISTRIBUTIONS

Observation model auxiliary variable ($v_i(t)$):

$$\begin{aligned} [v_i(t) | \cdot] &\propto [y_i(t) | v_i(t)] [v_i(t) | \mathbf{u}'_i(t) \boldsymbol{\gamma}_i, \mathbf{1}] \\ &\propto (1_{\{y_i(t)=0\}} 1_{\{v_i(t)\leq 0\}} + 1_{\{y_i(t)=1\}} 1_{\{v_i(t)>0\}}) \times \mathcal{N}(v_i(t) | \mathbf{u}'_i(t) \boldsymbol{\gamma}_i, \mathbf{1}) \\ &= \begin{cases} \mathcal{T}\mathcal{N}(\mathbf{u}'_i(t) \boldsymbol{\gamma}_i, \mathbf{1})_{-\infty}^0, & y_i(t) = 0 \\ \mathcal{T}\mathcal{N}(\mathbf{u}'_i(t) \boldsymbol{\gamma}_i, \mathbf{1})_0^\infty, & y_i(t) = 1 \end{cases} \end{aligned}$$

Individual-level regression coefficients ($\boldsymbol{\gamma}_i$):

$$\begin{aligned} [\boldsymbol{\gamma}_i | \cdot] &\propto [\mathbf{v}_i | \mathbf{U}_i \boldsymbol{\gamma}_i, \mathbf{1}] [\boldsymbol{\gamma}_i | \boldsymbol{\mu}_\gamma, \boldsymbol{\Sigma}_\gamma] \\ &\propto \mathcal{N}(\mathbf{v}_i | \mathbf{U}_i \boldsymbol{\gamma}_i, \mathbf{1}) \mathcal{N}(\boldsymbol{\gamma}_i | \boldsymbol{\mu}_\gamma, \boldsymbol{\Sigma}_\gamma) \\ &\propto \exp \left\{ -\frac{1}{2} (\mathbf{v}_i - \mathbf{U}_i \boldsymbol{\gamma}_i)' (\mathbf{v}_i - \mathbf{U}_i \boldsymbol{\gamma}_i) \right\} \\ &\quad \times \exp \left\{ -\frac{1}{2} (\boldsymbol{\gamma}_i - \boldsymbol{\mu}_\gamma)' \boldsymbol{\Sigma}_\gamma^{-1} (\boldsymbol{\gamma}_i - \boldsymbol{\mu}_\gamma) \right\} \\ &\propto \exp \left\{ -\frac{1}{2} (-2(\mathbf{v}'_i \mathbf{U}_i) \boldsymbol{\gamma}_i + \boldsymbol{\gamma}'_i \mathbf{U}'_i \mathbf{U}_i \boldsymbol{\gamma}_i) \right\} \\ &\quad \times \exp \left\{ -\frac{1}{2} (-2(\boldsymbol{\mu}'_\gamma \boldsymbol{\Sigma}_\gamma^{-1}) \boldsymbol{\gamma}_i + \boldsymbol{\gamma}'_i \boldsymbol{\Sigma}_\gamma^{-1} \boldsymbol{\gamma}_i) \right\} \\ &\propto \exp \left\{ -\frac{1}{2} (-2(\mathbf{v}'_i \mathbf{U}_i + \boldsymbol{\mu}'_\gamma \boldsymbol{\Sigma}_\gamma^{-1}) \boldsymbol{\gamma}_i + \boldsymbol{\gamma}'_i (\mathbf{U}'_i \mathbf{U}_i + \boldsymbol{\Sigma}_\gamma^{-1}) \boldsymbol{\gamma}_i) \right\} \\ &= \mathcal{N}(\mathbf{A}^{-1} \mathbf{b}, \mathbf{A}^{-1}), \end{aligned}$$

where $\mathbf{U}_i = \{\mathbf{u}_i(t), \forall t\}$ is a matrix of covariates for individual i and times $t \in \mathcal{T}$; $\mathbf{v}_i = \{v_i(t), \forall t\}$ is a vector of auxiliary variables for individual i and times $t \in \mathcal{T}$; $\mathbf{A} = \mathbf{U}'_i \mathbf{U}_i + \boldsymbol{\Sigma}_\gamma^{-1}$; and $\mathbf{b}' = \mathbf{v}'_i \mathbf{U}_i + \boldsymbol{\mu}'_\gamma \boldsymbol{\Sigma}_\gamma^{-1}$.

Population-level regression coefficients ($\boldsymbol{\mu}_\gamma$):

$$\begin{aligned}
 [\boldsymbol{\mu}_\gamma | \cdot] &\propto \prod_{i=1}^N [\boldsymbol{\gamma}_i | \boldsymbol{\mu}_\gamma, \Sigma_\gamma] [\boldsymbol{\mu}_\gamma | \mathbf{0}, \sigma_{\mu_\gamma}^2 \mathbf{I}] \\
 &\propto \prod_{i=1}^N \mathcal{N}(\boldsymbol{\gamma}_i | \boldsymbol{\mu}_\gamma, \Sigma_\gamma) \mathcal{N}(\boldsymbol{\mu}_\gamma | \mathbf{0}, \sigma_{\mu_\gamma}^2 \mathbf{I}) \\
 &\propto \exp \left\{ \sum_{i=1}^N \left(-\frac{1}{2} (\boldsymbol{\gamma}_i - \boldsymbol{\mu}_\gamma)' \Sigma_\gamma^{-1} (\boldsymbol{\gamma}_i - \boldsymbol{\mu}_\gamma) \right) \right\} \\
 &\quad \times \exp \left\{ -\frac{1}{2} (\boldsymbol{\mu}_\gamma - \mathbf{0})' (\sigma_{\mu_\gamma}^2 \mathbf{I})^{-1} (\boldsymbol{\mu}_\gamma - \mathbf{0}) \right\} \\
 &\propto \exp \left\{ -\frac{1}{2} \left(-2 \left(\sum_{i=1}^N \boldsymbol{\gamma}_i' \Sigma_\gamma^{-1} \right) \boldsymbol{\mu}_\gamma + \boldsymbol{\mu}_\gamma' (N \Sigma_\gamma^{-1}) \boldsymbol{\mu}_\gamma \right) \right\} \\
 &\quad \times \exp \left\{ -\frac{1}{2} \left(\boldsymbol{\mu}_\gamma' (\sigma_{\mu_\gamma}^2 \mathbf{I})^{-1} \boldsymbol{\mu}_\gamma \right) \right\} \\
 &\propto \exp \left\{ -\frac{1}{2} \left(-2 \left(\sum_{j=1}^J \boldsymbol{\gamma}_j' \Sigma_\gamma^{-1} \right) \boldsymbol{\mu}_\gamma + \boldsymbol{\mu}_\gamma' \left(N \Sigma_\gamma^{-1} + (\sigma_{\mu_\gamma}^2 \mathbf{I})^{-1} \right) \boldsymbol{\mu}_\gamma \right) \right\} \\
 &= \mathcal{N}(\mathbf{A}^{-1} \mathbf{b}, \mathbf{A}^{-1}),
 \end{aligned}$$

where $\mathbf{A} = N \Sigma_\gamma^{-1} + (\sigma_{\mu_\gamma}^2 \mathbf{I})^{-1}$ and $\mathbf{b}' = \boldsymbol{\gamma}' \Sigma_\gamma^{-1}$, where $\boldsymbol{\gamma}$ is the vector sum $\sum_{j=1}^J \boldsymbol{\gamma}_j$.

Precision matrix of individual-level regression coefficients (Σ_{γ}^{-1}):

$$\begin{aligned}
[\Sigma_{\gamma}^{-1} | \cdot] &\propto \prod_{i=1}^N [\gamma_i | \boldsymbol{\mu}_{\gamma}, \Sigma_{\gamma}] [\Sigma_{\gamma}^{-1} | \mathbf{S}_0^{-1}, \nu] \\
&\propto \prod_{i=1}^N \mathcal{N}(\gamma_i | \boldsymbol{\mu}_{\gamma}, \Sigma_{\gamma}) \text{Wish}(\Sigma_{\gamma}^{-1} | \mathbf{S}_0^{-1}, \nu) \\
&\propto |\Sigma_{\gamma}|^{-\frac{N}{2}} \exp \left\{ -\frac{1}{2} \sum_{N=1}^N (\gamma_i - \boldsymbol{\mu}_{\gamma})' \Sigma_{\gamma}^{-1} (\gamma_i - \boldsymbol{\mu}_{\gamma}) \right\} \\
&\quad \times |\mathbf{S}_0|^{-\frac{\nu}{2}} |\Sigma_{\gamma}^{-1}|^{\frac{\nu-p-1}{2}} \exp \left\{ -\frac{1}{2} \text{tr}(\mathbf{S}_0 \Sigma_{\gamma}^{-1}) \right\} \\
&\propto |\Sigma_{\gamma}|^{-\frac{N+\nu-p-1}{2}} \exp \left\{ -\frac{1}{2} \left[\sum_{i=1}^N \text{tr}((\gamma_i - \boldsymbol{\mu}_{\gamma})' \Sigma_{\gamma}^{-1} (\gamma_i - \boldsymbol{\mu}_{\gamma})) + \text{tr}(\mathbf{S}_0 \Sigma_{\gamma}^{-1}) \right] \right\} \\
&\propto |\Sigma_{\gamma}|^{-\frac{N+\nu-p-1}{2}} \exp \left\{ -\frac{1}{2} \left[\sum_{i=1}^N \text{tr}((\gamma_i - \boldsymbol{\mu}_{\gamma}) (\gamma_i - \boldsymbol{\mu}_{\gamma})' \Sigma_{\gamma}^{-1}) + \text{tr}(\mathbf{S}_0 \Sigma_{\gamma}^{-1}) \right] \right\} \\
&\propto |\Sigma_{\gamma}|^{-\frac{N+\nu-p-1}{2}} \exp \left\{ -\frac{1}{2} \left[\text{tr} \left(\sum_{i=1}^N ((\gamma_i - \boldsymbol{\mu}_{\gamma}) (\gamma_i - \boldsymbol{\mu}_{\gamma})') \Sigma_{\gamma}^{-1} + \mathbf{S}_0 \Sigma_{\gamma}^{-1} \right) \right] \right\} \\
&\propto |\Sigma_{\gamma}|^{-\frac{N+\nu-p-1}{2}} \exp \left\{ -\frac{1}{2} \left[\text{tr} \left(\sum_{i=1}^N ((\gamma_i - \boldsymbol{\mu}_{\gamma}) (\gamma_i - \boldsymbol{\mu}_{\gamma})') + \mathbf{S}_0 \right) \Sigma_{\gamma}^{-1} \right] \right\} \\
&= \text{Wish} \left(\left(\sum_{i=1}^N ((\gamma_i - \boldsymbol{\mu}_{\gamma}) (\gamma_i - \boldsymbol{\mu}_{\gamma})') + \mathbf{S}_0 \right)^{-1}, N + \nu \right).
\end{aligned}$$

MCMC ALGORITHM FOR PARAMETER ESTIMATION

One can implement a MCMC algorithm to estimate the parameters of the observation and process models using the sequence of steps outlined below.

1. Define initial values for: $\gamma_i^{(0)}$ for $i = 1, \dots, N$; $\boldsymbol{\mu}_{\beta}^{(0)}$; and $\Sigma_{\gamma}^{(0)}$.
2. Set $k = 1$.
3. For each harbor seal, $i = 1, \dots, N$, update the temporal process model parameters (i.e., γ_i and \mathbf{v}_i).
 - (a) Update $\mathbf{v}_i(t)^{(k-1)}$ using a Gibbs step:

$$\left[v_i(t)^{(k)} | \cdot \right] \sim \begin{cases} \mathcal{T}\mathcal{N} \left(\mathbf{u}'_i(t) \gamma_i^{(k-1)}, \mathbf{1} \right)^0, & y_i(t) = 0 \\ \mathcal{T}\mathcal{N} \left(\mathbf{u}'_i(t) \gamma_i^{(k-1)}, \mathbf{1} \right)_0^{\infty}, & y_i(t) = 1 \end{cases}$$

(b) Update $\boldsymbol{\gamma}_i^{(k-1)}$ using a Gibbs step:

$$[\boldsymbol{\gamma}_i^{(k)} | \cdot] \sim \mathcal{N}(\mathbf{A}^{-1}\mathbf{b}, \mathbf{A}^{-1}),$$

where $\mathbf{A} = \mathbf{U}_i' \mathbf{U}_i + (\boldsymbol{\Sigma}_\gamma^{-1})^{(k-1)}$ and $\mathbf{b}' = (\mathbf{v}_i^{(k)})' \mathbf{U}_i + (\boldsymbol{\mu}_\gamma^{(k-1)})' (\boldsymbol{\Sigma}_\gamma^{-1})^{(k-1)}$.

(c) Repeat Steps 3(a) and 3(b) for each individual $i = 1, \dots, N$.

4. Update $\boldsymbol{\mu}_\gamma^{(k-1)}$ using a Gibbs step:

$$[\boldsymbol{\mu}_\gamma^{(k)} | \cdot] \sim \mathcal{N}(\mathbf{A}^{-1}\mathbf{b}, \mathbf{A}^{-1}),$$

where $\mathbf{A} = N(\boldsymbol{\Sigma}_\gamma^{-1})^{(k-1)} + (\sigma_\gamma^2 \mathbf{I})^{-1}$ and $\mathbf{b}' = (\boldsymbol{\gamma}^{(k)})' (\boldsymbol{\Sigma}_\gamma^{-1})^{(k-1)}$, where $\boldsymbol{\gamma}^{(k)}$ is the vector sum $\sum_{i=1}^N \boldsymbol{\gamma}_i^{(k)}$.

5. Update $(\boldsymbol{\Sigma}_\gamma^{-1})^{(k-1)}$ using a Gibbs step:

$$[(\boldsymbol{\Sigma}_\gamma^{-1})^{(k)} | \cdot] \sim \text{Wish} \left(\left(\sum_{i=1}^N \left((\boldsymbol{\gamma}_i^{(k)} - \boldsymbol{\mu}_\gamma^{(k)}) (\boldsymbol{\gamma}_i^{(k)} - \boldsymbol{\mu}_\gamma^{(k)})' \right) + \mathbf{S}_0 \right)^{-1}, N + \nu \right)$$

6. Save $\mathbf{v}_i^{(k)}$ and $\boldsymbol{\gamma}_i^{(k)}$ for $i = 1, \dots, N$; $\boldsymbol{\mu}_\beta^{(k)}$; and $\boldsymbol{\Sigma}_\gamma^{(k)}$.

7. Set $k = k + 1$ and return to Step 3. The algorithm is iterated by repeating Steps 3 through 6 until a sufficiently large sample has been obtained from which to approximate the posterior distribution.

REFERENCES

- Albert, J. H., and S. Chib. 1993. Bayesian analysis of binary and polychotomous response data. *Journal of the American Statistical Association* **88**:669–679.
- Dorazio, R. M., and D. T. Rodríguez. 2012. A Gibbs sampler for Bayesian analysis of site-occupancy data. *Methods in Ecology and Evolution* **3**:1093–1098.
- Johnson, D. S., P. B. Conn, M. B. Hooten, J. C. Ray, and B. A. Pond. 2012. Spatial occupancy models for large data sets. *Ecology* **94**:801–808.

APPENDIX C4. The posterior distribution of $\mu_i(t)$ for each individual harbor seal (red gradient); brighter reds indicate higher posterior probability. Black points symbolize telemetry locations recorded while the individual was hauled-out of the water (dry), whereas blue crosses symbolize telemetry locations recorded while the individual was at sea (wet). Note that many telemetry locations occur beyond the extent of the maps.

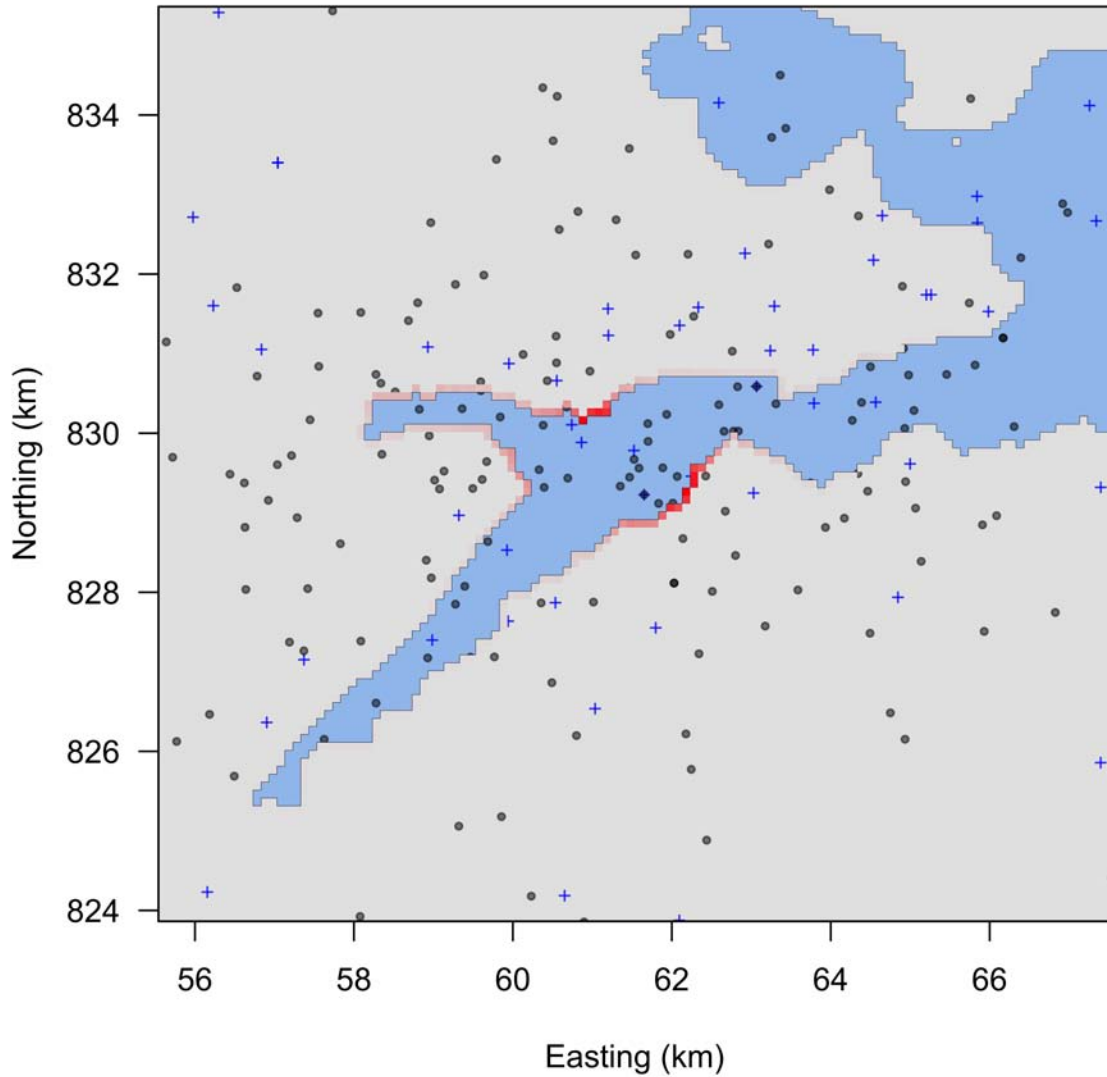


Figure C4.1. The posterior distribution of $\mu_i(t)$ for individual PV94KOD01, an adult male that was monitored from 10/06/94 to 03/31/95. Of the 427 recorded telemetry locations, 260 were obtained while the individual was hauled-out of the water.

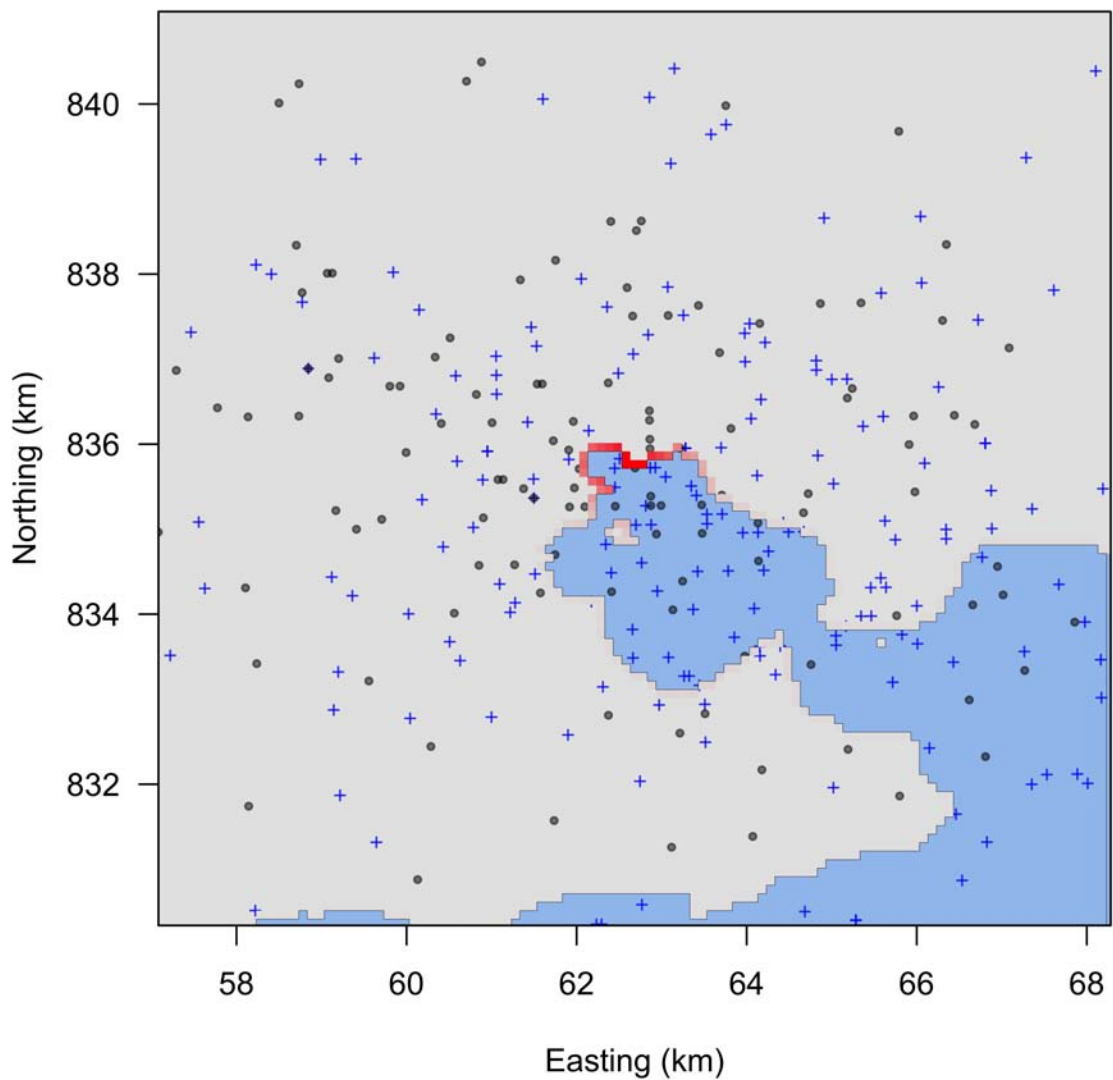


Figure C4.2. The posterior distribution of $\mu_i(t)$ for individual PV94KOD02, an adult male that was monitored from 10/06/94 to 03/31/95. Of the 682 recorded telemetry locations, 194 were obtained while the individual was hauled-out of the water.

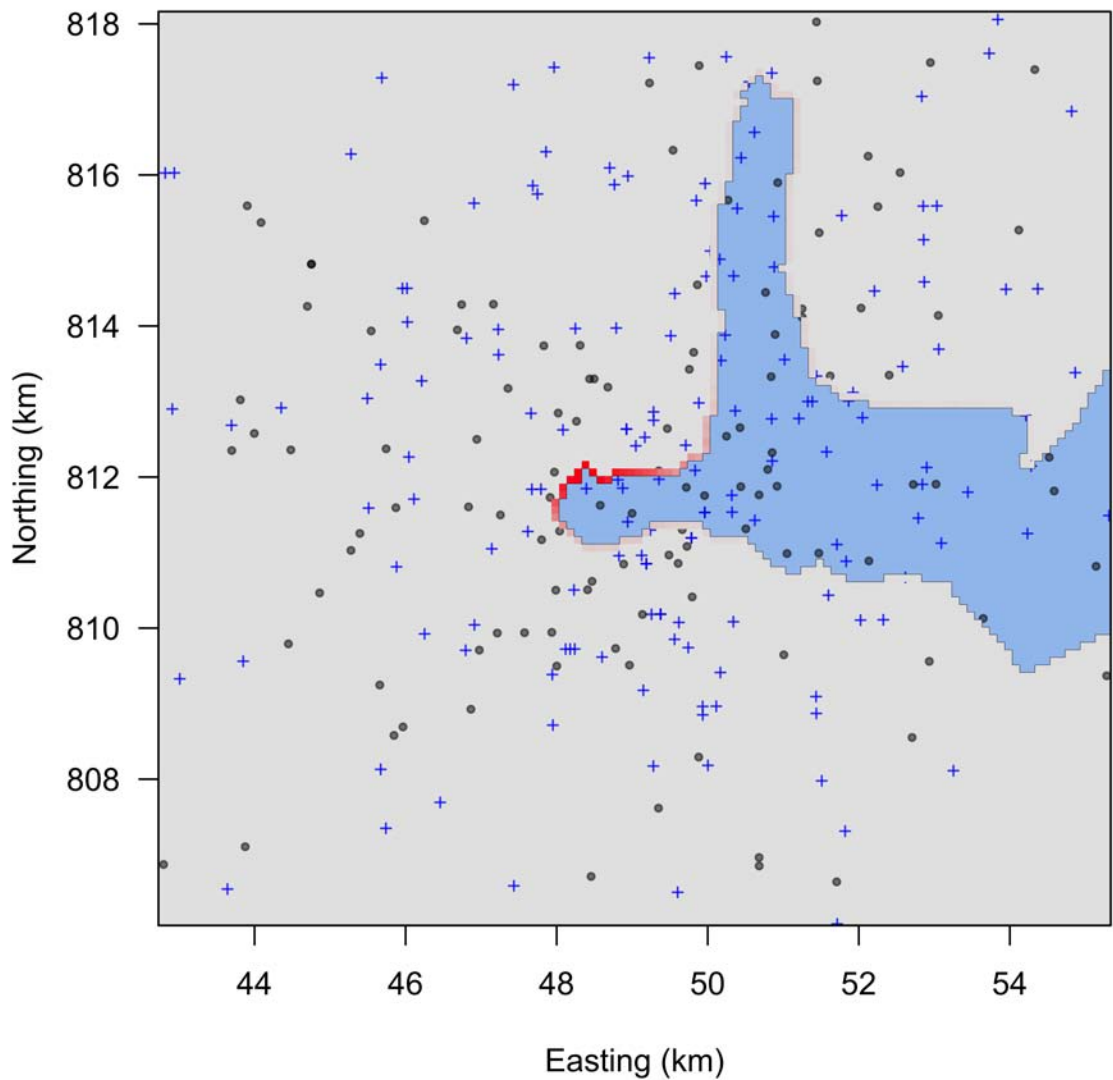


Figure C4.3. The posterior distribution of $\mu_i(t)$ for individual PV94KOD08, an adult male that was monitored from 10/09/94 to 03/31/95. Of the 693 recorded telemetry locations, 220 were obtained while the individual was hauled-out of the water.

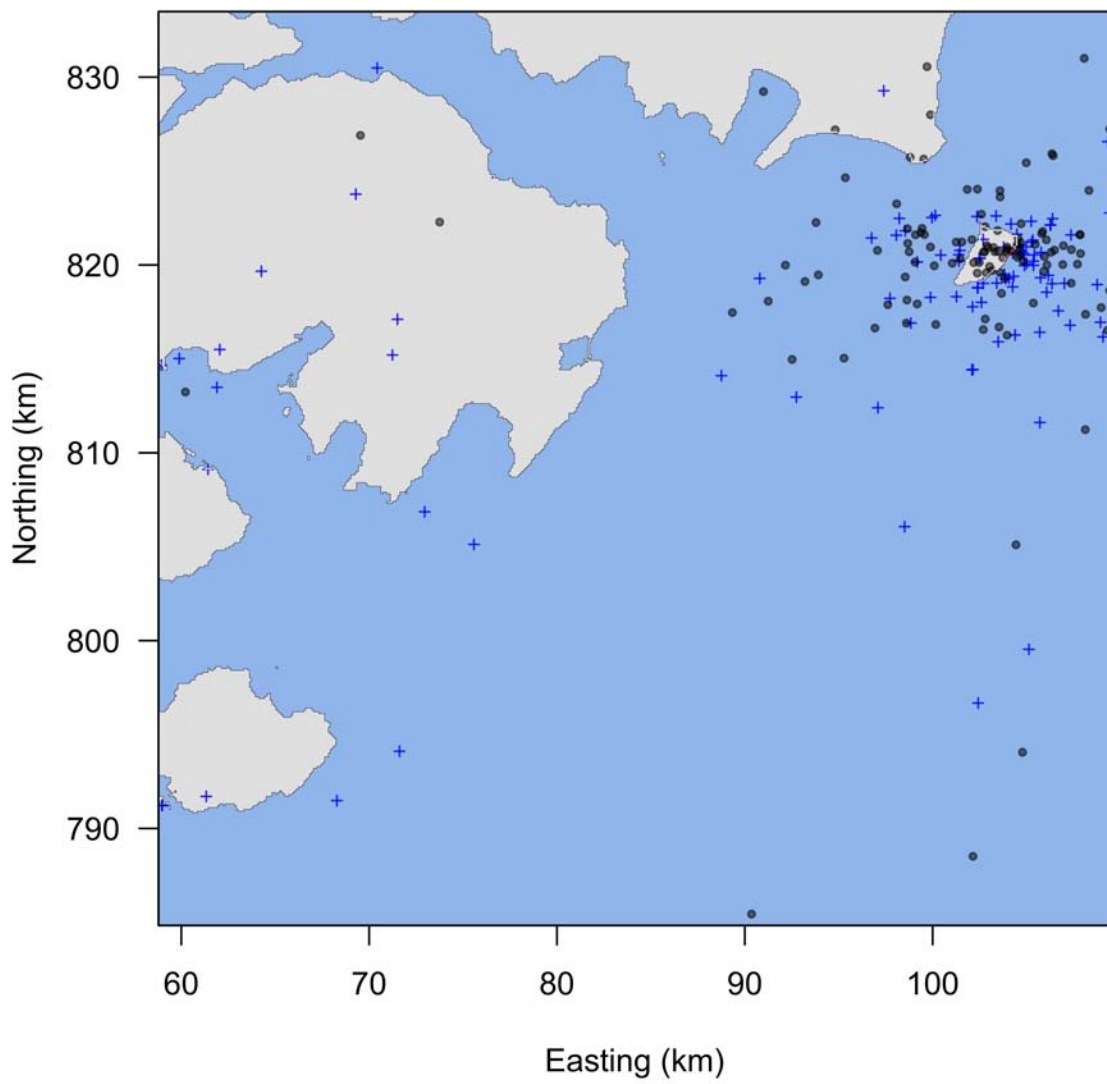


Figure C4.4. The posterior distribution of $\mu_i(t)$ for individual PV94KOD09, a subadult female that was monitored from 10/09/94 to 03/31/95 . Of the 315 recorded telemetry locations, 166 were obtained while the individual was hauled-out of the water.

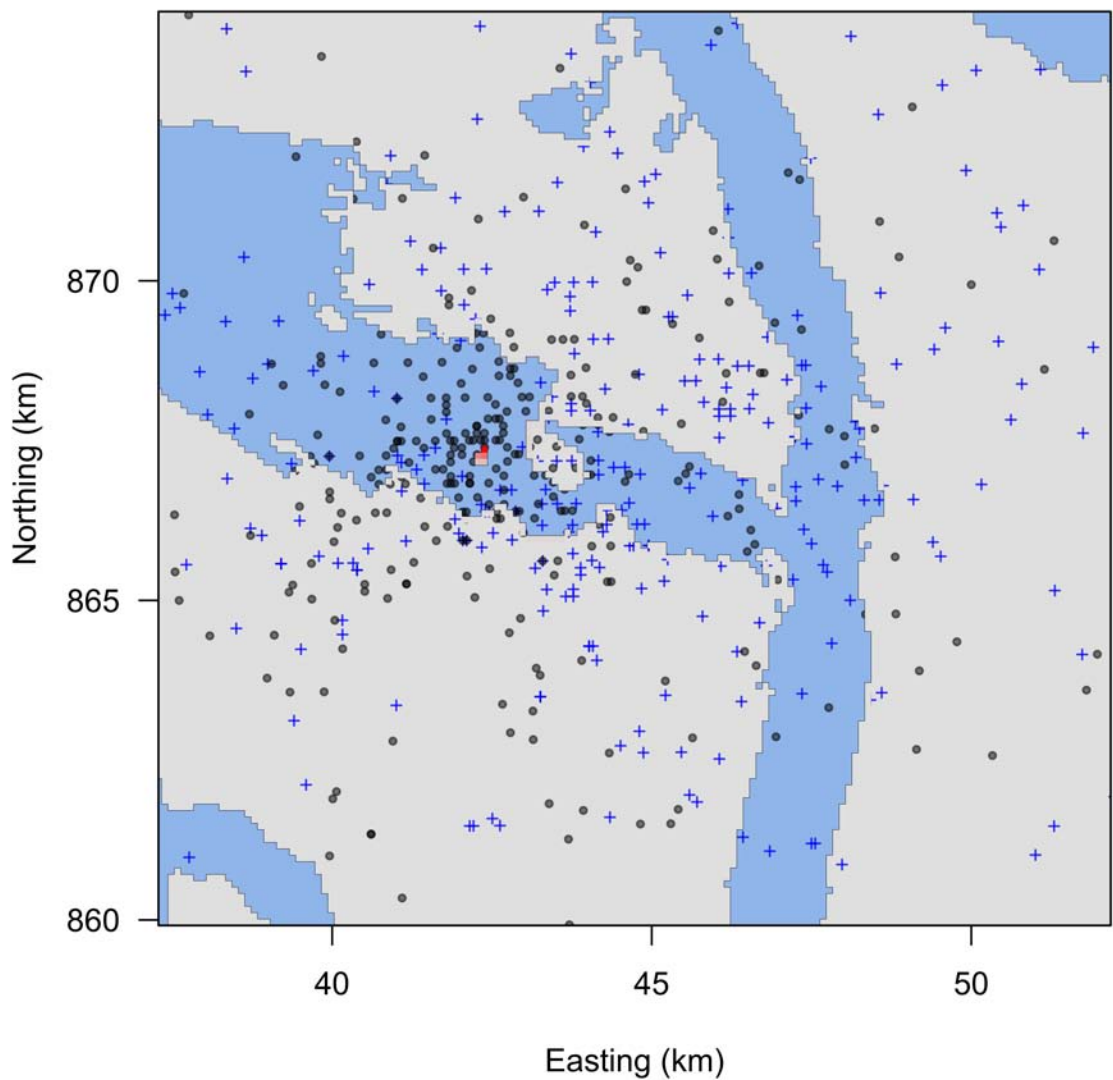


Figure C4.5. The posterior distribution of $\mu_i(t)$ for individual PV95KOD01, an adult male that was monitored from 03/29/95 to 07/29/95. Of the 1036 recorded telemetry locations, 418 were obtained while the individual was hauled-out of the water.

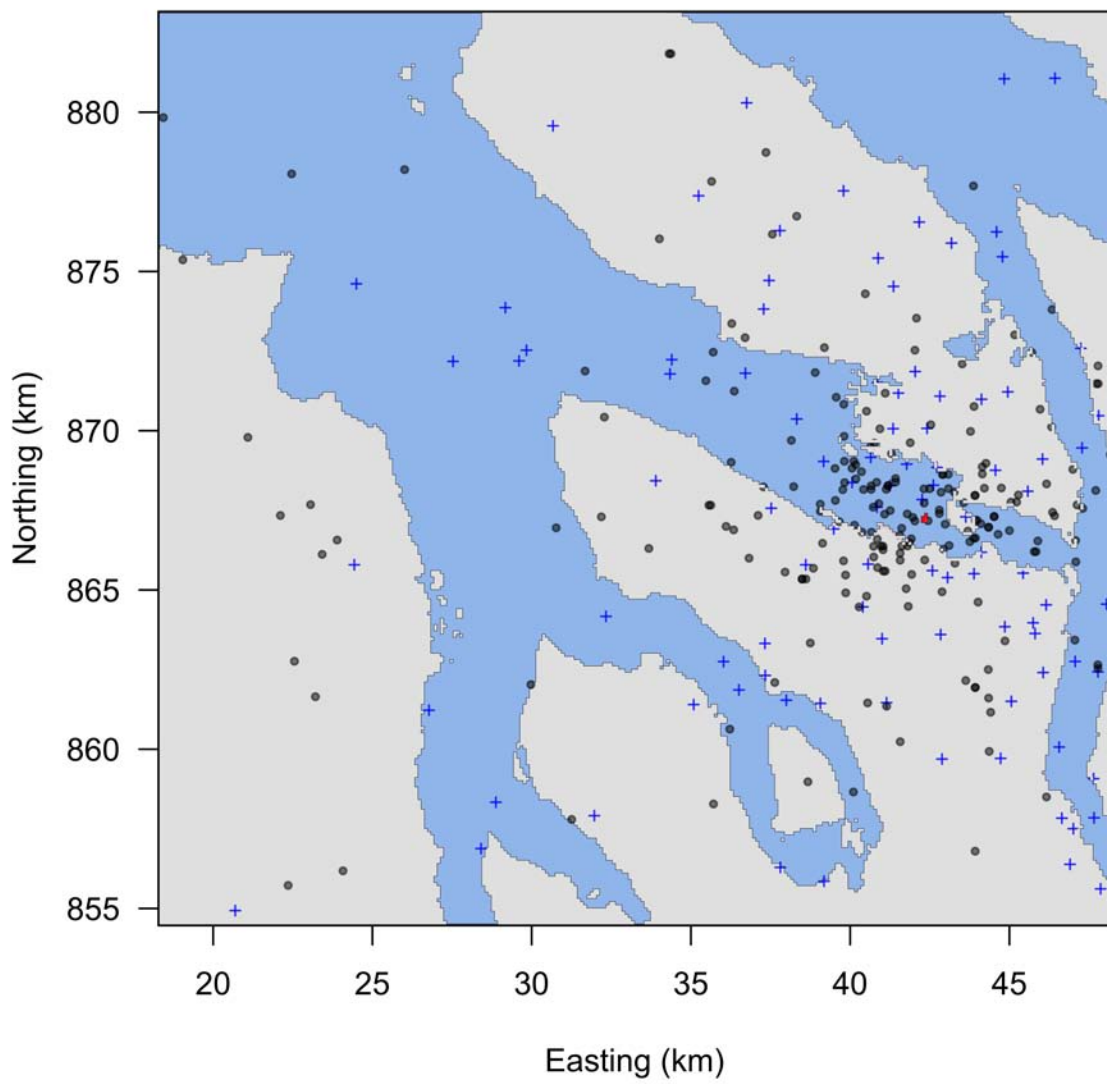


Figure C4.6. The posterior distribution of $\mu_i(t)$ for individual PV95KOD03, an adult female that was monitored from 03/30/95 to 06/14/95. Of the 512 recorded telemetry locations, 284 were obtained while the individual was hauled-out of the water.

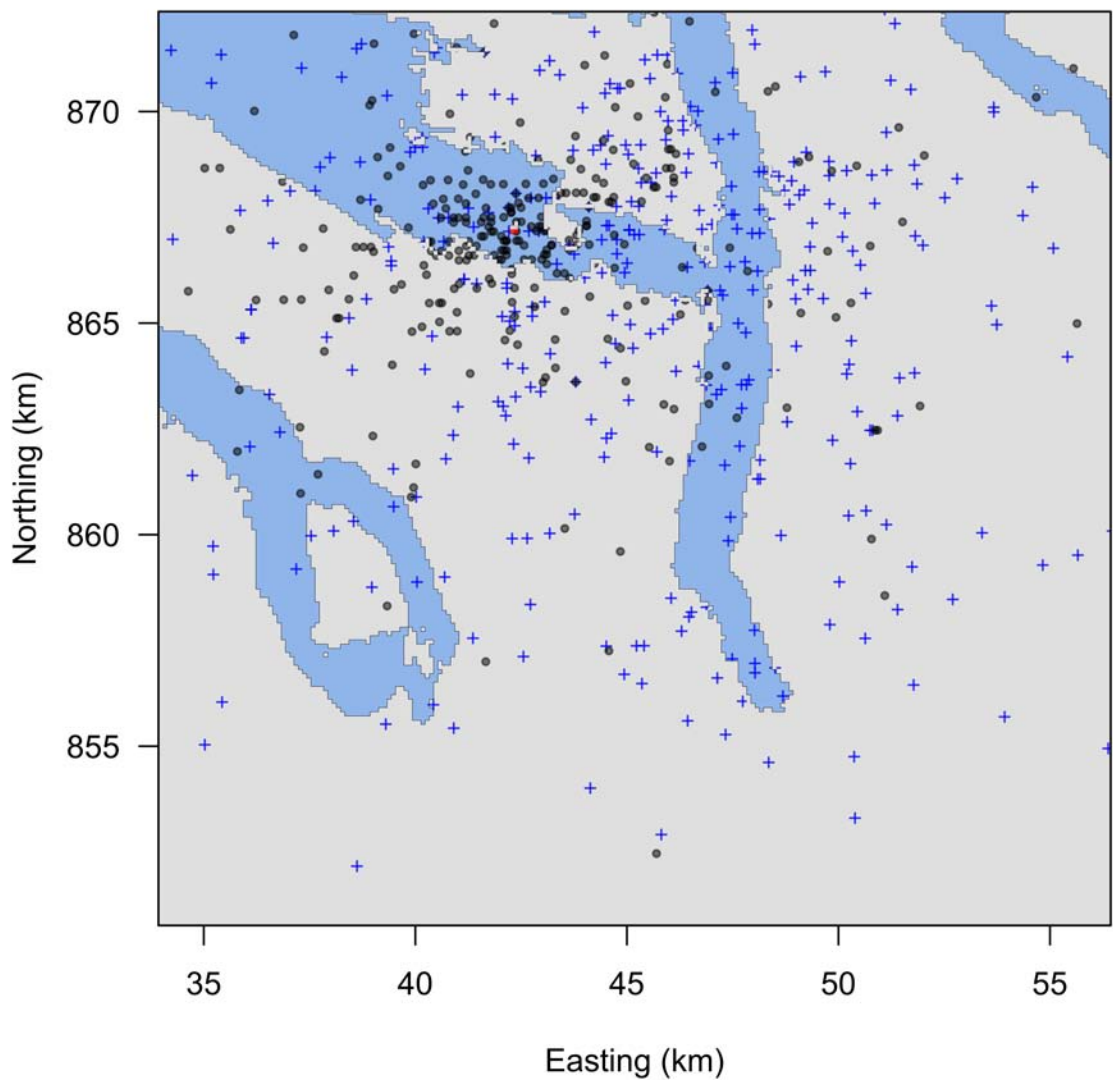


Figure C4.7. The posterior distribution of $\mu_i(t)$ for individual PV95KOD05, a subadult female that was monitored from 03/30/95 to 07/13/95. Of the 1000 recorded telemetry locations, 369 were obtained while the individual was hauled-out of the water.

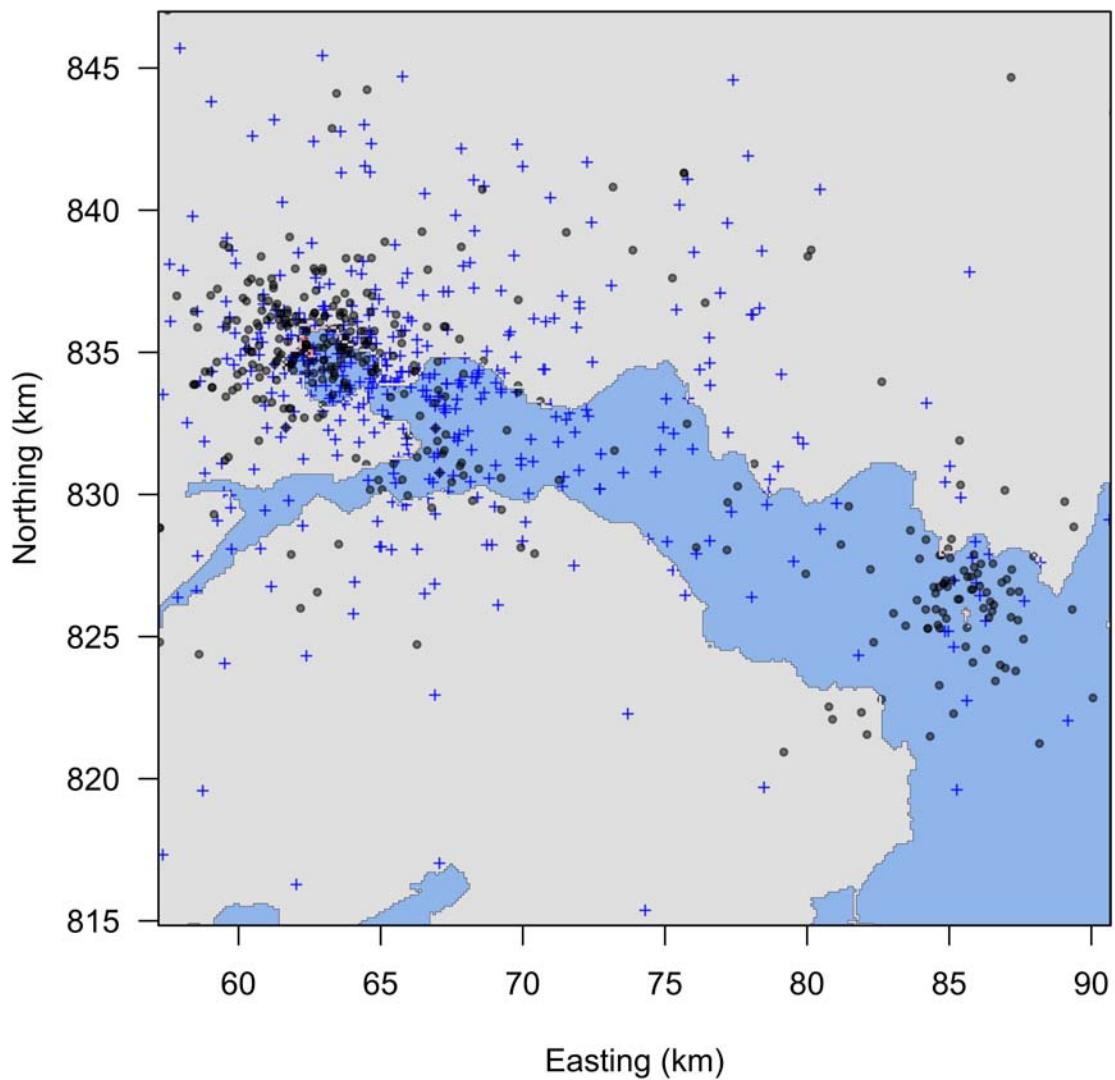


Figure C4.8. The posterior distribution of $\mu_i(t)$ for individual PV95KOD09, a subadult female that was monitored from 10/09/95 to 06/04/96. Of the 1009 recorded telemetry locations, 438 were obtained while the individual was hauled-out of the water.

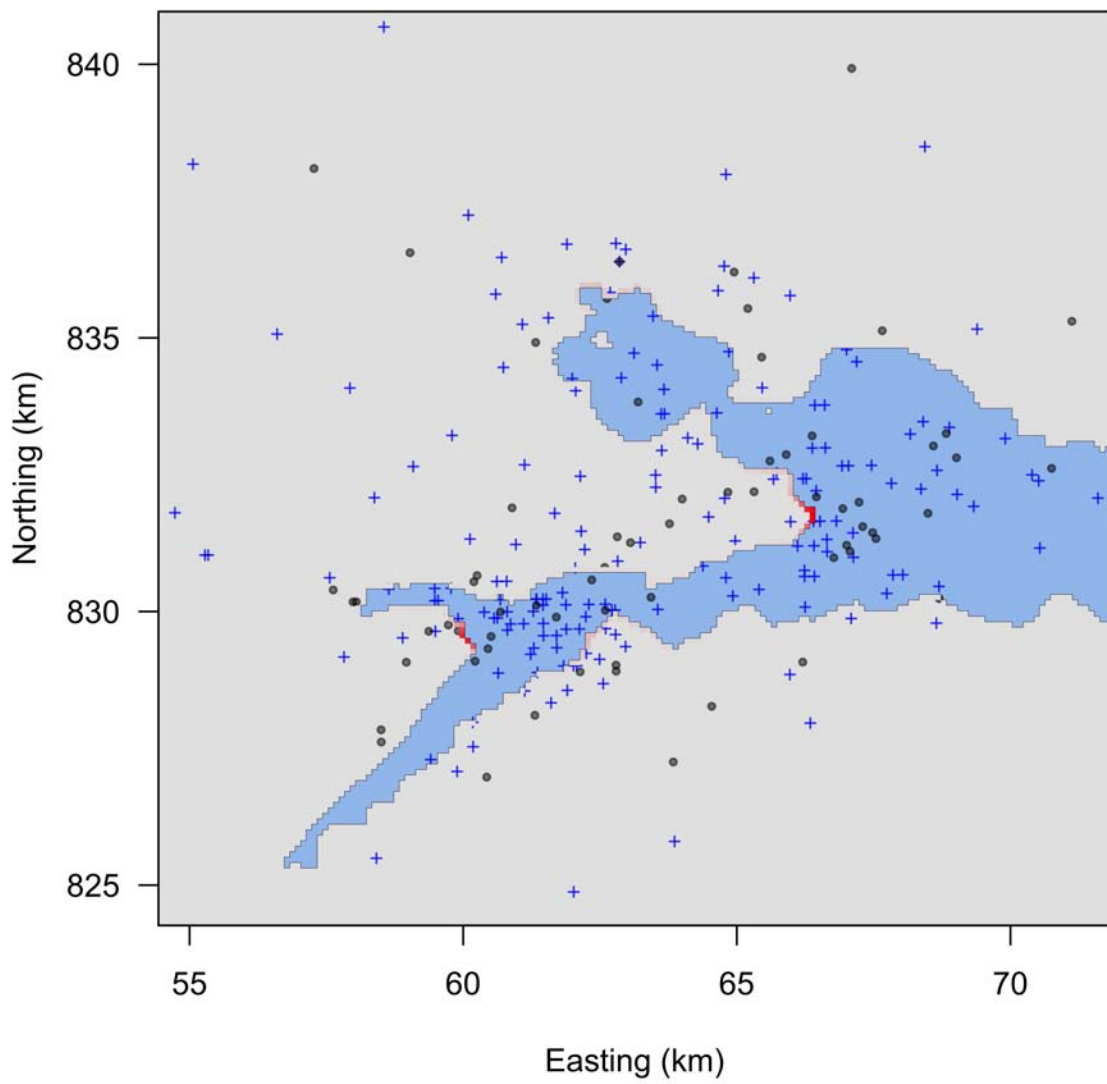


Figure C4.9. The posterior distribution of $\mu_i(t)$ for individual PV95KOD10, a male pup that was monitored from 10/12/95 to 05/27/96. Of the 301 recorded telemetry locations, 77 were obtained while the individual was hauled-out of the water.

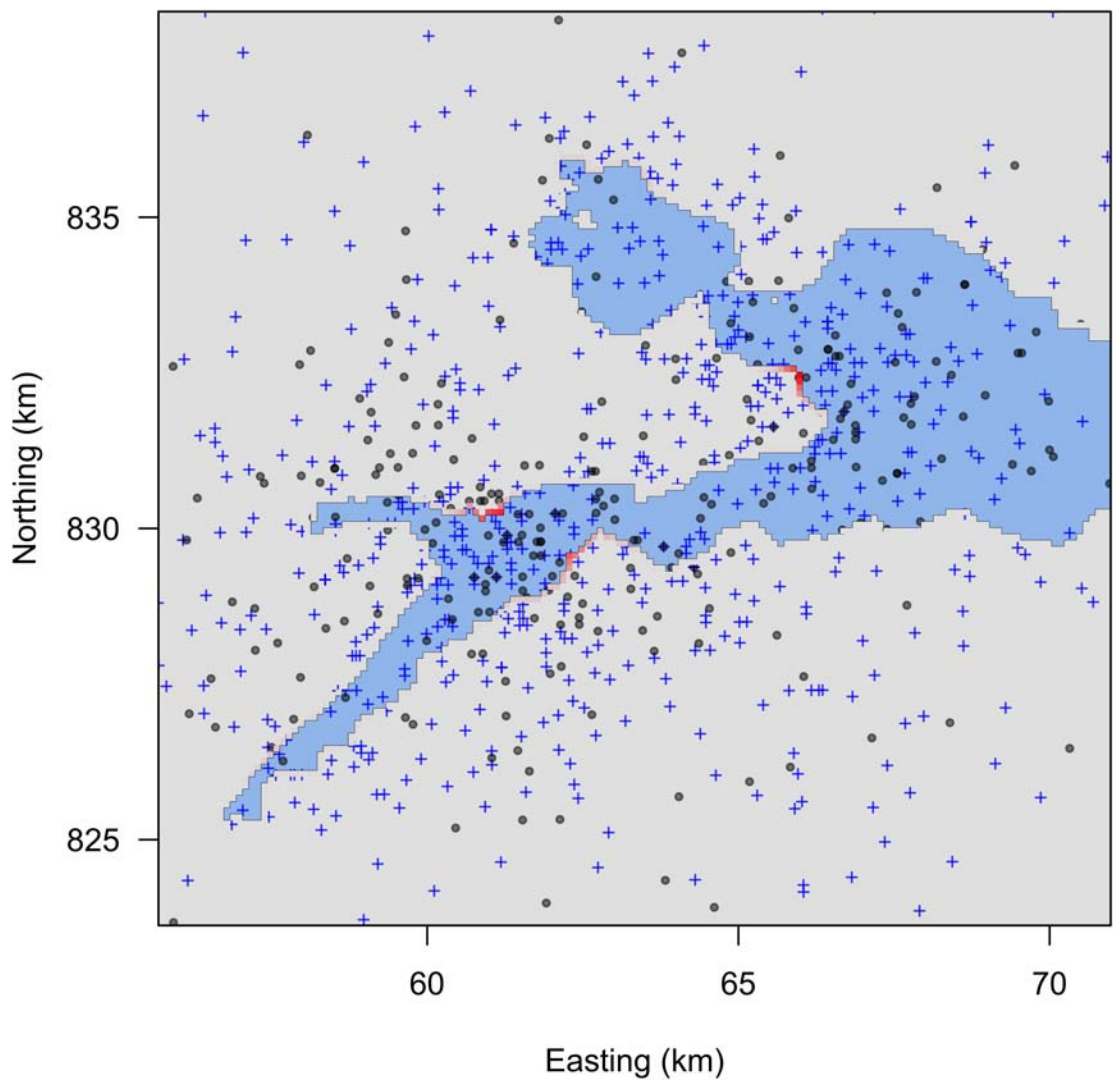


Figure C4.10. The posterior distribution of $\mu_i(t)$ for individual PV95KOD12, an adult female that was monitored from 10/10/95 to 06/27/96. Of the 1460 recorded telemetry locations, 340 were obtained while the individual was hauled-out of the water.

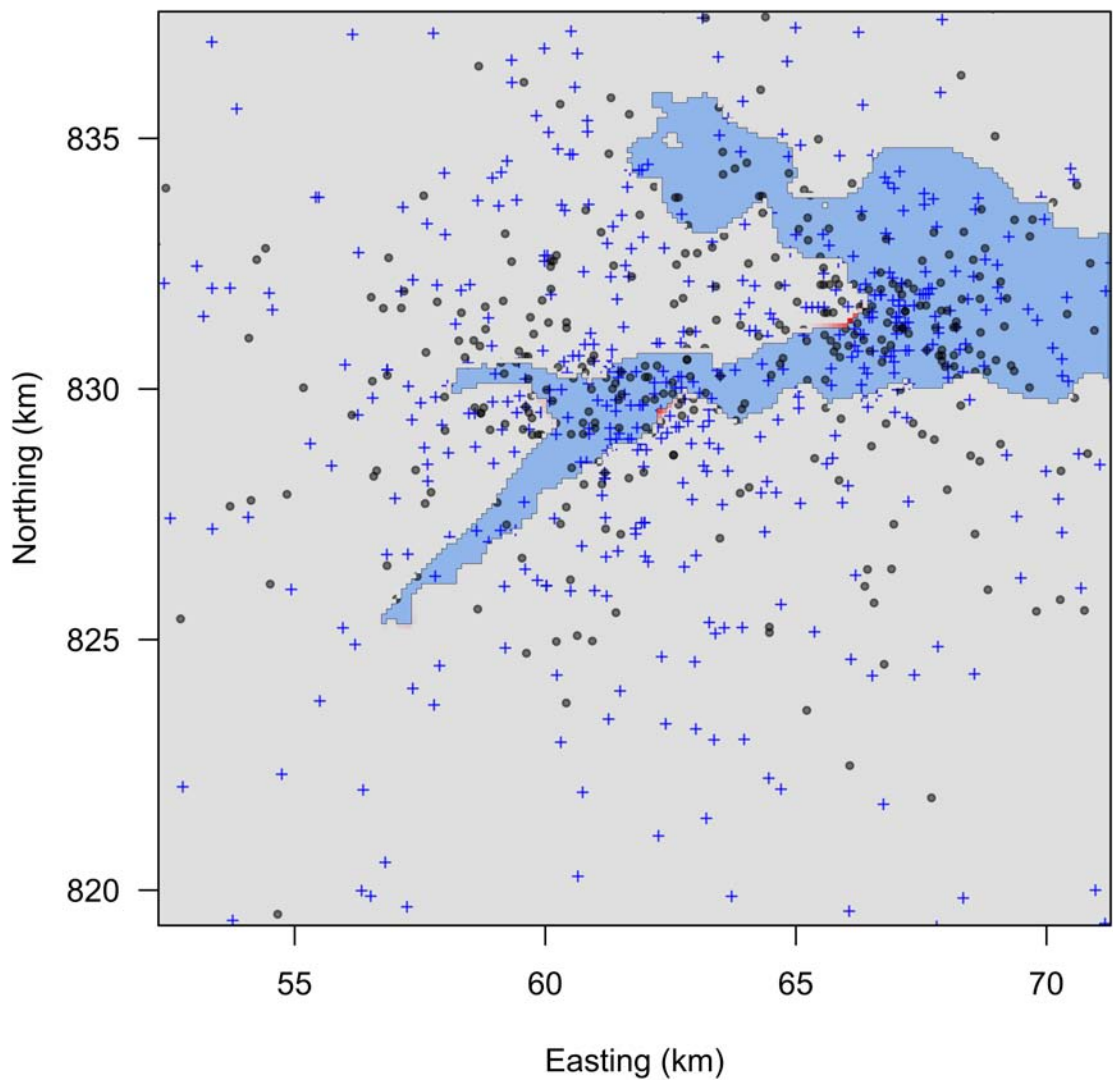


Figure C4.11. The posterior distribution of $\mu_i(t)$ for individual PV95KOD13, an adult male that was monitored from 10/10/95 to 06/16/96. Of the 1301 recorded telemetry locations, 435 were obtained while the individual was hauled-out of the water.

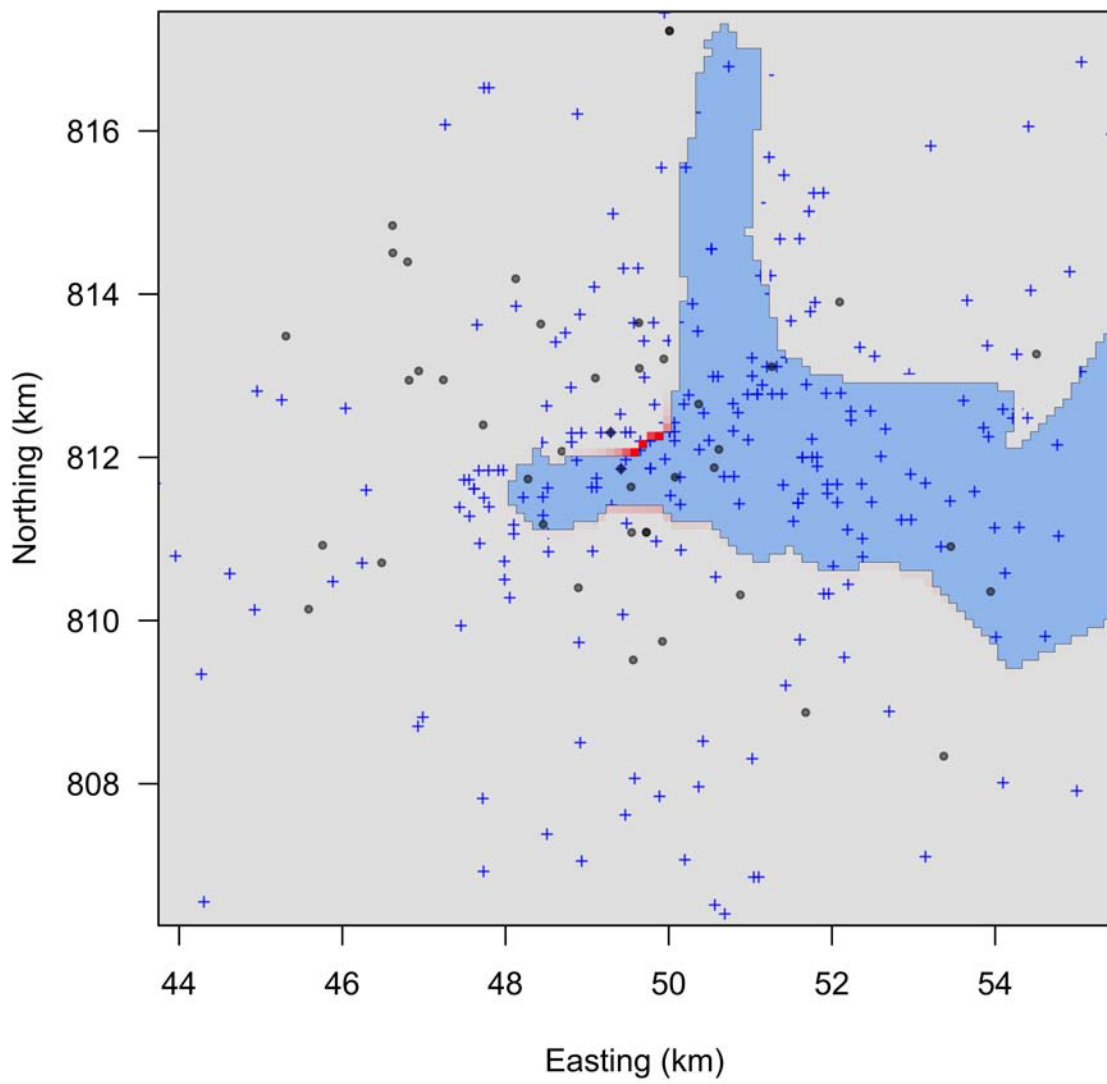


Figure C4.12. The posterior distribution of $\mu_i(t)$ for individual PV95KOD15, a female pup that was monitored from 10/10/95 to 05/13/96. Of the 379 recorded telemetry locations, 64 were obtained while the individual was hauled-out of the water.

APPENDIX C5. Summary of observation model parameter estimates. Reported quantities are based on 100,000 MCMC samples after convergence.

Table C5.1. Posterior mean and 95% credible intervals for the animal movement parameter (τ_i) in the observation model.

Individual	Sex	Age class	Posterior mean	Lower 95% credible bound	Upper 95% credible bound
PV94KOD01	Male	Adult	26488	21603	32157
PV94KOD02	Male	Adult	4710	3215	6669
PV94KOD08	Male	Adult	5917	3801	8407
PV94KOD09	Female	Subadult	3964	2774	5422
PV95KOD01	Male	Adult	5521	4543	6515
PV95KOD03	Female	Adult	15735	12831	18838
PV95KOD05	Female	Subadult	8081	6108	10107
PV95KOD09	Female	Subadult	3286	2637	4024
PV95KOD10	Male	Pup	2085	1529	2766
PV95KOD12	Female	Adult	7819	6808	8814
PV95KOD13	Male	Adult	2548	1821	3429
PV95KOD15	Female	Pup	1972	1543	2460

Table C5.2. Posterior mean and 95% credible intervals (in parentheses) for σ_{ic} (km).

Individual	Argos location quality class					
	3	2	1	0	A	B
PV94KOD01	3.64 (1.04, 10.17)	2.70 (1.48, 4.60)	3.15 (2.37, 4.09)	45.03 (38.66, 52.18)	11.34 (9.06, 14.18)	95.69 (82.99, 110.73)
PV94KOD02	5.50 (2.86, 10.69)	4.27 (2.47, 6.74)	2.30 (1.62, 3.26)	10.40 (9.21, 11.67)	16.39 (12.98, 20.74)	61.74 (55.99, 68.30)
PV94KOD08	3.91 (2.13, 7.05)	3.13 (1.77, 5.35)	75.02 (56.00, 98.94)	35.91 (31.65, 40.55)	14.88 (12.48, 17.34)	109.37 (98.89, 121.26)
PV94KOD09	2.75 (0.59, 8.73)	3.71 (2.16, 6.49)	3.10 (2.34, 4.13)	68.13 (58.46, 79.18)	71.88 (56.56, 91.25)	102.23 (85.96, 121.68)
PV95KOD01	1.26 (0.77, 2.12)	1.19 (0.85, 1.67)	1.64 (1.28, 2.12)	9.79 (8.72, 10.94)	5.22 (4.43, 6.14)	50.19 (46.46, 54.30)
PV95KOD03	2.31 (0.93, 4.58)	3.08 (1.80, 4.83)	2.57 (2.00, 3.35)	13.51 (11.78, 15.46)	10.11 (8.18, 12.55)	57.72 (50.74, 65.55)
PV95KOD05	1.39 (0.74, 2.46)	1.17 (0.82, 1.83)	2.37 (2.01, 2.79)	13.33 (11.73, 15.08)	9.72 (7.51, 11.95)	75.35 (69.41, 81.92)
PV95KOD09	1.51 (0.86, 2.50)	1.71 (1.33, 2.18)	2.11 (1.81, 2.45)	8.85 (7.64, 10.19)	8.02 (7.02, 9.19)	29.79 (26.91, 32.98)
PV95KOD10	1.09 (0.44, 2.56)	1.53 (0.74, 2.56)	1.49 (1.05, 2.10)	3.64 (2.75, 4.82)	4.02 (2.94, 5.36)	32.31 (27.58, 37.87)
PV95KOD12	2.39 (1.46, 3.95)	2.50 (1.75, 3.58)	2.81 (2.34, 3.36)	7.53 (6.60, 8.55)	6.75 (5.54, 8.07)	68.65 (63.99, 73.64)
PV95KOD13	1.47 (0.74, 2.78)	2.32 (1.78, 3.00)	5.35 (4.53, 6.28)	10.04 (9.01, 11.10)	15.03 (13.44, 16.78)	39.74 (36.95, 42.83)
PV95KOD15	1.63 (0.49, 4.09)	1.14 (0.58, 1.96)	1.66 (1.11, 2.36)	9.57 (6.88, 12.83)	4.33 (3.52, 5.26)	16.43 (14.52, 18.59)

Table C5.3. Posterior mean and 95% credible intervals (in parentheses) for a_{ic} .

Individual	Argos location quality class					
	3	2	1	0	A	B
PV94KOD01	0.58 (0.10, 0.98)	0.36 (0.12, 0.86)	0.33 (0.17, 0.60)	0.19 (0.16, 0.22)	0.33 (0.20, 0.52)	0.66 (0.46, 0.91)
PV94KOD02	0.38 (0.09, 0.90)	0.28 (0.09, 0.76)	0.36 (0.16, 0.72)	0.38 (0.30, 0.47)	0.69 (0.48, 0.95)	0.79 (0.65, 0.95)
PV94KOD08	0.21 (0.04, 0.66)	0.45 (0.10, 0.96)	0.07 (0.06, 0.08)	0.11 (0.09, 0.12)	0.32 (0.23, 0.44)	0.48 (0.37, 0.60)
PV94KOD09	0.52 (0.07, 0.97)	0.14 (0.05, 0.31)	0.68 (0.42, 0.96)	0.12 (0.12, 0.13)	0.14 (0.10, 0.18)	0.49 (0.31, 0.76)
PV95KOD01	0.75 (0.35, 0.99)	0.79 (0.41, 0.99)	0.60 (0.30, 0.91)	0.19 (0.15, 0.23)	0.73 (0.56, 0.93)	0.43 (0.36, 0.52)
PV95KOD03	0.36 (0.05, 0.93)	0.64 (0.19, 0.98)	0.77 (0.45, 0.99)	0.37 (0.28, 0.48)	0.70 (0.50, 0.94)	0.48 (0.38, 0.61)
PV95KOD05	0.14 (0.03, 0.41)	0.73 (0.37, 0.99)	0.30 (0.18, 0.51)	0.28 (0.23, 0.34)	0.28 (0.20, 0.39)	0.64 (0.53, 0.76)
PV95KOD09	0.33 (0.07, 0.84)	0.37 (0.19, 0.64)	0.31 (0.20, 0.45)	0.34 (0.27, 0.43)	0.84 (0.66, 0.99)	0.33 (0.27, 0.40)
PV95KOD10	0.29 (0.03, 0.83)	0.41 (0.13, 0.92)	0.22 (0.11, 0.37)	0.68 (0.34, 0.98)	0.19 (0.10, 0.35)	0.15 (0.09, 0.22)
PV95KOD12	0.27 (0.16, 0.48)	0.14 (0.07, 0.23)	0.43 (0.33, 0.55)	0.26 (0.21, 0.30)	0.70 (0.57, 0.86)	0.39 (0.33, 0.45)
PV95KOD13	0.58 (0.11, 0.98)	0.16 (0.10, 0.23)	0.17 (0.14, 0.21)	0.26 (0.21, 0.33)	0.52 (0.42, 0.66)	0.39 (0.32, 0.46)
PV95KOD15	0.11 (0.01, 0.57)	0.13 (0.04, 0.31)	0.26 (0.12, 0.47)	0.29 (0.14, 0.62)	0.26 (0.16, 0.41)	0.18 (0.13, 0.23)

Table C5.4. Posterior mean and 95% credible intervals (in parentheses) for ρ_{ic} .

Individual	Argos location quality class					
	3	2	1	0	A	B
PV94KOD01	0.52 (0.03, 0.98)	0.52 (0.20, 0.80)	0.70 (0.20, 0.95)	0.85 (0.80, 0.90)	0.42 (0.06, 0.68)	0.39 (0.11, 0.59)
PV94KOD02	0.41 (0.02, 0.87)	0.61 (0.08, 0.91)	0.67 (0.20, 0.89)	0.58 (0.47, 0.67)	0.63 (0.50, 0.74)	0.69 (0.60, 0.76)
PV94KOD08	0.43 (0.02, 0.92)	0.29 (0.01, 0.70)	0.99 (0.98, 1.00)	0.90 (0.86, 0.93)	0.70 (0.57, 0.79)	0.48 (0.34, 0.60)
PV94KOD09	0.51 (0.03, 0.98)	0.87 (0.26, 0.99)	0.70 (0.43, 0.87)	0.99 (0.99, 1.00)	0.91 (0.83, 0.96)	0.32 (0.03, 0.56)
PV95KOD01	0.34 (0.02, 0.79)	0.27 (0.01, 0.66)	0.69 (0.41, 0.85)	0.78 (0.69, 0.84)	0.57 (0.45, 0.67)	0.50 (0.40, 0.58)
PV95KOD03	0.38 (0.02, 0.90)	0.68 (0.12, 0.95)	0.34 (0.02, 0.72)	0.66 (0.55, 0.74)	0.69 (0.56, 0.79)	0.69 (0.58, 0.77)
PV95KOD05	0.39 (0.02, 0.83)	0.48 (0.03, 0.87)	0.68 (0.22, 0.86)	0.75 (0.68, 0.82)	0.63 (0.50, 0.73)	0.62 (0.54, 0.69)
PV95KOD09	0.34 (0.01, 0.82)	0.30 (0.02, 0.61)	0.40 (0.06, 0.63)	0.77 (0.70, 0.83)	0.66 (0.53, 0.76)	0.67 (0.59, 0.75)
PV95KOD10	0.57 (0.04, 0.96)	0.44 (0.02, 0.89)	0.69 (0.17, 0.91)	0.42 (0.03, 0.78)	0.62 (0.32, 0.82)	0.36 (0.14, 0.54)
PV95KOD12	0.95 (0.82, 0.99)	0.87 (0.65, 0.96)	0.69 (0.58, 0.78)	0.71 (0.63, 0.78)	0.54 (0.44, 0.63)	0.57 (0.49, 0.63)
PV95KOD13	0.41 (0.02, 0.83)	0.90 (0.80, 0.95)	0.87 (0.80, 0.92)	0.60 (0.50, 0.69)	0.61 (0.52, 0.69)	0.49 (0.40, 0.57)
PV95KOD15	0.50 (0.03, 0.96)	0.38 (0.02, 0.88)	0.46 (0.03, 0.81)	0.72 (0.43, 0.94)	0.51 (0.17, 0.73)	0.64 (0.52, 0.74)

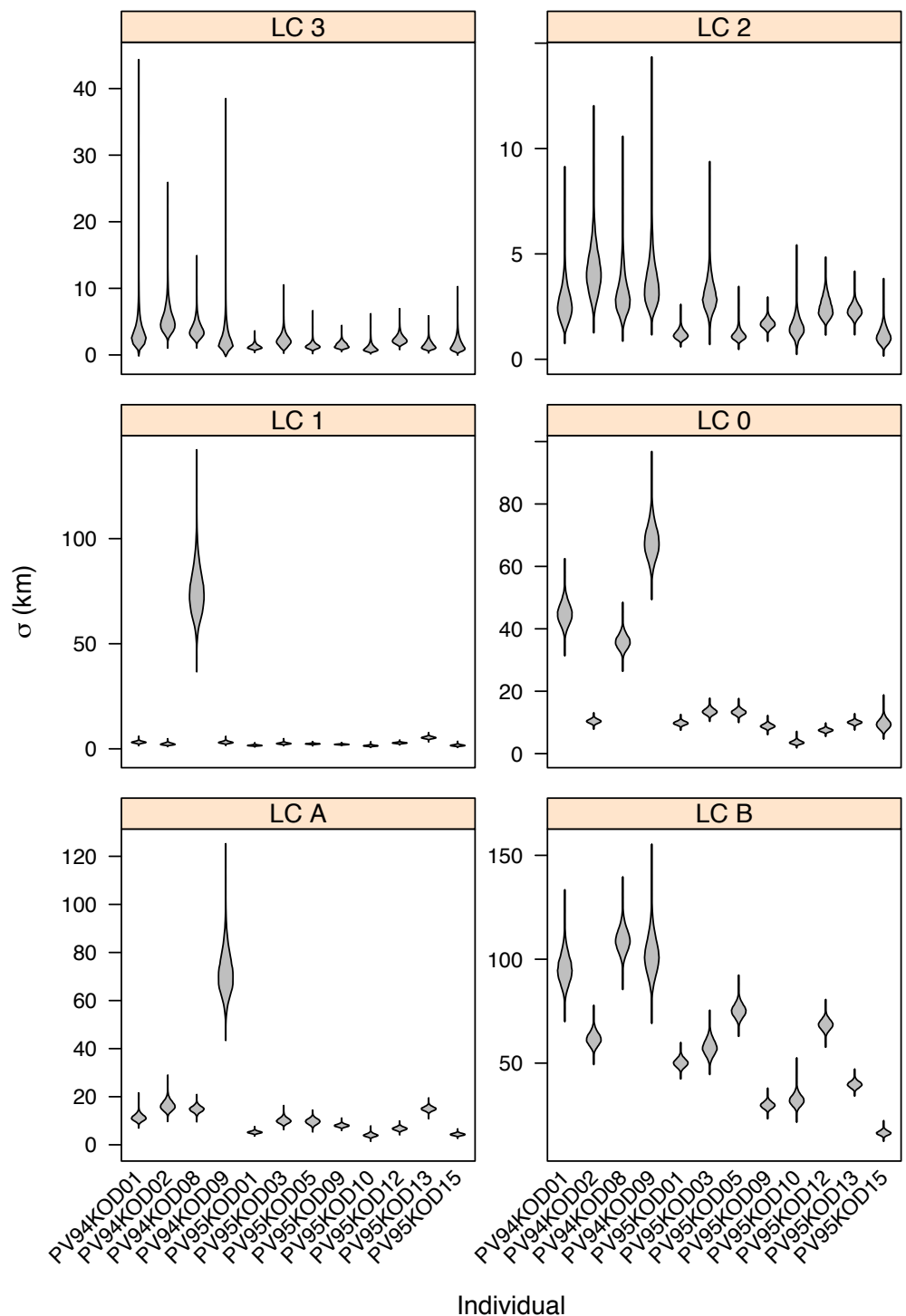


Figure C5.1. Posterior distributions of σ_{ic} .

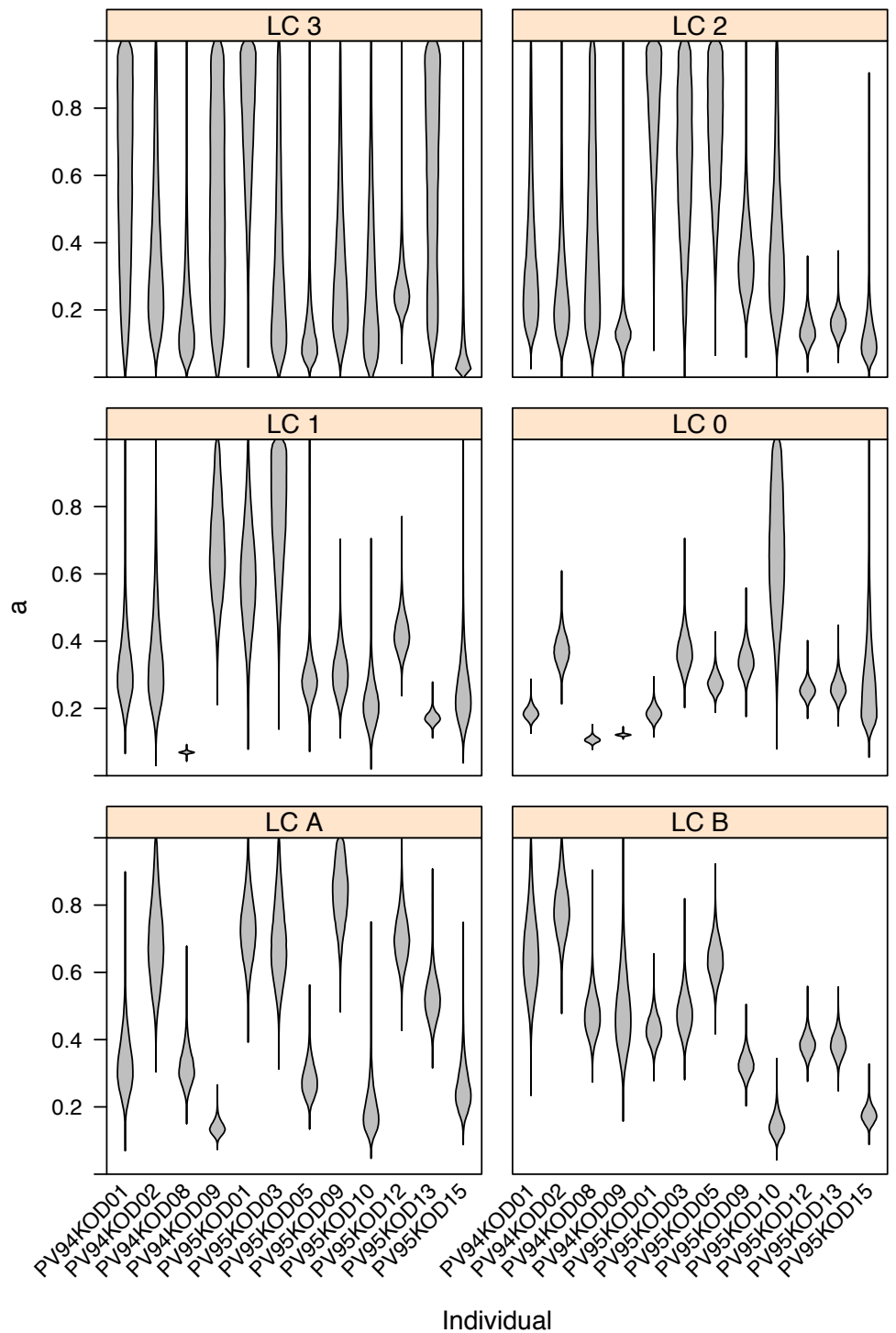


Figure C5.2. Posterior distributions of a_{ic} .

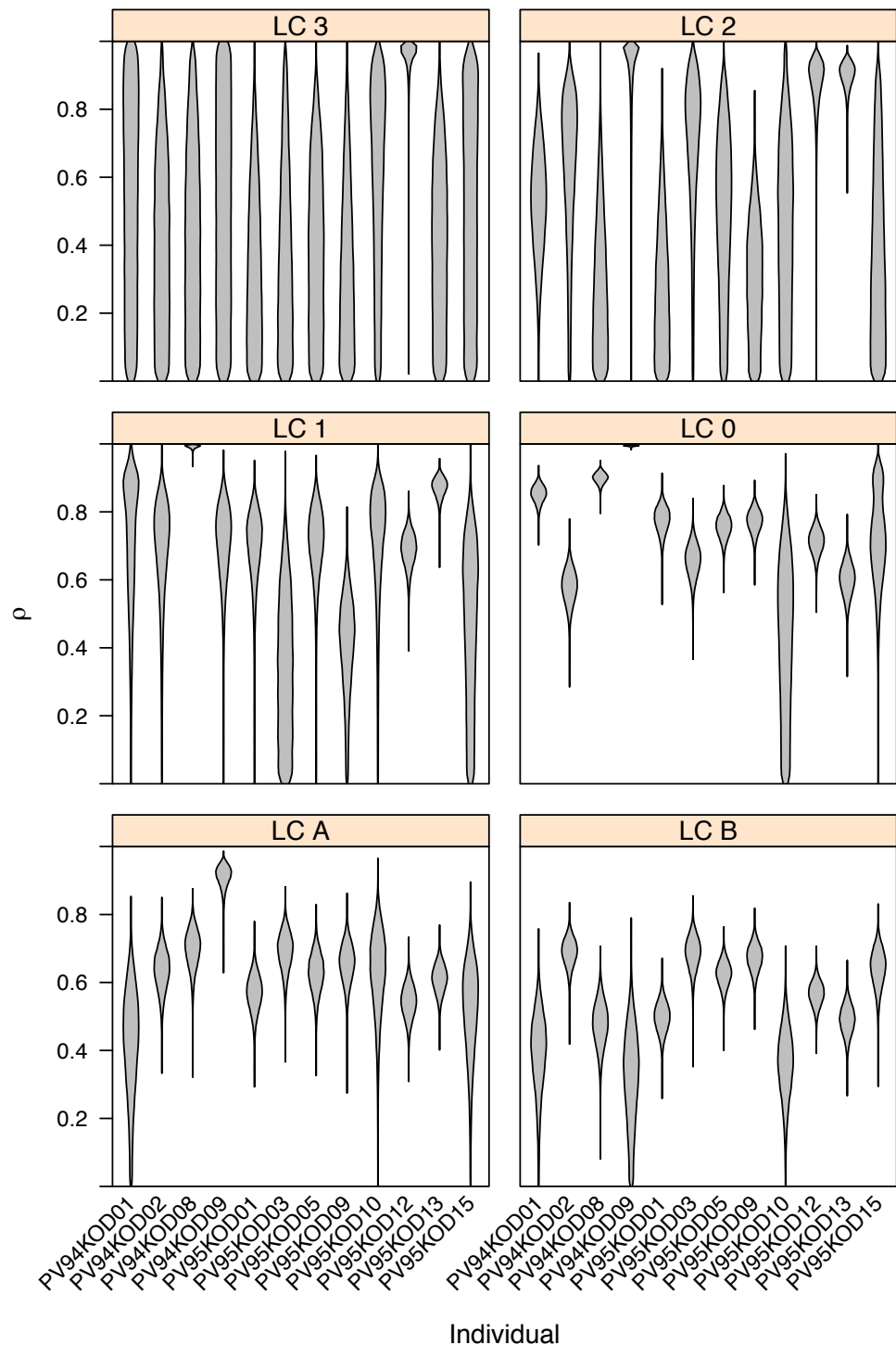


Figure C5.3. Posterior distributions of ρ_{ic} .

APPENDIX C6. Inference concerning haul-out site selection for the subset of harbor seals that did not exhibit complete separation between the counts w_{ij} and the two wave exposure categories.

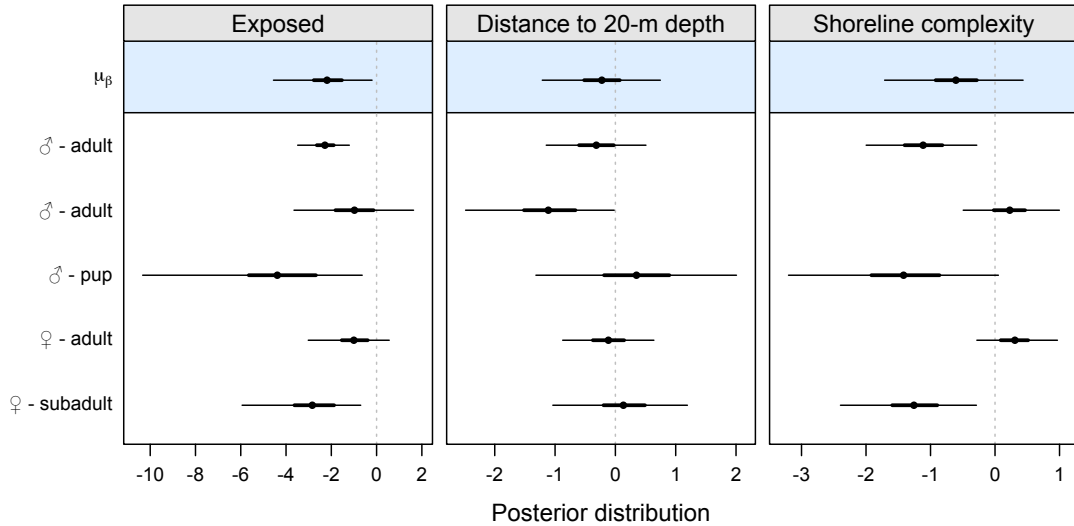


Figure C6.1. Individual- and population-level inference concerning parameters examined in the haul-out site selection model for the subset of 5 harbor seals for which complete separation between w_{ij} and wave exposure did not occur. The top row (blue box) represents inference concerning the population-level parameter (μ_β) that represents an average affect across the 5 harbor seals analyzed. The remaining rows show individual-level parameters (β_i), and individual seals are labeled according their sex and age class. The points indicate the posterior mean, the thick lines represent the 50% credible interval, and the thin lines represent the 95% credible interval.